

Aus dem Institut für Mineralogie und Petrographie
Universität Freiburg (Schweiz)



EVOLUTION OF METAL CATALYST DURING CVD SYNTHESIS OF CARBON NANOTUBES

INAUGURAL-DISSERTATION

zur Erlangung der Würde eines *Doctor rerum naturalium* der Mathematisch-
Naturwissenschaftlichen Fakultät der Universität Freiburg in der Schweiz

vorgelegt von

Kuno Matzinger

aus

Basel (BS), Luzern (LU), Littau (LU)

Dissertation Nr. 1504
ABC Druck & Kopie GmbH, Luzern
2006

Von der Mathematisch-Naturwissenschaftlichen Fakultät der Universität Freiburg in der Schweiz
angenommen, auf Antrag von Prof. Dr. Bernard Grobéty, Prof. Dr. Andreas Strasser, Prof. Dr.
Andreas Züttel und Dr. Andri Vital.

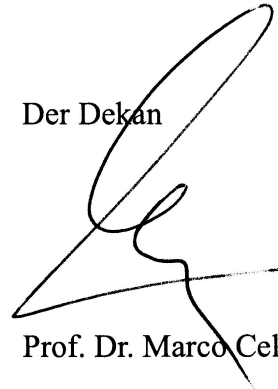
Freiburg, 17. Februar 2006

Der Leiter der Dissertation



Prof. Dr. Bernard Grobéty

Der Dekan



Prof. Dr. Marco Celio

Table of Contents

Abstract.....	1
Résumé.....	2
Zusammenfassung.....	3
Chapter 1 Introduction.....	4
1.1 Introduction to the World of Nanotubes	5
1.2 Structures of Carbon Materials	6
1.2.1 Graphite.....	6
1.2.2 Diamond.....	7
1.2.3 Fullerenes.....	7
1.2.4 Carbon Nanotubes.....	8
1.2.5 Carbon Fibres.....	11
1.2.6 Carbon Whiskers.....	11
1.2.7 Glassy Carbon.....	11
1.2.8 Liquid Carbon	11
1.3 Synthesis of Carbon Nanotubes	11
1.3.1 Arc-Discharge Technique.....	11
1.3.2 Laser Ablation Technique	12
1.3.3 Electrolysis Method	12
1.3.4 Synthesis from Bulk Polymer	13
1.3.5 Low-Temperature Solid Pyrolysis	13
1.3.6 Chemical Vapour Deposition (CVD) Methods	13
1.3.6.1 Horizontal Furnace.....	13
1.3.6.2 Vertical Furnace	14
1.3.6.3 Plasma Enhanced Chemical Vapour Deposition (PECVD).....	14
1.4 Physical Properties of Carbon Nanotubes.....	15
1.5 Applications of Carbon Nanotubes and Future Directions	15
1.6 Catalysis in the CVD Production of Carbon Nanotubes.....	16
1.7 Goals and Results of the Present Work.....	18
1.8 References.....	19
Chapter 2 Investigation Methods	24
2.1 CVD Facility.....	25
2.1.1 High Temperature X-ray Diffractometer Chamber.....	25
2.1.2 Temperature Calibration	25
2.1.3 Calculation of Peak-Positions at different Temperatures.....	27

2.1.4 Description of the Gas System.....	28
2.2 Scanning Electron Microscopy	28
2.3 Sample Preparation	29
2.4 Softwares.....	30
2.5 References.....	30
Chapter 3 The Evolution of Iron and Nickel Nitrate Films during CVD Synthesis of Carbon Nanotubes: An <i>in-situ</i> High Temperature X-Ray Diffraction Investigation	31
<p>K. Matzinger, A. Lepora, B. Grobéty and A. Züttel extended abstract at CARBON 2004, An International Conference on Carbon at Brown University, Providence, Staten Island, USA, 11.-16. July 2004</p>	
Chapter 4 The Evolution of Nickel Nitrate Hexahydrate coated Glass Substrate during CVD Synthesis of Carbon Nanotubes: An <i>in-situ</i> High Temperature X-Ray Diffraction Investigation	36
<p>K. Matzinger and B. Grobéty submitted to Carbon</p>	
Chapter 5 The Evolution of Cobalt Nitrate Hexahydrate coated Glass Substrate during CVD Synthesis of Carbon Nanotubes: An <i>in-situ</i> High Temperature X-Ray Diffraction Investigation	46
<p>K. Matzinger and B. Grobéty to be submitted to Journal of Applied Physics A</p>	
Chapter 6 The Evolution of Molybdenum Oxide coated Glass Substrate during CVD Synthesis of Carbon Nanotubes: An <i>in-situ</i> High Temperature X-Ray Diffraction Investigation	60
<p>K. Matzinger and B. Grobéty to be submitted</p>	
Appendices.....	69
1. The Evolution of Chromium Nitrate Nonahydrate coated Glass Substrate during CVD Synthesis of Carbon Nanotubes: An <i>in-situ</i> High Temperature X-Ray Diffraction Investigation	69

2. Log-Book of all obtained X-Ray Diffraction Experiments	73
3. Oxygen Fugacity and Carbon Activity Calculations	87
4. Metal-O-C Phase Diagrams	89
5. Calculations of Solid Volume Changes.....	90
6. Calculations of Unit Cell Parameters.....	94
7. Calibration Conversion from Reference Gases.....	95
8. SEM Samples.....	96
Acknowledgements	98
Curriculum Vitae	99

Abstract

The revolutionary discovery of carbon nanotubes (CNT) in 1991 led to intense research activities in the domain of carbon science. The fascinating properties of these unique material has opened a great number of potential applications e.g. as electron field emitters, one-dimensional conductors, supercapacitors, reinforcing fibres or hydrogen storage. Despite these stunning technical progresses there is still much struggle in the development of a synthesis method suitable for commercial applications. A leading candidate is the chemical vapour deposition (CVD) technique. Nucleation and growth of CNTs are induced by the decomposition of carbon-containing gases (CO , CO_2 , C_2H_2 , etc) over a metallic catalyst at temperatures between 600°C and 1200° . CVD is a widely used technique to generate CNTs in large quantities and much progress has been made from the point of view of the yield, the synthesis costs or the purity of the products. But the great conundrum of CVD process remains the growth mechanism. A key reaction step for nanotube growth seems to be diffusion of carbon through the metal catalyst and the most active metals are iron, cobalt and nickel but their catalytic action depends on the type of precursor, the type of substrate and of the reactive gases used. Highly controversial is the actual chemical nature of the active catalyst e.g. if it is present as metal, carbide or as mixed phase. So far few investigations of the chemical and morphological evolution of the catalyst during CVD process have been performed. This thesis focuses on the evolution of nickel-, cobalt-, chromium- and molybdenum-based catalysts under a nitrogen/acetylene and a nitrogen/acetylene/hydrogen atmosphere at 600°C and 750°C . In order to elucidate the nature of the catalyst during synthesis runs an X-ray diffractometer equipped with a heating stage and an atmosphere controlling system was used to study *in-situ* the evolution of metal nitrate films. Samples quenched after different pyrolysis time were investigated by SEM and TEM. The microscopic images showed that nickel, cobalt and molybdenum can act under typical nanotube synthesis conditions as catalyst for CNT nucleation and growth, but not chromium. Grain size reduction resulting from a sufficient solid volume loss during redox reactions in the catalyst precursor and the transformation of these precursors to a metallic phase are the main requirements for nanotube growth. The reaction sequences observed during the reduction of the precursor are put in relation with the nucleation and growth of nanotubes. Diffusion

of carbon through the metal particle, indicated by an increase of metal cell parameters identified in diffractograms as peak shifts, was observed whenever carbon nanotubes were generated. In the nickel and cobalt system no carbide phases were detected. In contrast to the iron system, where the break-down of metastable carbides act as a second boost of nanotube formation, the appearance of carbides in the molybdenum system after 20 minutes stops further carbon nanotube growth. In any case hydrogen pre-treatment promotes nanotube growth.

Résumé

La découverte révolutionnaire des nanotubes de carbone (CNT) en 1991 a provoqué une intensification des travaux de recherche dans le domaine de la science du carbone. Les propriétés fascinantes de ce matériau offrent une multitude d'applications potentielles, par exemple comme émetteur de champs, conducteur uni-dimensionnel, condensateur haute capacité ("supercap"), fibres de renforcement ou encore comme réservoir d'hydrogène. Malgré d'immenses progrès techniques, l'amélioration des méthodes de synthèse en vue d'une application commerciale est encore au centre des recherches. La technique de dépôt en phase vapeur (CVD) est un candidat prometteur. Dans cette technique, la nucléation et la croissance des CNTs sont induites par la décomposition de gaz carburés (CO , CO_2 , C_2H_2 , etc.) sur un catalyseur métallique à des températures comprises entre 600°C et 1200°C . La CVD est largement utilisée pour la fabrication à grande échelle de CNTs et beaucoup de progrès ont été faits en ce qui concerne la quantité, les frais de synthèse et la pureté des produits. Toutefois, le mécanisme de croissance des nanotubes par CVD reste peu connu. La diffusion du carbone à travers le catalyseur métallique est souvent considérée comme l'étape déterminante lors de la croissance des CNTs. Les métaux les plus réactifs sont le fer, le cobalt et le nickel, mais leur effet catalytique est dépendant de plusieurs facteurs tels que la nature du précurseur, le substrat utilisé et les gaz de réaction. La nature chimique actuelle du catalyseur actif est très controversée; on ne sait pas par exemple s'il est présent sous forme de métal, de carbure ou en phase mélangée. Jusqu'à présent, très peu d'analyses *in-situ* de l'évolution chimique et morphologique du catalyseur durant le processus CVD ont été faites. Le comportement de catalyseurs à base de nickel, cobalt, chrome ou molybdène a été analysé sous une atmosphère azote/acétylène ou azote/acétylène/hydrogène à des températures de 600°C et de 750°C . Pour mieux comprendre les propriétés des phases métalliques pendant le processus de synthèse, un diffractomètre à rayons X équipé avec une table chauffante et un système de contrôle atmosphérique a été utilisé pour étudier *in-situ* l'évolution des revêtements de nitrate métallique. Les échantillons ont été ensuite trempés à différents stades de pyrolyse pour être finalement observés au MEB et MET. Les images au microscope ont montré que le nickel ainsi que le cobalt et le molybdène peuvent agir comme catalyseurs pour la nucléation et la croissance

des CNTs, cependant pas le chrome. La réduction de la taille des grains résultant d'une perte suffisante de volume solide pendant les réactions rédox dans le précurseur catalytique, ainsi que la transformation de ces précurseurs en une phase métallique sont les principales conditions nécessaires à la croissance de CNTs. Les stades de réaction observés pendant la réduction du précurseur ont été mis en relation avec la nucléation et la croissance des nanotubes. La diffusion de carbone à travers les particules métalliques, marquée par un agrandissement des paramètres cellulaires du métal et identifiée sur les diffractogrammes par un déplacement des pics, est observée à chaque fois que des nanotubes de carbone sont générés. Avec le nickel et le cobalt, aucune phase de carbure ne s'est formée. Avec le fer, la décomposition des phases métastables de carbure agit comme une seconde activation de la croissance des nanotubes alors que le molybdène va favoriser la formation de carbures qui vont stopper la croissance des CNTs après 20 minutes. Dans tous les cas, il a été démontré qu'un traitement préliminaire à l'hydrogène favorise la croissance des nanotubes.

Zusammenfassung

Die revolutionäre Entdeckung von Kohlenstoff-Nanoröhrchen (CNT) im Jahre 1991 liess die Forschungsarbeiten im Bereich der Kohlenstoffwissenschaft intensivieren. Die faszinierenden Eigenschaften dieses einzigartigen Materials ermöglichten eine Vielzahl von potenziellen Anwendungen wie zum Beispiel als Elektronen Feldemissionsquelle, eindimensionale Konduktoren, Superkapazitäten, Verstärkungsfaden oder Wasserstoffspeicher. Trotz der atemberaubenden technischen Fortschritte bemüht man sich immer noch um die Entwicklung einer Synthesemethode für die kommerzielle Anwendung. Ein vielversprechender Kandidat ist die Technik der chemischen Gasphasenabscheidung (CVD). Die Keimbildung und das Wachstum von CNTs werden induziert durch die Zersetzung von kohlenstoffhaltigen Gasen (CO , CO_2 , C_2H_2 , usw.) über einem metallischen Katalysator bei Temperaturen zwischen 600°C und 1200°C . CVD ist eine weit verbreitete Technik für die Fabrikation von CNT in grossen Quantitäten und Fortschritte betreffend der Menge, der Synthesekosten und der Reinheit der Produkte, wurden erzielt. Doch das grosse Rätsel der CVD Methode bleibt der Wachstumsmechanismus. Der Hauptreaktionsschritt für das Wachstum von Nanoröhrchen scheint die Diffusion von Kohlenstoff durch den Metallkatalysator zu sein. Die reaktivsten Metalle sind Eisen, Kobalt und Nickel, doch deren katalytische Wirkung ist abhängig von der Art des Ausgangsmaterials, des benutzten Substrates und der Reaktionsgase. Sehr umstritten ist die aktuelle chemische Beschaffenheit des aktiven Katalysators, zum Beispiel ob er als Metall, Karbid oder als gemischte Phase vorliegt. Bis jetzt wurden nur sehr wenige *in-situ* Analysen der chemischen und morphologischen Evolution des Katalysators während des CVD Prozesses durchgeführt.

Diese Doktorarbeit befasst sich mit der Evolution von nickel-, kobalt-, chrom- und molybdän-basierenden Katalysatoren unter Stickstoff/Acetylen und Stickstoff/Acetylen/Wasserstoff Atmosphäre bei 600°C und 750°C . Um die Eigenschaften von metallischen Phasen während des Syntheseablaufs aufzuklären, wurde ein Röntgendiffraktometer mit einem Heiztisch und einem Atmosphärenkontrollsystem ausgestattet, welches das *in-situ* Studium der Evolution von Metallnitrat-Filmen ermöglicht. Die Proben wurden dafür bei verschiedenen Pyrolysezeiten abgeschreckt und im REM und TEM untersucht.

Die Mikroskopiebilder zeigen, dass Nickel sowie Kobalt und Molybdän unter typischen Nanoröhrchen Synthesebedingungen als Katalysatoren für CNTs Keimbildung und Wachstum agieren können, jedoch nicht Chrom. Korngrößenreduktion, resultierend aus dem ausreichenden Festkörpervolumenverlust während der Redox Reaktion im katalytischen Ausgangsmaterial, und die Transformation des Ausgangsmaterials zu einer metallischen Phase sind die Hauptvoraussetzungen für das CNT Wachstum. Die beobachteten Reaktionsabschnitte während der Reduktion des Ausgangsmaterials werden in Verbindung gebracht mit der Keimbildung und dem Wachstum von Nanoröhrchen. Kohlenstoffdiffusion durch die metallischen Partikel, angezeigt durch eine Vergrösserung der Zellparameter des Metalls und identifiziert in Diffraktogramme als Peak-Verschiebung, wurde beobachtet wann immer CNTs gebildet wurden. Im Nickel- und Kobaltsystem wurden keine Karbidphasen entdeckt. Doch im Vergleich zum Eisensystem, wo die Zerlegung von metastabilem Karbid als zweiter Schub von Nanoröhrchen Bildung dient, wird das CNT Wachstum im Molybdänsystem nach der Bildung von Karbiden nach 20 Minuten gestoppt. In jedem Fall begünstigt eine Vorbehandlung mit Wasserstoff die Nanoröhrchen Bildung.

CHAPTER 1

Introduction

1.1 Introduction to the World of Nanotubes

Carbon an element which has the affinity to bond with itself is forming a rich variety of structures and morphologies. Until recently only two types of all-carbon crystalline structures were known – diamond and graphite. The first carbon fibres were prepared by Thomas A. Edison to provide a filament for an early model of an electric light bulb. Specially selected bamboo filaments were pyrolysed to produce a coiled carbon resistor, which could be heated ohmically [1]. Further research on filamentous carbon proceeded more slowly, since the carbon spiral coil was soon replaced by tungsten filaments. The second stimulus to carbon fibre research came in the 1950's from the space and aircraft industry, which was searching for strong, stiff light-weight fibres with superior mechanical properties. This stimulation led to the synthesis of single crystal carbon whiskers [2], which have become a benchmark for the discussion of mechanical and elastic properties of carbon fibres. Intense efforts were invested in reducing fibre defects and crack propagation as well as in development of highly oriented pyrolytic graphite, which preceded the synthesis of carbon fibres by a catalytic chemical vapour deposition (CVD) process [3]. Research on vapour grown carbon fibres reported occasionally the occurrence of very small diameter filaments [4], but no detailed systematic studies of such thin filaments were carried out.

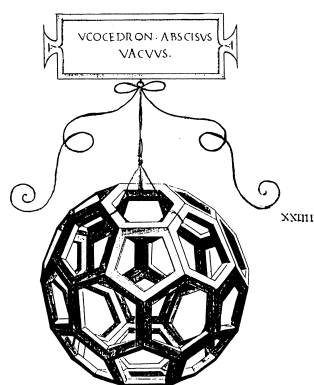


Fig. 1: A regular truncated icosahedron designed by Leonardo da Vinci in 1509 [6].

The discovery of C_{60} by Smalley and Kroto [5] in 1985 (Nobel prize in chemistry in 1996) as a side product of a new laser-vaporisation synthesis method started a new era in carbon science. The geometry of the molecule is that of a regular truncated icosahedron, a shape already known to Leonardo da Vinci [Figure 1] and Albrecht Dürer [Figure 2] in the 16th century.

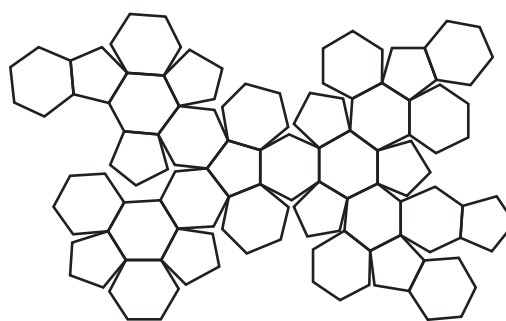


Fig. 2: Albrecht Dürer's drawing (~1500) of the construction of the icosahedron truncum by folding up a sheet of cardboard [6].

These molecules are called “Buckminsterfullerenes” or short “Buckyballs”, in honor of the brilliant philosopher, architect, engineer, mathematician, poet and cosmologist Richard Buckminster Fuller (1895-1983), an eminent futurist and global thinker.

Smalley [7] speculated about the existence of carbon nanotubes (CNT) of dimensions comparable to C_{60} . Dresselhaus [8] suggested, based on symmetry considerations, that tubes consisting of wrapped graphite sheets and capped at either end by fullerene hemispheres should be possible. First, progress after discovery was slow, but since Krätschmer and Huffman [9] developed a simple technique to vaporise graphite by arc discharge, research activities gained pace. Iijima [10] engaged in a detailed TEM study of the soot produced by Krätschmer-Huffman's arc-evaporation technique. Cylindrical deposits which were formed on the graphite cathode revealed a wide spectrum of novel graphitic structures. The most striking discovery among others was long hollow fibres – carbon nanotubes.

All nanotubes observed by Iijima in 1991 invariably contain at least two graphitic layers and are therefore called multi-walled carbon nanotubes (MWNT) with an inner diameter of 4 nm or more. An extremely important development was the synthesis of single-walled nanotubes (SWNT) only two years later [11,12]. Their appearance is quite different to that of MWNT. The individual tubes have smaller diameters (typically ~ 1nm) and are curled and looped rather than straight. The discovery of SWNT had been the basis for a large body of theoretical studies. One of the most striking predictions was that, depending on the wrapping scheme, carbon nanotubes could be either semi-conducting or metallic, which has been corroborated experimentally in 1998 [13]. Likewise important were the successful filling of nanotubes with molten lead [14] or the synthesis of aligned

SWNTs in bundles [15]. Overall, the volume of nanotube research is still growing at an astonishing rate.

The discovery of carbon nanotubes inspired interest of scientists in many fields. Physicists have been attracted by their extraordinary electronic and mechanical properties and the quasi-one dimensional behaviour of nanotubes; chemists by the molecular nature of the solid tubes and the immense potential to form new compounds; material scientists and device engineers by the possibility to assemble the nanotubes into two-dimensional ordered nanostructures which have potential use in optical, electrical or mechanical devices. Even earth scientists are drawn by fullerenes found in very old age carbon-rich mineral deposits, so-called shungites [16]. The inspiration of potential applications in this various scientific areas leads to an astonishing growing rate in the nanotube research field.

1.2 Structures of Carbon Materials

All information in this chapter was taken from the three following books [6,17,18]. Carbon is the sixth element of the periodic table and has a $1s^2 2s^2 2p^2$ electronic ground state configuration. The energetics of the valence electrons in the crystalline phase is unique in Nature since the energy difference between the upper 2p energy level and the lower 2s level is small compared with the binding energy of the chemical bond. Mixing of these electronic wave functions is facilitated and three hybridization states are possible: sp , sp^2 and sp^3 [Figure 3].

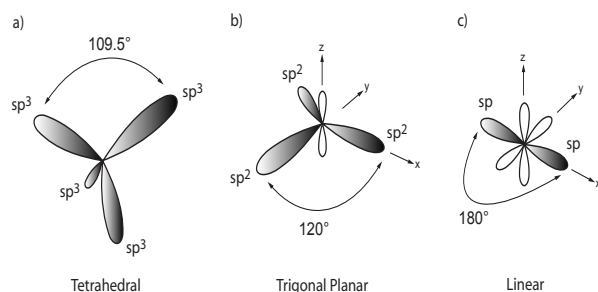


Fig. 3: The 3 different hybridisation states of carbon a) sp^3 , b) sp^2 , c) sp^1 [6]

In the sp^3 hybridisation the 2s orbital hybridises with all three 2p orbitals and form four equivalent sp^3

orbitals arranged tetrahedrally around the nucleus. A simple example for a sp^3 hybridization provide the carbon atoms in ethane (C_2H_6).

If the 2s orbitals hybridise with two of the 2p orbitals three sp^2 orbitals are formed and one unhybridised 2p orbital is left. The sp^2 orbitals are in a plane oriented at 120° to each other and can form σ bonds by overlapping with sp^2 orbitals of neighbouring atoms as seen in C_2H_4 (ethylene). The remaining p orbitals on both C atoms perpendicular oriented to the plane form a π bond by overlapping with the corresponding orbitals of the neighbouring C atoms ($C=C$).

In the sp^1 hybridisation a linear combination of the 2s orbital with one of the 2p orbital is formed. Two sp^1 hybridised carbon atoms are bonded by overlapping their sp^1 orbitals (σ bond). The remaining two p orbitals of each carbon atom form a π bond. This hybridisation can be seen in acetylene (C_2H_2) and is represented by $C\equiv C$ [Table 1].

dimension	0-D	1-D	2-D	3-D
isomer	C_{60} fullerene	nanotube carbyne	graphite fiber	diamond amorphous
hybridization	sp^2	sp^2 (sp)	sp^2	sp^3
density [g/cm ³]	1.72	1.2 - 2.0 2.68 - 3.13	2.26 ~2	3.515 2 - 3
bond length [Å]	1.40 (C=C) 1.46 (C-C)	1.44 (C=C)	1.42 (C=C) 1.44 (C-C)	1.54 (C=C)
electric properties	semiconductor $E_g = 1.9$ eV	metal or semiconductor	semimetal	insulating $E_g = 5.47$ eV

Tab. 1: Compilation of different isomers made of carbon [17].

1.2.1 Graphite

Graphite is the solid form of carbon stable at room temperature and its structure is made of layers in which each carbon atom is bound to three others. The stacking sequence of this open honeycomb network with an in-plane nearest-neighbour distance a_{C-C} of 1.421 Å, an in-plane lattice constant a_0 of 2.456 Å and a c-axis lattice constant c_0 of 6.708 Å is generally ABAB with a resulting interlayer spacing of 3.34 Å (= hexagonal Bernal graphite [Figure 4]).

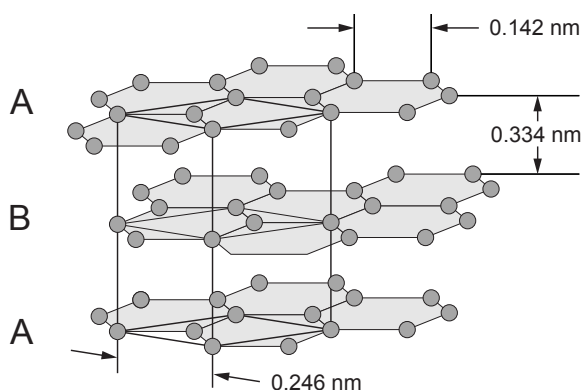


Fig. 4: The structure of hexagonal (Bernal) graphite (ABAB stacking) with the unit cell [18].

The atoms are arranged in layers and are bonded with sp^2 σ bonds and a delocalised π bond [Table 1]. The unit cell contains 4 atoms and the space group is $P6_3/mmc$. In poorly crystallized graphites, the inter-planar spacing is significantly larger (3.44 Å) and the graphene layers are randomly rotated with respect to each other about the c -axis. Such graphites are termed turbostratic and are zero-gap semi-conductor. The Bernal AB stacking of graphite is more stable than the ABC stacking.

1.2.2 Diamond

The high pressure phase of carbon is diamond. Each carbon atom is coordinated tetrahedrally by four others and the resulting structure is cubic. This structure is a consequence of the sp^3 hybridization of the bonding orbitals [Table 1]. The c -axis lattice constant a_0 is 3.567 Å and a nearest-neighbour distance a_{c-c} of 1.544 Å (10% larger than that of graphite). The diamond crystal can be viewed as two interpenetrating fcc structures (zinc blend type) displaced by $(\frac{1}{4}, \frac{1}{4}, \frac{1}{4}) a_0$ along the body diagonal, with cubic space group $Fd3m$ [Figure 5].

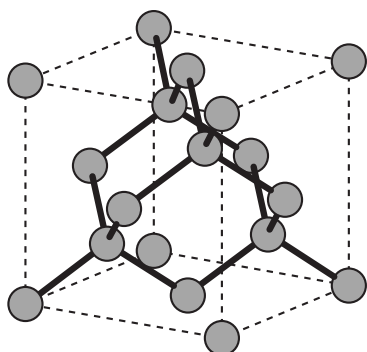


Fig. 5: Diamond in the cubic form [18].

Diamond is the hardest material known (Mohs hardness 10) and is a wide-gap semi-conductor. Not surprising the density is considerably higher than the density of graphite (56% higher than in graphite). Diamond has a very high thermal conductivity ($\sim 25 \text{ Wcm}^{-1}\text{K}^{-1}$) and the melting point is around 4500 K. At room pressure, diamond is less stable than graphite and is converted to graphite at a temperature of 1700°C. The Lonsdaleite, a metastable high pressure phase of carbon has wurtzite structure.

1.2.3 Fullerenes

Fullerene, in honor of the chemist Richard Buckminster Fuller, is a closed cage carbon molecule containing only hexagonal and pentagonal rings. While the number of pentagons has to be exactly 12, the number of hexagons is arbitrary. Such bodies fulfill the Euler's theorem for polyhedra.

$$f + v = e + 2 \quad f: \text{faces, } v: \text{vertices, } e: \text{edges}$$

The most frequent fullerene is the C_{60} molecule with an (ir)regular truncated icosahedral structure that has 90 edges of equal length, 60 equivalent vertices, 20 hexagonal faces and 12 additional pentagonal faces. Each of the carbon atoms in C_{60} is joined to three neighbours through sp^2 bonds, although there must be a small amount of sp^3 character due to the curvature. Fullerenes exhibit therefore a hybridization configuration of $sp^{2+\eta}$ ($0 > \eta > 1$) that is expected to have a higher excitation energy than that of the symmetric sp^2 hybridization [Table 1]. The lengths for the single bonds in pentagons ($= a_5$ see figure 6) are 1.46 Å but the lengths for double bonds in hexagons ($= a_6$ see figure 6) only 1.40 Å. The bond lengths in C_{60} are not exactly equal ($a_5 - a_6 \approx 0.06$ Å) and the shape is therefore, strictly speaking, not a regular truncated icosahedron [Figure 6].

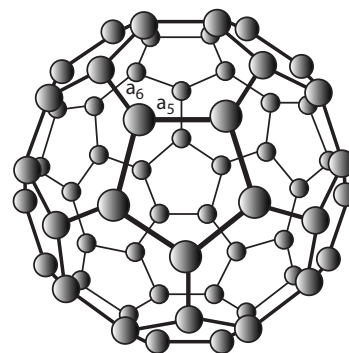


Fig. 6: C_{60} Buckminsterfullerene with single bonds in pentagons (a_5) and double bonds in hexagons (a_6) [18].

Two pentagons in fullerene molecules are usually not adjacent to each other (= isolated pentagon rule), since this would lead to higher local curvature on the fullerene, and hence more strain. C_{60} is the smallest fullerene satisfying the isolated pentagon rule and it is expected that it has filled molecular levels since the bonding requirements of all the valence electrons are satisfied. C_{60} contain the highest degree of symmetry of any known molecule (I_h , 120 symmetry operations), and the high binding energy accounts for the stability. The outer diameter of these molecules can be estimated as 10.34 Å. The next largest fullerenes to satisfy the isolated pentagon rule are C_{70} , C_{76} , C_{78} , C_{80} , ... Carbon clusters as large as C_{240} and C_{330} and clusters in the range of C_{600} – C_{700} have been observed in mass spectra but have not yet been proved to be fullerenes. It is possible that these high-mass molecules C_n ($n > 200$) maybe single-walled or even multi-walled fullerene anions.

1.2.4 Carbon Nanotubes

Carbon nanotubes are the most interesting and enthralling isomer of carbon. The hybridization configuration sp^2 is not only able to form a planar structure as occurring in graphite. The graphene

sheet can also be wrapped up into a closed polyhedra (0-dimensional) e.g. as in fullerenes or rolled up into cylinders (1-dimensional) as in carbon nanotubes [Table 1]. Single-wall nanotubes consisting of a single, enrolled graphene sheet have a diameter between 0.7 and 10.0 nm and are either infinite in length or with caps at each end. The atomic arrangement of the caps is the same as the one found in fullerenes. The unique nature of a single-walled nanotube is that it behaves as a macro-molecule and as a crystal at the same time. To illustrate their structure we simply cut a C_{60} (20 hexagonal faces and 12 pentagonal faces) molecule in half and place a graphene cylinder in between. Two symmetrically different structures are possible.

A “zig-zag” nanotube [Figure 7a] will be formed when a C_{60} is divided normal to one of the three-fold axes (chiral angle $\theta = 0^\circ$, see below), and an “armchair” nanotube [Figure 7b] when bisecting C_{60} normal to one of the five-fold axes ($\theta = 30^\circ$). In practice, it is believed that most of the nanotubes do not reveal this highly symmetric form but have structures between the two end-member structures e.g. in which the hexagons are arranged helically around the tube axis ($0^\circ < \theta < 30^\circ$). These structures are chiral [Figure 7c], exhibit a mirror symmetry plane normal to the tubule axis and can be specified

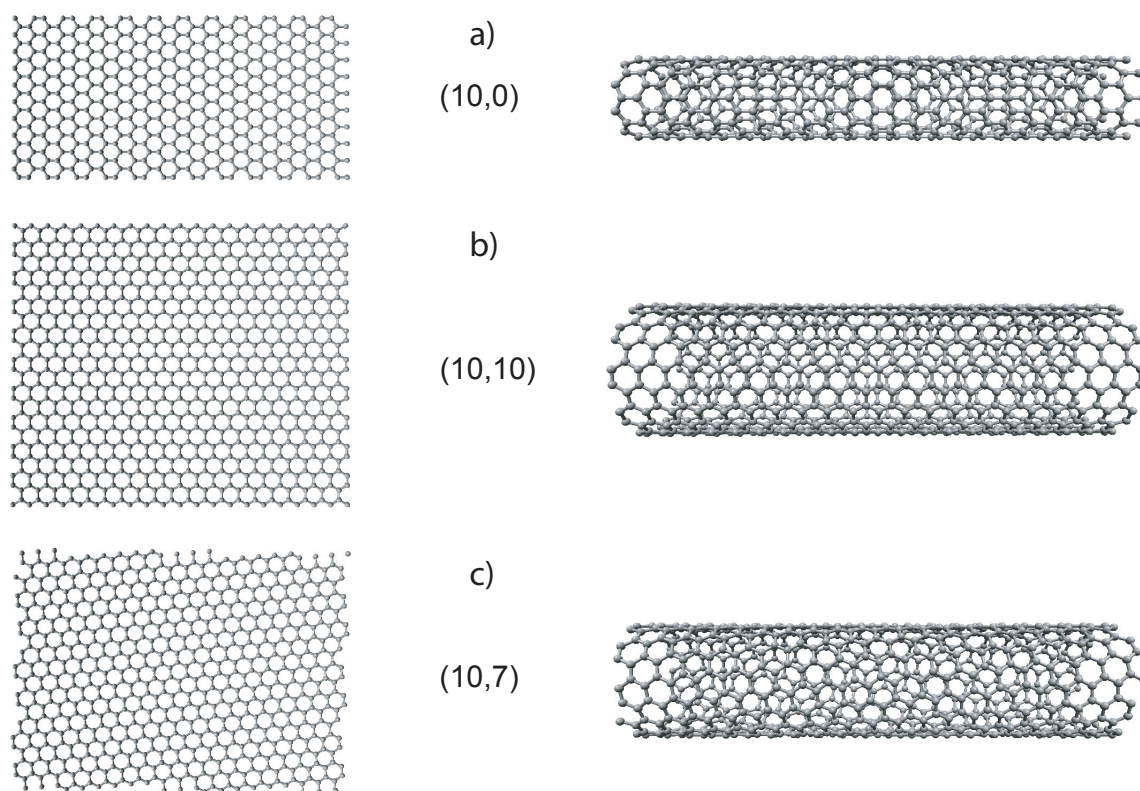


Fig. 7: Schematic theoretical model for a single-wall carbon tubule with the tubule axis normal to: a) the $\theta = 0^\circ$ direction (a “zig-zag” tubule), b) the $\theta = 30^\circ$ direction (an “armchair” tubule), and c) a general direction $0^\circ < \theta < 30^\circ$ (a “chiral” tubule). Numbers in brackets: n, m . Drawn with Nanotube Modeler [19].

mathematically in terms of the chiral vector c_h .

$$c_h = na_1 + ma_2 \equiv (n, m) \quad (1)$$

The chiral vector c_h is defined on the honeycomb lattice of carbon atoms by unit vectors a_1 and a_2 and the chiral angle θ between c_h and the so-called zigzag-direction $(n,0)$ on the graphite lattice. The lattice vector $T = OB$ is the basis translation vector of the 1D tubule unit cell perpendicular to c_h . The rotation angle ψ and the translation τ constitute the basic symmetry operation $R = (\psi/\tau)$ for the carbon nanotubes. To form a (n,m) – nanotube we simply have to superimpose the two ends OA along the vector c_h . Possible vectors specified by the pairs of integers (n,m) for general carbon nanotubes are leading to zigzag $(n,0)$, armchair (n,n) or chiral (n,m) tubules. The unit cell of a nanotube is defined by the rectangle $OAB'B$ [Figure 8].

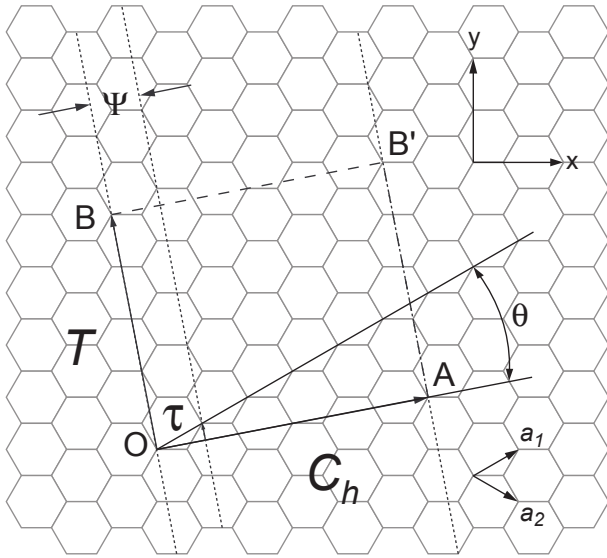


Fig. 8: Definition of a unit cell of a carbon nanotube [6].

In terms of the integers n , m the tubule diameter d_t is given by

$$d_t = \frac{C_h}{\pi} = \frac{\sqrt{3}a_{c-c} * \sqrt{(m^2 + mn + n^2)}}{\pi} \quad (2)$$

where a_{c-c} is the nearest-neighbour carbon-carbon distance (1.44 Å in carbon nanotubes), C_h is the length of the chiral vector c_h , and the chiral angle θ is given by

$$\theta = \sin^{-1} \frac{\sqrt{3}m}{2\sqrt{(n^2 + m^2 + mn)}}. \quad (3)$$

Table 2 shows the most important parameters and formulas for the mathematical description of nanotubes. The thinnest possible single-wall nanotube $(5,0)$ which can be capped by half a C_{60} fullerene, has a tubule diameter d_t of 6.88 Å. This value is consistent with experimental observations. The smallest observed carbon nanotubes had a diameter of 4 Å (corresponds to a C_{20} dodecahedron) [20] but they were either non-capped or had non-fullerene (polyhedral cap or a symmetrical flat cap). SWNT occur often in bundles which are hold together by weak Van der Waals forces.

Many of the experimentally observed carbon tubules are multilayered (MWNT), consisting of capped coaxially stacked cylinders separated by ~ 3.5 Å. Each of the cylinders can be specified by the chiral vector c_h with the indices (n,m) or equivalently by the combination of the tubule diameter d_t and the chiral angle θ [Figure 9].

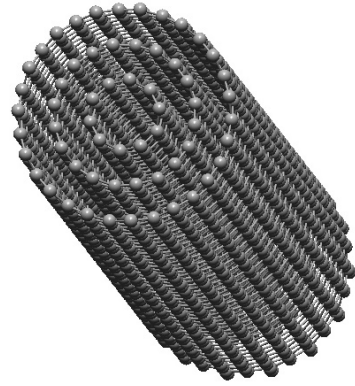


Fig. 9: A multi-walled carbon nanotubes with in total 3 graphene layers $(5,0)$ drawn with Nanotube Modeler [19].

Because of the different numbers of carbon atoms around the various concentric tubules, it is not possible to achieve an AB or an ABC interlayer stacking of graphite in carbon nanotubes. MWNT's are therefore considered to be turbostratic with a minimum interlayer separation distance between 3.39 Å to 3.90 Å (smaller diameter tubes have the largest spacings) which is in the range of interlayer spacing found in turbostratic graphite (3.44 Å). Multi-walled nanotubes can exhibit very complicated internal structure, sometimes involving the formation of closed compartments or one or more layers traversing the central core.

Symbol	Name	Formula	Value
a_{C-C}	carbon-carbon distance		1.421 Å (graphite)
a	length of unit vector	$\sqrt{3}a_{C-C}$	2.46 Å
$\mathbf{a}_1, \mathbf{a}_2$	unit vectors	$\left(\frac{\sqrt{3}}{2}, \frac{1}{2}\right)a, \left(\frac{\sqrt{3}}{2}, -\frac{1}{2}\right)a$	in (x,y) coordinates
$\mathbf{b}_1, \mathbf{b}_2$	reciprocal lattice vectors	$\left(\frac{1}{\sqrt{3}}, 1\right)\frac{2\pi}{a}, \left(\frac{1}{\sqrt{3}}, -1\right)\frac{2\pi}{a}$	in (x,y) coordinates
\mathbf{C}_h	chiral vector	$\mathbf{C}_h = n\mathbf{a}_1 + m\mathbf{a}_2 \equiv (n,m)$	n, m : integers
θ	chiral angle	$\sin \theta = \frac{\sqrt{3}m}{2\sqrt{n^2 + m^2 + nm}}$ $\cos \theta = \frac{2n + m}{2\sqrt{n^2 + m^2 + nm}}$ $\tan \theta = \frac{\sqrt{3}m}{2n + m}$	$0 \leq \theta \leq 30^\circ$
L	circumference of nanotube	$L = \mathbf{C}_h = a\sqrt{n^2 + m^2 + nm}$	$0 \leq m \leq n$
d_t	diameter of nanotube	$d_t = \frac{L}{\pi} = \frac{\sqrt{n^2 + m^2 + nm}}{\pi} a$	
d	the highest common divisor of (n,m)		
d_R	The highest common divisor of (2n+m, 2m+n)	$d_R = \begin{cases} d & \text{if } n - m \text{ not a multiple of } 3d \\ 3d & \text{if } n - m \text{ a multiple of } 3d \end{cases}$	
\mathbf{T}	translation vector of 1D unit cell	$\mathbf{T} = t_1\mathbf{a}_1 + t_2\mathbf{a}_2$ $t_1 = \frac{2m + n}{d_R}$ $t_2 = -\frac{2n + m}{d_R}$	t_1, t_2 : integers
T	length of \mathbf{T}	$T = \frac{\sqrt{3}L}{d_R}$	
N	number per hexagons per 1D unit cell	$N = \frac{2(n^2 + m^2 + nm)}{d_R}$	$2N \equiv \frac{n_c}{\text{unit cell}}$
\mathbf{R}	symmetry vector ⁺⁺	$\mathbf{R} = p\mathbf{a}_1 + q\mathbf{a}_2 \equiv (p,q)$ $D = mp - nq, 0 \leq p \leq \frac{n}{d}, 0 \leq q \leq \frac{m}{d}$	p, q : integers [*]
M	number of 2π revolutions	$M = \frac{[(2n + m)p + (2m + n)q]}{d_R}$	M : integers
\mathbf{R}	basic symmetry operation ⁺⁺	$\mathbf{NR} = M\mathbf{C}_h + d\mathbf{T}$	
τ	translation operation	$\tau = \frac{d\mathbf{T}}{N}$	τ : length
ψ	rotation operation	$\psi = \tau * \mathbf{R}$	ψ : radians

* : (p,q) are uniquely determined by $d = mp - nq$, subject to conditions stated in table, except for zigzag tubes which $\mathbf{C}_h = (n,0)$, and we define $p = 1, q = -1$, which gives $M = 1$.

++: \mathbf{R} and R refer to the same symmetry operation.

Tab. 2: Different parameters of carbon nanotubes [17].

1.2.5 Carbon Fibres

The first application of graphitic carbon fibres was over a century ago when Thomas Edison produced carbon fibres by pyrolysis of fibrous organic materials. There are two different methods to produce carbon fibres. They can be synthesized by stabilizing polyacrylonitrile polymer (PAN) or coal-tar pitch precursors at 350°C followed by a heat treatment at 1000°C to carbonise the filaments while removing impurities (H, N, O). To improve the mechanical properties a second heat treatment consisting of an increase of temperature from 1300°C to 3000°C is necessary. In the 2nd process, graphite fibres are synthesized by decomposing hydrocarbons at temperature between 700°C and 2500°C in a hydrogen atmosphere. These vapour grown carbon fibres (= VGCF) reveal a structure closely related to carbon nanotube structure [21].

1.2.6 Carbon Whiskers

Carbon whiskers are single carbon sheet rolled in a scroll-like structure [Figure 10]. They are formed in a DC (direct current) carbon arc under a high pressure of inert gas and have been discovered by Bacon [2]. The structure is much more regular than in the pyrolytically produced carbon fibres. Graphite whiskers typically have diameters in the order of 5 μm, and can be up to 3 cm in length. They reveal exceptional mechanical properties namely tensile strengths up to 20 GPa and a Young's modulus of approximately 800 GPa.

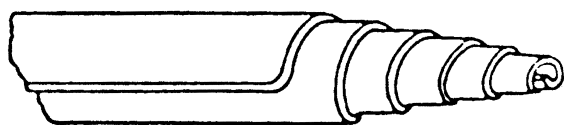


Fig. 10: Sketch of a scroll-like structure of graphite whiskers [17].

1.2.7 Glassy Carbon

By controlled degradation of certain polymers at temperatures in the range of 900 – 1000°C another common carbon material, glassy carbon (GC), is formed. GC consists of tangled, poorly ordered ribbon microstructures. Within the ribbons, the

carbon atoms are ordered like in graphite layers.

1.2.8 Liquid Carbon

At atmospheric pressure carbon liquefies at 4450 K [22] which is the highest melting point of any elemental solid. Since the vaporization temperature for carbon ($T_v = 4700$ K) is only slightly higher than the melting point the vapour pressure in equilibrium with liquid carbon is very high. This is, together with the large carbon-carbon bonding energy, favourable to form carbon clusters like C_{60} rather than independent atoms when emitted from a molten carbon surface.

There are several more forms and structures of carbon such as carbon blacks, carbynes, carbolites and amorphous carbon which are not further described in this paragraph.

1.3 Synthesis of Carbon Nanotubes

In contrast to fullerenes, such as C_{60} , which have been found in interstellar dust, carbon nanotubes have not been found in natural state neither in space nor on earth. All nanotubes have been produced synthetically. There are two principal manufacturing routes for carbon nanotubes. The synthesis is either based on the sublimation of elemental carbon precursor within an inert atmosphere, such as the electric arc-discharge process and the laser ablation method, or on chemical transformation of carbon containing precursor such as the catalytic decomposition of hydrocarbons, the production by electrolysis, the heat treatment of polymer, or the low temperature solid pyrolysis.

1.3.1 Arc-Discharge Technique

The first carbon nanotubes observed by Iijima were produced by the Krätschmer-Huffman [9] electric arc-discharge technique [Figure 11]. A potential of 20 – 30 V is applied between two graphite rods placed in a helium or argon flushed reaction chamber. The electrodes are then moved against each other until arcing occurs at a distance of approximately 1 mm or less. The resulting plasma has a temperature around 3700°C. The whole system needs to be water-cooled and kept at a constant pressure of helium. Two synthesis types are distinguished:

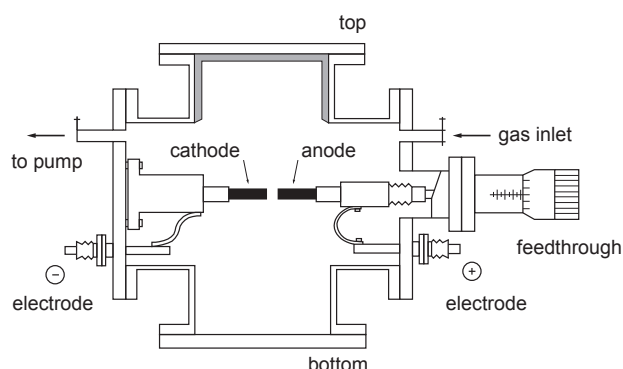


Fig. 11: Schematic illustration of an arc-evaporation apparatus for the production of fullerenes and nanotubes [18].

When only pure graphite is used as electrode material, carbon nanoparticles and multi-walled nanotubes are formed (2 – 25 nm in diameter, 1 μm in length) on the cathode surface. The soot on the reactor walls contains fullerenes, amorphous carbon and graphitic structures, but no MWNT's. When a metal is co-evaporated with the graphite the products at the cathodes consist of MWNT's, empty or filled graphitic nanoparticles and a high density of SWNT's. The soot can reveal SWNT's and MWNT's or no nanotubes at all depending on the metal catalyst used.

1.3.2 Laser Ablation Technique

The first fullerenes were synthesized with the laser ablation technique developed by Kroto and Smalley [23]. The same approach can be used to produce CNT's within an inert atmosphere (helium or argon). Carbon from a solid disk of graphite is vaporized by laser irradiation. The graphite target is placed in the middle of an evacuated long quartz tube and first heated to 1200°C. The tube is then filled with a flowing inert gas and a laser beam, focused on the graphite target, is scanned across the surface and maintains an uniform vaporization rate. The ejected carbon fragments are swept by the flowing gas from the high-temperature zone downstream and deposited on a water-cooled copper collector at the end of the apparatus and at the walls of the quartz tube [Figure 12]. The deposited material consist of MWNT's (4 – 24 graphitic layers, and length of 300 nm) when using pure graphite, and perfectly closed SWNT's arranged in ropes (5 – 20 nm in diameter and several hundreds of μm in length) when small amount of transition metal has been added to the

carbon target. To improve the method a second laser pulse is used to provide more uniform vaporization and to minimize the amount of carbon deposited as soot.

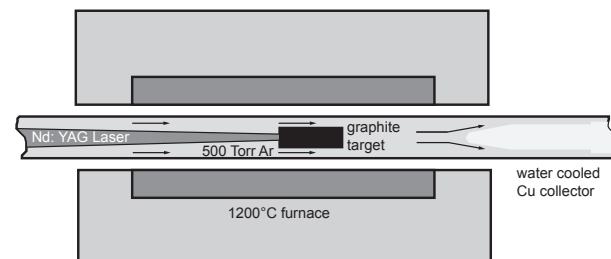


Fig. 12: Schematic illustration of a laser ablation apparatus [18].

1.3.3 Electrolysis Method

The production of carbon nanotubes via electrolysis is obtained by passing an electric current in a molten ionic salt between graphite electrodes [24]. A carbon cathode rod is immersed in a carbon crucible (anode) made by a high-purity graphite cylinder which is filled with lithium chloride. The crucible is heated to 604°C (melting point of LiCl) in air or an inert atmosphere of argon while a current between 1 and 30 A is maintained through the melt for several minutes. While the surface of the cathode is eroded, its residues are dispersed throughout the melt. After cooling, the residues are washed out from the lithium chloride with a toluene (C_7H_8) solution [Figure 13]. The products obtained by electrolysis are encapsulated particles, onion-like structures and MWNT's with diameters in the range of 2 – 20 nm and length of up to 5 μm .

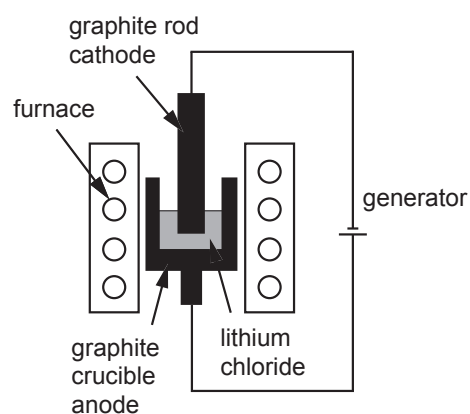


Fig. 13: Schematic representation of an electrolysis experimental system [25].

1.3.4 Synthesis from Bulk Polymer

Carbon nanotubes can also be synthesized by chemical route using polymers that mainly consist of carbon [26]. By simple thermal treatment, elements other than carbon are removed. The carbon residue contains MWNT's (5 – 20 nm in diameter, 1 μm in length), small carbon graphitic particles and amorphous sheet-like carbons.

1.3.5 Low-Temperature Solid Pyrolysis

In a graphite resistance furnace at relatively low temperature (1200°C – 1900°C) carbon nanotubes can be synthesized by conventional pyrolysis of refractory metastable carbon-containing compounds for example nanosize silicon carbonitride powder [27]. Capped MWNT's (10 – 25 nm in diameter, 0.1 – 1.0 μm in length) are formed *in-situ* on the surface of the raw material.

1.3.6 Chemical Vapour Deposition (CVD) Methods

When carbon-containing gases such as acetylene (C_2H_2), methane (CH_4), benzene (C_6H_6) or carbon monoxide are decomposed over metal surfaces (Fe, Ni, Co,...) at temperatures between 500°C and 1100°C the liberated carbon atoms may form carbon nanotubes. The CVD method has been used for the manufacturing of carbon fibres for a long time. The first evidence that this technique could be also used to synthesize carbon nanotubes has been given by Yacamàn et al. [28].

The CVD process has several advantages over other synthesis methods. CNT's can grow at a relatively low temperature and their size [29], growth rate, diameter, length and crystallinity can be manipulated by changing the type and morphology of the catalysts [30]. The CVD method allows also the growth of well aligned nanotubes [31], the fabrication of high quality single-wall [32] and multi-wall carbon nanotubes with specific properties [33]. CVD synthesis may result in individual, well dispersed nanotubes [31,33,34] grown directly onto substrates or in bulk masses [35]. A major advantage of CVD is that the nanotubes can be used directly without further purification unless removal of the catalyst particle is necessary. A major pitfall of this method is, however, the high defect densities in the nanotube structure, which is probably due to relatively low

growth temperature that does not provide sufficient thermal energy to anneal the defects. Growing perfect MWNT's by CVD remains a challenge to this day. Several modifications of the CVD method exist and are discussed more in detail below.

1.3.6.1 Horizontal Furnace

Horizontal furnaces are the most popular vessels for the CVD production of carbon nanofibres and nanotubes [36,37]. The reactant gases are directed over the substrate/catalysts placed in a removable ceramic holder in the middle of an electrically heated quartz tube. The reaction chamber is first flushed with a carrier gas (argon, hydrogen or nitrogen) and subsequently heated up to the growth temperature before the carbon containing gaseous feedstock is introduced. The synthesis is usually conducted at temperatures below 1000°C to reduce the formation of undesirable amorphous carbon depositions. In general, there is a compromise between carbon nanotubes yield and the quality of the tubes. A high flow rate reduces the formation of amorphous carbon [Figure 14].

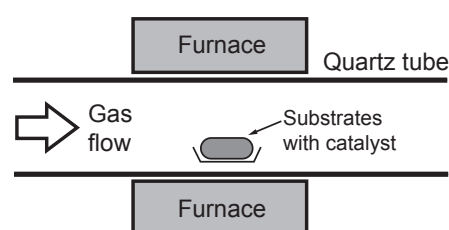


Fig. 14: Illustration of a horizontal CVD furnace used to grow carbon nanotubes [38].

Four structural forms of carbon are found within the CVD products: amorphous carbon layers on the surface or graphite layers covering the metal particles, filaments of amorphous carbon and straight, curved or helical MWNT's. The latter have often an amorphous carbon coating and catalytic particles at their tip. The vessel used during the present work is slightly different from an original CVD furnace. The heat is generated by a point source. Due to the size of the chamber large thermal gradients occur. These disadvantages, however, are compensated by the possibility to do *in-situ* X-ray diffraction investigations.

1.3.6.2 Vertical Furnace

This configuration is usually employed for the continuous production of carbon fibres, nanofibres and nanotubes [39]. The carbon source is injected together with the catalyst at the top of a vertical arranged tube furnace. Resulting filaments are growing during the flight through the heating zone and are collected at the bottom of the chamber [Figure 15].

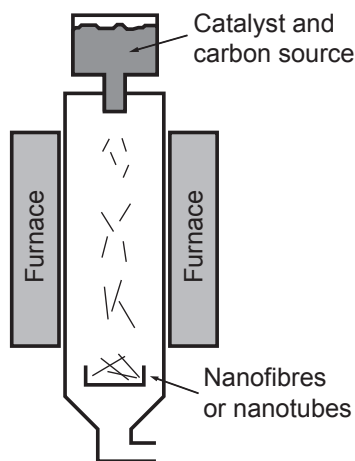


Fig. 15: Illustration of a vertical CVD furnace used to grow carbon nanotubes [38].

The ultrafine metal catalyst particles are either introduced into the reactor directly or formed *in-situ* using adapted precursors such as metallocenes. Compared to the horizontal furnace the residence time is relatively short. The high purity and the high yield of the products made this method nevertheless suitable for the production of nanotubes in quantities of tons a year used in electrodes of lithium-ion batteries [40] and as fillers in conductive polymers [41].

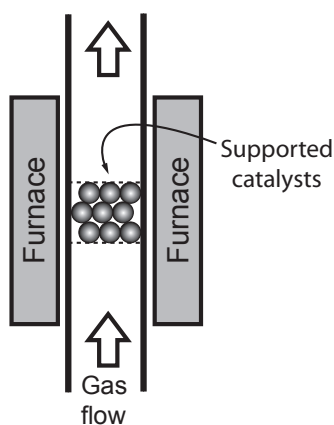


Fig. 16: Illustration of a fluidized-bed CVD reactor [38].

A fluidized bed reactor is a variation of the vertical furnace and is targeted at the synthesis of nanotubes on a large-scale [42]. Therefore the solid particles are fluidized through suspension in an upward flow of carbon feedstock gases. The supported catalyst particles are placed on a quartz filter in the centre of the furnace and due to the fluidization process are remaining much longer in the furnace [Figure 16]. Up to tens of kilograms of multi-wall carbon nanotubes a day have been produced [43].

1.3.6.3 Plasma Enhanced Chemical Vapour Deposition (PECVD)

This relatively new technique adds a completely new aspect to the traditional horizontal and vertical furnace techniques. The flat substrate which is prior coated with a metal catalyst is placed inside a plasma generated using DC- (direct current), RF- (radio frequency) or MW-plasma (micro wave) excitation [38]. The ionized gas mixture consists of methane (CH_4) and hydrogen (H_2) with a ratio of 1% CH_4 to 99% H_2 , at pressures between 1 and 40 mbar at temperatures around 900°C [44].

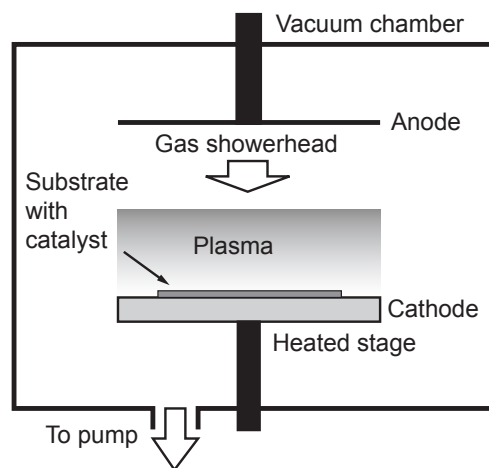


Fig. 17: Illustration of a plasma-enhanced CVD reactor [38].

Plasma deposition conditions are very stable which leads to highly controllable and reproducible nanotube growth. Ren et al. [31] reported the growth of single, freestanding vertical nanotubes and Merkulow et al. [45] developed a simple DC-PECVD system to grow vertically aligned carbon nanofibres. One of the most significant results recently was the demonstration of room temperature growth of nanofibres using RF-PECVD [38].

1.4 Physical Properties of Carbon Nanotubes

Since the carbon nanotubes diameter frequently fall into the size range less than 10 nm, quantum effects become important. This led, combined with their unusual symmetries, structure and morphology, theoreticians to predict some exceptional electronic, magnetic, vibrational and mechanical properties.

The large surface area ($\sim 10 - 20 \text{ m}^2/\text{g}$) anticipates some useful mechanical and chemical applications. The strength of the carbon bonds makes nanotubes one of the strongest and stiffest materials. Its axial elastic modulus is predicted to be at least 1000 GPa (measured by their thermal vibrational amplitudes) and is increasing with tube diameter. Nanotubes can sustain extreme strains (40%) in tension without showing bond rupture nor signs of brittle behaviour or plastic deformation and are therefore considered to be highly elastic.

One of the most remarkable characters of carbon nanotubes is to be, depending on their diameter and precise structure, a metal or a semi-conductor [13]. The electronic properties of graphite are highly anisotropic: within the graphene layers electron mobility is high, but perpendicular to the planes relatively low depending on the degree of crystalline order. For carbon nanotubes the same effect is observed, while all armchair SWNT (n,n) are expected to be metallic, only one-third of zig-zag tubes ($n,0$) and chiral nanotubes (n,m) should be metallic, with the remainder being semi-conducting. It is believed that the transport behaviour of nanotubes is essentially that of a quantum wire, so that conduction occurs through well-separated, discrete electron states and, therefore, the transport along the tubes may be ballistic in nature. Electrons move therefore with negligible resistance and could be used for the construction of ultrafast devices, such as a nanoscale heterojunction between a metallic and a semi-conducting tube. In fact, the conductive path and the resulting resistivity inside the tube is very complex depending on temperature, diameter, presence of defects and its structure.

Due to the presence of ring currents graphite reveal a relatively large negative magnetic susceptibility which is highly anisotropic. In the case of nanotubes the diamagnetic susceptibility is even larger and increases with decreasing temperature. It was found to be much greater for tubes aligned parallel than tubes aligned perpendicular to the field.

The non-linear optical properties of carbon nanotubes depend on the diameter and symmetry of the tubes. Nanotube films with tubes oriented perpendicular

to the film plane (nanotube lawn) were found to be optically isotropic, while for films with tubes lying in the film plane the optical properties depend strongly on whether the light is polarised parallel or perpendicular to the tubes. Vibrational properties of nanotubes are depending on the symmetry of the tubes, hence they maybe either IR active or Raman active. The number of IR and Raman active modes is independent of the nanotube diameter and provides a method of determining the chirality of nanotubes.

1.5 Applications of Carbon Nanotubes and Future Directions

A lot of suggestions for potential applications were triggered by theoretical considerations and preliminary investigations, but most of them have not yet been turned into commercial products. The most remarkable innovations are exploiting the electronic properties of nanotubes such as the development of flat panel displays using aligned carbon nanotube films as the electron emission source [46]. Individual opened tubes are also used as probes in scanning tunnelling (STM) or atomic force microscopy (AFM) [47]. The electronic properties of nanotubes make them potential candidates for quantum wires [48]. The heterojunction device built by Tans et al. uses single semi-conducting SWNT as single-molecule field-effect transistor [49]. Gas discharge tube (GDT) devices containing carbon nanotubes coated electrodes provide protection to telecom network from lightning and ac power cross faults [50]. The second major application field exploit the strength and elasticity of carbon nanotubes. Beside the intrinsic mechanical strength, CNT's are ideal in reinforced polymer fibre composite materials since the interface between the fibre and the matrix is strong ($\sim 200 - 300 \text{ MPa}$) [51].

The possibility to fill MWNT's and SWNT's by capillarity with molten salt [52] (Ag, Au, Pt) and metals [14] (Pb, Mo, V) opened the horizon for some promising applications such as nanowires and nanocontainers. Biological molecules were introduced into opened nanotubes and it is conceivable that tubes filled or coated with iodine or gadolinium might be used as biosensors and contrast medias in therapeutic radiology and imaging. The potential to fill SWNT's with gases [53] (hydrogen, argon) and the ability to control their release storage make them useful candidates as hydrogen-storage materials, used in fuel cells or batteries, or as containers for gaseous nuclear waste. Doping of SWNT bundles

with K, Rb, I or Br is leading to super-conducting transitions as it was observed by doped graphite and C_{60} [54].

Nanotechnology is still in its infancy. Although several applications exist, most of them are still distant from industrial application. Limiting factors are primarily the unsatisfactory ability to manipulate structures at the atomic scale, and the lack of manufacturing techniques that can produce nanotubes of reasonable purity and quality in kilogram quantities for an affordable price. So far, rather “low-tec” – applications such as the use of nanotubes as filler in composites have been developed beyond pilot status to commercial products.

1.6 Catalysis in the CVD Production of Carbon Nanotubes

It has been known for over a century that filamentous carbon can be formed by the catalytic decomposition of a carbon-containing gas over metal surfaces at elevated temperatures. In the metal industry carbon deposits are a nuisance and the prevention of carbon accumulation is a high priority objective in many processes involving hydrocarbon conversion reactions [36]. The presence of such carbon deposits creates problems including blockage of reactors, reduction of heat transfer properties, and catalyst deactivation due to encapsulation of the metallic component [55]. Before 1990, research on carbon deposition was motivated by the need to avoid filamentous carbon growth. By using controlled atmosphere electron microscopy and based on the observation that the activation energy for filamentous growth and the activation energy for bulk carbon diffusion in nickel was about the same, a basic growth model was deduced, which resembled already to the current models proposed for CNT nucleation and growth [56]. The first stage consists of absorption and decomposition of the hydrocarbon on the “front” surface of the metal particle to hydrogen and carbon. The carbon dissolves into the particle from the leading face to form a metal-carbon solid solution. When supersaturation of carbon in metal particles is reached carbon precipitation at the rear of the particle occur and crystalline nanofibres are formed [Figure 18]. Precipitation on the contact between metal and support is possible, because this area is not in direct contact with the atmosphere and the carbon activity is, therefore, lower on the leading edge. The pictures presented by Baker and

Harris show a lighter contrast along the centre of the filaments, suggesting that they were actually nanotubes.

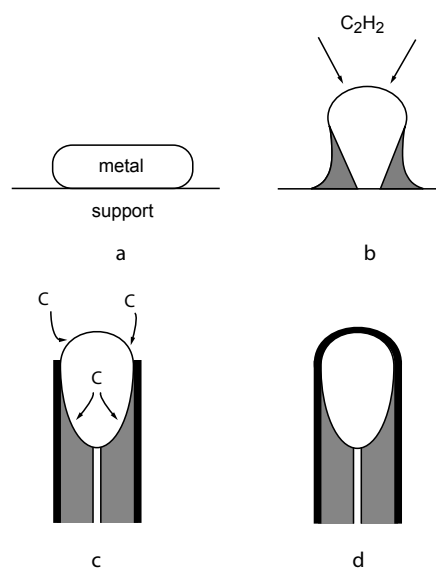


Fig. 18: Model proposed by Baker and Harris for the catalytic growth of carbon filaments [56].

In their model they postulated diffusion of carbon through the catalyst particle as rate-determining step in the formation of carbon nanostructures. Baker [57] suggested a temperature gradient in the particle provoked by the exothermic decomposition of the carbon-containing gas at the front face and the endothermic precipitation of solid carbon at the rear phase. Over years the state of the catalyst in carbon deposition has been discussed, especially the formation of carbides during reaction process and if present its catalytic activity. Oberlin and co-workers [4], by using electron diffraction analysis, identified small cementite (Fe_3C) crystals at the tip of each filamentous carbon tube and claimed in their growth model as necessary for filament formations. Cementite as the active phase was refuted by Baker since there was no growth of carbon fibres observed when high purity cementite was the starting catalyst [58] and Yang [59] demonstrated that the surface of Fe_3C was essentially inactive for benzene decomposition but in the presence of hydrogen in the gas phase metallic phase was generated and carbon nanofibre growth occurred.

Later Sacco and Alstrup [60] proposed that a metal carbide phase formed at the gas-particle interface is responsible for diffusion and the resulting carbon concentration gradient between surface and bulk [61].

The models for the formation of carbon filaments

have been sophisticated over the years. Today there are two main growth modes in use. [Figure 19] In the base-growth mode, the tubes remain closed at the tip and the carbon is added at the base e.g. at the contact of the tubes with the catalyst particle, which remain attached to the substrate. In the tip-growth model the catalyst particle is detached from the substrate. The carried-along particle is responsible for supplying the needed carbon for the tube growth [62]. The carbon is added at the back of the particle. Perturbation in the chemistry of the leading face of the particle may lead to a carbon overgrowth at the tip, cutting the direct contact between catalyst and feeding gas, which effectively prevent further hydrocarbon decomposition.

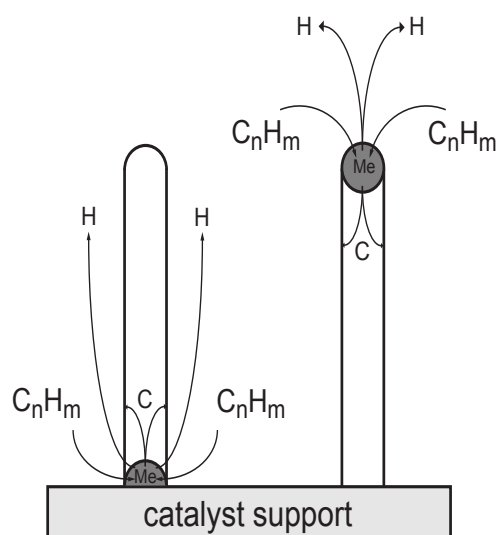


Fig. 19: The two general growth modes of nanotube in chemical vapour deposition. Left in diagram: base growth mode. Right in diagram: tip growth mode [63].

Despite tremendous progress in yields, lowering of the synthesis costs and the improved purity of the products obtained by CVD, there is still much debate about what really controls CNT's growth and what the catalytic mechanisms are. Diffusion as rate-determining step in the growth of carbon nanostructures is widely accepted, but the origin of the driving force for carbon diffusion is still obscure. X-ray diffraction observation by Sikder et al. [64] revealed an expansion of the metal unit cell upon CVD. This expansion is suggested to be taken place due to the diffusion of carbon into the metal layer while forming a metal-carbide solid solution. Further adaptation of the growth models were undertaken by Kukovitsky [65] who proposed a vapour-liquid-solid (VLS) growth mechanism. They concluded that, due to their reduced size and shape, catalyst particles

have to be in a liquid state during the growth process. The agreement between the enthalpy of filament growth and the enthalpy of carbon diffusion in the bulk metals, however, suggest that the catalyst is in the solid state [66].

The transition metals Cr, Mn, Fe, Co and Ni are suitable catalysts for CNT synthesis and hydrocarbon decomposition. But not all metal catalysts known to promote hydrocarbon cracking will lead to the formation of nanotubes [67], such as noble metals like platinum and gold. The catalytic activity of certain metals can also be influenced by the nature of the reacting gases [68]. Nickel seemed to be more active in a C_2H_2/H_2 mixtures, while iron seemed to be the preferable catalyst in CO/H_2 atmospheres [67]. Particularly the presence of hydrogen promotes carbon decomposition as well as the addition of co-catalysts such as a second metal (Cu, Sn, K) or a non-metal (S) [69]. An extensive comparison of the influences of the used carbon containing gas species, reaction temperature and support materials during CVD on the formation of carbon nanotubes are presented in table 3 [Table 3].

As for carbon filaments, the role of carbides in the synthesis of CNT's is not clear, Rodriguez and co-workers [69] investigated the interaction of copper-nickel particles with ethylene (C_2H_4) and observed carbon nanotubes but no evidence for the existence of a bulk carbide during these experiments. In contradiction to the above mentioned experiment Ni_3C particles and multi-walled carbon nanotubes were observed on an electrodeposited nickel coating on a copper substrate treated by ammonia [97]. Bladh [67] proposed an inside-out growth mechanism for MWNT's where carbon is expelled from metastable carbide particles, and Saito [98] proposed a similar scenario for SWNT's growing radially from Ni_3C particles. Although they seem to be metastable carbides present at the synthesis conditions, there is no agreement about whether they are active species for CNT's growth or not [4,97,98]. The idea of the formation of an assortment of intermediate states during interaction of hydrocarbon molecules with metal surfaces is well known from surface science studies. It is supposed that the decomposition of these intermediates leads to the formation of carbidic carbon which exhibits higher activity compared to bulk carbide thus subsequent growth of nanofibres is possible [99].

Catalyst precursor compound ^a	Carbon precursor	Additive	Reaction temperature [°C]	Support material	Description of synthesized material	References
Fe(NO ₃) ₃	CH ₄		900	Al ₂ O ₃ (powder)	SWNT and bundles, MWNT	[62]
MoO ₂ , Fe(NO ₃) ₃	CO, C ₂ H ₄		750-850	Al ₂ O ₃ (powder)	SWNT and bundles, MWNT	[32]
Fe(NO ₃) ₃ , Ni(NO ₃) ₂ , Co(NO ₃) ₂	CH ₄		1000	Al ₂ O ₃ (powder), SiO ₂ (powder)	SWNT and bundles	[70]
MoO ₂	CH ₄		850-1000	Al ₂ O ₃ (aerogel)	Bundles of SWNT	[71]
MoO ₂	CO		1200	Al ₂ O ₃ (powder)	SWNT	[37]
Co(NO ₃) ₂	CO		700	SiO ₂ (gel)	Bundles of SWNT	[72,73]
Cobalt and iron salts ^b	CH ₄	H ₂	1000	MgO (powder)	SWNT and bundles	[74]
Cobalt, nickel and iron salts ^b	C ₂ H ₄		1080	Al ₂ O ₃ (powder), SiO ₂ (powder)	SWNT and bundles	[75]
Fe(NO ₃) ₃ , Ni(NO ₃) ₂ , Mg(NO ₃) ₂ , Co(NO ₃) ₂	CH ₄	H ₂	1000-1070	MgO or Mg _{0.8} Al ₂ O ₄ (from combustion)	SWNT and MWNT individual and bundles	[76,77]
Fe(NO ₃) ₃	CH ₄		850	MgO and Si (wafer)	SWNT and bundles	[78]
Cobalt, Molybdenum ^b	CH ₄ , C ₂ H ₂		900	SiO ₂ (oxidized Si)	SWNT and MWNT	[79,80]
Fe(NO ₃) ₃ , MoO ₂	CH ₄	H ₂	900-1000	Al ₂ O ₃ (on Si wafer)	SWNT and bundles	[81,82,83]
Iron ^b	CH ₄		600-800	Sapphire	Bundles of SWNT and MWNT	[84]
Fe ₂ O ₃ , Iron and Nickel ^b	CH ₄		750-1000	SiO ₂ (oxidized Si)	Bundles of MWNT	[85]
Fe(NO ₃) ₃	C ₂ H ₂		600-650	Al ₂ O ₃ (powder)	MWNT	[86]
Iron, Molybdenum ^b	CO, CH ₄	H ₂	900	Si (wafer)	SWNT and bundles	[87]
Fe(NO ₃) ₃ , Ni(NO ₃) ₂ , Co(NO ₃) ₂	C ₂ H ₂	H ₂	750-1000	Al ₂ O ₃ (powder), SiO ₂ (powder)	SWNT and MWNT	[88]
Mg(NO ₃) ₂ + (NH ₄) ₆ *Mo ₇ O ₂₄	CH ₄	H ₂	1200	MgO (powder)	MWNT	[89]
Ni(NO ₃) ₂	C ₂ H ₂	H ₂	450-800	Al ₂ O ₃ (powder)	MWNT	[90]
Cobalt, nickel ^b	C ₂ H ₂	NH ₃	800-900	SiO ₂ (oxidized Si)	MWNT	[91]
Nickel, nickel-copper ^b	CH ₄ , CO	H ₂	450-650	SiO ₂ (oxidized Si)	MWNT	[92]
Copper, Iron, Nickel ^b	C ₂ H ₂	H ₂	750	Al ₂ O ₃ (powder), SiO ₂ (powder), TiO ₂ , CaO	MWNT, No tubes on CaO	[93]
Fe(NO ₃) ₃ , Ni(NO ₃) ₂ , Co(NO ₃) ₂	C ₂ H ₂		580-1000	SiO ₂ (powder), Si (wafer)	MWNT	[94]
Fe(NO ₃) ₃ , Ni(NO ₃) ₂ , Co(NO ₃) ₂	CH ₄	H ₂	< 520	Al ₂ O ₃ (powder)	MWNT	[95]
Cobalt/Nickel + Pd, Pt or Cr ^b	C ₂ H ₂	NH ₃ , H ₂	500-550	SiO ₂ (oxidized Si)	MWNT, carbon onions	[96]

^aWater of hydration not included in the formula

^bChemical composition not specified

Tab. 3: Compilation of results obtained by CVD using different metal nitrate phases as precursors and different gases, temperatures and support materials.

1.7 Goals and Results of the Present Work

In order to better understand the mechanisms of carbon nanotube formation during CVD synthesis a large number of investigations have been undertaken in which parameters such as temperature, catalyst composition and concentration have been systematically examined [29,30,65,71,74,79,80,90,94,100,101]. Scarce information, however, is available on the processes that occur within the catalyst during synthesis. A major problem with most investigations is that the analysis of the catalyst was done *ex-situ* and conclusions were drawn by

comparing pre- and post-synthesis results. Lepora et al. [102] analysed iron catalysts *in-situ* and showed that the catalyst underwent major chemical changes during the synthesis which are impossible to deduce from post-synthesis analyses. They showed that cementite is formed immediately after acetylene is added to the atmosphere, but that the latter decomposes after certain reaction duration. The formation of carbon nanotubes was observed during all stages of catalyst evolution e.g. during cementite formation but also during its decomposition.

This project extends the analysis made by Lepora

[102] to the evolution of other transition metal catalyst e.g. Ni, Co, Cr, Mo under a nitrogen-acetylene atmosphere between 600°C and 750°C. The evolution was followed *in-situ* with an X-ray diffractometer that was equipped with a heating stage and a gas-mixing system. The catalysts were deposited as transition metal nitrate films on glass substrates. Phase evolution during heating procedure under nitrogen, hydrogen and oxygen atmosphere and subsequent treatment with acetylene was examined. One of the goals of this investigation was to test whether or not carbides are formed and what their role was during the CVD process. The grain size distribution, a limiting factor for nanotube growth, was systematically analyzed and its evolution compared with the simultaneous chemical changes. The results of the *in-situ* investigations corroborate certain reaction steps of the proposed nanotube growth mechanism e.g. the diffusion of carbon through the catalyst particle. Quenching experiments with the same furnace configuration were obtained under various atmosphere conditions and increasing pyrolysis times in order to investigate the evolution of the catalyst and if present the nanotubes *ex-situ* by Transmission and Scanning Electron Microscopy (TEM, SEM).

The results of this *in-situ* X-ray diffraction investigations and SEM/TEM studies pinpointed that for nickel and cobalt precursors, like for iron, it is the pure metal that acts under typical NT synthesis conditions as catalyst. The nickel and the cobalt particles dissociate acetylene and serve as nanotube nucleation sites. No carbides are formed during the synthesis runs. The cell parameter of both metals measured immediately after acetylene exposure, however, are larger than the values for the pure metals. With synthesis time, these values decrease to approach the parameters of the pure metals. The increased cell parameters are due to carbon dissolved in the metal structures. Carbon diffuses, thus, into the bulk of the particles shortly after the admittance of acetylene. The decrease of the cell parameter with time indicates that carbon 1. diffuses out of the particles and 2. that carbon leaving the particles is not fully compensated for by carbon from outside. These *in-situ* observations are, thus, compatible in the initial stages with the proposed CNT nucleation and growth mechanism based on diffusion of carbon through the particles, followed by precipitation of carbon at surface in shape of a tube. The decrease in cell parameter, however, indicates also that the concentration of carbon dissolved decreases with

time, which may indicate that after a certain time the bulk catalyst is not the carbon source anymore.

Molybdenum and chromium precursors behaved differently from nickel and cobalt. Reduction to pure metals was only possible when a hydrogen pre-treatment was done before the exposure to acetylene. In the case of molybdenum, the metal reacts immediately to carbide. Nanotube nucleation was only observed during the period the Mo catalyst was present as metal, suggesting that Mo-carbide is, if at all, only a poor catalyst.

The role of particle size could be very nicely demonstrated in experiment with cobalt precursor. Oxygen fugacity during purging of the camera with nitrogen is close to the Co_3O_4 - CoO buffer, and either of the phases could be present at the start of acetylene admission. Only experiments in which the spinel phase was present at the start of acetylene exposure contained nanotubes. This is probably due to the cobalt oxides breakdown which plays an important role for the early carbon incorporation and ongoing diffusion.

1.8 References

- [1] Edison TA, US Patent 470'925 (1892).
- [2] Bacon R. Growth, structure and properties of carbon whiskers. *J Appl Phys* 1960; 31: 283-290.
- [3] Dresselhaus MS, Dresselhaus G, Sugihara K, Spain IL, and Goldberg HA. Graphite fibers and filaments. (Springer-Verlag, Berlin, 1988), Vol. 5 of Springer Series in Materials Science.
- [4] Oberlin A, Endo M, and Koyama T. Filamentous growth of carbon through benzene decomposition. *J Crystal Growth* 1975; 32: 335-349.
- [5] Kroto HW, Heath JR, O'Brian SC, Curl RF, and Smalley RE. C_{60} : Buckminsterfullerene. *Nature* 1985; 318: 162-163.
- [6] Dresselhaus MS, Dresselhaus G, Eklund PC. Science of fullerenes and carbon nanotubes. Academic Press, San Diego, California, 1996.
- [7] Smalley RE, Semiconductor cluster surface chemistry. DoD Workshop in Washington, DC (December 1990).
- [8] Dresselhaus MS, Dresselhaus G, and Eklund PC. Symmetry for lattice modes in C_{60} and alkali-metal-doped C_{60} . *Phys Rev B* 45 1992; 12: 6923-6930.

- [9] Krätschmer W, Lamb LD, Fostiropoulos K, and Huffman DR. Solid C_{60} : a new form of carbon. *Nature* 1990; 347: 354-356.
- [10] Iijima S. Helical microtubules of graphitic carbon. *Nature* 1991; 354: 56-58.
- [11] Iijima S and Ichihashi T. Single-shell carbon nanotubes of 1 nm diameter. *Nature* 1993; 363: 603.
- [12] Bethune DS, Kiang CH, de Vries MS, Gorman G, Savoy R, Vasquez J, and Beyers R. Cobalt-catalysed growth of carbon nanotubes with single-atomic-layer walls. *Nature* 1993; 363: 605.
- [13] Wildoer JWG, Venema LC, Rinzler AG, Smalley RE, Dekker C. Electronic structure of atomically resolved carbon nanotubes. *Nature* 1998; 391: 59-62.
- [14] Ajayan PM, Iijima S. Capillarity-induced filling of carbon nanotubes. *Nature* 1993; 361: 333.
- [15] Thess A, Lee R, Nikolaev P, Dai H, Petit P, Robert J, Xu C, et al. Crystalline ropes of metallic carbon nanotubes. *Science* 1996; 273: 483-487.
- [16] Buseck PR, Tspursky SJ, Hettich R. Fullerenes from the geological environment. *Science* 1992; 257: 215-217.
- [17] Saito R, Dresselhaus G, Dresselhaus MS. Physical properties of carbon nanotubes. Imperial College Press, London, 1998.
- [18] Harris PJF, Carbon nanotubes and related structures – New materials for the twenty-first century. Cambridge University Press, Cambridge, UK, 1999.
- [19] Nanotube Modeler, JCrystalSoft 2004 – 2005, <http://www.icrystal.com>.
- [20] Qin LC, Zhao X, Hirahara K, Miyamoto Y, Ando Y, Iijima S. The smallest carbon nanotube, *Nature* 2000; 408: 50.
- [21] Ebbesen TW, Carbon nanotubes. Edited by T.W. Ebbesen, CRC Press (Boca Raton, New York, London, Tokyo) 1999.
- [22] Bundy FP. Solid state physics under pressure: Recent advance with anvil devices. Edited by Minomura S, (Reidel, Dordrecht 1985).
- [23] Kroto HW, Heath JR, O'Brian SC, Curl RF, and Smalley RE. C_{60} : Buckminsterfullerene. *Nature* 1985; 318: 162-163.
- [24] Hsu WK, Terrones M, Hare JP, Terrones H, Kroto HW, Walton DRM. Electrolytic formation of carbon nanostructures. *Chem. Phys. Lett.* 1996; 262: 161.
- [25] Journet C, Bernier P. Production of carbon nanotubes. *Appl. Phys. A.* 1998; 67: 1-9.
- [26] Cho WS, Hamada E, Kondo Y, Takayanagi K, Synthesis of carbon nanotubes from bulk polymer. *Appl. Phys. Lett.* 1996; 69: 278.
- [27] Li YL, Yu YD, Liang Y. A novel method for synthesis of carbon nanotubes: Low temperature solid pyrolysis. *J. Mater. Res.* 1997; 12: 613.
- [28] Yacamàn MJ, Yoshida MM, Rendon L, Santiesteban JG. Catalytic growth of carbon microtubules with fullerene structure. *Appl. Phys. Lett.* 1993; 62: 202-204.
- [29] Huang ZP, Wang DZ, Wen JG, Sennett M, Gibson H, Ren ZF. Effect of nickel, iron and cobalt on growth of aligned carbon nanotubes. *Appl Phys A-Mater* 2002; 74 (3): 387-391.
- [30] Lee CJ, Park J, Yu JA. Catalyst effect on carbon nanotubes synthesized by thermal chemical vapour deposition. *Chem Phys Lett* 2002; 360 (3-4): 250-255.
- [31] Ren ZF, Huang ZP, Xu JW, Wang JH, Bush P, Siegal MP, et al. Synthesis of large arrays of well-aligned carbon nanotubes on glass. *Science* 1998; 282: 1105.
- [32] Hafner JH, Bronikowski MJ, Azamian BR, Nikolaev P, Rinzler AG, Colbert DT, Smith KA, Smalley RE. Catalytic growth of single-wall carbon nanotubes from metal particles. *Chem. Phys. Lett.* 1998; 296: 195-202.
- [33] Fan SS, Chapline MG, Franklin NR, Tomblor TW, Cassell AM, Dai H. Self-oriented regular arrays of carbon nanotubes and their field emission properties. *Science* 1999; 283: 512-514.
- [34] Teo KBK, Chhowalla M, Amaratunga GAJ, Milne WI, Hasko DG, Pirio G, et al. Uniform patterned growth of carbon nanotubes without surface Carbon. *Appl. Phys. Lett.* 2001; 79: 1534-1536.
- [35] Singh C, Shaffer MSP, Koziol KKK, Kinloch IA, Windle AH. Towards the production of large-scale aligned carbon nanotubes. *Chem. Phys. Lett.* 2003; 372: 860-865.
- [36] Rodriguez NM. A review of catalytically grown carbon nanofibres. *J. Mater. Res.* 1993; 8(10): 3233-3250.
- [37] Dai H, Rinzler AG, Nikolaev P, Thess A, Colbert DT, Smalley RE. Single-wall nanotubes produced by metal-catalyzed disproportionation of carbon monoxide. *Chem. Phys. Lett.* 1996; 260: 471-475.
- [38] Teo KBK, Singh C, Chhowalla M, Milne WI. Catalytic synthesis of carbon nanotubes and

- nanofibres. Encyclopedia of Nanoscience and Nanotechnology, edited by H.S. Nalwa, Volume X.
- [39] Zhu HW, Xu CL, Wu DH, Wei BQ, Vajtai R, Ajayan PM. Direct synthesis of long single-walled carbon nanotube strands. *Science* 2002; 296: 884-886.
- [40] Endo M, Kim YA, Hayashi T, Nishimura K, Matusita T, Miyashita K, Dresselhaus MS. Vapor-grown carbon fibers (VGCFs): Basic properties and their battery applications. *Carbon* 2001; 39: 1287-1297.
- [41] Baughman RH, Zakhidov AA, de Heer WA. Carbon nanotube: The route toward applications. *Science* 2002; 297: 787-792.
- [42] Mauron Ph, Emmenegger C, Sudan P, Wenger P, Rentsch S, Züttel A. Fluidised-bed CVD synthesis of carbon nanotubes on Fe₂O₃/MgO. *Diamond and Related Material* 2003; 12: 781-786.
- [43] Wang Y, Wei F, Luo G, Yu H, Gu G. The large-scale production of carbon nanotubes in a nano-agglomerated fluidized-bed reactor. *Chem. Phys. Lett.* 2002; 364: 568-572.
- [44] Kuetzel OM, Groening O, Emmenegger C, Schlapbach L. Electron field emission from phase pure nanotube films grown in a methane/hydrogen plasma. *Appl. Phys. Lett.* 1998; 73: 2113-2115.
- [45] Merkulov VI, Lowndess DH, Wei YY, Eres G, Voelkl E. Patterned growth of individual and multiple vertically aligned carbon nanofibers. *Appl. Phys. Lett.* 2000; 76: 3555-3557.
- [46] Wang QH, Setlur AA, Lauerhaas JM, Day, JH Seelig EW, Chang RPH, A nanotube-based field-emission flat panel display. *Appl. Phys. Lett.* 1998; 72: 2192.
- [47] Dai H, Hafner JH, Ginzler AG, Colbert, DT Smalley RE. Nanotubes as nanoprobe in scanning probe microscopy. *Nature* 1996; 384 (6605): 147-150.
- [48] Tans SJ, Devoret MH, Dai H, Thess A, Smalley RE, Geerligs LJ, et al. Individual single-wall carbon nanotubes as quantum wires. *Nature* 1997; 386 (6624): 474-477.
- [49] Tans SJ, Verschueren ARM, Dekker C. Room-temperature transistor based on a single carbon nanotube. *Nature* 1998; 393 (6680) 49-52.
- [50] Rosen R, Simendinger W, Debbault C, Shimoda H, Flemming L, et al. Quantum-dot concentrator and thermodynamic model for the global redshift. *Appl. Phys. Lett.* 2000, 76: 1197-1199.
- [51] Wagner HD, Lourie O, Feldman Y, Tenne R, Stress-induced fragmentation of multiwall carbon nanotubes in a polymer matrix. *Appl. Phys. Lett.* 1998 ; 72 : 188.
- [52] Ugarte D, Châtelain A, de Heer WA, Nanocapillarity and chemistry in carbon nanotubes. *Science* 1996; 274: 1897.
- [53] Dillon AC, Jones KM, Bekkedahl TA, Kiang CH, Bethune DS, Heben MJ, Storage of hydrogen in single-walled carbon nanotubes. *Nature* 1997; 386: 377.
- [54] Rao AM, Eklund PC, Bandow S, Thess A, Smalley RE, Evidence for charge transfer in doped carbon nanotube bundles from raman scattering. *Nature* 1997; 388: 255.
- [55] Bennett MJ. Carbon deposition: A major technological problem. *Mater. Corros.* 1998; 49 (5): 345-351.
- [56] Baker RTK, Harris PS, The formation of filamentous carbon. *Chem. Phys. Carbon* 1978; 14: 83.
- [57] Baker RTK, Barber MA, Harris PS, Feates FS, Waite RJ, Nucleation and growth of carbon deposits from nickel catalyzed decomposition of acetylene, *J. Catal.* 1972; 26 (1): 51-54.
- [58] Baker RTK, Alonzo JR, Dumesic JA, Yates DJC, Effect of the surface state of iron on filamentous carbon formation, *J. Catal.* 1982; 77: 74-84.
- [59] Yang KL, Yang RT, The accelerating and retarding effects of hydrogen on carbon deposition on metal surfaces. *Carbon* 1986; 24: 687-693.
- [60] Sacco A, Thacker P, Chang TN, Chiang ATS, The initiation and growth of filamentous carbon from alpha-Iron in H₂, CH₄, H₂O, CO₂ and CO gas-mixtures. *J. Catal.* 1984; 85 (1): 224-236.
- [61] Alstrup I, A new model explaining the carbon-filament growth on nickel, iron and Ni-Cu alloy catalysts. *J. Catal.* 1988; 109 (2): 241-251.
- [62] Cassell A, Raymakers J, Kong J, Dai H, Large scale CVD synthesis of single-walled carbon nanotubes. *J. Phys. Chem.* 1999; 103: 6484-6492.
- [63] Dresselhaus MS, Dresselhaus G, Avouris Ph (Eds.). *Carbon Nanotubes*. Springer-Verlag, Berlin, Heidelberg 2001.
- [64] Sikder AK, Sharda T, Misra DS, Chandrasekaram D, Veluchamy P, Minoura H, et al. *Diamond Deposition on Ni/Ni-diamond*

- coated stainless steel substrate. *J. Mater. Res.* 1999; 14 (3): 1148-1152.
- [65] Kukovitsky EF, L'vov SG, Sainov NA. VLS-growth of carbon nanotubes from the vapour. *Chem. Phys. Lett.* 2000; 317: 65-70.
- [66] Hou H, Schaper AK, Weller F, Greiner A. Carbon nanotubes and spheres produced by modified ferrocene pyrolysis. *Chem. Mater.* 2002; 14: 3990-3994.
- [67] Bladh K, Falk LKL, Rohmund F, On the iron-catalysed growth of single-walled carbon nanotubes and encapsulated metal particles in the gas phase. *Appl. Phys. A-Mater.* 2000; 70 (3): 317-322.
- [68] Zhu XY, White JM, Interaction of ethylene and acetylene with Ni(111): A SSIMS study. *Surf. Sci.* 1989; 214: 240.
- [69] Rodriguez NM, Kim MS, Baker RTK. Deactivation of copper nickel-catalysts due to changes in surface composition. *J. Catal.* 1993; 140: 16-29.
- [70] Kong J, Cassell AM, Dai H. Chemical vapor deposition of methane for single-walled carbon nanotubes. *Chem. Phys. Lett.* 1998; 292: 567-574
- [71] Su M, Zheng B, Liu J. A scalable CVD method for the synthesis of single-walled carbon nanotubes with high catalyst productivity. *Chem. Phys. Lett.* 2000; 322: 321-32
- [72] Alvarez WE, Kitiyanan B, Borgna A, Resasco DE. Synergism of Co and Mo in the catalytic production of single-wall carbon nanotubes by decomposition of CO. *Carbon* 2001; 39: 547-558
- [73] Kitiyanan B, Alvarez WE, Harwell JH, Resasco DE. Controlled production of single-wall carbon nanotubes by catalytic decomposition of CO on bimetallic Co-Mo catalysts. *Chem. Phys. Lett.* 2000; 317: 497-503
- [74] Colomer JF, Stephan C, Lefrant S, Van Tendeloo G, Willems I, Konya Z, Fonseca A, Laurent C, Nagy JB. Large-scale synthesis of single-wall carbon nanotubes by catalytic chemical vapor deposition (CCVD) method. *Chem. Phys. Lett.* 2000; 317: 83-89
- [75] Colomer JF, Bister G, Willems I, Konya Z, Fonseca A, Laurent C, Nagy JB. Synthesis of single-wall carbon nanotubes by catalytic decomposition of hydrocarbons. *Chem. Commun.* 1999; 1343-1344
- [76] Flahaut E, Govindaraj A, Peigney A, Laurent C, Rousset A, Rao CNR. Synthesis of single-walled carbon nanotubes using binary (Fe, Co, Ni) alloy nanoparticles prepared in situ by the reduction of oxide solid solutions. *Chem. Phys. Lett.* 1999; 300: 236-242
- [77] Flahaut E, Peigney A, Laurent C, Rousset A. Synthesis of single-walled carbon nanotube-Co-MgO composite powders and extraction of the nanotubes. *J. Mater. Chem.* 2000; 10: 249-252
- [78] Yan H, Li Q, Zhang J, Liu Z. Possible tactics to improve the growth of single-walled carbon nanotubes by chemical vapor deposition. *Carbon* 2002; 40: 2693-2698
- [79] Yoon YJ, Bae JC, Baik HK, Cho SJ, Lee SJ, Song KM, Myung NS. Nucleation and growth control of carbon nanotubes in CVD process. *Physica B Condensed Matter.* 2002; 323: 318-320
- [80] Yoon YJ, Bae JC, Baik HK, Cho SJ, Lee SJ, Song KM, Myung NS. Growth control of single and multi-walled carbon nanotubes by thin film catalyst. *Chem. Phys. Lett.* 2002; 366: 109-114
- [81] Kong J, Soh HT, Cassell AM, Quate CF, Dai H. Synthesis of individual single-walled carbon nanotubes on patterned silicon wafers. *Nature* 1998; 395: 878-818
- [82] Franklin NR, Li Y, Chen RJ, Javey A, Dai H. Patterned growth of single-walled carbon nanotubes on full 4-inch wafers. *Appl. Phys. Lett.* 2001; 79: 4571-4573
- [83] Soh HT, Quate CF, Morpurgo AF, Marcus CM, Kong J, Dai H, Integrated nanotube circuits: Controlled growth and ohmic contacting of single-walled carbon nanotubes. *Appl. Phys. Lett.* 1999; 75: 627-629
- [84] Hongo H, Yudasaka M, Ichihashi T, Nihey F, Iijima S. Chemical vapor deposition of single-wall carbon nanotubes on iron-film-coated sapphire substrates. *Chem. Phys. Lett.* 2002; 361: 349-354
- [85] Homma Y, Yamashita T, Finnie P, Tomita M, Ogino T. *Japan. J. Appl. Phys.* 2002; 41: L89-91
- [86] Emmenegger C, Bonard JM, Mauron Ph, Sudan P, Lepora A, Grobety B, Züttel A, Schlupbach L. Synthesis of carbon nanotubes over Fe catalyst on aluminum and suggested growth mechanism. *Carbon* 2003; 41: 539-547
- [87] Huang S, Woodson M, Smalley RE, Liu J. Growth mechanism of oriented long single-walled carbon nanotubes using "Fast-Heating"

- chemical vapour deposition process. *Nano Lett* 2004; 4 (6): 1025-1028
- [88] Ivanov V, Fonseca A, Nagy JB, Lucas A, Bernaerts A, Zhang XB, Catalytic production and purification of nanotubules having fullerene-scale diameters. *Carbon* 1995; 33 (12): 1727-1738.
- [89] Pérez-Mendoza M, Vallés C, Maser WK, Martínez MT, Benito AM. Influence of molybdenum on the chemical vapour deposition production of carbon nanotubes. *Nanotechnology* 2005; 16: 224-225
- [90] Zheng GB, Kouda K, Sano H, Uchiyama Y, Shi YF, Quan HJ. A model for the structure and growth of carbon nanofibres synthesized by the CVD method using nickel as a catalyst. *Carbon* 2004; 42: 635-640
- [91] Lee CJ, DW Kim, Lee TJ, Choi YC, Park YS, Lee YH, Kim JM. Synthesis of aligned carbon nanotubes using thermal chemical vapour deposition. *Chem. Phys. Lett.* 1999; 312: 461-468.
- [92] Alstrup I, Tavares, MT Bernardo CA, Sorensen O, Rostrup-Nielson JR. Carbon formation on nickel and nickel-copper alloy catalysts. *Mater. Corr.* 1998; 49: 367-372
- [93] Vander Wal RL, Ticich TM, Curtis VE. Substrate-support interactions in metal-catalyzed carbon nanofiber growth. *Carbon* 2001; 39: 2277-2289.
- [94] Klinke C, Bonard JM, Kern K. Comparative study of the catalytic growth of patterned carbon nanotube films. *Surf. Sci.* 2001; 492: 195-201.
- [95] Wang X, Hu Z, Chen X, Chen Y. Preparation of carbon nanotubes and nano-particles by microwave plasma-enhanced chemical vapor deposition. *Scripta Mater.* 2001; 44: 1567-1570.
- [96] Lee CJ, Park J, Kim JM, Huh Y, Lee JY, No KS. Low-temperature growth of carbon nanotubes by thermal chemical vapor deposition using Pd, Cr, and Pt as co-catalyst. *Chem. Phys. Lett.* 2000; 327: 277-283.
- [97] Singh MK, Singh PP, Titus E, Misra ES, LeNormand F. High density of multi-walled carbon nanotubes observed on nickel electroplated copper substrates by microwave plasma chemical vapour deposition. *Chem. Phys. Lett.* 2002; 354 (3-4): 331-336.
- [98] Saito Y. in *Carbon Nanotubes*, edited by Endo M, Iijima S, Dresselhaus MS. Pergamon Press, New York, 1996; 153-162.
- [99] McCarty JG, Hou PY, Sheridan D, Wise H, in *coke formation on metal surfaces*. Edited by Albright LF and Baker RTK. ACS Symposium Series 1981; 2020: 252.
- [100] Jung M, Eun KY, Lee JK, Baik YJ, Lee KR, Park JW. Growth of carbon nanotubes by chemical vapour deposition. *Diam. Relat. Mater.* 2001; 10 (3-7): 1235-1240.
- [101] Baker RTK, Harris PS, Thomas RB, Waite RJ. Formation of filamentous carbon from iron, cobalt and chromium catalyzed decomposition of acetylene. *J. Catal.* 1973; 30 (1): 86-95.
- [102] Lepora A, Métraux C, Grobety B, Emmenegger C, Zuettel A. The evolution of iron nitrate films during CVD synthesis of carbon nanotubes: An *in-situ* high temperature X-ray diffraction investigation. in press.

CHAPTER 2

Investigation Methods

2.1 CVD Facility

Laboratory CVD set-ups are usually composed of a quartz tube with an external wire furnace. During synthesis, a constant gas flow is directed over the catalyst-carrying substrate placed in the centre of the tube. The apparatus used for this project is not a common CVD facility but the principle and the synthesis mechanism remain the same. A cylindrical heating chamber attached to an X-ray diffractometer replaced the quartz tube at the conventional CVD system. The gas flow was controlled by two gas mass flow controllers.

2.1.1 High Temperature X-ray Diffractometer Chamber

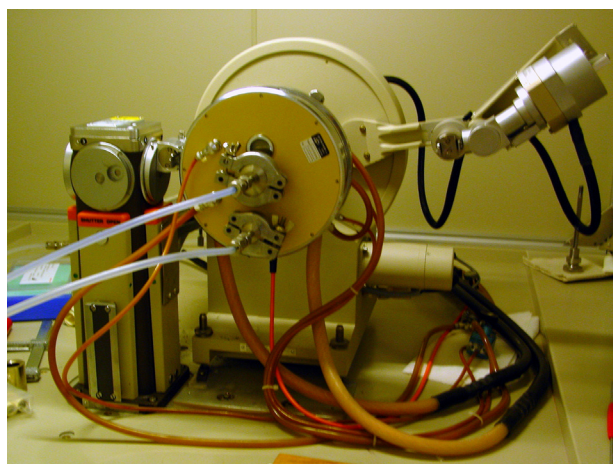


Fig. 1: Picture of the used HT X-ray diffractometer

The apparatus used for the *in-situ* diffractometry is a Philips PW 1830 diffractometer. The X-rays were generated by a Cu source at a current of 40 mA and voltage of 40 kV. The diffracted X-ray intensity was measured by a scintillation detector mounted on a goniometer with Bragg-Brentano geometry and equipped with divergence and soller slits on both the tube and the detector side. The diffractograms were recorded in step scan mode with $0.02^\circ/\text{step}$ and variable recording times per step. A high temperature X-ray camera (model HTK 10, Anton PAAR, Graz, Austria) [Figure 1] controlled by a temperature control unit (TCM 2000, Anton PAAR, Graz, Austria) is mounted on the diffractometer and serves as reaction chamber comparable to conventional CVD facilities [Figure 2].

The sample holder is a 1 cm wide platinum strip which serves as heat source. By resistance heating

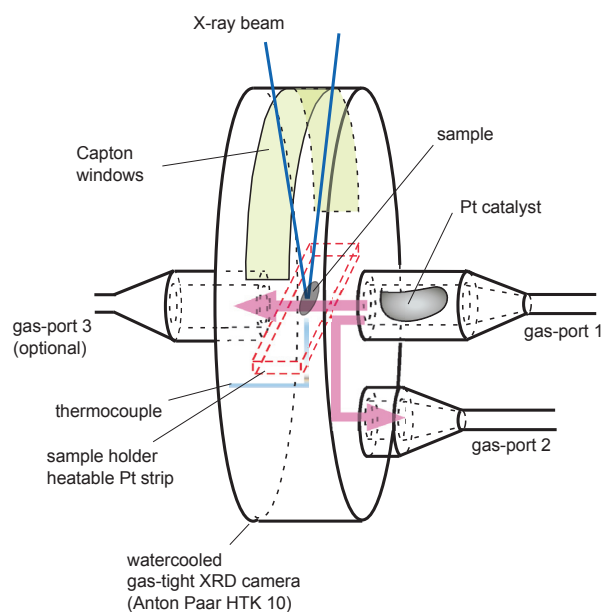


Fig. 2: Schematic illustration of the HT X-ray chamber

temperatures up to 1500°C can be reached. The camera is equipped with X-ray transparent capton-windows. Gas in- and outlet are at the front of the camera, at the level of the sample and 3 cm below, respectively.

A disadvantage of this set-up is the limited time resolution. Phase changes are followed by scanning corresponding peaks. The accuracy of kinetic measurements is, therefore, limited by the scanning speed, e.g. for the measurement parameters used in the present experiments time resolution is around 30 seconds.

The temperature is controlled by a thermoelement attached on the lower side of the platinum strip. The catalyst precursors were deposited on glass platelets (AF 45, PGO GmbH, Iserlohn, Germany) and placed in the centre of this platinum strip. In contrast to externally heated gas mixing furnaces used in conventional CVD synthesis of CNT, there is a large temperature gradient between the hot-spot and the water-cooled camera walls. A careful temperature calibration is, therefore, indispensable.

2.1.2 Temperature Calibration

The thermocouple was calibrated via the thermal expansion of platinum [1] and the α - β transition temperature in quartz [2,3]. The platinum sample holder was used as reference sample. Unit cell

parameter refinements at 25°C gave a cell parameter of 3.9206 Å. This value is 0.0025 Å smaller than the parameter for pure Pt e.g. 3.9231 Å. This deviation is due to a slight iron contamination of the strip caused by previous experiments with iron oxides. Patterns of the strip were taken from room temperature in 200°C steps up to 1000°C. Cell parameters were refined using UnitCell [4] and the linear thermal expansion was calculated [1], taking the cell parameter of the contaminated strip as reference and the following thermal expansion expression for pure platinum, disregarding the effect of the contamination on the thermal expansion coefficient.

$$\alpha_{\text{Pt}} \Delta T_{19.85^\circ\text{C}} = -1.766 * 10^{-2} + (8.862 * 10^{-4} * T) + (1.76 * 10^{-7} * T^2) - (1.144 * 10^{-10} * T^3) + (8.93 * 10^{-14} * T^4) \quad (1)$$

The unit cell refinement corrects also for zero and sample displacement shifts (see next chapter). The cell parameter at temperature T is, thus, given by

$$a_{\text{Pt at } X^\circ\text{C}} = a_{\text{Pt measured } 25^\circ\text{C}} + \alpha_{\text{Pt}} \Delta T_{X^\circ\text{C}} \quad (2)$$

and therefore

$$a_{\text{Pt } 600^\circ\text{C calculated}} = a_{\text{Pt measured } 25^\circ\text{C}} + \alpha_{\text{Pt}} \Delta T_{600^\circ\text{C}} = 3.9206 + 3.9206 * (0.5643 * 100\%) = 3.9427 \quad (3)$$

$\alpha_{\text{Pt} \Delta T_{600^\circ\text{C}}}$: Percent linear thermal expansion coefficient of platinum (= 0.56428 when relative to 19.85°C [1]) [Table 1].

Temp. (°C)	linear thermal expansion coefficient rel. to 0°C (*10 ⁻⁴)	percent linear thermal expansion rel. to 19.85°C
-20	8.790	-0.03531
0	8.862	-0.01766
19.85	8.931	0.00000
50	9.029	0.02708
100	9.183	0.07261
150	9.324	0.11889
200	9.457	0.16585
250	9.583	0.21345
300	9.705	0.26167
350	9.826	0.31051
400	9.949	0.35994
450	10.076	0.41001
500	10.210	0.46072
550	10.354	0.51213
600	10.511	0.56428
650	10.511	0.61725
700	10.511	0.67112
750	10.511	0.72598
800	10.511	0.78194
850	10.511	0.83913
900	10.511	0.89767
950	10.511	0.95772
1000	10.511	1.01944
25	8.933	0.00460
1003	12.573	1.02320
812	11.304	0.79555
607	10.515	0.57165
405	10.081	0.36492
194	9.452	0.16018

Tab. 1: Linear thermal expansion coefficient of platinum referred to 19.85°C after Edsinger [1]

The increase of the cell parameter was almost linear [Figure 3].

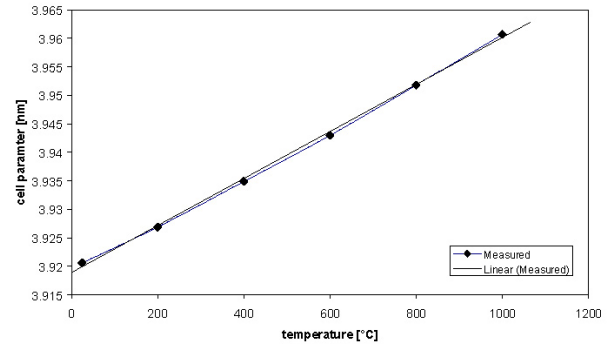


Fig. 3: Measured cell parameter for contaminated platinum strip for various temperatures. The punctuated line indicates a linear increase

The actual temperature of the strip was determined by comparing the measured expansion with calculated and tabulated values for pure platinum, assuming that the error due to the use of the thermal expansion expression for pure platinum is smaller than the measurement error.

Except for 200°C, all actual temperatures were slightly above the temperatures indicated by the thermocouple [Table 2].

induced Temp [°C]	average cell parameter [Å]		actual Temp [°C]
	calculated	measured	
25	3.9231	3.9206	-
200	3.9296	3.9269	194
400	3.9438	3.9349	405
600	3.9660	3.943	607
800	3.9970	3.9518	812
1000	4.0378	3.9607	1003

Tab. 2: Comparison of measured with calculated expansion leads to the actual temperature [1].

The most likely reasons for the deviation are 1. the age of the thermocouple and 2. the contamination of the thermocouple due to iron contamination [Figure 4].

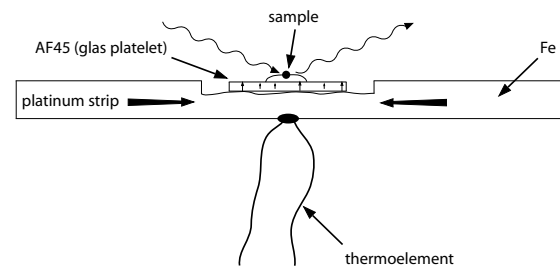


Fig. 4: Schematic illustration of the used platinum strip.

These values represent the average temperature of the strip area covered by the X-ray beam.

To assess the influence of the glass plate used as sample support for the experiments, the α - β transition temperature of quartz powder [2], which was deposited on such a glass plate, was calibrated.

As expected, the values read from the thermocouple were 15 - 20 °C above the temperature indicated in the literature. The observed difference between the theoretical transition temperature and the indicated value is composed of the thermocouple error (+ 7° C at 600°C) and the additional heating necessary to compensate the diffusive losses due to the intervening glass plate. Additional losses are due to the unevenness of the platinum strip. Grooves in the Pt-strip may be filled with air and lead to an inhomogeneous thermal conductivity. The actual temperature on the surface of the glass plate is thus 22 – 27°C lower than indicated by the thermocouple and this deviation was taken into account when setting the temperatures for the experiments.

2.1.3 Calculation of Peak-Positions at different Temperatures

The accuracy and the precision of the peak positions are affected by several factors. Peak shifts are mainly due to errors in the zero position of the goniometer and to wrong sample height. The calibration of the goniometer geometry was based on the peak position of platinum. All sample measurements contain Pt-peak, because the glass substrate does not cover the entire strip. These Pt-peaks were used as internal standards at temperature after correction for sample displacement and correction for thermal expansion and zero shift. The latter can be important since the platinum strip is quite soft and may change the shape during heating. Following equations [5] were used to determine the theoretical peak position:

$$n * \lambda = 2 * d * \sin\theta \quad \rightarrow \quad \sin\theta = \arcsin \frac{n * \lambda}{2 * d} \quad (4)$$

for cubic unit cell:

$$d^2 = \frac{a^2}{h^2 + k^2 + l^2} \quad (5)$$

$$a = \sqrt{d^2 * (h^2 + k^2 + l^2)} = \sqrt{\left(\frac{n * \lambda}{2 * \sin\theta}\right)^2 * (h^2 + k^2 + l^2)}$$

a: unit cell parameter (ang), corrected for thermal

expansion at temperature [Tab. 1]

λ : wavelength (nm)

d: interplanar spacing (nm)

θ : diffraction angle (degree)

$h^2+k^2+l^2$: reciprocal lattice parameters

For example, the platinum (1 1 1) peak position in units of 2θ at 600°C is at angle:

$$2\theta = 2 * \arcsin\left(\frac{\lambda}{2 * d}\right) = 2 * \arcsin\left(\frac{\lambda}{2 * \sqrt{\frac{a^2}{h^2 + k^2 + l^2}}}\right) \quad (6)$$

$$= 2 * \arcsin\left(\frac{1.54056}{2 * \sqrt{\frac{3.9427^2}{1^2 + 1^2 + 1^2}}}\right) = 39.554$$

The position of the (1 1 1) peak for other temperatures are listed in table 3 [Table 3 a.]. All other peak positions for platinum can be calculated in the same way. Catalyst peak positions were corrected using the shift observed for the closest platinum peak [Table 3 b.].

Temp (°C)	(1 1 1)	(2 0 0)	(2 2 0)	(3 1 1)	(2 2 2)
25	39.790	46.275	67.518	81.327	85.780
200	39.723	46.197	67.395	81.169	85.609
400	39.639	46.097	67.240	80.970	85.394
600	39.554	45.997	67.083	80.769	85.177
800	39.463	45.889	66.914	80.552	84.942
1000	39.370	45.780	66.744	80.334	84.707

at 600°C	calculated	measured	difference
(1 1 1)	39.554	39.14	0.414
(2 0 0)	45.997	45.64	0.357
(2 2 0)	67.083	66.7	0.383
(3 1 1)	80.769	80.38	0.389
(2 2 2)	85.177	84.8	0.377

Tab. 3: Calculated peak positions of platinum at various temperatures a.) and peak position correction of platinum peaks at 600°C b.).

2.1.4 Description of the Gas System

One important part of a CVD apparatus to form carbon nanotubes is a reliable gas flow control. The present system consists of two mass flow controllers (AFC-2600, AALBORG, Orangeburg, New York USA), a command module (2PROC, AALBORG) and three electromagnetic valves. The original flow controllers were calibrated for CO₂. The gases used for the synthesis were acetylene, hydrogen and nitrogen. A correction factor was therefore indispensable (see appendix).

The mass flow meters were controlled by a digital

2-channel command module which allows to adjust the desired gas stream. The flow range used in the experiments was at the lower end of the available mass flow controllers (1 – 3 % of full scale, error according to manufacturer is $\pm 1\%$). Experiments showed that a stable gas stream rate was only achieved after about 5 minutes which caused serious problems in the adjustment of experiments with short gas exposure time (kinetic measurements). The introduction of electromagnetic valves (V1, V2 and V3) in the gas system gave the possibility to pre-adjust gas flow rate before passing through the reaction chamber (V2 close, V3 open). After constant flow rates were reached, simple switching of the electromagnetic valves allowed to direct the adjusted gas flow through the chamber (V2 open, V3 close). The nitrogen feeding tube remained open and the flow rate constant during all experiments. Due to this simple construction the accuracy of the experiments was increased drastically [Figure 5].

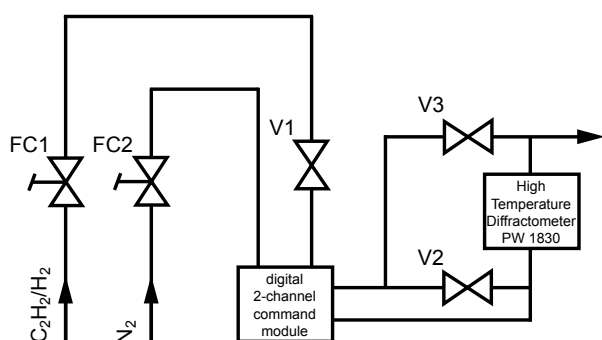


Fig. 5: Sketch of the gas controlling system

Three different high purity grade gases were used for the experiments:

Nitrogen: N_2 99.995%,
impurities: $O_2 < 10$ ppm, $H_2O < 10$ ppm

Acetylene: C_2H_2 99.6%,
impurities: $N_2, PH_3 < 10$ ppm

Hydrogen: H_2 99.99%,
impurities: $O_2 < 5$ ppm, $H_2O < 10$ ppm,
 $N_2 < 300$ ppm

All gases were used without prior cleaning nor drying and the pressure for all gases was constantly kept at 0.5 bar before the passage into the electromagnetic valves. The flow rate for nitrogen was kept constant at 250 ml/min (=250 sccm), and that for hydrogen and acetylene was adjusted to either 25 sccm or 75 sccm. A relative control of the gas flow was obtained

by directing the outlet gas stream into a water bin and comparing the amount of bubble formation.

In the nickel and chromium system, the oxygen partial pressure equilibrium of the oxide-metal buffers, e.g. NiO-Ni and Cr_2O_3 -Cr are well below the oxygen impurities present in the “inert” nitrogen gas used in the experiments. Some of the equilibrium f_{O_2} in the molybdenum and cobalt systems are, however, close to the oxygen fugacity of the nitrogen gas used ($10^{-6} - 10^{-4}$). Phase evolutions in these systems are thus very much susceptible to small changes in the oxygen impurity level of the gas (see appendix).

2.2 Scanning Electron Microscopy

The Scanning Electron Microscope used was a Philips FEI XL30 SFEG SIRIUS. The investigations were performed on drop-coated samples (0.01 mol/l) on glass platelets (AF45, Präzisions Glas & Optik GmbH, Iserlohn, Germany). The specimens are fixed with a conducting carbon cement (Leit-C by Göcke, BAL-TEC distribution) on aluminium stubs (sample holder) and dried on air for at least 24 hours. This guaranteed an optimal contact between the specimen and the sample holder. All samples were coated with a 10 nm thick Au-layer using a BAL-TEC SCD 050 Sputter in order to prevent charging of the specimen. Generally 4 specimens were positioned at the same time on a specially conceived multiple sample holder.

The scanning electron microscope is equipped with a field emission gun designed for working with low voltages and high magnification. The microscope can be run in two operation modes: HR (high resolution) and UHR (ultra high resolution) [Figure 6].

In UHR mode, the sample is immersed in the magnetic field of the final lens, whereas in HR mode the sample is at a certain distance at the lens. The main difference between the normal and immersion lens is that the latter does not have an air gap in the lens but outside the lens. Therefore the specimen has to be placed on a small working distance to obtain ray path through the yoke into the specimen and then via the stage to the specimen chamber back to the column. Likewise the beam energy has to be kept small and the column needs to be centred to the specimen chamber. In this lens configuration a strong magnetic field is generated between the lens and the specimen in which the samples are immersed [Figure 7].

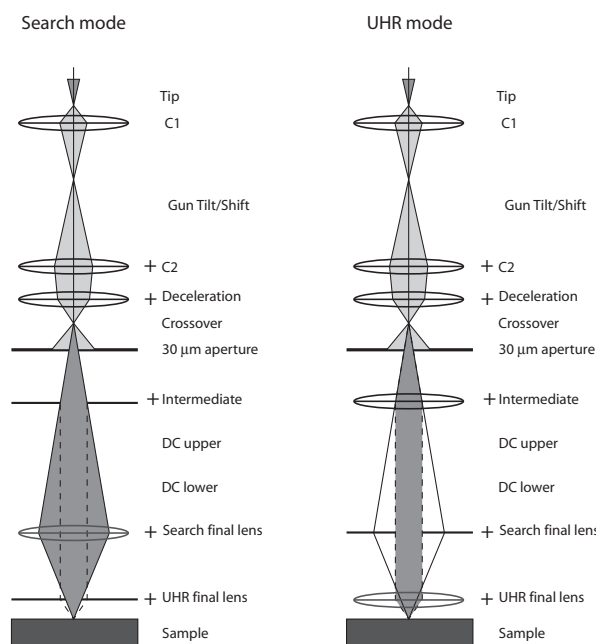


Fig. 6: Electron path in a “normal” (HR) and an immersion (UHR) operation mode.

It is therefore not possible to look at magnetic samples with the immersion lens because particles could detach from the substrate and be drawn into the column damaging the emission tip. The huge spot size and the high acceleration voltage needed when using the UHR mode increase the possibility of detaching particles from the glass platelets.

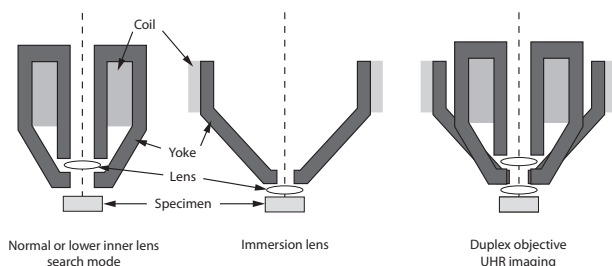


Fig. 7: field free (HR) and immersion lens (UHR) and a duplex objective lens mode.

Since nickel, cobalt, iron, chromium and its alloys are magnetic, it was not advisable to perform sample investigations in the UHR mode and we therefore used only high resolution mode. Working distance for all samples were chosen between 14.5 mm and 15 mm depending on the thickness of the specimen layer. The acceleration voltage was adjusted to 20 kV to minimize the effect of magnetism. These settings allowed a magnification (25'000-fold) sufficient for our investigation goals.

2.3 Sample Preparation

In our experiments we used thin alkali free borosilicate glass platelets (6 x 12 x 0.2 mm, AF 45, PGO GmbH, Iserlohn, Germany) as substrate. The surface is scribe-cut and unbeveled and its softening temperature (883°C) is well above the temperatures used during the experiments. We used two different preparation procedures depending on the objectives – phase changes or SEM investigations.

Samples used for the investigations of phase changes during synthesis were prepared according to following method: About 5 mg crystals were weight in (precision balance, STETTLER AE 361) and mixed together with 3 drops of ethanol in a mortar. To achieve an optimal mixing, the salt was crushed and homogenized. By pipetting, the pasty liquid was deposited on the substrate and subsequently dried on air before mounting it on the platinum strip in the reaction chamber of the diffractometer. The pipetting procedure is not as reproducible as other methods like the usual spin coating and therefore may lead to morphological inhomogeneities.

Another preparation technique was obtained for samples investigated by the scanning electron microscope. Here we used the so-called drop coating method: One drop of the nitrate solution (approx. 35 – 40 μ l) in three different concentrations, 1 mol/l, 0.1 mol/l and 0.05 mol/l dissolved in ethanol were deposited by pipetting on the glass platelets and subsequent dried on air. In comparison to the spin coating method where the surface of the substrate is regularly covered by a very thin layer, the drop coating technique offers the advantage that the liquid layer thickness varies continuously from the centre to the rim of the drop allowing to study systematically the influence of the catalyst layer thickness on CNT production.

2.4 Softwares

The software [“Automatic Powder Diffraction” (APD) from Philips Electronics N.V. 1997] was used for controlling of diffractometer and heating stage. The software allows to write variable temperature control programs, to plot the results and to obtain quantitative analysis. All raw data originating from the HT-diffractometer were transformed in Excel-readable formats by the aid of the freeware ConvX. Peak determination was obtained by the extensive

database of JCPDS-ICDD (International Centre for Diffraction Data) by the aid of the software PCPDFWIN Version 1.3 (1997).

2.5 References

- [1] Edsinger RE, Reilly ML, Schooley JF. Thermal expansion of platinum and platinum-rhodium alloys. *J. Res. NBS* (20899) 1986; 91 (6): 333-356.
- [2] Heaney PJ, Veblen DR. Observation of the α - β phase transition in quartz: A review of imaging and diffraction studies and some new results. *American Mineralogist* 1991; 76: 1018-1032.
- [3] Tucker MG, Keen DA, Dove MT. A detailed structural characterization of quartz on heating through the α - β phase transition. *Mineral. Mag.* 2001; 65 (4): 489-507
- [4] Freeware programmed by Tim Holland and Simon Redfern.
- [5] Ladd MFC, Palmer RA. Structure determination by X-ray crystallography. Plenum Press, New York 1994, Third edition.
- [6] Operating Manual for AFC-2600 Mass Flowmeters & Controllers, AALBORG® Instruments & Controls, Inc. Orangeburg, New York USA.

CHAPTER 3

THE EVOLUTION OF IRON AND NICKEL NITRATE FILMS DURING CVD SYNTHESIS OF CARBON NANOTUBES: AN *IN-SITU* HIGH TEMPERATURE X-RAY DIFFRACTION INVESTIGATION

K. Matzinger¹, A. Lepora¹, B. Grob ty¹ and A. Z ttel²

¹Geosciences Department, University of Fribourg, 1700 Fribourg, Switzerland

²Physics Department, University of Fribourg, 1700 Fribourg, Switzerland

extended abstract at CARBON 2004, An International Conference on Carbon at Brown University, Providence, Staten Island, USA, 16. July 2004

Abstract

The Transition metals are necessary catalyst for the synthesis of carbon nanotubes by chemical vapour deposition (CVD). The chemical and morphological evolution of iron nitrate films deposited on glass substrates and exposed to acetylene-nitrogen gas mixture at temperatures between 600°C and 750°C were studied by *in-situ* X-ray diffraction, scanning and transmission electron microscopy. The iron nitrate solution leads to a deposit of an amorphous iron oxide coating which crystallizes to hematite (Fe₂O₃) during heating under nitrogen, the nickel nitrate solution forms a nickel nitrate deposit that transforms to nickel oxide (NiO) at a temperature of 200°C. At 600°C, Fe₂O₃ transforms to iron carbide (Fe₃C, cementite) as soon as acetylene is added, no iron is formed; NiO, however, transforms to the metal without intervening carbide. The polycrystalline substrates for both metals are fragmented due to the large solid volume loss and a large reduction in grain size is observed. Nanotubes occur after several minutes of CVD treatment for both metals. After 40 minutes, cementite transforms to iron and graphite (metal dusting). At the onset of dusting a second boost in tube production is observed. These results suggest that the catalytic processes leading to nanotube growth are different depending on the transition metal used. This may explain the contradictory statements about the role of carbides for CVD synthesis found in the literature. Models for both Fe and Ni will be presented.

1. Introduction

Chemical vapor deposition (CVD) is a widely used technique to produce CNTs in large quantities [1]. The decomposition of gases with carbon containing species (CO , CO_2 , C_2H_2 etc.) over a metallic catalyst at temperatures between 600°C and 1200°C leads to the nucleation and growth of CNTs. Much progress has been made from the point of view of the yield, the synthesis costs, and the purity of the products obtained by CVD, but there is still much debate about what really controls CNTs growth. The most active metals are Fe, Co and Ni, but their catalytic action depends on the type of precursor [2], the type of the substrate [3] and of the reactive gases used [4]. Highly controversial is the actual chemical nature of the active catalyst e.g. if it is present as metal, carbide or as mixed phase. Although carbides are often metastable (e.g. Fe_3C), because they require carbon activities in the gas phase > 1 to be stabilized, they have often been detected in the reactor and inside the tubes [5], but there is no agreement about whether they are active species for CNTs growth [6], or if they are only post-reaction phases [7].

One reason for the uncertainties regarding the catalytic action of metal particles during CNTs synthesis by CVD is the scarce number of *in-situ* analyses of the chemical and morphological evolution of the catalyst. Most *in-situ* analysis concentrated on the growth process of the carbon tubes [8] and the evolution of the reactive gases [9], but not on the evolution of the catalyst.

This paper focuses on the evolution of iron and nickel-based catalysts under a nitrogen-acetylene atmosphere between 600°C and 750°C . An X-ray diffractometer equipped with a heating stage and an atmosphere controlling system was used to study *in-situ* the evolution of iron and nickel nitrate films, in order to elucidate the nature of the metal phase during the synthesis runs. Quenching experiments with the same furnace were conducted with increasing pyrolysis time, in order to investigate the timing of the nanotubes appearance by *ex-situ* Scanning Electron Microscopy (TEM, SEM).

2. Experimental

The catalyst precursors $\text{Fe}(\text{NO}_3)_3 \cdot 9(\text{H}_2\text{O})$ (Merck, Germany) and $\text{Ni}(\text{NO}_3)_2 \cdot 6(\text{H}_2\text{O})$ (Fluka, Buchs, Switzerland) were either deposited as crystals or as solution dissolved in ethanol onto glass substrates (0.07 mMol iron- and 0.05 mMol nickel nitrate

hydrate). The crystal samples were used to monitor the catalyst evolution, whereas the solution samples were analyzed for nanotube growth.

The apparatus for the *in-situ* diffractometry was a high temperature X-ray camera (model HTK 10, Anton PAAR, Graz, Austria) mounted on a Philips PW 1830 diffractometer. Gas flow was controlled by two mass flow controllers (AFC-2600, AALBORG, Orangeburg, New York, USA). The phase evolution in the catalyst was studied for two different temperatures: 600°C and 750°C . The goniometer was equipped with a scintillation detector and the phase changes were monitored by scanning individual peaks of the reactant. The diffractograms were recorded in step scan mode ($0.02^\circ/\text{step}$, $1\text{sec}/\text{step}$) between 20° and 80° (2θ). The temperature was raised at a rate of $70^\circ\text{C}/\text{min}$ to the desired temperature under nitrogen. After an annealing time of 10 minutes, acetylene (2 vol% or 6 vol%) was added to the nitrogen atmosphere.

The Scanning Electron Microscope (Philips FEI XL30 SFEG SIRIUS) investigations were performed on solution-coated glass substrate (7-10 keV acceleration potential). TEM investigations were made with a Philips CM20 microscope, operated at 200 keV and equipped with an EDAX energy dispersive spectrometer.

3. Results and Discussion

During the heating up stage under nitrogen, the iron nitrate hydrate transformed to an amorphous layer that started to crystallize as hematite (Fe_2O_3) around 300°C , the nickel nitrate hydrate dehydrated and the nitrate decomposed at 250°C to NiO. As soon as acetylene was introduced to the iron catalyst, the oxide phases were reduced. At 600°C , hematite disappeared within 2 minutes and was replaced by magnetite (Fe_3O_4) and wuestite (FeO).

The first non-oxide phase, cementite (Fe_3C), appeared after 1 to 2 minutes. During this first transformation stage no metallic iron could be detected. After 40 minutes the cementite peaks started to decrease and peaks of elemental iron could be detected in the diffractograms. However, nickel oxide, was reduced within seconds to pure nickel. No nickel carbides were detected neither directly after the C_2H_2 flooding of the chamber nor after 3 hours. The nickel peaks, however, shifted to lower 2θ -values. This shift is interpreted as a change in carbon concentration in solid solution with nickel (Figure 1). At 750°C the rate of the reduction reactions for the iron catalyst

was considerably accelerated. The main product of the reduction reaction was again cementite and in contrast to the experiments run at lower temperatures no iron could be detected even after prolonged annealing.

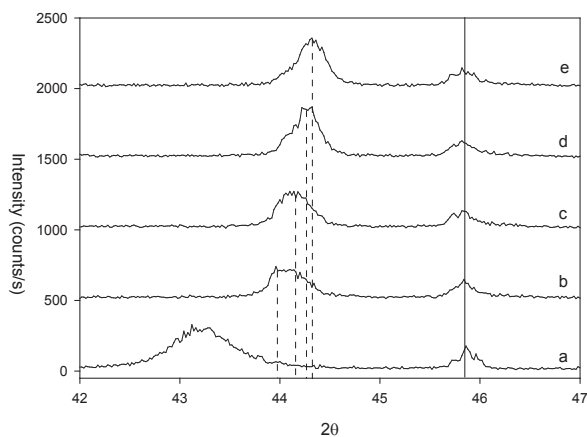


Fig. 1: X-ray diffractograms of nickel catalyst samples annealed at 600°C (a) crystals dissolved in ethanol before acetylene exposure. (b) Sample after 30 seconds, (c) after 1 hour, (d) after two hours and (e) after three hours exposed to acetylene (2 vol%). Observe the shift in the nickel peak position (stippled lines) with increase in acetylene exposure. The continuous line indicates the stable peak position of platinum.

After the heating up cycle, the catalyst films formed a polygonal microstructure with an average grain size of 200 nm for hematite and 40 nm for the nickel oxide. The oxide reduction under the acetylene atmosphere reduced considerably the grain size (Figure 2a).

The final microstructure is a sponge-like aggregate of cementite (Figure 2b) and metallic nickel respectively. The iron carbide grains had a large size distribution ranging from a few, up to 80 nm whereas the nickel particles had a more homogeneous grain

size e.g. around 20 nm. CNTs were only nucleating on grains smaller than 40 nm in diameter. The first tube-shaped carbon deposition for both catalysts were observed 1 minute after the addition of the acetylene and consisted of rods several tens of nanometer thick and some hundred nanometers in length.

Yields and size homogeneity for both catalysts appeared to be proportional to the acetylene concentration (Figure 3) and inversely proportional with film thickness. Areas with a thick catalyst layer showed heterogeneous deposits of amorphous carbon, encapsulated particles, and nanotubes with a large diameter. In general, the tube diameter was correlated with the grain size of the catalyst.

The wall thickness determined from TEM images showed that the CNTs are multiwalled. Both open and closed tips are present, often enclosing catalyst particles. The carbide nature of the iron containing particles was confirmed by electron diffraction. A temperature increase of 150°C had a strong enhancing effect on nanotubes production for the iron catalyst, not so for the nickel catalyst. The reason is probably the stronger tendency of nickel metal particles to coalesce. After a short time at this temperature, most nickel particles were too large to serve as nucleation site for the tubes.

The predominance of carbides for the iron catalyst at the onset of CNTs formation seems to be in contradiction with the arguments put forward by Rodriguez [10]. Based on the fact, that activation energy for CNTs growth on a given metal is very close to the activation energy of carbon diffusion in the same metal, and that experiments made with pure iron carbide catalysts were unable to produce CNTs, he concluded that carbides play no active role in CNT formation. The diffusion data [11] were obtained by measuring growth rates of single NTs on

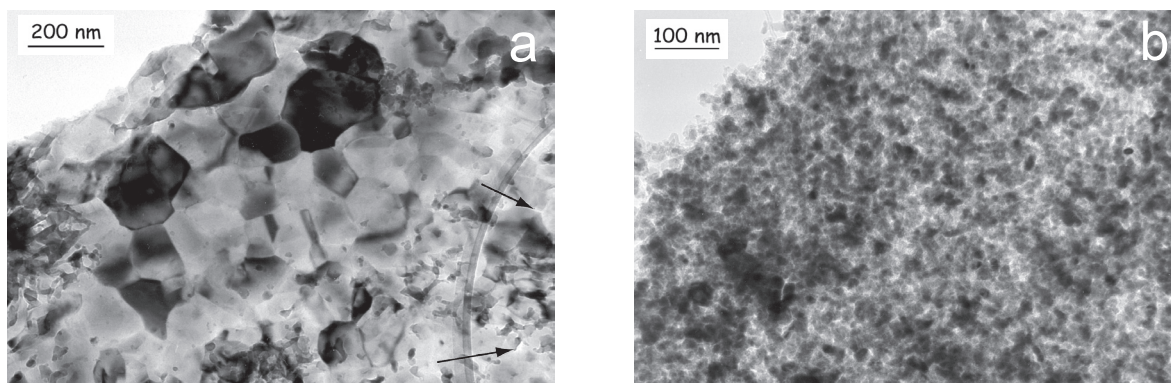


Fig. 2: Bright Field TEM images of iron catalyst samples annealed under acetylene at 600°C for (a) 30 sec: Polygonal iron oxides layer (centre); a change of grain size is visible towards the rim. The sample has been annealed. The arrows point to intergranular pores. Texture obtained after 5 minutes of annealing. A clear reduction of the grain size is visible. Most cementite grains and interstitial pores are covered/filled with carbon. (d) After 10 minutes the first carbon nanotubes are visible.

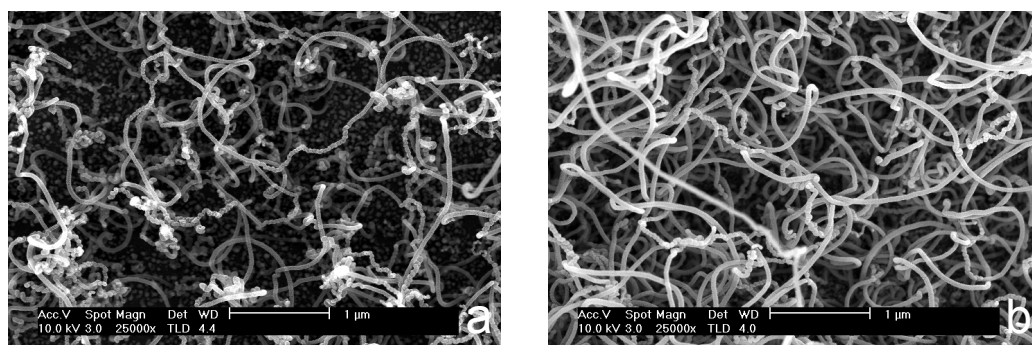


Fig. 3: SEM images of samples (0.05 mol/l nickel nitrate hydrate dissolved in ethanol) (a) sample exposed for 1 hour to 2% acetylene and (b) to 6% acetylene.

different metal nanoparticles *in-situ* by Controlled Atmosphere Electron Microscopy (CAEM). No *in-situ* structural analyses of the nanoparticles have been presented in this paper, so the nature of the catalyst during the experiment is not really known. The authors observed fragmentation of iron nanoparticles during the experiments, which may well be explained by decarburization and associated metal wasting. The absence of nanotube growth in the presence of iron carbide particles may be related to the fact, that the catalyst in CNT synthesis has two roles to play. Poor performance in the first catalytic process, e.g. the breakdown of the carbon bearing gas species, does not preclude the ability to serve as nucleation site for CNTs and vice versa. The low temperature growth of CNTs on Co-Ni particles as an example, is only possible when a co-catalyst (Pd, Pt, Cr) is added to break down acetylene [12]. The large quantities of CNTs produced in the present experiments at 750°C, during which no iron is formed, show that iron carbide particles are able to serve as CNT nucleation sites. The role of cementite in the breakdown of acetylene is less clear, because in the sample strip in the HTK-camera is made of platinum, an excellent catalyst for that process.

4. Conclusions

The experiments have shown that iron and nickel catalyst under typical NT synthesis conditions behave differently. Strictly speaking, iron is not a “catalyst” but an active reactant of the system. For both catalysts, the morphological and crystallographic nature of the catalyst at the end of the synthesis does in no way translate the complex transformations occurring during the run, and the above experiments show the valuable information that can be gained from *in-situ* analysis of the catalyst. Both morphological and

chemical changes such as size reduction and metal dusting (iron) influence the timing and the yield of nanotube formation. Differences in yields and morphology of nanotubes for synthesis performed under different run conditions may, therefore, not be related to intrinsic changes in the nanotube growth rates, but to differences in the evolution of the catalyst. Similar behaviors can be expected from other transition metals used as catalysts for NTs growth.

5. References

- [1] Dresselhaus MS, Dresselhaus G, Sugihara K, Spain IL, and Goldberg HA. Graphite fibers and filaments. Springer Series in Materials Science 5, (Springer Verlag, New York, 1988).
- [2] Fonseca A, Hernadi K, Piedigrosso P, Colomer JF, Mukhopadhyay K, Doome R, Lazarescu S, Biro LP, Lambin P, Thiry PA, Bernaerts D, Nagy JB. Appl. Phys. A-Mat. Sci. & Proc., 67, 11 (1998).
- [3] Kukovecz A, Konya Z, Nagaraju N, Willems I, Tamasi A, Fonseca A, Nagy JB, Kiricsi I. Phys. Chem. Chem. Phys. 2, 3071 (2000).
- [4] Nerushev OA, Dittmar S, Morjan RE, Rohmund F, Campbell EEB. J. Appl. Phys. 93, 4185 (2003).
- [5] Hou HQ, Schaper AK, Jun Z, Weller F, Greiner F. Chem Mat. 15, 580 (2003)
- [6] Ivanov V, Fonseca A, Nagy JB, Lucas A, Lambin P, Bernaerts D, Zhang XB. Carbon 33, 1727 (1995).
- [7] Coquay P, Peigney A, De Grave E, Vandenberghe RE, Laurent C. J. Phys. Chem. B, 106, 13199 (2002).
- [8] Kim DH, Jang HS, Kim CD, Cho DS, Yang

- HS, Kang HD, Min BK, Lee HR. *Nano Let.*, 3, 863 (2003).
- [9] Woo YS, Jeon DY, Han IT, Lee NS, Jung JE, Kim JM. *Diamond Rel. Mat.* 11, 56-66 (2002).
- [10] Rodriguez NM, *J.Mater.Res.* 8, 3233 (1993).
- [11] Baker RTK, Alonzo JR, Dumesic JA, and Yates DJC. *J. Catal.* 77, 74 (1982).
- [12] Lee CJ, Park J, Kim JM, Huh Y, Lee JY, and No KS. *Chem.Phys.Lett.* 327, 277 (2000).

CHAPTER 4

THE EVOLUTION OF NICKEL NITRATE HEXAHYDRATE COATED GLASS SUBSTRATE DURING CVD SYNTHESIS OF CARBON NANOTUBES: AN *IN- SITU* HIGH TEMPERATURE X-RAY DIFFRACTION INVESTIGATION

K. Matzinger and B. Grobéty

Dep. of Geoscience, Applied Mineralogy Group, University of Fribourg, Pérolles, 1700 Fribourg

submitted to Carbon

Abstract

The chemical and morphological evolution of a nickel catalyst was studied by *in-situ* X-ray diffraction and high resolution Scanning Electron Microscopy (SEM). Glass substrates coated with nickel nitrate solution as catalyst were exposed to an acetylene-nitrogen gas mixture at temperatures between 600°C and 750°C in the camera of a high temperature X-ray diffractometer. In all experiments the formation of carbon nanotubes (CNT) were observed. The nickel nitrate solution decomposed during heating under nitrogen to a fine crystallized nickel oxide coating. After addition of acetylene, the nickel oxide transformed very quickly to small nickel particles. This transformation is accompanied by a huge solid volume loss that is responsible for the strong fragmentation of the catalyst layer. The size of the particles was a function of the film thickness. The nickel peaks observed in the *in-situ* measured X-ray diffractograms shifted continuously with progressing synthesis time. The shift is interpreted as a change in the amount of carbon dissolved in the metallic catalyst. No metastable carbide was formed.

Keywords: A. carbon nanotubes; B. chemical vapour deposition; C. x-ray diffraction; D. crystal structure

1. Introduction

Filamentous carbon produced during the decomposition of hydrocarbons in presence of metal catalysts such as iron, cobalt, nickel and some of their alloys, have been known for many years. Especially in the metal industry the prevention of carbon deposit accumulation is a high priority objective in many processes involving hydrocarbon conversion reactions [1]. The presence of such carbon deposits create problems including blockage of reactors, reduction of heat transfer properties, and catalyst deactivation due to encapsulation of the metallic component [2].

The groundbreaking observation that many of the small carbon filaments are in fact tubes has turned the nuisance into a potential material for nanotechnology application [3] such as electron field emitters [4,5], one-dimensional conductors [6,7], supercapacitors electrodes [8], transistor [9,10] reinforcing fibres in composite materials [11], probe tips for atomic force microscopy (AFM) or scanning tunneling microscopy (STM) [12] and molecular filtration membranes [13]. One of the most attractive applications based is to use CNT's as individual electron emitter for flat panel displays [14].

Various methods such as electric arc discharge [15,16], laser vaporization [15,16], electrolysis [16], pyrolysis [15,16], plasma-enhanced or chemical vapour deposition (CVD) [17,18] have been developed for the production of CNT. CVD is currently one of the most promising and flexible methods to produce CNT in a larger quantities [19,20]. During the CVD process, the carbon containing gas species (C_2H_2 , CO_2 , etc) decompose over a metallic catalyst at temperatures between 600°C and 1000°C. The carbon is absorbed by the catalyst particle and nucleates as CNT at the surface. The CVD process has several advantages over other synthesis methods. CNT can grow at a relatively low temperature and their size can be controlled by varying the size of the catalyst [1,21]. Furthermore the growth rate, the diameter and the crystallinity can be manipulated by selecting the catalysts [22,23]. Despite tremendous progress in the yields, the lowering of the synthesis costs and the improvement in purity of the products obtained by CVD, the mechanisms of CNT growth and nucleation are still much debated. A basic model was developed by Baker and coworkers [24] which has been extended by many authors [15,25,26,27,28,29,30]. The key steps in their model are the adsorption and the decomposition of a hydrocarbon on a metal surface

to produce carbon species which dissolve and diffuse through the bulk and ultimately precipitate at the rear of the particle to form nanotubes or -fibres. Such a mechanism is based on the observation that the activation energies for CNT nucleation and growth on specific metals are very similar to the activation energies for carbon bulk diffusion in the same metals [31,32]. The question that is still open is if carbides form during this reaction process and if they are present what catalytic activity they have. Rodriguez stressed that the active species for filament and nanotube formation are metals and not carbides [1,33]. Electron diffraction analysis carried out by Oberlin and coworkers [19] revealed the existence of cementite (Fe_3C) after the interaction of iron with benzene/hydrogen. Although these carbides are often metastable at synthesis conditions, there is no agreement about whether they are active species for CNT growth or not [1,19,34,35,36]. Rodriguez and co-workers [33] investigated the interaction of copper-nickel particles with ethylene (C_2H_4) but no evidence for the existence of a bulk carbide phase was found in these experiments. In contrast, Ni_3C phases were observed on an electrodeposited nickel coating on a copper substrate treated by ammonia [34]. Ivanov [35] proposed in his work by using arc-discharge method cobalt carbides as the active catalyst, and not metallic Co, for the production of nanotubes using cobalt nitrate coated SiO_2 substrates. A major problem with most investigations is that they were done *ex-situ* and conclusions were drawn by comparing pre- and post-synthesis results. Lepora et al. [36] analysed iron catalysts *in-situ* and showed that the catalyst underwent major chemical changes during the synthesis which are impossible to deduce from post-synthesis analyses. They showed that cementite is formed immediately after acetylene is added to the atmosphere, but that the carbide decomposes after a certain reaction duration. Simultaneous with the cementite break-down a boost in CNT growth is observed.

This paper focuses on the *in-situ* investigation of the evolution of a nickel-based catalyst under a nitrogen-acetylene atmosphere at 600°C and 750°C.

2. Experimental Methods

2.1 Starting Materials

The substrate (thin glass AF 45, PGO GmbH, Iserlohn, Germany) was coated with a nickel nitrate

hexahydrate ($\text{Ni}(\text{NO}_3)_2 \cdot 6(\text{H}_2\text{O})$; Fluka, Buchs, Switzerland, crystallized $\geq 98.0\%$) and was either deposited as crystals or dissolved in ethanol onto the glass substrate. The support material, an alkali free borosilicate glass, has a softening temperature (883°C) well above the temperatures used during the experiments. About 5 mg of crystals or one drop of nitrate solution (approx. 35 - 40 μl) in three different concentrations, 1 mol/l, 0.1 mol/l and 0.05 mol/l of $\text{Ni}(\text{NO}_3)_2 \cdot 6\text{H}_2\text{O}$, were deposited by pipetting or spin coating on the substrate and subsequently dried on air, resulting in a bulge like precursor film with radially decreasing thickness. The crystals were slightly wetted with ethanol to guarantee a better adhesion to the substrate. The glass platelets were chosen because of their non-crystallinity and ease to use in the XRD set-up.

The gases were of high purity grade: N_2 99.995%, impurities: $\text{O}_2 < 10$ ppm, $\text{H}_2\text{O} < 10$ ppm; C_2H_2 99.6%, impurities: $\text{N}_2, \text{PH}_3 < 10$ ppm. All gases were used without prior cleaning nor drying.

2.2 High Temperature Diffractometer Experiments

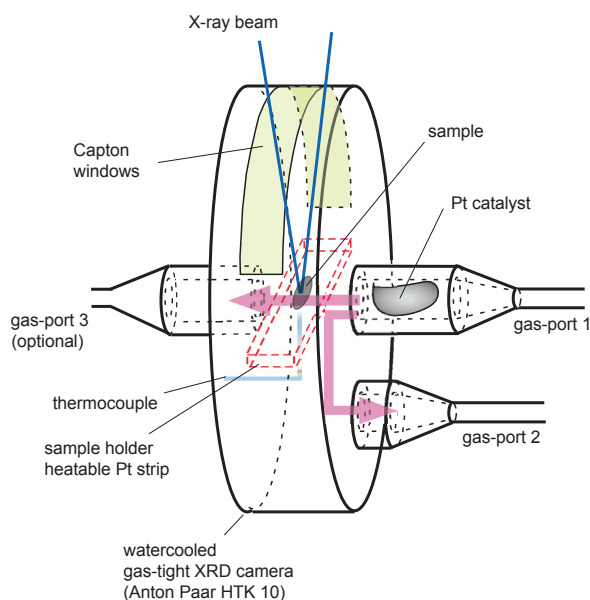


Fig. 1: High temperature powder X-ray camera used for the diffractometry under controlled atmosphere.

The apparatus for the *in-situ* diffractometry was a high temperature X-ray camera (model HTK 10, Anton PAAR, Graz, Austria) [Figure 1] controlled by a temperature control unit (TCM 2000, Anton PAAR, Graz, Austria) mounted on a Philips PW 1830 diffractometer (see [36]). Nitrogen and acetylene gas

flow was controlled by two mass flow controllers (AFC-2600, AALBORG, Orangeburg, New York, USA).

The glass substrates were placed on the heated platinum strip in the centre of the cylindrical camera. Temperature was controlled by a thermocouple on the lower side of the platinum strip. In contrast to externally heated gas mixing furnaces used in conventional CVD CNT synthesis, there is a large temperature gradient between the hot-spot and the water-cooled camera walls. The thermocouple was calibrated via thermal expansion of platinum, using peaks originating from the sample holder strip [39], and via α - β - quartz transition at 573°C [40], with an estimated uncertainty of $\pm 5^\circ\text{C}$.

The phase evolution was studied for two different temperatures: 600°C and 750°C . Gas flow and experiment duration were identical to the synthesis conditions used in a gas-mixing furnace by Emmenegger et al. [5]. The goniometer was equipped with a scintillation detector and the phase changes were monitored by scanning individual peaks (reference: appropriate JCPDS cards) of the reactant phases (nickel nitrate hexahydrate: 16.16° (020), JCPDS No. 25-0577; nickel nitrate: 21.03° (111), JCPDS No. 14-0593; nickel oxide: 43.27° (200), JCPDS No. 47-1049) and the product phase (nickel: 44.50° (111), JCPDS No. 04-0850). Due to the sample holder was a platinum strip, in all diffractograms obtained during the measurements, platinum peaks originating from the sample holder occurred (platinum: 39.76° (111), 46.24° (200), 67.45° (220), 81.82° (311), JCPDS No. 04-0802) and served as reference peaks. The diffractograms were recorded in step scan mode between 20° and 80° (2θ). We used for samples with crystals and 0.05 mol/l, 0.1 mol/l and 1.0 mol/l nitrate solution with a step size of $0.02^\circ/\text{step}$ and a measuring time of 1 sec/step. These parameters represent the best compromise between time resolution, and sensitivity.

The Pt peaks at room temperature were shifted to smaller angles due to a slight iron contamination and a small displacement error. The unit cell parameters were refined with the program UnitCell (programmed by Tim Holland and Simon Redfern). The refinement allowed the determination of the total 2θ shift of the peaks. The splitting of the Pt peaks observed in the patterns taken at high temperature is due to interferences with the glass platelets, because it is absent in diffractograms taken from the bare Pt strip.

At the beginning of each run, the camera was flushed

with nitrogen and the temperature then raised at a rate of 70°C/min to the desired temperature under nitrogen. After an annealing time of 10 minutes, acetylene (25 sccm or 75 sccm) was added to the nitrogen atmosphere. Parameters such as nickel nitrate hexahydrate concentration, temperature, gas flow rate and time were systematically varied between experiments.

2.3 Electron Microscopy

The Scanning Electron Microscope (Philips FEI XL30 SFEG SIRIUS) investigations were performed on drop-coated samples (0.01 mol/l or 1.0 mol/l) on glass platelets (AF45) annealed. To prevent electrical charging of the samples during SEM investigation, all samples were gold coated with a BAL-TEC SCD 050 Sputter-coater. Imaging was done under high resolution mode and with an acceleration voltage between 7 to 10 keV. EDS measurements were done with an acceleration voltage between 15 and 20 keV. Working distance for all samples was adjusted to 5 mm.

3. Results

3.1 Morphological and Chemical Evolution of the Catalyst

The nickel nitrate hydrate ($\text{Ni}(\text{NO}_3)_2 \cdot X \text{H}_2\text{O}$) appears in four different states of hydration (X : 2, 4, 6, 8). Nickel nitrate hexahydrate was used as starting

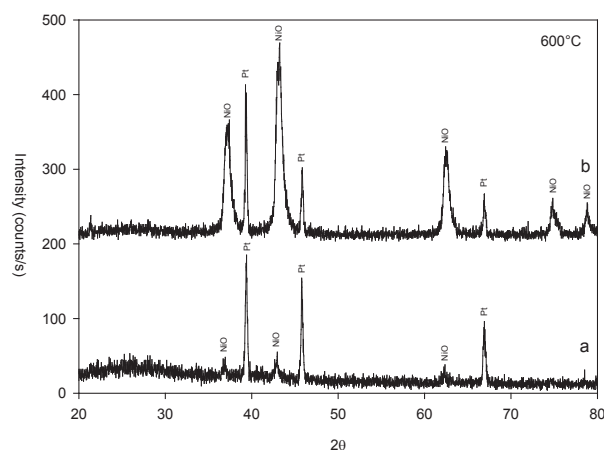


Fig. 2: X-ray diffractograms of samples annealed for 2 hours at 600°C under nitrogen (a) solution of 0.1 mol/l dissolved in ethanol. (b) Crystals dissolved in ethanol.

material. The X-ray diffractogram contained some additional, non-identified, peaks, probably due to variation of the hydration state within the sample. The glass platelet was coated with the starting material completely dissolved in alcohol. The lowest solution concentration for which XRD signals from the catalyst were observable is 0.05 mol/l. The phase evolution of solution samples, independent of concentration, and crystal samples is identical and the same X-ray diffractograms are obtained [Figure 2].

Under nitrogen, as well as under air, the dehydration reaction of nickel nitrate hydrate started at 56°C [41]. At about 100°C the first peaks of nickel nitrate occurred. The nickel nitrate evolution during subsequent heating up to 400°C depended upon the atmosphere composition. Under nitrogen all hydrate phases were fully decomposed to nickel nitrate at 220°C and the first NiO appeared at 250°C. The nitrate peaks disappeared completely at 350°C. Under air, the dehydration has already been completed at 160°C. First signs of NiO, a large saddle in the 2θ -region of the nickel oxide (200) peak appeared around 220°C, but clear NiO peaks were only observed above 350°C [Figure 3].

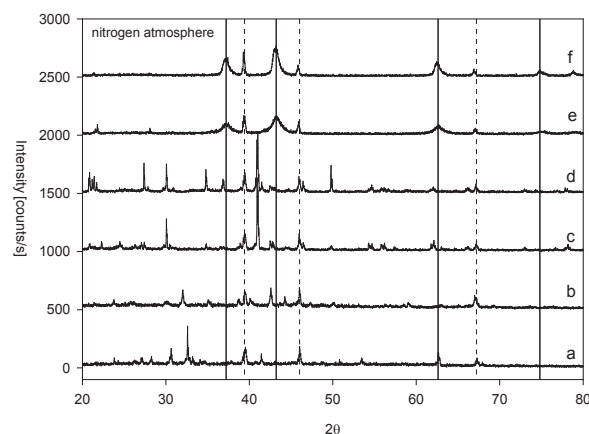


Fig. 3: X-ray diffractograms of quenched samples annealed at various temperatures under nitrogen heating conditions. (a) Nickel nitrate hydrate crystals at room temperature (25°C). Sample annealed at 100°C (b) 200°C (c) 250°C. (d) 400°C (e) and 600°C (f). Continuous lines represent NiO, stippled lines platinum and remaining peaks $\text{Ni}(\text{NO}_3)_2$.

Between 400°C and the maximum temperature 750°C no new phases appeared neither in air nor in a nitrogen atmosphere. The nickel oxide peaks are very broad at the beginning and get narrower with increasing temperature. Average grain diameters calculated with the Scherrer equation using the full width at half maximum of the NiO (200) peak ranged from 6.4 nm at 320°C to 12.7 nm at 600°C

[Figure 4]. At the start of the acetylene addition, the catalyst phase present was always nickel oxide.

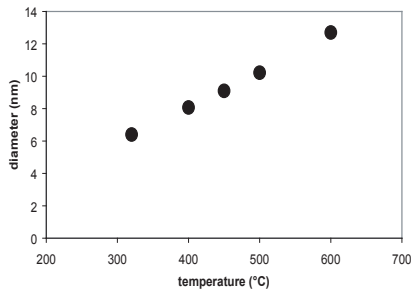


Fig. 4: Grain size evolution of NiO during the heating up stage.

At 600°C, as soon as acetylene is introduced, nickel oxide is reduced within seconds to pure nickel. No nickel carbide was detected during the entire run [Figure 5]. The average particle diameter is considerably larger than for the oxide precursor and varies between 24 nm after 10 min and 32 nm after 220 min of acetylene exposure. The lattice parameters calculated from the (111) and (200) peaks (calibrated against the platinum peaks corrected for the iron impurity) were larger than the parameters reported for pure nickel. With increasing annealing time the value decreased to 3.534 Å [Figure 6], close to the parameter for pure nickel at 600°C (3.531 Å).

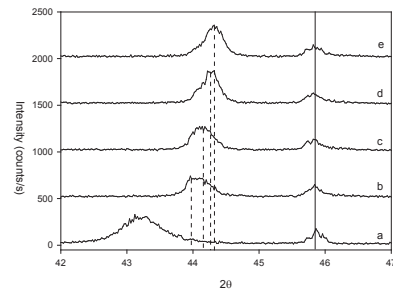


Fig. 5: X-ray diffraction patterns of quenched samples annealed at 600°C for 2 hours under nitrogen atmosphere. (a) Crystals dissolved in ethanol before acetylene exposure. The left peak belongs to NiO. (b) Sample after 30 seconds. (c) After 1 hour, (d) after two hours and (e) after three hours acetylene exposure. The continuous line connects platinum, the stippled lines Ni peaks.

Increasing the annealing temperature to 750°C reveals exactly the same evolution, but the transformation rates are faster.

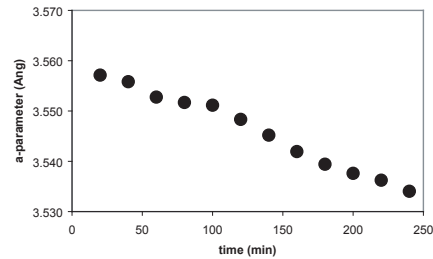


Fig. 6: Evolution of the unit cell parameter of the nickel phase with time at 600°C.

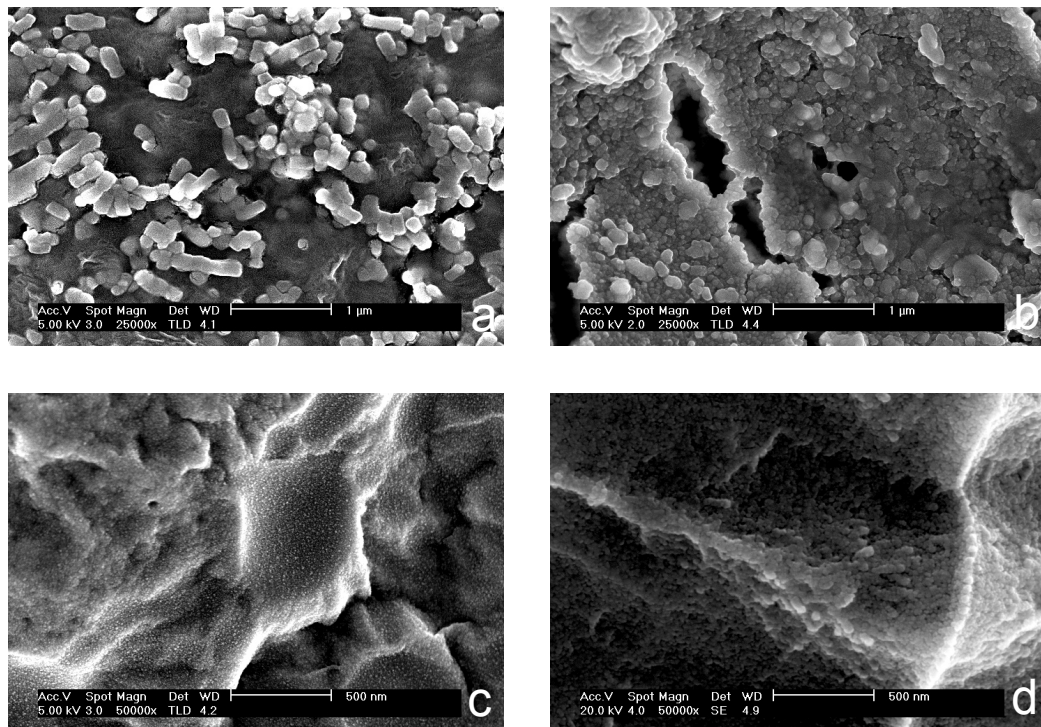


Fig. 7: SEM images of 0.05 mol/l nickel nitrate hydrate samples dissolved in ethanol and heated up on various temperatures under nitrogen atmosphere condition. Sample annealed for 2 hours at (a) 100°C, (b) 200°C, (c) 400°C and (d) 600°C.

The SEM pictures taken from samples prepared by depositing a drop of the nickel nitrate solution on a glass platelet confirm the grain size evolution deduced from the observed peak broadening. Samples with 0.05 mol/l nickel nitrate hydrate solution heated up to 100°C reveal a coalesced rough surface covered by well crystallized cubic nickel nitrate particles with an average particle size of about 200 – 500 nm, forming a corrugated, brain-like surface [Figure 7a]. Around 200°C the decomposition of nickel nitrate to nickel oxide starts reducing the size to 100 – 300 nm. The surface of the now sponge-like structure is less rough and some cracks and holes are visible [Figure 7b].

Above 330°C the last remnants of nickel nitrate

crystals disappeared [Figure 7c] and the surface of the film disintegrated to very fine powder with grain diameters smaller than 10 nm. At 600°C the surface film is rougher with grains larger than 15 nm [Figure 7d]. When the thickness is larger than 50 nm, individual particles coalesce to a continuous surface only disrupted by cracks. The sintering of the grains seems, however, to affect only the surface, not the interior of the layer. The thickness and the continuity of this sintered layer are proportional to flow rate and temperature. In thinner part of the layer, coalescence is less pronounced and leads to 200 to 400 nm well separated large grains still surrounded by small particles. The evolution was identical for a solution of 1.0 mol/l nickel nitrate hydrate.

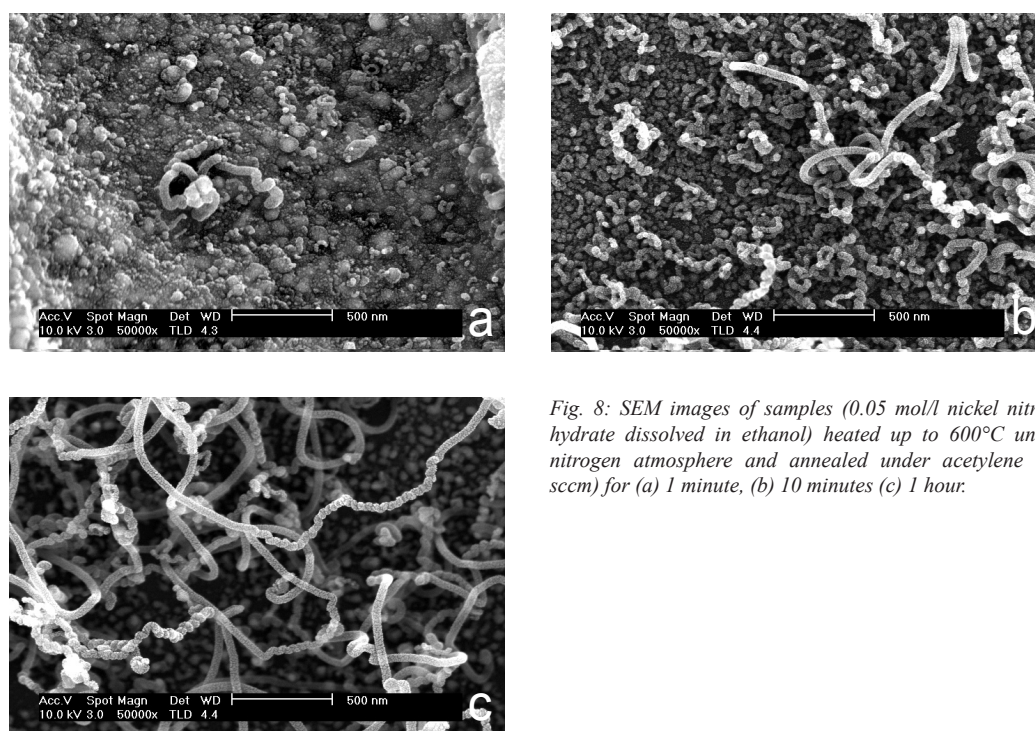


Fig. 8: SEM images of samples (0.05 mol/l nickel nitrate hydrate dissolved in ethanol) heated up to 600°C under nitrogen atmosphere and annealed under acetylene (25 sccm) for (a) 1 minute, (b) 10 minutes (c) 1 hour.

3.2 Formation of Nanotubes

All samples with a nitrate solution catalyst precursor, which were exposed to acetylene is at 600°C, contained nanotubes, but never samples prepared with coarse nitrate crystals. The first tube-shaped carbon deposition on the glass support are observed 1 minute after the addition of the acetylene and consists of rods several tens of nanometer thick and some hundred nanometers in length. They appear only in the thin areas of the nickel layer and have often wounded shapes [Figure 8a]. No nanotubes were found on the thicker part of the nickel layer

except at the border of cracks and inside them. With increasing annealing time (> 10 min), longer and thinner nanotubes appear, which are randomly oriented [Figure 8b]. Samples annealed one hour exhibit a loose carpet of fine nanotubes with a diameter ranging between 20 and 50 nm [Figure 8c] and lengths of several microns.

An increase of the acetylene flow rate by a factor three has a strong enhancing effect on the concentration and the length of nanotubes. After 1 hour of annealing an extended network of fine tubes occurred [Figure 9a,b].

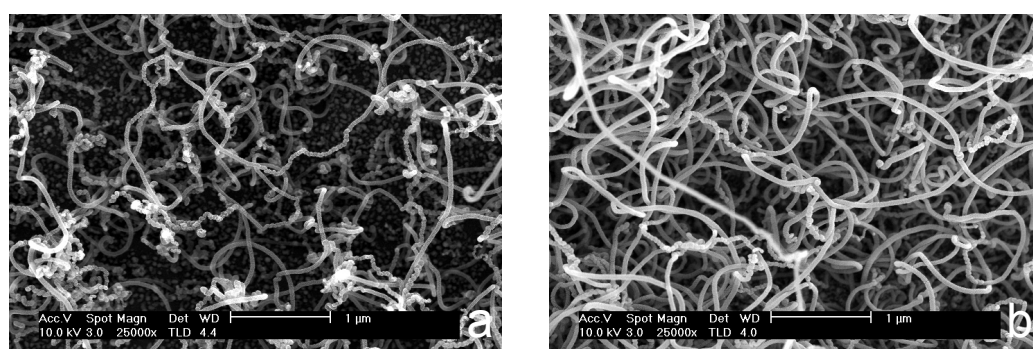


Fig. 9: SEM images of samples (0.05 mol/l nickel nitrate hydrate dissolved in ethanol) heated up to 600°C under nitrogen atmosphere and annealed for 1 hour under (a) 25 sccm acetylene and (b) 75 sccm acetylene.

At 750°C the concentration of CNT's for the same settings of solution concentration and gas flow was smaller. Their average diameter varied between 20 nm and 200 nm and their lengths reached only a

few microns. The thicker tubes are shorter and less wounded than the thinner tubes [Figure 10a, b]. At the surface of the catalyst layer, large grains (up to 1 μm) occurred.

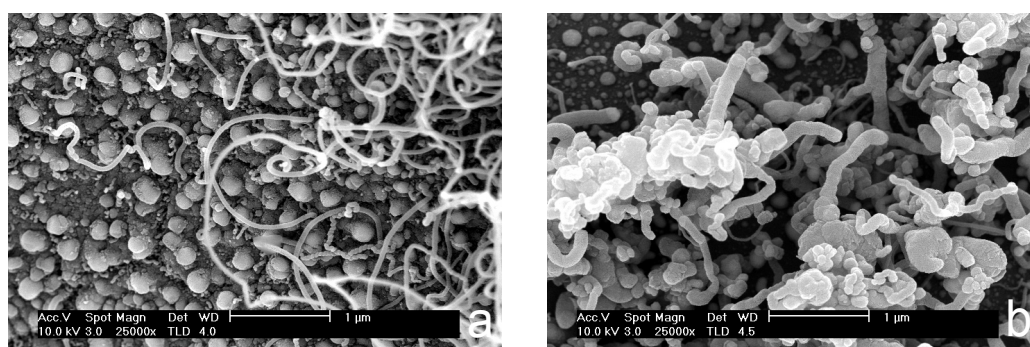


Fig. 10: SEM images of samples (0.05 mol/l nickel nitrate hydrate dissolved in ethanol) exposed for 1 hour to 75 sccm acetylene at (a) 600°C and (b) at 750°C.

4. Discussion

The denitrification and reduction of the initial nickel nitrate is accompanied by a huge solid volume change between reactants and products. The most important loss of solid volume (81.34% relative to the reactant) is associated with the transformation of nickel nitrate to cubic nickel oxide. The volume loss connected with the reduction of the oxide is half as large (39.96%). The total solid volume loss between the catalyst precursor (nickel nitrate) and the catalyst (pure nickel particles) is more than 88.8% and therefore twice the volume loss in comparison to the iron system discussed by A. Lepora et al.

[36]. The smallest particles occur at the onset of denitrification. The observed grain growth during the heating up phase could possibly be avoided by a faster heating rate. Despite the overall solid volume loss during the reaction, the average metallic nickel particle size is larger than the size of the oxide grains before acetylene addition. This is the result of agglomeration and recrystallization of grains in the thicker part of the catalyst film.

The location of nanotube growth is clearly related to this initial film thickness. The first tubes were observed where the catalyst particle size dropped below 50 nm [Figure 11] which is in accordance to the work of Z.P. Huang [21].

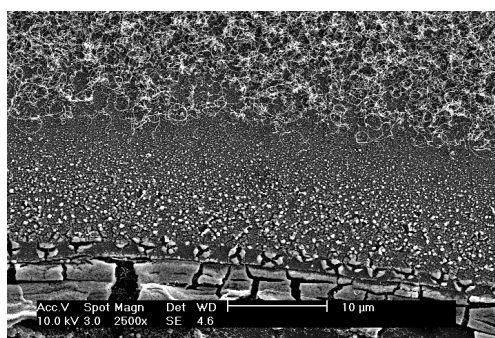


Fig. 11: SEM image of a sample (crystals of nickel nitrate hydrate dissolved in 1 drop of ethanol) exposed for 10 minutes to acetylene at 600°C. Carbon nanotubes appear as soon as the catalyst particle size drops below 50 nm.

The lower concentration at 750°C is clearly also the consequence of the faster agglomeration rate of the nickel particles, which leads to an increase of the tube diameters (s. Fig. 10b).

No carbide peaks were observed during the experiments. The increased nickel unit cell parameter at the beginning of the acetylene exposure is indicative of the presence of dissolved carbon. Sikder et al. [41] observed the same unit cell expansion in CVD diamond synthesis experiment where nickel substrates were used. Analysis of the nickel substrate revealed 1-2 wt% of carbon. The initial expansion in our experiments is of the same order. This shows that carbon is dissolved within the nickel catalyst when exposed to acetylene. This is compatible with the CNT growth models asking for a diffusive flow of carbon through the catalyst particle. The decrease of the expansion indicates a decrease in the carbon concentration dissolved in the catalyst and thus a decrease in diffusive flow and a decrease in CNT growth rate. The smaller carbon concentration is probably due the coating and shielding of the catalyst film by CNT and other carbon deposition.

5. Conclusions

Nickel acts, like iron, under typical NT synthesis conditions as catalyst in the reaction sequence. The nickel particles dissociate acetylene and serve as nanotube nucleation sites. No nickel carbide appears in the reaction system at all. The observed unit cell expansion, however, suggests that carbon is dissolved in the nickel particle during synthesis.

6. References

- [1] Rodriguez NM. A review of catalytically grown carbon nanofibres. *J Mater Res* 1993; 8(10): 3233-3250.
- [2] Bennett MJ. Carbon deposition: A major technological problem. *Mater Corros* 1998; 49 (5): 345-351.
- [3] Iijima S. Helical microtubules of graphitic carbon. *Nature* 1991; 354 (6348): 56-58.
- [4] Kuettel OM, Groening O, Emmenegger C, Schlapbach L. Electron field emission from phase pure nanotube films grown in a methane/hydrogen plasma. *Appl Phys Lett* 1998; 73 (15): 2113-2115.
- [5] Emmenegger C, Mauron P, Zuetzel A, Nuetzenadel C, Schneuwly A, Schlapbach L, et al. Carbon nanotube synthesized on metallic substrates. *Appl Surf Sci* 2000; 162: 452-456.
- [6] Hamada N, Sawada S, Oshiyama A. New one-dimensional conductors – graphitic, microtubules. *Phys Rev Lett* 1992; 68 (10): 1579-1581.
- [7] Saito R, Fujita M, Dresselhaus G, Dresselhaus MS. Electronic-structure of chiral graphene tubules. *Appl Phys Lett* 1992; 60 (18): 2204-2206.
- [8] Niu CM, Sichel EK, Hoch R, Moy D, Tennent H. High power electrochemical capacitors based on carbon nanotube electrodes. *Appl Phys Lett* 1997; 70 (11): 1480-1482.
- [9] Tans SJ, Verschueren ARM, Dekker C. Room-temperature transistor based on a single carbon nanotube. *Nature* 1998; 393 (6680) 49-52.
- [10] Tans SJ, Devoret MH, Dai H, Thess A, Smalley RE, Geerligs LJ, et al. Individual single-wall carbon nanotubes as quantum wires. *Nature* 1997; 386 (6624): 474-477.
- [11] Zuetzel A, Sudan P, Mauron P, Kiyobayashi T, Emmenegger C, Schlapbach L. Hydrogen storage in carbon nanostructures. *Int J Hydrogen Energy* 2002; 27 (2): 203-212.
- [12] Dai H, Hafner JH, Ginzler AG, Colbert DT, Smalley RE. Nanotubes as nanoprobe in scanning probe microscopy. *Nature* 1996; 384 (6605): 147-150.
- [13] Che GL, Lakshmi BB, Fisher ER, Martin CR. Carbon nanotubule membranes for electrochemical energy storage and production. *Nature* 1998; 393 (6683): 346-349.
- [14] Fan SS, Chapline MG, Franklin NR, Tomblor

- TW, Cassel AM, Dai H. Self-oriented regular arrays of carbon nanotubes and their field emission properties. *Science* 1999; 283 (5401): 512-514.
- [15] Harris PJF. Carbon nanotubes and related structures – New materials for the twenty-first century. Cambridge University Press 1999; 18-24.
- [16] Journet C, Bernier P. Production of carbon nanotubes. *Appl Phys A-Mater* 1998; 67 (1): 1-9.
- [17] Jung M, Eun KY, Lee JK, Baik YJ, Lee KR, Park JW. Growth of carbon nanotubes by chemical vapour deposition. *Diam Relat Mater* 2001; 10 (3-7): 1235-1240.
- [18] Lee CJ, Kim DW, Lee TJ, Choi YC, Park YS, Lee YH, et al. Synthesis of aligned carbon nanotubes using thermal chemical vapour deposition. *Chem Phys Lett* 1999; 312 (5-6) 461-468.
- [19] Oberlin A, Endo M, Koyama T. Filamentous growth of carbon through benzene decomposition. *J Cryst Growth* 1976; 32 (3): 335-349.
- [20] Dresselhaus MS, Dresselhaus G, Sugihara K, Spain IL, Goldberg HA. Graphit, fibers and filaments. Springer Series in Materials Science 1988; 5: 382.
- [21] Huang ZP, Wang DZ, Wen JG, Sennett M, Gibson H, Ren ZF. Effect of nickel, iron and cobalt on growth of aligned carbon nanotubes. *Appl Phys A-Mater* 2002; 74 (3): 387-391.
- [22] Lee CJ, Park J, Yu JA. Catalyst effect on carbon nanotubes synthesized by thermal chemical vapour deposition. *Chem Phys Lett* 2002; 360 (3-4): 250-255.
- [23] Bladh K, Falk LKL, Rohmund F. On the iron-catalysed growth of single-walled carbon nanotubes and encapsulated metal particles in the gas phase. *Appl Phys A-Mater* 2000; 70 (3): 317-322.
- [24] Baker RTK, Barber MA, Harris PS, Feates FS, Waite RJ. Nucleation and growth of carbon deposits from nickel catalyzed decomposition of acetylene. *J Catal* 1972; 26 (1): 51-54.
- [25] Baker RTK, Harris PS. The formation of filamentous carbon. *Chem Phys Carbon* 1978; 14: 83.
- [26] Amelinckx S, Zhang XB, Bernaerts D, Zhang XF, Ivanov V, Nagy JB. A formation mechanism for catalytically grown helix-shaped graphite nanotubes. *Science* 1994; 265 (5172): 635-639.
- [27] Baker RTK, Terry S, Harris PS. Unique form of filamentous carbon. *Nature* 1975; 253 (5486): 37-39.
- [28] Tavares MT, Bernardo CA, Alstrup I, Rostrup-Nielsen JR. Reactivity of carbon deposited on nickel copper alloy catalysts from the decomposition of methane. *J Catal* 1986; 100 (2): 545-548.
- [29] Sacco A, Thacker P, Chang TN, Chiang ATS. The initiation and growth of filamentous carbon from alpha-iron in H₂, CH₄, H₂O, CO₂ and CO gas-mixtures. *J Catal* 1984; 85 (1): 224-236.
- [30] Alstrup I. A new model explaining the carbon-filament growth on nickel, iron and Ni-Cu alloy catalysts. *J Catal* 1988; 109 (2): 241-251.
- [31] Baker RTK, Harris PS, Thomas RB, Waite RJ. Formation of filamentous carbon from iron, cobalt and chromium catalyzed decomposition of acetylene. *J Catal* 1973; 30 (1): 86-95.
- [32] Baker RTK, Chludzinski JJ, Dudash NS, Simoens AJ. The formation of filamentous carbon from decomposition of acetylene over vanadium and molybdenum. *Carbon* 1983; 21 (5): 463-468.
- [33] Rodriguez NM, Kim MS, Baker RTK. Deactivation of copper nickel-catalysts due to changes in surface-composition. *J Catal* 1993; 140 (1): 16-29.
- [34] Singh MK, Singh PP, Titus E, Misra DS, LeNormand F. High density of multi-walled carbon nanotubes observed on nickel electroplated copper substrates by microwave plasma chemical vapour deposition. *Chem Phys Lett* 2002; 354 (3-4): 331-336.
- [35] Ivanov V, Fonseca A, Nagy JB, Lucas A, Bernaerts D, Zhang XB. Catalytic production and purification of nanotubules having fullerene-scale diameters. *Carbon* 1995; 33 (12): 1727-1738.
- [36] Lepora A, Métraux C, Grobety B, Emmenegger Ch, Züttel A. The evolution of iron nitrate films during CVD synthesis of carbon nanotubes: An *in-situ* high temperature X-ray diffraction investigation. in press.
- [37] Goodman DW, Kelley RD, Madey TE, Yates JT Jr. Kinetics of the hydrogenation of Co over a single-crystal nickel-catalyst. *J Catal* 1980; 63 (1): 226-234.
- [38] Klinke C, Bonard JM, Kern K. Comparative study of the catalytic growth of patterned carbon nanotube films. *Surf Sci* 2001; 492 (1-

- 2): 195-201.
- [39] Edsinger RE, Reilly ML, Schooley JF. Thermal expansion of platinum and platinum-rhodium alloys. *J Res NBS* (20899) 1986; 91 (6): 333-356.
- [40] Heaney PJ, Veblen DR. Observations of the alpha-beta-phase transition in quartz – A review of imaging and diffraction studies and some new results. *Am Mineral* 1991; 76 (5-6): 1018-1032.
- [41] Sikder AK, Sharda T, Misra DS, Chandrasekaram D, Veluchamy P, Minoura H, et al. Diamond deposition on Ni/Ni-diamond coated stainless steel substrate. *J Mater Res* 1999; 14 (3): 1148-1152.

CHAPTER 5

THE EVOLUTION OF COBALT NITRATE HEXAHYDRATE COATED GLASS SUBSTRATE DURING CVD SYNTHESIS OF CARBON NANOTUBES: AN *IN- SITU* HIGH TEMPERATURE X-RAY DIFFRACTION INVESTIGATION

K. Matzinger and B. Grobéty

Dep. of Geoscience, Applied Mineralogy Group, University of Fribourg, Pérolles, 1700 Fribourg

to be submitted to Journal of Applied Physics A

Abstract

The presence of metallic catalysts is required for the synthesis of carbon nanotubes by chemical vapor deposition (CVD). The chemical and morphological evolution of a cobalt catalyst was studied by *in-situ* X-ray diffraction, high resolution Scanning Electron Microscopy (SEM) and Transmission Electron Microscopy (TEM). Glass substrates coated with cobalt nitrate solution as catalyst were exposed to an acetylene-nitrogen and a hydrogen-acetylene-nitrogen gas mixture at temperatures of 600°C and 750°C in the camera of a high temperature X-ray powder diffractometer. The formation of carbon nanotubes (CNT) is dependent on the acetylene flow rate and the annealing temperature. CNT's were only observed where the oxidation state of cobalt is mixed (e.g. Co_3O_4) before acetylene exposure, no nanotubes could be observed when the initial phase was CoO. The cobalt nitrate solution decomposes during heating under nitrogen to a fine crystallized Co_3O_4 coating. Addition of the synthesis gas mixture reduces the oxide to small metallic cobalt particles, but no metastable carbide is formed. This transformation is accompanied by a huge solid volume loss that is responsible for the strong fragmentation of the catalyst layer. We have shown by X-ray diffraction that carbon diffuses through the metal particles during the formation of carbon nanotubes and that carbon oversaturation in metallic cobalt particles may be one of the driving forces for carbon nanotube growth.

Keywords: A. carbon nanotubes; B. chemical vapour deposition; C. x-ray diffraction; D. carbon solubility

1. Introduction

Filamentous carbon deposits on the metal surfaces of reactor vessels used for cracking of hydrocarbons have been known for a long time [1]. The presence of such carbon deposits create problems including blockage of reactors, reduction of heat transfer properties, and catalyst deactivation due to encapsulation of the metallic component [2]. The groundbreaking observation that many of the small carbon filaments have in fact tube morphology has turned the nuisance into a potential material for nanotechnology application. [3] such as electron field emitters [4,5], one-dimensional conductors [6,7], supercapacitors electrodes [8], transistor [9,10] reinforcing fibres in composite materials [11], probe tips for scanning tunnelling and atomic force microscopy [12] and molecular filtration membranes [13]. One of the most attractive applications based on CNT technology is as an electron emitter for flat panel displays [14].

Various methods such as electric arc discharge [15,16], laser vaporization [15,16], electrolysis [16], pyrolysis [15,16], plasma-enhanced or thermal chemical vapor deposition [17,18] have been developed for the production of CNTs. CVD is currently one of the most promising and flexible method with regard to applications and therefore a widely used technique to produce CNTs in larger quantities [19,20]. During the CVD process, the decomposition of gases with carbon containing species (C_2H_2 , CO_2 , etc) over a metallic catalyst at temperatures between $600^\circ C$ and $1000^\circ C$ leads to the nucleation and growth of CNTs. The CVD process has several advantages over other synthesis methods. CNTs grow at a relatively low temperature and their size can be controlled by varying the size of the catalyst [1,21,22]. Furthermore the growth rate, the density, the diameter and the crystallinity can be manipulated by changing the nature of the catalyst and varying gas flow, gas composition and growth temperature [22,23,24].

Despite a great number of systematic studies, there is still no clear picture of what really controls CNTs growth and what the catalytic mechanisms are.

Not all metal catalysts known to promote hydrocarbon cracking will lead to the formation of nanotubes. Platinum, an excellent cracking catalyst does not promote CNT nucleation [25]. The most active metals are transition metals, especially Fe, Ni, Mo and Co. Their effectiveness depends on different parameters such as the nature of the synthesis gas, the flow rate, synthesis temperature etc. Pure cobalt

has been used as catalyst (Khassin et al., 1998, CO, $800^\circ C$ [26], Flahaut et al., 1999, CH_4 , $1070^\circ C$ [27], Alvarez et al., 2001, CO, $600 - 800^\circ C$ [28], Hernadi et al., 2002, C_2H_2 , $627 - 827^\circ C$ [29], Lee et al., 2002, C_2H_2 , $950^\circ C$ [23], and Bartsch et al., 2005 [30]), but it is most attractive in combination with a second transition metal (Fe, Ni, Mo) (Flahaut et al., 1999, Co-Fe, Co-Ni, CH_4 , 1070° [27]; Lee et al., 1999, C_2H_2 , Co-Ni, 900° [18]; Alvarez et al., 2001, CO, $600 - 800^\circ C$ [28]; Yoon et al., 2002, CH_4 , Co-Mo, $1070^\circ C$ [31]; Liao et al., 2003, CO, Co-Mo, $700^\circ C$ [32]; Kohno et al., 2004, C_2H_6 , Co-Mo, Co-Pt, $700^\circ C$ [33]). CNT yields from such bimetallic catalysts are often considerably larger than for monometallic catalysts. Possible enhancing effects in bimetallic catalyst are the increase in carbon solubility, the decrease of melting temperature and the prevention of carbide formation.

In-situ monitoring of the catalyst evolution and of the interaction with the reacting system with suitable imaging, and diffraction or spectroscopic techniques are essential to understand the mechanisms of catalytic activity. Although X-ray based spectroscopy (e.g. XPS, EXAFS) and X-ray diffraction (XRD) have routinely been used for this purpose for diverse catalytic reactions [34,35,36, and references therein], there are few *in-situ* investigations performed during CNT synthesis experiments. Baker [37] observed carbon filament growth using a Transmission Electron Microscope (TEM) equipped with an environmental cell. Recently, similar *in-situ* experiments allowed to achieve atomic resolution imaging of nickel catalyst particles during the growth of carbon nanofibres [38]. X-ray diffraction is often used to characterize the synthesis products, but *in-situ* X-ray monitoring is limited so far to iron and nickel catalysts [39,40]. Alvarez et al. [28] followed by *in-situ* EXAFS and XANES spectroscopy the evolution of a Co-Mo catalyst during CNT synthesis (gas: CO) and were able to show that oxygen was present until 30 minutes after the inlet of carbon monoxide. Hernadi et al. [29] observed in samples with alumina supported cobalt catalyst exposed to acetylene only binding energies of metallic Co-Co bonds in their XPS spectra. In the samples with iron as catalyst, Fe-C bonds typical for cementite were found. Direct measurement of the growth rate of nanotubes have been realized using *in-situ* time resolved reflectivity measurements of a catalyst covered silica support during CVD synthesis [41,42].

One of the consequences of the lack of *in-situ* information is that the mechanism of carbon nanotube formation is still the subject of some controversy

particularly with regard to the active state of the catalyst particle responsible for the growth. A basic model was developed by Baker and co-workers [43] which has been extended and enlarged by many authors [15,44,45,46,47,48,49]. The key steps in their model are the adsorption and the decomposition of a hydrocarbon molecule on a metal surface to produce elemental carbon which dissolve and diffuse through the bulk and, after supersaturation is reached, reprecipitates at the surface of the particle. In suitable conditions the precipitates has the shape of a nanotube. Such a mechanism is based on the observation that the activation energies for CNT nucleation and growth on specific metals are very similar to the activation energies for carbon bulk diffusion in the same metals [50,51]. The question that is still open is, if carbides form during this reaction process and, if they are present, what catalytic activity they have. Rodriguez stressed that the active species for filament and nanotube formation are metals and not carbides [1]. Electron diffraction analysis carried out by Oberlin and co-workers [19] revealed the existence of cementite (Fe_3C) together with carbon filaments after the interaction of iron with benzene/hydrogen. Rodriguez and co-workers [52] investigated the interaction of copper-nickel particles with ethylene (C_2H_4) but no evidence for the existence of a bulk carbide was found in these experiments. In contradiction to the above mentioned experiments Ni_3C phases were observed on an electrodeposited nickel coating on a copper substrate treated by ammonia [53]. Ivanov [54] claimed that cobalt carbide was the active catalyst, and not Co, in his arc discharge synthesis using cobalt nitrate coated on a SiO_2 substrates as precursor. Although they are often metastable carbides at the synthesis conditions, there is no agreement about whether they are active species for CNTs growth or not [1,19,53,54]. A major problem with most investigations is that they were done *ex-situ* and conclusions were drawn by comparing pre- and post-synthesis results (lit). Lepora et al. [55] analysed iron catalysts *in-situ* and showed that the catalyst underwent major chemical changes during the synthesis which are impossible to deduce from post-synthesis analyses. They showed that cementite is formed immediately after acetylene is added to the atmosphere, but that the carbide decomposes after a certain reaction duration. Matzinger et al. analysed nickel catalysts on glass platelets exposed to acetylene/nitrogen gas mixture but no existence of nickel carbides occurred [39].

In order to better understand the catalytic growth

various scientists systematically examined the parameter temperature, catalyst composition and concentration [17,22,24,56] but scarce information of what really happened to the catalyst during CVD process can be found. This paper focuses on the evolution of a cobalt-based catalyst under a nitrogen-acetylene atmosphere between 600°C and 750°C .

2. Experimental Methods

2.1 Starting Materials

The substrate (thin glass AF 45, PGO GmbH, Iserlohn, Germany) was coated with a cobalt nitrate hexahydrate ($\text{Co}(\text{NO}_3)_2 \cdot 6(\text{H}_2\text{O})$; Fluka, 60833, Buchs, Switzerland, crystallized $\geq 98.0\%$) and was either deposited as crystals or as solution dissolved in ethanol onto the glass substrate. The support material, an alkali free borosilicate glass, has a softening temperature (883°C) well above the temperatures used during the experiments. About 5 mg of crystals or one drop of nitrate solution (approx. 35 - 40 μl) in three different concentrations, 1 mol/l, 0.1 mol/l and 0.05 mol/l of $\text{Co}(\text{NO}_3)_2 \cdot 6\text{H}_2\text{O}$, were deposited by pipetting or spin coating on the substrate and subsequently dried on air. The crystals were slightly wetted with ethanol to guarantee a better adhesion to the substrate. The glass platelets were chosen because of their non-crystallinity and ease to use in the XRD set-up.

The gases were of high purity grade: N_2 99.995%, impurities: $\text{O}_2 < 10$ ppm, $\text{H}_2\text{O} < 10$ ppm; C_2H_2 99.6%, impurities: N_2 , $\text{PH}_3 < 10$ ppm. All gases were used without prior cleaning nor drying.

2.2 High Temperature Diffractometer Experiments

The apparatus for the *in-situ* diffractometry was a high temperature X-ray camera (model HTK 10, Anton PAAR, Graz, Austria) controlled by a temperature control unit (TCM 2000, Anton PAAR, Graz, Austria) mounted on a Philips PW 1830 diffractometer as described in Matzinger et al. [39]. Gas flow was controlled by two mass flow controllers (AFC-2600, AALBORG, Orangeburg, New York, USA) and the handling of the gases was by the aid of a command module (2PROC, AALBORG) and three electromagnetic valves.

The glass substrates were placed on the heated platinum strip in the middle of the cylindrical camera. Temperature is controlled by a thermoelement on the lower side of the platinum strip. In contrast to externally heated gas mixing furnaces used in conventional CVD synthesis of carbon nanotubes, there is a large temperature gradient between the hot-spot and the water-cooled camera walls that will certainly affect the reaction in the gas phase. The thermocouple was calibrated via thermal expansion of platinum [57] and via α - β quartz transition at 573°C [58], with an estimated uncertainty of $\pm 5^\circ\text{C}$.

The phase evolution was studied for two different temperatures 600°C identical to the synthesis conditions used in a gas-mixing furnace by Emmenegger et al. [5], and 750°C. The goniometer is equipped with a scintillation detector and the phase changes were monitored by scanning individual peaks of the reactant phases (cobalt nitrate hexahydrate: 27.12° (013), JCPDS No. 25-1219; cobalt nitrate: 40.42° (222), JCPDS No. 19-0356; cobalt oxide (Co₃O₄): 36.85° (311), JCPDS No. 42-1467; cobalt oxide (CoO): 42.40° (200), JCPDS No. 43-1004) and product phase (cobalt: 44.21° (111), JCPDS No. 15-0806). Care has been taken that all diffractograms contained minimum one platinum peak originating from the sample holder. (platinum: 39.76° (111), 46.24° (200), 67.45° (220), 81.82° (311), JCPDS No. 04-0802). The platinum reflections served base for calibration. The diffractograms were recorded in step scan mode between 10° and 80° (2θ) with a step size of $0.02^\circ/\text{step}$ and a measuring time of 1 sec/step. These parameters represent the best compromise between time resolution and sensitivity.

The camera was flushed with nitrogen and temperature was raised at a rate of $70^\circ\text{C}/\text{min}$ to the desired temperature under nitrogen. After an annealing time of 10 minutes, acetylene (25 sccm or 75 sccm) was added to the nitrogen atmosphere. Parameters such as cobalt nitrate hexahydrate concentration, temperature, gas flow rate and time were systematically varied between experiments. Grain size determination was obtained by the Scherrer equation and confirmed by SEM observations.

2.3 Electron Microscopy

The Scanning Electron Microscope (Philips FEI XL30 SFEG SIRIUS) investigations were

performed on drop-coated samples (0.01 mol/l) on glass platelets (AF45). All samples were coated by a BAL-TEC SCD 050 Sputter-coater with a 10 nm thick Au-layer. The SEM settings for scan and high resolution mode were defined by an acceleration voltage between 7 to 10 keV. Working distance for all samples was adjusted to 5 mm. Due to the strong magnetic properties of most of the SEM specimen scanning has to be dealt with great care.

3. Results

3.1 Phase Evolution of the Catalyst

The cobalt nitrate hydrate ($\text{Co}(\text{NO}_3)_2 \cdot X \text{H}_2\text{O}$) appears in 5 different states of hydration (X : 1, 2, 4, 6, 8). We used cobalt nitrate hexahydrate as starting material. The observed X-ray peaks corresponded to the reference pattern (JCPDS No. 25-1219), although some additional peaks occur which belonged to less hydrated phases. The starting material dissolved completely in ethanol.

The lowest solution concentration for which XRD signals from the catalyst are observable is 0.1 mol/l. The number and positions of peaks in the X-ray diffractograms did not change with nitrate concentration and were also the same for the samples in which crystal were used without prior dissolution as samples [Figure 1].

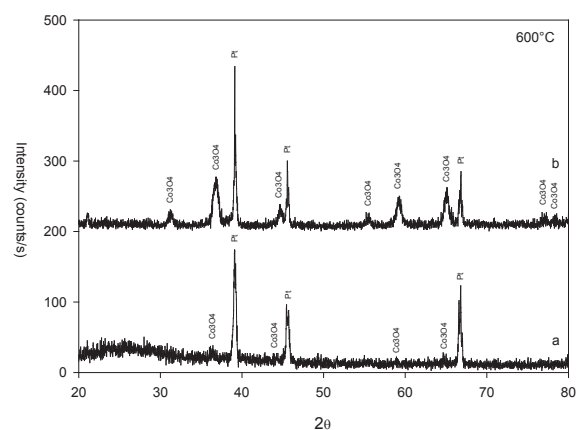


Fig. 1: X-ray diffractograms of samples annealed for 2 hours at 600°C under nitrogen (a) solution of 0.1 mol/l dissolved in ethanol. (b) Crystals dissolved in ethanol.

Under nitrogen, as well as under air, the dehydration reaction of cobalt nitrate hydrate starts at 55°C [59]. During heating up to 250°C cobalt nitrate hydrate showed different behaviour depending upon the atmosphere composition. Under air a progressive

dehydration occurs from the tetrahydrate phase at 60°C to the dihydrate phase between 70°C to 110°C and to the monohydrate phase between 110°C up to 230°C. During the last state of dehydration all X-ray peaks disappear almost completely, indicating the formation of an amorphous layer. At 250°C, peaks of the spinel phase Co_3O_4 (JCPDS No. 42-1467) were visible. Under nitrogen atmosphere the dehydration reaction proceeded faster. The cobalt nitrate hydrate decomposed not to an amorphous phase but to crystalline cobalt nitrate at 150°C (JCPDS No. 19-0356). The nitrate was stable up to a temperature of 210°C. Above this temperature, the nitrate was replaced by a fine grained oxide mixture composed of Co_3O_4 and CoO that coexisted with cobalt nitrate up to 250°C. Between 250°C and the maximum temperature applied in the present experiments (750°C), only Co_3O_4 and/or CoO occurred [Figure 2]. No further phase changes neither in normal nor

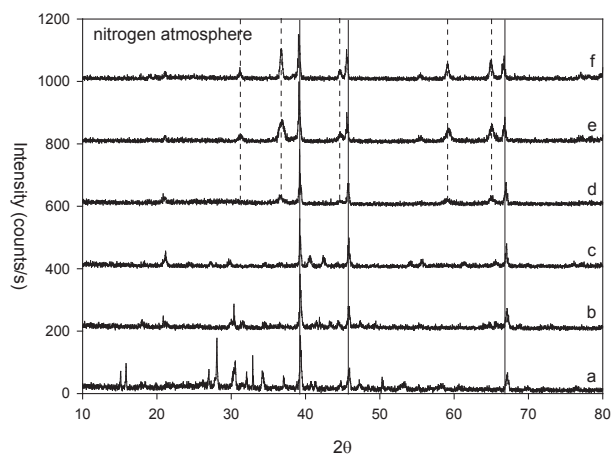


Fig. 2: X-ray diffractograms of quenched samples annealed at various temperatures under nitrogen heating conditions. (a) Cobalt nitrate hydrate crystals at room temperature (25°C). Sample annealed at 100°C (b). Cobalt nitrate hydrate dehydrates subsequent from higher dehydration states to lower and formation of cobalt nitrate takes place. Low signal intensity because of formation of a probable X-ray amorphous layer occurs (c) at 200°C and only cubic cobalt nitrate can be observed. At 300°C all cobalt nitrate has been decomposed to Co_3O_4 (d). Sample annealed at 600°C reveals only cobalt oxide peaks (e) and (f) at 750°C. The stippled lines represent Co_3O_4 position, continuous lines that for platinum.

in nitrogen atmosphere have been observed. The X-ray derived grain size of both oxides continuously increased with heating. The average value at 600°C for the spinel phase varied between 13 nm and 20 nm [Figure 3]. The ratio $\text{Co}_3\text{O}_4/\text{CoO}$ changed from experiment to experiment and ranged from pure Co_3O_4 to pure CoO . The introduction of hydrogen at 400°C after heating under nitrogen led to an instant reduction of the cobalt oxide(s) to pure metallic

cobalt. The size of the cobalt particles increased to 25 – 30 nm during successive heating under hydrogen up to 600°C.

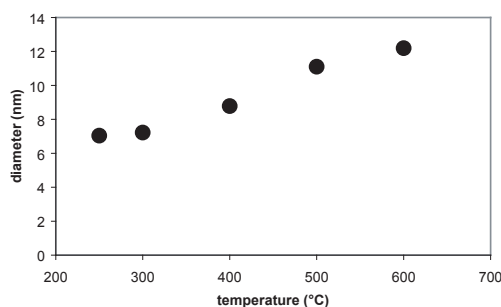


Fig. 3: Cobalt oxide (spinel phase) grain size evolution during heating sequence from 250°C to 600°C.

At 600°C acetylene was introduced at two different flow rates. Only flow rates above 25 sccm (20 ml/min) were sufficient to obtain complete reduction of the oxides to metallic cobalt. In samples containing only Co_3O_4 , reduction started 60 seconds after the acetylene inlet. CoO formed as intermediate phase and reached a maximum after 90 sec. After 120 seconds all Co_3O_4 has been reduced. Metallic Co appeared for the first time after about 120 seconds.

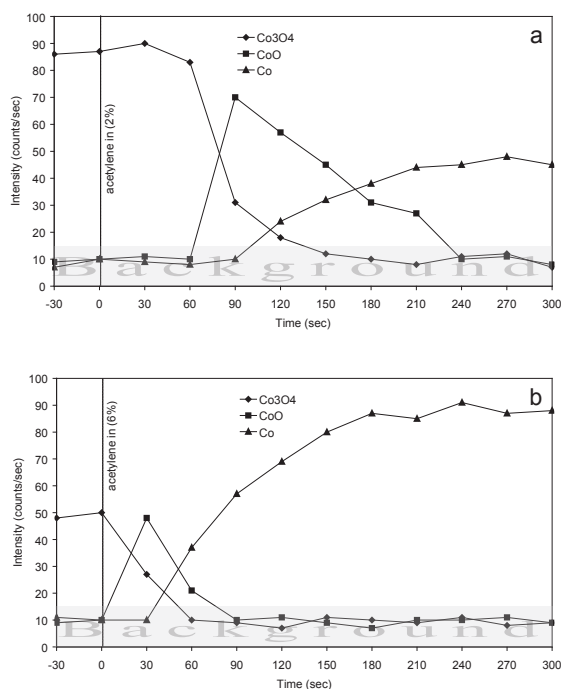


Fig. 4: Phase evolution of cobalt oxide precursors during exposure of (a) 25 sccm and (b) 75 sccm C_2H_2 at 600°C. Increasing flow rate accelerates the formation of metallic cobalt.

After 240 sec, complete reduction of all oxides was achieved. [Figure 4a]. At 75 sccm acetylene flow

rate, Co_3O_4 disappears after 60 seconds and after 90 seconds all CoO has been fully reduced to pure Co . Metallic Co was detected after 60 seconds [Figure 4b]. With CoO as oxide precursor before acetylene inlet, the reduction to pure cobalt was accelerated and took not longer than 2 minutes. The final product of the reduction reactions was in all experiments metallic cobalt. No cobalt carbides were detected neither directly after C_2H_2 flooding of the chamber nor after 3 hours. At 750°C the evolution was identical but occurred faster. In samples pre-treated with hydrogen and consisting of metallic cobalt at acetylene inlet, no phase changes within the catalyst have been observed.

Peak positions of metallic cobalt formed from the spinel phase showed a considerable shift from the expected values towards lower 2θ -angles [Figure 5a]. The shift observed in experiments where cobalt was formed from the reduction of CoO was considerably smaller [Figure 5b]. With synthesis time, the peak shifts became smaller and after 3 hours values characteristic of pure cobalt at 600°C were reached. In experiment where the oxides were reduced by hydrogen, the peak shift was even smaller [Figure 5c].

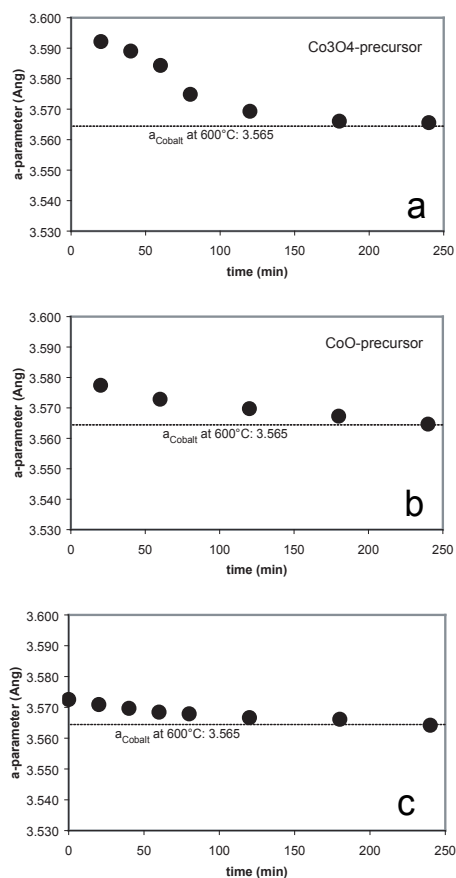


Fig. 5: Peak shift of metallic cobalt with ongoing acetylene exposure when using (a) Co_3O_4 or (b) CoO as precursors and peak shift of metallic cobalt when treated with hydrogen (c).

Before exposure to acetylene the average X-ray derived grain size of both CoO and spinel particles was between 15 and 20 nm. The grain size of the metal particles was smaller than the precursor oxide particles. The values remained constant or showed a gentle increase with synthesis time [Figure 6a]. The metal particles obtained by hydrogen reduction at 400°C had an average of 15 nm, which increased with treatment time to a maximum value of 25 to 30 nm [Figure 6b]. This value did not change after subsequent acetylene treatment [Figure 6c].

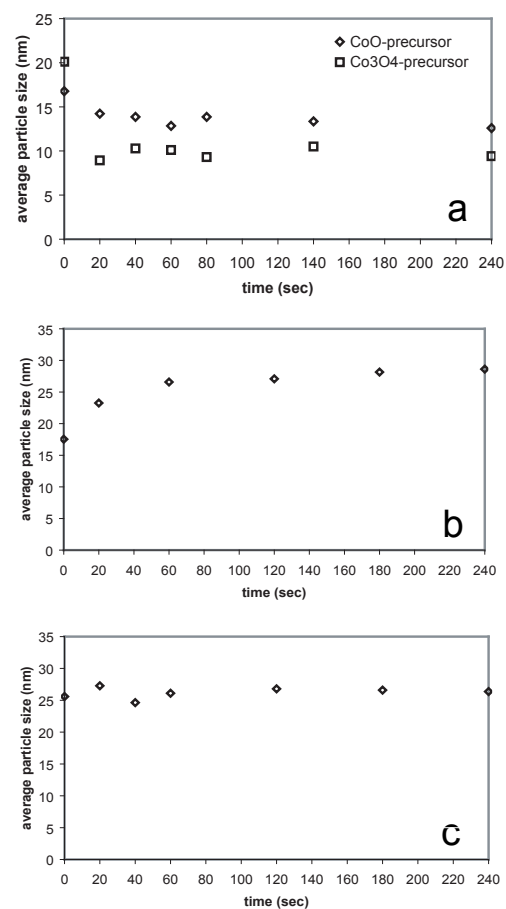


Fig. 6: Grain size evolution of metallic cobalt particles exposed to acetylene (a) when using different precursors, (b) exposed to hydrogen or (c) pre-treated with hydrogen and subsequent acetylene exposure.

3.2 Morphological Evolution of the Catalyst and Formation of Nanotubes

The SEM pictures for the description of the morphological evolution were taken from samples prepared by depositing a drop of the 0.01 mol/l cobalt nitrate solution on glass platelets. At 100°C the partially hydrated nitrate layer consisted either of a fine meshwork of reticulated needle-like crystals with a length of about $1\ \mu\text{m}$ and forming large bundles or a rough, bumpy surface with oval holes (diameter: $0.5 - 1\ \mu\text{m}$) [Figure 7a]. After complete

dehydration ($> 200^{\circ}\text{C}$) very fine cube shaped cobalt nitrate crystals were observed with an average particle size of about 10 nm [Figure 7b].

The size of the spinel grains resulting from the

decomposition of the nitrate had slightly larger diameters, 10 – 30 nm at 400°C [Figure 7c], which remained the same after further heating to 600°C [Figure 7d].

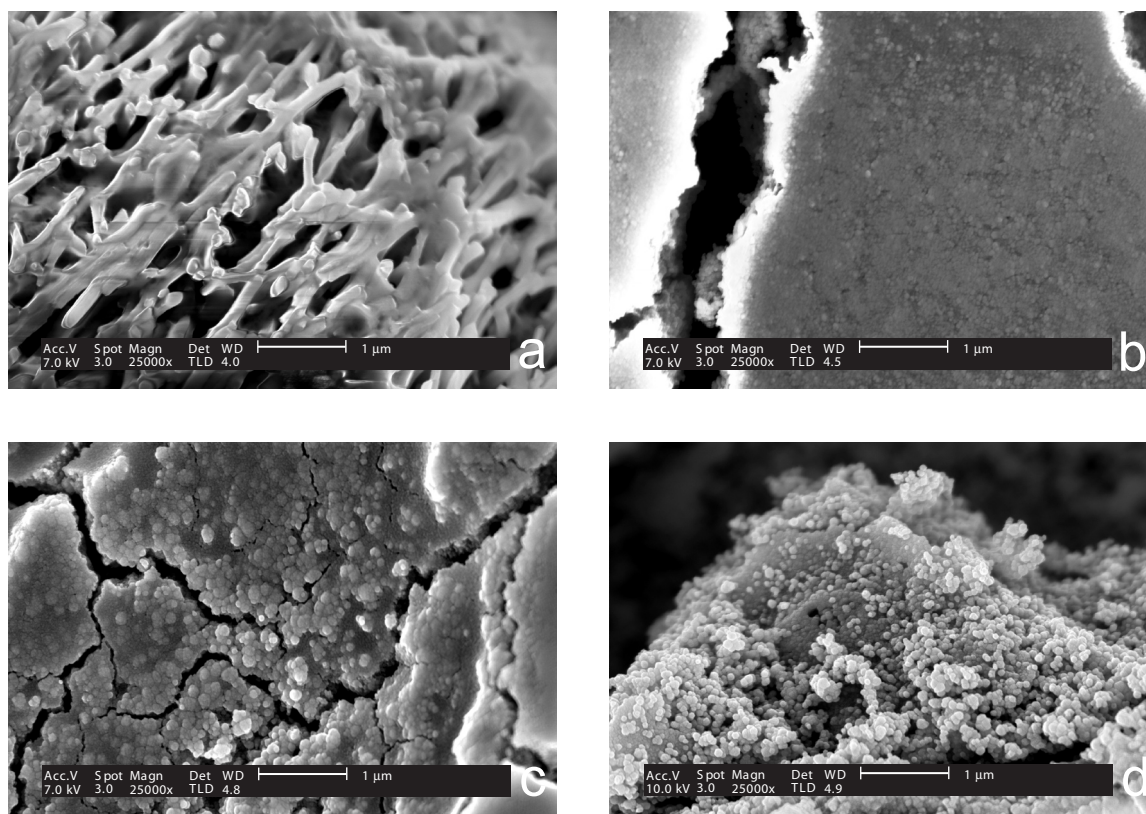


Fig. 7: SEM images of 0.05 mol/l cobalt nitrate hydrate samples dissolved in ethanol and heated up on various temperatures under nitrogen atmosphere condition. Sample annealed for 2 hours at (a) 100°C , (b) 200°C , (c) 400°C , (d) 600°C .

Carbon nanotubes only were growing, when Co_3O_4 occurred before acetylene inlet. No nanotube growth has been observed when the cobalt oxide appears in the CoO state, independent of temperature and acetylene flow rate. In the latter case, the surface shows signs of strong coalescence of carbon-covered cobalt grains [Figure 8] leading to mushroom-like particles with diameters up to one micron. After 1 minute

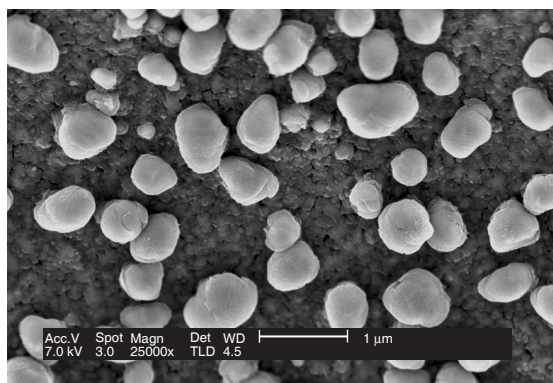


Fig. 8: Carbon-covered metallic cobalt grains after acetylene treatment when using CoO as precursor.

exposure to acetylene (25 sccm), SEM pictures of samples with the spinel phase as precursor showed a clear increase in porosity and crack density, but no nanotubes yet [Figure 9a]. The first tube-shaped carbon deposition on the glass support are observed about 2 minutes after the addition of acetylene and consisted of rods some tens of nanometer thick and some hundred nanometers in length. The cobalt particles close to the surface of thicker areas coalesced leading to a smoother topography. With increasing annealing time (> 10 min), longer and thinner nanotubes appear which are randomly oriented [Figure 9b]. Samples annealed for one hour exhibit a loose assemblage of fine nanotubes with diameter ranging between 10 and 30 nm and lengths up to several microns [Figure 9c].

An increase of the acetylene flow rate at 600°C by a factor three, has not only a strong enhancing effect on the nanotube yield [Figure 9d], but accelerates also the first appearance of nanotubes (~ 1 minute). The nanotube density for a synthesis temperature of

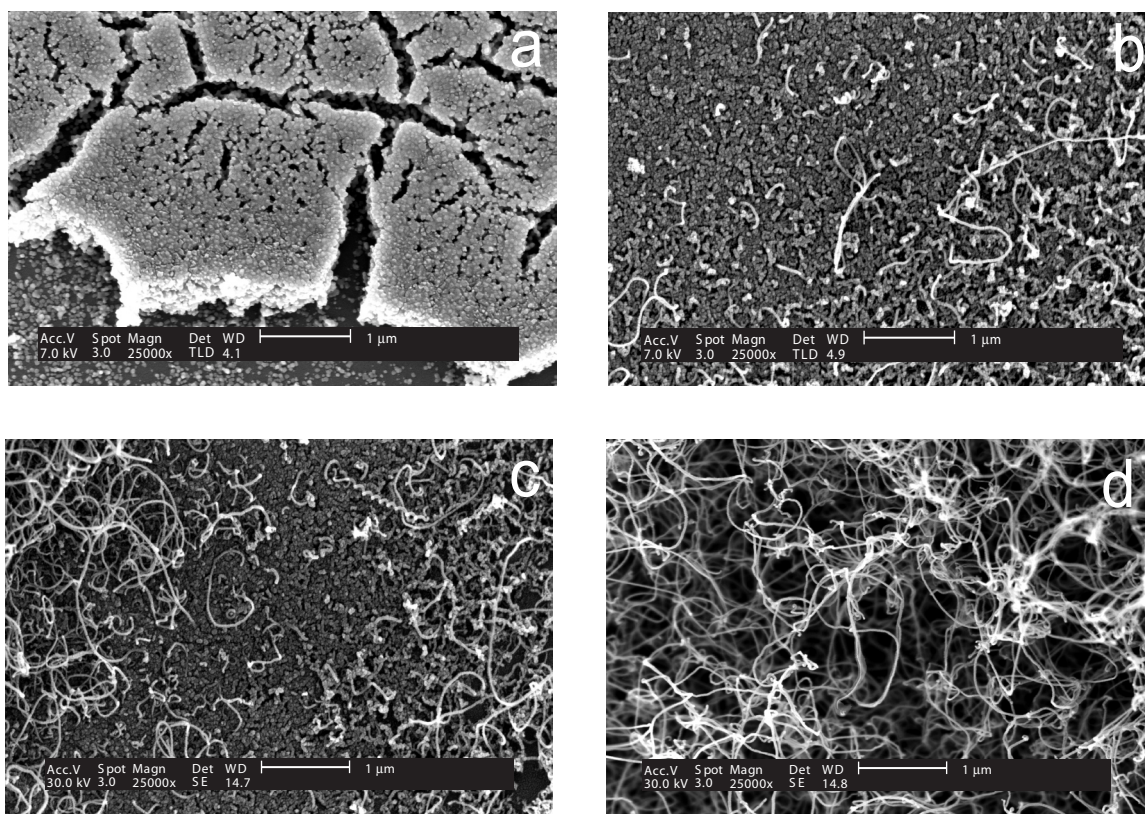


Fig. 9: SEM images of 0.05 mol/l cobalt nitrate hydrate samples dissolved in ethanol and treated at 600°C with acetylene for (a) 1 minute, (b) 2 minutes, (c) 10 minutes and (d) 60 minutes.

750°C [Figure 10a] is similar to the concentration observed for 600°C [Figure 10b]. The average diameter of the tubes varies between 10 and 70 nm and their length reaches several microns. A pronounced coalescence and formation of larger

cobalt particles was observed, similar to the samples, which had CoO as precursors (s. Fig. 7). These large particles had a characteristic zoned contrast in BSE images, e.g. a bright centre with a darker rim [Figure 10a].

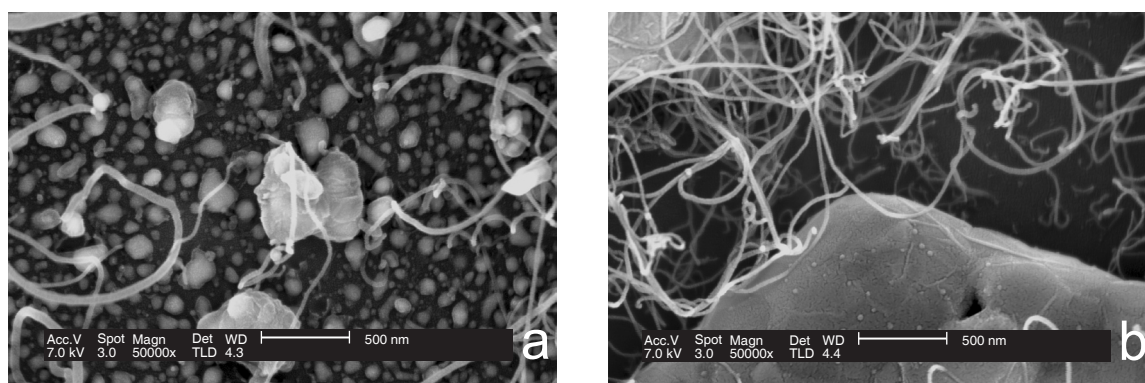


Fig. 10: SEM images show similar nanotube density for constant gas flow rate at (a) 750°C and (b) 600°C.

In the samples pre-treated with hydrogen [Figure 11a], only short (0.2 – 1.0 μm) and very thick (20 – 100 nm) carbon filaments were observed after

10 minutes of acetylene exposure [Figure 11b]. No further growth or nucleation of filaments occurred after this time (60 minutes) [Figure 11c].

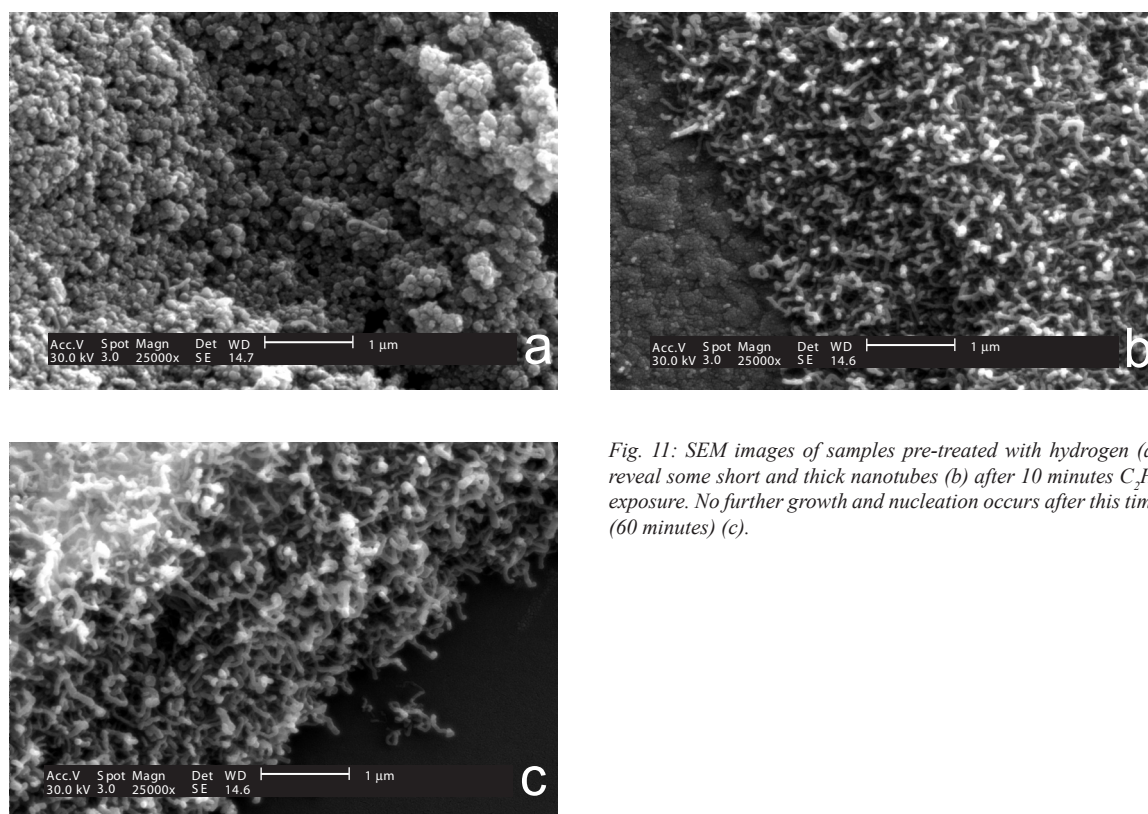


Fig. 11: SEM images of samples pre-treated with hydrogen (a) reveal some short and thick nanotubes (b) after 10 minutes C_2H_2 exposure. No further growth and nucleation occurs after this time (60 minutes) (c).

4. Discussion

The variable presence of either Co_3O_4 resp. CoO or both after termination of the heating step is due to oxygen impurities of the nitrogen atmosphere in the chamber. The partial pressure of oxygen O_2 in equilibrium with the Co_3O_4/CoO buffer at $600^\circ C$ is $1.5 \cdot 10^{-4}$ bar, which is in the same order of magnitude as the oxygen impurities in the nitrogen gas used for the experiments (10 ppm). Slight differences in oxygen concentration from bottle to bottle and oxygen leaking into the gas conduits and the chamber are, therefore, the likely reason for the difficulties to get reproducible phase composition before acetylene exposure.

The sudden changes in average particle size of the catalyst precursors is related to solid volume losses associated with the different phase transformation occurring during the heating procedure. The first and largest solid volume reduction occurs at the breakdown of the nitrate to the oxide phases. There is not a large difference in solid volume loss between the transformation of nitrate to Co_3O_4 (78.36 vol%) and the transformation directly to CoO (81 vol%). The almost equal grain size of the two phases observed at $250^\circ C$ is compatible with these similar solid volume losses. The reduction of the spinel phase

to metallic cobalt is associated with a slightly larger volume reduction (49%) than the reduction of CoO to the metal phase (42.37%), which may explain the slightly larger grain size of cobalt resulting from the latter transformation (s. Fig. 6a). Substantial grain growth of metallic cobalt seems only to occur in samples pretreated with hydrogen between $400^\circ C$ and $600^\circ C$.

Grains size seems not to be the limiting factor for the formation of nanotubes in the present experiments. The average cobalt particle size in the experiment with the spinel phase as precursor is similar to the ones with CoO as precursor (13 – 35 nm at $600^\circ C$). These diameters are smaller than the upper limits reported in the literature beyond which no tubular carbon is formed. Nerushev et al. [60] observed growth of nanotubes on iron particles as large as 500 nm. The maximum “fertile” size for nickel particles observed by Kukovitzky et al. [61] was 100 nm. Size selectivity seems, therefore, not to be the reason for the very small concentration of nanotubes in the hydrogen pretreated samples and samples with CoO as precursors.

The metallic cobalt present in the reduced samples has fcc structure, which is stable at this temperature. The same cubic phase was obtained in CNT synthesis experiments with $Co(CO_3)NO$ as precursor [62,63].

The lattice parameter increase observed in the present experiment is due to carbon dissolved in the metal particle. The relationship between concentration of carbon in solution at room temperature and the lattice parameter is given by Cadeville and Lapierre [64]:

$$a_{\text{ssL}} (\text{\AA}) = a_{\text{Co}} + 0.0076 * C (\text{at}\%) \quad (1)$$

This relationship is strictly linear only up to 1 at% C. Above that concentration, carbon pair and cluster formation within the alloy reduce the lattice expansion and the value calculated by the above equation gives only a minimum concentration. The lattice parameter measured at the first appearance of metallic cobalt in the sample with spinel precursors is 3.572 \AA (= back calculated from the lattice parameters observed at 600°C to room temperature), which corresponds to a minimum of 3.5 ± 0.5 at% carbon. The concentration decreases with time to reach the value of the pure metal after approximately 100 minutes of acetylene exposure. The lattice parameter in the case of CoO as precursor is only (3.550 \AA), which corresponds to a carbon solubility of 1.58 ± 0.5 at%. The value for the hydrogen treated sample is smaller than both previous values (1.05 ± 0.5 at% H₂). The previous authors, who observed the cubic phase [62,63], gave no indications about possible peak shifts. The carbon solubility in transition metals as function of bulk solubility S_0 , temperature T , particle radius r , volume of the metal molecule V , and surface tension σ (surface tension data taken from German [65]) is given by the equation from Adamson [66]:

$$S = S_0 * \exp\left(\frac{4 * \sigma * V}{k * T * d}\right) \quad (2)$$

The bulk solubility of cubic cobalt at 600°C extrapolated from high temperature data given by Dunn et al. [67] is 0.1 at%. A sensible increase of the solubility is only observable for particles with diameters smaller than 5 to 6 nm [Figure 12]. The carbon concentration observed in our samples is, therefore, about one order of magnitude above the equilibrium saturation. The samples in which CNT formation have been observed e.g. with the spinel phase as precursor, have an initial carbon concentration twice as high as the samples without. The supersaturation is possible, because the carbon species, which is in contact with the metal particles is metastable relative to the stable phase e.g. graphite.

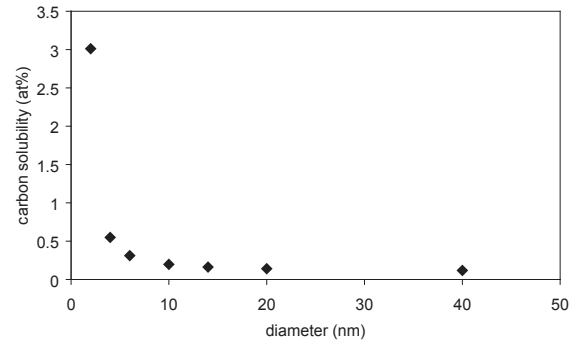


Fig. 12: Carbon solubility in cobalt particles at 600°C in dependence of the grain size.

The degree of supersaturation was estimated by the chemical potential difference between graphite and the metastable phase present [68]:

$$x = x_0 * \exp\left(\frac{\Delta G_{\text{gr} \rightarrow \text{mph}}}{k * T}\right) \quad (3)$$

The upper limit for the supersaturation x/x_0 given in the literature is around 4. Estimations obtained from metal-carbon eutectic shifts [69] give smaller values, between 1.5 and 2. The supersaturation observed in our samples is considerably larger than indicated by these previous authors. The saturation factor value of 4 by Parmon [68] was obtained using the difference in free energy between graphite and as metastable phase amorphous carbon. The value of 1.05 ± 0.5 at% C observed in the sample pretreated with hydrogen is compatible with such a supersaturation value. For the samples, which had oxides as precursors, however, the supersaturation is much larger. The question is, if amorphous carbon is a correct representative for the carbon species, produced through the decomposition of acetylene. Carbon adsorbed on the metal surface may have a larger free energy than amorphous carbon thus allowing a higher supersaturation to be reached. Another possible explanation for the high supersaturation may be that a certain amount of particles are not solid but liquid during the synthesis run. Liquid metals have indeed a much higher carbon solubility than the corresponding solids. The reduced particle size is a possible factor that may lower the melting temperature. The observed peak shift would be dominated by oversaturated particles that solidified due to growth or coalescence with other grains. The dependence of the melting temperature with particle radius is given by Geguzin [70] as:

$$T_{mp} = T_0 \exp\left(-\frac{2 \cdot \sigma \cdot V_m}{r \cdot \Delta H_m}\right) \quad (4)$$

with T_0 the bulk melting temperature, ΔH_m the melting enthalpy, σ the surface tension and V_m the molar volume of the melting phase. For transition metals a dramatic decrease of T_{mc} for radii < 4 nm occurs [Figure 13]. For the smallest average particle

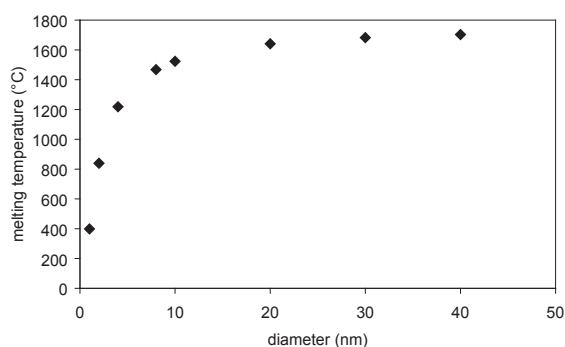


Fig. 13: Melting temperature decrease of metallic cobalt with decreasing grain size.

radii observed in our experiments the calculated melting temperature is still considerably higher than the experiment temperature (e.g. $\approx 1430^\circ\text{C}$ for an 8 nm sized particle diameter). It can, however, not be excluded, that some particles have radii below the critical radii for 600°C (2 – 3 nm). An additional factor lowering the melting temperature is the carbon in solution. Judging from the particle sizes seen in SEM pictures the majority of the particles, also the ones seeding nanotubes, are considerably larger and this effect is certainly not the main culprit for the high supersaturation observed.

The increasing supersaturation from samples pretreated with hydrogen over samples with CoO to samples with Co_3O_4 as precursor, indicates that the oxide breakdown play a role in the early carbon incorporation into the metal particle and the degree of reached supersaturation. During the spinel breakdown, more oxygen is released than during the breakdown of CoO. This may favour counter diffusion and incorporation of carbon into the resulting metal particle. For the hydrogen pretreated sample, no oxygen release occurs with acetylene inlet e.g. no carbon diffusion enhancing effect is to be expected.

The degree of supersaturation is an important parameter in proposed models for CNT nucleation

growth. Kuznetsov et al. [71] have calculated the minimum radius of a graphite-like nucleus on the surface of a catalyst particle that will survive and develop into a carbon nanotube. For a supersaturation factor of 2 and a temperature of 600°C , the critical radius, which is equal to the inner diameter of the smallest tube that can grow, is around 5 nm. There are many examples of CVD experiments, where nanotubes with much smaller diameters have been grown at these temperatures [28,60]. A supersaturation factor of 30 or more, as observed in the present experiment, would reduce the critical radius to 1 nm, which is more compatible with the smallest diameters observed.

The decrease in carbon concentration indicates that the supply is diminishing with time. There are different models presented in the literature for the slowing growth rate and final stoppage of CNT growth. For base growth, the growing nanotubes themselves may seal the catalytic layer off from the feed gas. This is especially true for dense, aligned growing CNT carpets. In our samples, the CNT concentration was too low to cut off the catalytic layer from the acetylene gas. The second model used to explain the stop in CNT growth is catalytic poisoning [42]. The poisoning occurs either by deactivation of active sites at surface of the catalyst particle or by the formation of a carbonaceous layer on the surface of the particle. This carbonaceous layer decreases the nanoparticle surface available for catalytic decomposition of the incoming feedstock molecules; thus it restricts the source flux of carbon atoms available for CNT growths. The characteristic time scale for growth stoppage they observed in their experiments, made under similar conditions as the present experiments, was in the order of 500 to 1000 seconds e.g. considerably shorter than the time it took in the present experiment for the carbon supersaturation to reach equilibrium. The products, however, obtained by Poretzky et al. [42] were very dense carpets and it is likely that the main reason for the growth stoppage was not catalytic poisoning but the cut off of the catalytic particles from the feed gas.

5. Conclusions

The present experiments give for the first time direct evidence for the presence of an oversaturated carbon solution during CNT growth. The degree of oversaturation seems to be a crucial parameter for the possible growth of CNT's

6. References

- [1] Rodriguez NM. A review of catalytically grown carbon nanofibres. *J Mater Res* 1993; 8(10): 3233-3250
- [2] Bennett MJ. Carbon deposition: A major technological problem. *Mater Corros* 1998; 49 (5): 345-351
- [3] Ijima S. Helical microtubules of graphitic carbon. *Nature* 1991; 354 (6348): 56-58
- [4] Kuettel OM, Groening O, Emmenegger C, Schlapbach L. Electron field emission from phase pure nanotube films grown in a methane/hydrogen plasma. *Appl Phys Lett* 1998; 73 (15): 2113-2115
- [5] Emmenegger C, Mauron P, Zuetzel A, Nuetzenadel C, Schneuwly A, Schlapbach L, et al. Carbon nanotube synthesized on metallic substrates. *Appl Surf Sci* 2000; 162: 452-456
- [6] Hamada N, Sawada S, Oshiyama A. New one-dimensional conductors – graphitic microtubules. *Phys Rev Lett* 1992; 68 (10): 1579-1581
- [7] Saito R, Fujita M, Dresselhaus G, Dresselhaus MS. Electronic-structure of chiral graphene tubules. *Appl Phys Lett* 1992; 60 (18): 2204-2206
- [8] Niu CM, Sichel EK, Hoch R, Moy D, Tennent H. High power electrochemical capacitors based on carbon nanotube electrodes. *Appl Phys Lett* 1997; 70 (11): 1480-1482
- [9] Tans SJ, Verschueren ARM, Dekker C. Room-temperature transistor based on a single carbon nanotube. *Nature* 1998; 393 (6680) 49-52
- [10] Tans SJ, Devoret MH, Dai H, Thess A, Smalley RE, Geerligs LJ, et al. Individual single-wall carbon nanotubes as quantum wires. *Nature* 1997; 386 (6624): 474-477
- [11] Zuetzel A, Sudan P, Mauron P, Kiyobayashi T, Emmenegger C, Schlapbach L. Hydrogen storage in carbon nanostructures. *Int J Hydrogen Energy* 2002; 27 (2): 203-212
- [12] Dai H, Hafner JH, Ginzler AG, Colbert DT, Smalley RE. Nanotubes as nanoprobe in scanning probe microscopy. *Nature* 1996; 384 (6605): 147-150
- [13] Che GL, Lakshmi BB, Fisher ER, Martin CR. Carbon nanotubule membranes for electrochemical energy storage and production. *Nature* 1998; 393 (6683): 346-349
- [14] Fan SS, Chapline MG, Franklin NR, Tomblor TW, Cassel AM, Dai H. Self-oriented regular arrays of carbon nanotubes and their field emission properties. *Science* 1999; 283 (5401): 512-514
- [15] Harris PJF. Carbon nanotubes and related structures – New materials for the twenty-first century. Cambridge University Press 1999; 18-24
- [16] Journet C, Bernier P. Production of carbon nanotubes. *Appl Phys A-Mater* 1998; 67 (1): 1-9
- [17] Jung M, Eun KY, Lee JK, Baik YJ, Lee KR, Park JW. Growth of carbon nanotubes by chemical vapour deposition. *Diam Relat Mater* 2001; 10 (3-7): 1235-1240
- [18] Lee CJ, Kim DW, Lee TJ, Choi YC, Park YS, Lee YH, et al. Synthesis of aligned carbon nanotubes using thermal chemical vapor deposition. *Chem Phys Lett* 1999; 312 (5-6) 461-468
- [19] Oberlin A, Endo M, Koyama T. Filamentous growth of carbon through benzene decomposition. *J Cryst Growth* 1976; 32 (3): 335-349
- [20] Dresselhaus MS, Dresselhaus G, Sugihara K, Spain IL, Goldberg HA. Graphite fibers and filaments. Springer Series in Materials Science 1988; 5: 382
- [21] Huang ZP, Wang DZ, Wen JG, Sennett M, Gibson H, Ren ZF. Effect of nickel, iron and cobalt on growth of aligned carbon nanotubes. *Appl Phys A-Mater* 2002; 74 (3): 387-391
- [22] Huh Y, Lee JY, Cheon J, Hong YK, Koo JY, Lee TJ, et al. Controlled growth of carbon nanotubes over cobalt nanoparticles by thermal chemical vapour deposition. *J Mater Chem* 2003; 13: 2297-2300
- [23] Lee CJ, Park J, Yu JA, Catalyst effect on carbon nanotubes synthesized by thermal chemical vapour deposition. *Chem Phys Lett* 2002; 360: 250-255
- [24] Lee CJ, Park J, Huh Y, Le JY. Temperature effect on the growth of carbon nanotubes using thermal chemical vapor deposition. *Chem Phys Lett* 2001; 343: 33-38
- [25] Bladh K, Falk LKL, Rohmund F. On the iron-catalysed growth of single-walled carbon nanotubes and encapsulated metal particles in the gas phase. *Appl Phys A-Mater* 2000; 70 (3): 317-322
- [26] Khassin AA, Yurieva TM, Zaikovskii VI, Parnon VN. Effect of metallic cobalt particles size on occurrence of CO disproportionation. Role of fluidized metallic cobalt-carbon

- solution in carbon nanotube formation. *React Kin and Catal Lett* 1998; 64 (1): 63-71
- [27] Flahaut E, Govindaraj A, Peigney A, Laurent Ch, Rousset A, Rao CNR. Synthesis of single-walled carbon nanotubes using binary (Fe, Co, Ni) alloy nanoparticles prepared *in situ* by the reduction of oxide solid solutions. *Chem Phys Lett* 1999; 300: 236-242
- [28] Alvarez WE, Kitiyanan B, Borgna A, Resasco DE. Synergism of Co and Mo in the catalytic production of single-wall carbon nanotubes by decomposition of CO. *Carbon* 2001; 39: 547-558
- [29] Hernadi K, Konya Z, Siska A, Kiss J, Oszko A, Nagy JB, Kirisci I. On the role of catalyst, catalyst support and their interaction in synthesis of carbon nanotubes by CCVD. *Mat Chem Phys* 2002; 77: 536-541
- [30] Bartsch K, Biedermann K, Gemming T, Leonhardt A. On the diffusion-controlled growth of multiwalled carbon nanotubes. *J Appl Phys* 2005; 97 (11)
- [31] Yoon YJ, Bae JC, Baik HK, Cho SJ, Lee SJ, Song KM, Myung NS. Nucleation and growth control of carbon nanotubes in CVD process, *Physica B* 2002; 323: 318-320
- [32] Liao XZ, Serquis A, Jia QX, Peterson DE, Zhu YT. Effect of catalyst composition on carbon nanotube growth. *Appl Phys Lett* 2003; 82 (16): 2694-2696
- [33] Kohno M, Orii T, Hirasawa M, Seto T, Murakami Y, Chiashi S, Miyauchi Y, Maruyama S. Growth of single-walled carbon nanotubes from size-selected catalytic metal particles. *Appl Phys A* 2004; 79: 787-790
- [34] Clausen BS, Topsoe H, Frahm R. Application of combined X-ray diffraction and absorption techniques for *in-situ* catalyst characterization. *Advances in Catal* 1998; 42: 315-344
- [35] Grunwaldt JD, Molenbroek AM, Topsoe NY, Topsoe H, Clausen BS. *In situ* investigations of structural changes in Cu/ZnO catalysts. *J Catal* 2000 ; 194 (2): 452-460
- [36] Grunwaldt JD, Clausen BS. Combining XRD and EXAFS with on-line catalytic studies for *in situ* characterization of catalysts. *Top Catal* 2002 ; 18 (1-2): 37-43
- [37] Baker RTK. Catalytic growth of carbon filaments. *Carbon* 1989; 27 (3): 315-323
- [38] Helveg S, Lopez-Cartes C, Sehested J, Hansen PL, Clausen BS, Rostrup-Nielsen JR, Abild-Pedersen F, Norskov JK. Atomic-scale imaging of carbon nanofibre growth. *Nature* 2004; 427: 426-429
- [39] Matzinger K, Grobóty B. The evolution of nickel nitrate hexahydrate coated silicon substrate during CVD synthesis of carbon nanotubes: An *in-situ* high temperature X-ray diffraction investigation. Submitted to *carbon* 2005
- [40] Nishimura K, Okazaki N, Pan LJ, Nakayama Y. *In-situ* study of iron catalysts for carbon nanotube growth using X-ray diffraction analysis. *Jap J Appl Phys Part 2* 2004; 43 (4A): L471-L474
- [41] Maruyama S, Einarsson E, Murakami Y, Edamura T. Growth process of vertically aligned single-walled carbon nanotubes. *Chem Phys Lett* 2005 ; 403 (4-6): 320-323
- [42] Puretzky AA, Geohegan DB, Jesse S, Ivanov IN, Eres G. *In-situ* measurements and modelling of carbon nanotube array growth kinetics during chemical vapour deposition. *Appl Phys A* 2005; 81: 223-240
- [43] Baker RTK, Barber MA, Harris PS, Feates FS, Waite RJ. Nucleation and growth of carbon deposits from nickel catalyzed decomposition of acetylene. *J Catal* 1972; 26 (1): 51-54
- [44] Baker RTK, Harris PS. The formation of filamentous carbon. *Chem Phys Carbon* 1978; 14: 83
- [45] Amelinckx S, Zhang XB, Bernaerts D, Zhang XF, Ivanov V, Nagy JB. A formation mechanism for catalytically grown helix-shaped graphite nanotubes. *Science* 1994; 265 (5172): 635-639
- [46] Baker RTK, Terry S, Harris PS. Unique form of filamentous carbon. *Nature* 1975; 253 (5486): 37-39
- [47] Tavares MT, Bernardo CA, Alstrup I, Rostrup-Nielsen JR. Reactivity of carbon deposited on nickel copper alloy catalysts from the decomposition of methane. *J Catal* 1986; 100 (2): 545-548
- [48] Sacco A, Thacker P, Chang TN, Chiang ATS. The initiation and growth of filamentous carbon from alpha-iron in H₂, CH₄, H₂O, CO₂ and CO gas-mixtures. *J Catal* 1984; 85 (1): 224-236
- [49] Alstrup I. A new model explaining the carbon-filament growth on nickel, iron and ni-cu alloy catalysts. *J Catal* 1988; 109 (2): 241-251
- [50] Baker RTK, Harris PS, Thomas RB, Waite

- RJ. Formation of filamentous carbon from iron, cobalt and chromium catalyzed decomposition of acetylene. *J Catal* 1973; 30 (1): 86-95
- [51] Baker RTK, Chludzinski JJ, Dudash NS, Simoens AJ. The formation of filamentous carbon from decomposition of acetylene over vanadium and molybdenum. *Carbon* 1983; 21 (5): 463-468
- [52] Rodriguez NM, Kim MS, Baker RTK. Deactivation of copper nickel-catalysts due to changes in surface-composition. *J Catal* 1993; 140 (1): 16-29
- [53] Singh MK, Singh PP, Titus E, Misra DS, LeNormand F. High density of multiwalled carbon nanotubes observed on nickel electroplated copper substrates by microwave plasma chemical vapor deposition. *Chem Phys Lett* 2002; 354 (3-4): 331-336
- [54] Ivanov V, Fonseca A, Nagy JB, Lucas A, Bernaerts D, Zhang XB. Catalytic production and purification of nanotubules having fullerene-scale diameters. *Carbon* 1995; 33 (12): 1727-1738
- [55] Matzinger K, Lepora A, Grobéty B, Zuetzel A. The evolution of iron and nickel films during CVD synthesis of carbon nanotubes: An *in-situ* high temperature X-ray diffraction investigation, Extended Abstract for Carbon 2004, 11 – 16 July 2004, Brown University, Providence, Staten Island, USA
- [56] Klinke C, Bonard JM, Kern K. Comparative study of the catalytic growth of patterned carbon nanotube films. *Surf Sci* 2001; 492 (1-2): 195-201
- [57] Edsinger RE, Reilly ML, Schooley JF. Thermal expansion of platinum and platinum-rhodium alloys. *J Res NBS* (20899) 1986; 91 (6): 333-356
- [58] Heaney PJ, Veblen DR. Observations of the alpha-beta-phase transition in quartz – A review of imaging and diffraction studies and some new results. *Am Mineral* 1991; 76 (5-6): 1018-1032
- [59] Lide DR. Handbook of Chemistry and Physics. CRC Press Inc. 1995-1996; Vol. 76: 4-73
- [60] Nerushev OA, Dittmar S, Morjan RE, Rohmund F, Campbell EEB. Particle size dependence and model for iron-catalyzed growth of carbon nanotubes by thermal vapour deposition. *J Appl Phys* 2003; 93 (7): 4185-4190
- [61] Kukovitsky EF, L'vov SG, Sainov NA, Shustov VA, Chernozatonskii LA. Correlation between metal catalyst particle size and carbon nanotube growth. *Chem Phys Lett* 2002; 355: 497-503
- [62] Liu S, Zhu J, Mastai Y, Felner I, Gedanken A. Preparation and characteristics of carbon nanotubes filled with cobalt. *Chem Mat* 2000; 12: 2205-2211
- [63] Rana RK, Koltypin Y, Gedanken A. Synthesis of carbon nanotubes from *in-situ* generated cobalt nanoparticles and carbon monoxide. *Chem Phys Lett* 2001; 344 (3-4): 256-262
- [64] Cadeville MC, Lapierre MF. Etude aux rayons X de la solution solide cobalt-carbone. *Scripta Metallurgica* 1972; 6: 399-404
- [65] German RM. Sintering Theory and Practice (New York: Wiley-Interscience) p: 550
- [66] Adamson AW. Physical Chemistry of Surfaces (4th ed.) 1982. Wiley, New York, p: 664
- [67] Dunn WW, McLellan RB, Oates WA. Solubility of carbon in cobalt and nickel. *Trans Metall Soc AIME* 1968; 242 (10): 2129
- [68] Parmon VN. Fluidization of the active component of catalysts in catalytic formation of carbon assisted by iron and nickel carbides. *Catal Lett* 1996; 42 (3-4): 195-199
- [69] Fedorov VB, Shoshorov MKh, Gusev OV, Musyaev IKh, Shipkov NN, Khakimova DK, Procenko NG. Fibrous and Dispersion-Strengthened Composition Materials (Nauka, Moscow, 1976) in Russian
- [70] Geguzin LS, Physics of Sintering (Nauka, Moscow, 1967) in Russian
- [71] Kuznetsov VL, Usoltesva AN, Chuvilin AL, Obratsova ED, Bonard JM. Thermodynamic analysis of nucleation of carbon deposits on metal particles and its implications for the growth of carbon nanotubes. *Phys Rev B* 2001; 64: 235401 (7)

CHAPTER 6

THE EVOLUTION OF MOLYBDENUM OXIDE COATED GLASS SUBSTRATE DURING CVD SYNTHESIS OF CARBON NANOTUBES: AN *IN-SITU* HIGH TEMPERATURE X-RAY DIFFRACTION INVESTIGATION

K. Matzinger and B. Grobéty

Dep. of Geoscience, Applied Mineralogy Group, University of Fribourg, Pérolles, 1700 Fribourg

to be submitted

Abstract

The presence of metallic catalysts is required for the synthesis of carbon nanotubes by chemical vapour deposition (CVD). The chemical and morphological evolution of a molybdenum catalyst was studied by *in-situ* X-ray diffraction and high resolution Scanning Electron Microscopy (SEM). Glass substrates coated with a molybdenum oxide suspension as catalyst were exposed to an acetylene/nitrogen or acetylene/hydrogen/nitrogen gas mixture at temperatures between 600°C and 750°C in the camera of a high temperature X-ray powder diffractometer. The reduction of MoO₂ to metallic Mo is only observed with extensive hydrogen pre-treatment at 750°C. A treatment with acetylene leads to the formation of at least three stable carbide phases, an orthorhombic and a hexagonal Mo₂C phase as well as a hexagonal MoC phase, and two intermediate metastable cubic MoO_xC_y and cubic Mo₂C phases which requires carbon supersaturation. In samples where minor amounts of metallic molybdenum were detected, growth of carbon nanotubes was observed during a short time span.

Keywords: A. carbon nanotubes; B. chemical vapour deposition; C. x-ray diffraction; D. crystal structure/grain size

1. Introduction

The revolutionary discovery of carbon nanotubes (CNT) in 1991 [1] started intense research activities in the domain of carbon science. The fascinating properties of these unique material has opened a great number of potential applications e.g. electron field emitters [2], hydrogen storage [3,4], nanoelectronic components and devices [5,6], probe tips for scanning tunnelling and atomic force microscopy [7].

Despite this huge interest, the synthesis methods suitable for industrial manufacturing of nanotubes are still in their infancy. [8] High quality materials are obtained by laser ablation and arc discharge methods, but purification process e.g. the elimination of impurities is difficult and expensive. The high temperature necessary for both techniques make them difficult to scale up in a cost-effective way. Chemical vapour deposition (CVD) seems to be the most flexible and well adapted method for industrial production. [9]. This method has been extensively used in the past to produce different forms of carbon filament and fibres [10,11] and recently for the production of both single- and multiwall carbon nanotubes at low cost and kilogram scale. [12,13]. The CVD process has several advantages over other synthesis methods. CNT's grow at a relatively low temperature and their size can be controlled by varying the size of the catalyst [14,15]. Furthermore the growth rate, the density, the diameter and the crystallinity can be manipulated by selecting the catalysts or varying the growth temperature [15,16,17]. Despite tremendous increase in production yields, the synthesis costs and the purity of the products obtained by CVD, the importance of different parameters that affect CNT nucleation and growth are still much debated.

Little in-situ information on the chemical and morphological evolution of the metal-based catalyst exposed to the gas flow in the CVD reaction chamber is available. These investigations have shown that the type and the grain-size of the catalyst has a strong effect on nanotube diameter, growth rate and wall thickness as well as on morphology and microstructures [14]. A minimal average grain size of a metallic phase and a sufficient diffusion rate of carbon through the nuclei are required to let carbon nanotubes grow [18].

Molybdenum has been used as an activator for the nanotube growth in CVD processes [19,20,21,22]. One of the main advantages when Mo containing bimetallic catalysts are used is the possibility to control the relative amount of SWNTs and MWNTs by modifying the Mo/Metal ratio [21,22,23]. Some

research groups reported no nanotube growth when molybdenum alone was used as catalyst. [22,24] Dai et al., however, reported the synthesis of SWNTs in similar conditions but higher temperatures (1200°C). [19]. The mechanism by which Mo favours the formation of carbon nanotubes supported in metal oxide substrates is not yet clarified. Pérez-Mendoza [22] postulated that Mo species is assisting the production of nanotubes in two different ways. First they ease the dispersion and avoid sintering of metallic catalyst particles and second they promote the aromatization of the hydrocarbon source molecules. Investigations with only a Mo catalyst are missing so far. Therefore this paper is focusing to the chemical and morphological evolution of MoO₂ during CVD process to test whether or not carbon nanotubes are formed.

2. Experimental Methods

2.1 Starting Materials

The experiments were performed with MoO₂ (Alfa Aesar Johnson Matthey GmbH, 76185 Karlsruhe, Germany, Nr. 242-637-9) dry powder on alcohol. The substrate (thin glass AF 45, PGO GmbH, Iserlohn, Germany) was coated with the suspension. The support material, an alkali free borosilicate glass, has a softening temperature (883°C) well above the temperatures used during the experiments. About 5 mg of crystals or one drop of nitrate solution (approx. 35 – 40 µl) in three different concentrations, 1 mol/l, 0.1 mol/l and 0.05 mol/l of MoO₂, were deposited by pipetting or spin coating on the substrate and subsequently dried on air. The crystals were slightly wetted with ethanol to guarantee a better adhesion to the substrate. The glass platelets were chosen because of their non-crystallinity and ease to use in the XRD set-up.

The gases were of high purity grade: N₂ 99.995%, impurities: O₂ < 10 ppm, H₂O < 10 ppm; C₂H₂ 99.6%, impurities: N₂, PH₃ < 10 ppm; H₂ 99.99%, O₂ < 5ppm, H₂O < 10 ppm, N₂ < 300 ppm. All gases were used without prior cleaning nor drying. The gas mixtures were compiled by a constant flow rate for nitrogen appointed to 300 ml/min (=300 sccm), and that for hydrogen and acetylene to either 25 sccm or 75 sccm.

2.2 High Temperature Diffractometer Experiments

The apparatus for the in-situ diffractometry was a high temperature X-ray camera (model HTK 10, Anton PAAR, Graz, Austria) controlled by a temperature control unit (TCM 2000, Anton PAAR, Graz, Austria) mounted on a Philips PW 1830 diffractometer. Gas flow was controlled by two mass flow controllers (AFC-2600, AALBORG, Orangeburg, New York, USA) and the handling of the gases was by the aid of a command module (2PROC, AALBORG) and three electromagnetic valves. Calibration of the high temperature diffractometer, sample handling and treatment of the different gases are obtained as described in Matzinger et al. [25].

The phase evolution was studied for two different temperatures, 600°C identical to the synthesis conditions used in a gas-mixing furnace by Emmenegger et al. [26] and 750°C. The goniometer is equipped with a scintillation detector and the phase changes were monitored by scanning individual peaks of the reactant phases: (-1 1 1) reflection of cubic MoO₂ (Tugarinovite) at 26.03° 2θ (JCPDS No. 32-0671); (1 0 -1) reflection of monoclinic MoO₃ (Molybdite) at 23.67° 2θ (JCPDS No. 47-1320); (2 1 0) reflection of hexagonal MoO₃ at 25.80° 2θ (JCPDS No. 21-0569); (0 0 1) reflection of tetragonal MoO_{2.80} at 22.56° 2θ (JCPDS No. 12-0517) and product phases: (1 1 0) reflection of metallic molybdenum at 40.51° 2θ (JCPDS No. 42-1120); (2 0 0) reflection of MoO_xC_y at 43.69° 2θ (JCPDS No. 17-0104); (1 1 1) reflection of cubic Mo₂C at 37.76° 2θ (JCPDS No. 15-0457); (1 0 0) reflection of β - Mo₂C at 34.35° 2θ (JCPDS No. 35-0787); (1 0 1) reflection of γ - MoC at 48.79° 2θ (JCPDS No. 45-1015). The scanning range for all measurements was chosen such, that minimum one platinum peak originating from the sample holder occurred in the diffractogram (platinum: (1 1 1) reflection at 39.76° 2θ, (2 0 0) reflection at 46.24° 2θ, (2 2 0) reflection at 67.45° 2θ, or reflection (3 1 1) at 81.82° 2θ). Platinum served as reference to correct the peak positions for instrument zero and sample displacement errors. The diffractograms were recorded in step scan mode between 20° and 70° (2θ). A step size of 0.02°/step and a measuring time of 1 sec/step represented the best compromise between time resolution and sensitivity. Grain size determination was obtained by the Scherer equation and confirmed by SEM observations.

2.3 Electron Microscopy

The Scanning Electron Microscope (Philips FEI XL30SFEG SIRIUS) investigations were performed on glass platelets (AF45) drop coated with powder suspension (0.01 mol/l). All samples were coated with a 10 nm thick Au-layer (BAL-TEC SCD 050 Sputter-coater). The Scanning Electron Microscope was operated at 20 keV and working distance for all samples was adjusted to about 15 mm.

3. Results

3.1 Morphological and Chemical Evolution of the Catalyst

Molybdenum oxide was used as starting material. The X-ray peaks of the starting material were compatible with the reference pattern from JCPDS cards. X-ray diffraction pattern reveal mostly monoclinic MoO₂ (Tugarinovite, JCPDS: 32-0671) and only sparse monoclinic MoO₃ (47-1320) and tetragonal MoO_{2.8} (12-0517) at 25°C. For both of the suspension samples, independent of concentration, and the crystal samples significant phase transformation could be observed during heating under oxygen from room temperature (25°C) to 750°C.

During heating under oxygen the traces of MoO_{2.8} disappeared at about 325°C. At this temperature MoO₂ starts to oxidize to a mixture of monoclinic, orthorhombic or a small amount of hexagonal (JCPDS: 21-0569) MoO₃. This transformation is completed at about 475°C. Above 650°C the monoclinic and orthorhombic polymorphs transform to monoclinic MoO₃. At 750°C only little orthorhombic MoO₃ remains and the hexagonal structure has completely disappeared.

Under nitrogen, the most frequent molybdenum oxide phase is monoclinic MoO₂. Only small amounts, if at all, of monoclinic MoO₃ was present. Above 600°C MoO₃ is increasing at the expense of monoclinic MoO₂ crystals [Figure 1].

The MoO₂ peaks kept the same shape during the entire heating procedure. Average grain diameters calculated with the Scherer equation using the full width at half maximum of the (-1 1 1) peak ranged from 36 nm at 25°C to 40 nm at 750°C. At the start of the acetylene addition, the catalyst phase present was always molybdenum oxide.

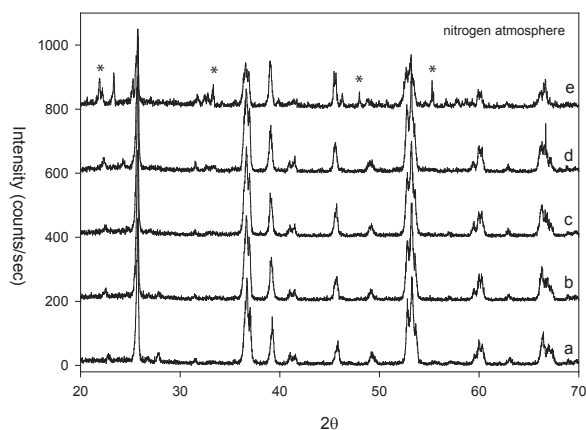


Fig. 1: X-ray diffractograms of quenched samples annealed at various temperatures under nitrogen heating conditions. (a) Molybdenum oxide crystals at room temperature (25°C). Sample at 300°C (b) reveals mostly MoO_2 and at 450°C (c) formation of polymorphic MoO_3 is observed. At 600°C all three polymorphs of molybdenum oxide are visible most of them is MoO_3 (d) and after a recrystallization at 750°C mostly monoclinic MoO_3 is the present phase (e). * represent the MoO_3 peaks.

At 600°C, but also at 750°C the addition of acetylene leads to a reduction of MoO_3 to MoO_2 , but no further reduction is observed. The reduction reaction is accompanied by a slight decrease in grain diameter from 36 to 33 nm at 600°C and from 38 to 31 nm at 750°C. At 750°C a decrease of the MoO_2 peak intensity is observed and simultaneously the appearance of an amorphous mound between 33° and 43° 2θ [Figure 2].

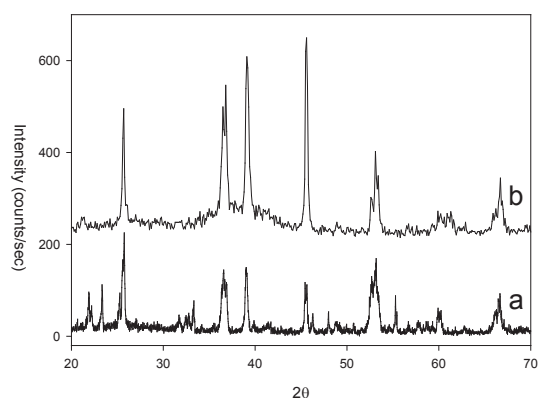


Fig. 2: X-ray diffractograms of molybdenum oxide at 750°C before (a) and after 20 minutes of acetylene treatment (b).

When hydrogen is introduced during the heating cycle at 400°C and maintained up to 600°C, the phase observed is MoO_2 . Replacing hydrogen by acetylene at 600°C has no effect on MoO_2 , e.g. neither metallic molybdenum nor carbides were detected, even after 3 hours of exposure. Pre-treatment of the samples with hydrogen between 400°C and 600°C does not change the situation. MoO_3 is reduced to MoO_2 , which remains stable also after acetylene inlet.

Further reduction of the molybdenum oxides was only observed in experiments where hydrogen was introduced at 400°C, and the samples were heated in hydrogen up to 750°C before acetylene was added. The hydrogen treatment reduced the starting oxide mix to MoO_2 , which reacted instantly to cubic MoO_xC_y and/or cubic Mo_2C (not clearly determinable) and minor amounts of metallic molybdenum at acetylene inlet [Figure 3a]. After 10 minutes the metallic Mo had completely disappeared. Peaks of hexagonal MoC (γ - MoC) appeared and the intensity of the cubic carbide phase started to decrease continuously. After 40 min peaks of the hexagonal Mo_2C (β - Mo_2C) appeared. All three carbide phases were present for the remaining of the experiment (max. 3 hours). No peak shifts are observed, except for cubic MoO_xC_y and/or Mo_2C , which showed a displacement to lower 2θ angles. The peak shift occurs immediately after the acetylene addition and a second time after 60 minutes. The grain size of the oxide, between 37 and 43 nm, was reduced to 7 and 10 nm for the cubic carbide. The grain size of the γ - MoC and β - Mo_2C phases were larger and reached 17 nm and 26 nm respectively. Due to peak overlap and low intensities, the grain size of the metallic molybdenum could not be extracted. The carbide grain size remained constant over the whole reaction duration.

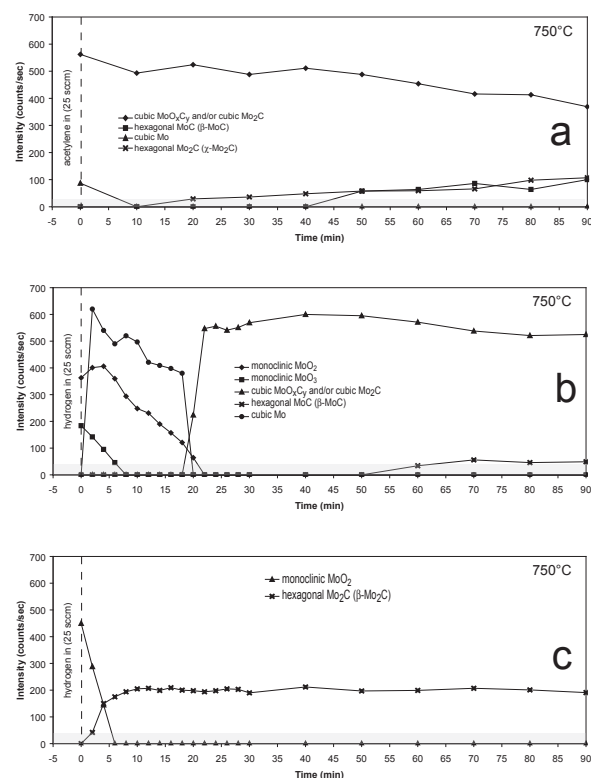


Fig. 3: Phase evolution of molybdenum oxide precursors during exposure of acetylene at 750°C when pretreated with hydrogen from 400°C (a) and phase evolution of MoO_2 - (b) and MoO_3 + MoO_2 - precursors when exposed to hydrogen (c). The transparent crossbars indicate the background.

In a few experiments with hydrogen pre-treatment, carbide formation was observed even without addition of acetylene [Figure 3b]. At 600°C in samples with MoO₂ and MoO₃, after nitrogen treatment, metallic molybdenum appeared right at hydrogen inlet accompanied by a decrease in the intensity of the oxide peaks. Cubic MoO_xC_y and/or Mo₂C appeared 15 min after hydrogen inlet replacing both the remaining oxides and metallic molybdenum. β-Mo₂C peaks appeared 60 min after hydrogen inlet. In the same case, at 750°C, β-Mo₂C formed right away and the peaks of the oxide phase disappeared completely after 5 minutes [Figure 3c]. The carbide formation was accompanied by a significant reduction of the grain size from 40 nm for

the oxide to 12 nm for the carbide phase.

3.2 SEM Observation and Formation of Carbon Nanotubes

The SEM images taken from samples prepared by deposition of a drop of the molybdenum oxide suspension on a glass platelet showed no significant change in grain size during the heating in nitrogen. At 600°C, the grains are mostly coalesced with grain sizes varying between 20 and 200 nm [Figure 4a]. In samples where the addition of hydrogen and/or acetylene led only to a reduction of MoO₃ to MoO₂, particle size remained almost the same [Figure 4b].

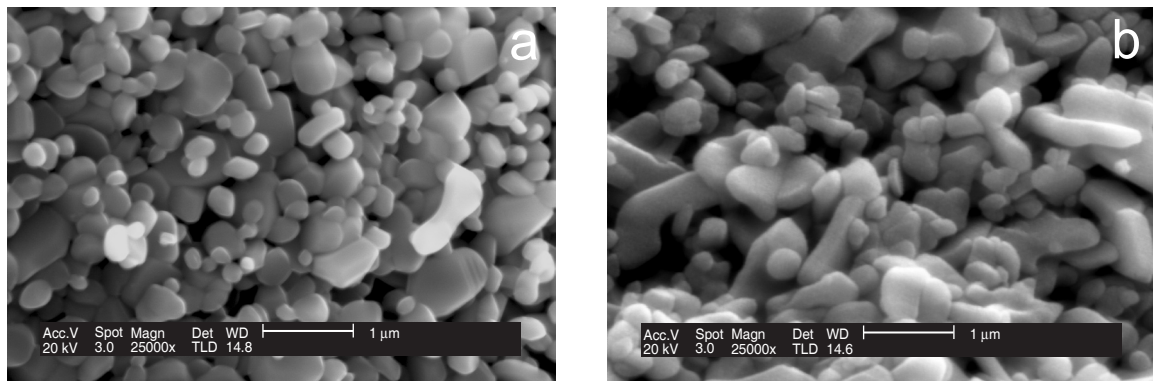


Fig. 4: SEM image of a MoO₂ precursor at 600°C before acetylene inlet (a) and after 20 minutes acetylene treatment (b).

At 750°, less coalescence was observed and the oval grains have diameters between 30 and 500 nm [Figure 5a]. After 20 minutes of acetylene exposure a slight decrease in the smallest grain sizes to approximately 25 nm is observed [Figure 5b].

EDS analysis of the sample showed that the carbon concentration measured from the oxide grains increased with time, probably representing carbon deposits at the surface of the grains.

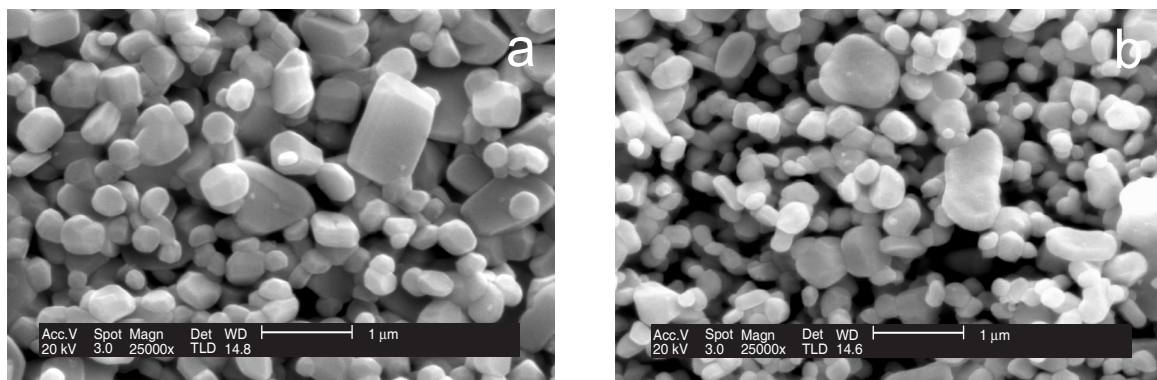


Fig. 5: SEM images of molybdenum oxide at 750°C before acetylene inlet (a) and after 20 minutes (b) C₂H₂ treatment.

The samples heated under hydrogen between 400°C and 750°C and taken before acetylene exposure had grain sizes between 10 and 50 nm [Figure 6a]. They were well rounded and showed little coalescence. Samples taken after 10 minutes of acetylene exposure

contained carbon nanotubes with tube diameters between 10 and 20 nm and lengths up to several microns. The tubes had often helical morphology [Figure 6b].

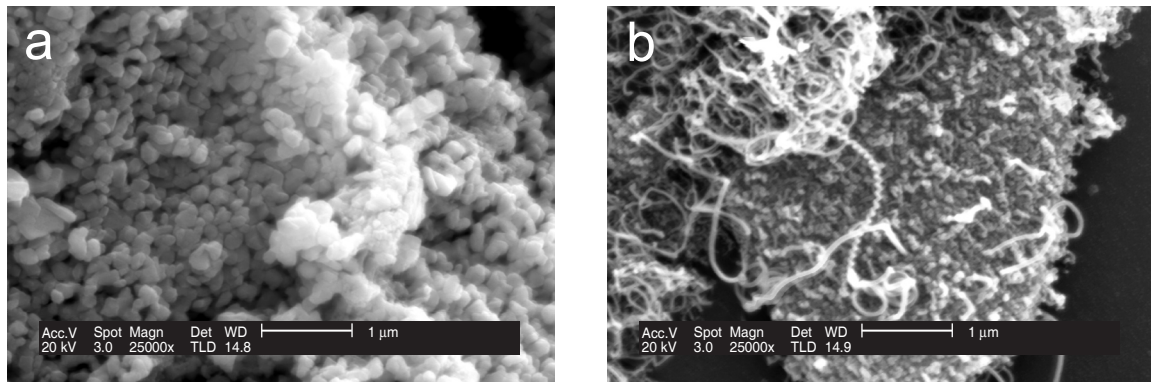


Fig. 6: SEM images of samples heated under hydrogen between 400°C and 750°C and taken before acetylene exposure (a). Sample taken after 10 minutes (b) of acetylene exposure contained carbon nanotubes.

The special samples treated only with hydrogen at 600°C and 750°C that showed the presence of carbides in the X-ray pattern contained isotropic grains with sizes between 50 and 200 nm

[Figure 7a]. Further hydrogen treatment led to a coarsening of the grains (500 nm to 1 μm after 1 hour) [Figure 7b]. No nanotubes could be observed.

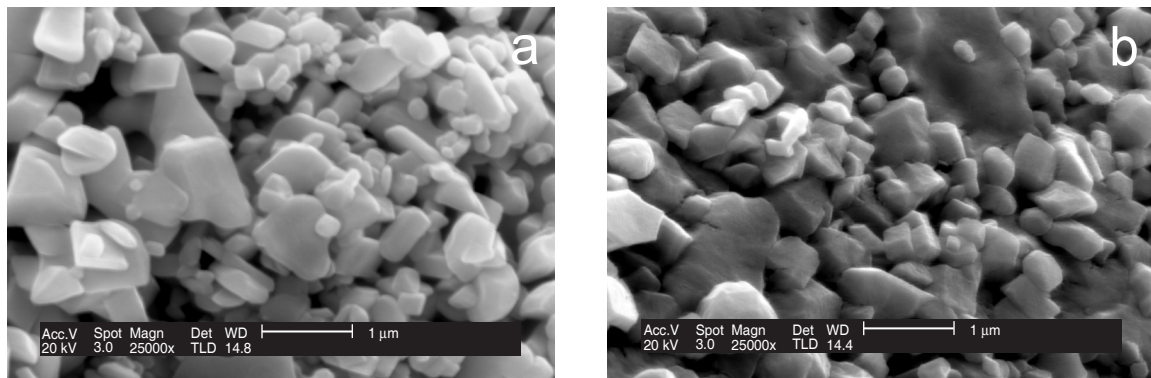


Fig. 7: SEM images of samples treated with hydrogen treatment at 750°C after 10 minutes (a) and after 60 minutes (b) contained isotropic carbide grains coarsening with increasing exposure time.

4. Discussion

The experiments which resulted in carbide/carbon nanotube formation without the introduction of acetylene were done after the X-ray camera was cleaned and annealed for 60 minutes at 1000°C under air to remove carbon deposition. The fact that reduction to molybdenum metal and/or carbides were only observed in a few experiments at 600°C (without acetylene inlet!) and only with extensive hydrogen pre-treatment at 750°C is a consequence of the very low equilibrium oxygen partial pressure of the MoO₂ to metallic Mo transition. For 600°C and 750°C the value for p_{O_2} is approximately $2.37 \cdot 10^{-26}$ and $2.08 \cdot 10^{-21}$ respectively. Previous experiments with different transition metal oxides have shown, that the camera design (caption windows, joint between backplate and cover) did not allow to routinely attain oxygen partial pressure below $> 10^{-25}$. The experiments at 600°C were nevertheless

attempted. Similar *in-situ* high temperature X-ray reduction experiments on MoO₃, though at lower temperatures (350°C), using a 5 vol% H₂ and 95 vol% Ar mixture as reducing agent, gave also MoO₂ as product [27]. The equilibrium partial pressure at 750°C is well within the range attainable with the equipment. The oxidation of the starting MoO₂ phase in air and in nitrogen to MoO₃, considering the potential oxygen impurity content of the latter, is consistent with the tabulated values of the redox equilibria. The experiments in which carbides were formed without acetylene inlet can only be explained by the presence of a carbon impurity in the camera. The latter was cleaned with acetone and heat-treated on air at 1000°C for one hour to oxidize carbon residues deposited on the camera wall. So far, we do not know the nature of this carbon source. These experiments had, however, the advantage that the concentration of the carbon species was low. The carbide evolution was thus slower and could be

better followed in the *in-situ* X-ray measurements than in the regular experiments.

There exist a great number of molybdenum oxide and carbide phases. Phase equilibria in the Mo-O-C system are thus complex, but have received a great deal of attention, since these oxides and carbides are used as catalytic agent in the synthesis of numerous compounds. In the Mo-C system at least six different stable phases have been identified. In the temperature range of interest in the present experiments, there are three stable carbide phases, an orthorhombic and a hexagonal Mo₂C phase as well as a hexagonal MoC phase. The products of carburization of molybdenum oxides reported in the literature are either metastable cubic MoC_{1-x} or the stable hexagonal Mo₂C [28], depending on the carbon content of the carburizing agent used [29]. In experiments with butane the MoC_{1-x} is prevalent, whereas with methane the stable hexagonal phase is present. MoO_xC_y has been observed as first carbon containing phase in the carburization of MoO₃ [30]. Cubic Mo₂C has been synthesized sono-chemically from Mo₂N under a methane/hydrogen atmosphere, the same experiments starting with MoO₃, however, resulted in the formation of hexagonal Mo₂C [31]. The product analyses in all these experiments have been made *ex-situ* and reflect the phase present at certain moments of the reaction or at the end of the experiment.

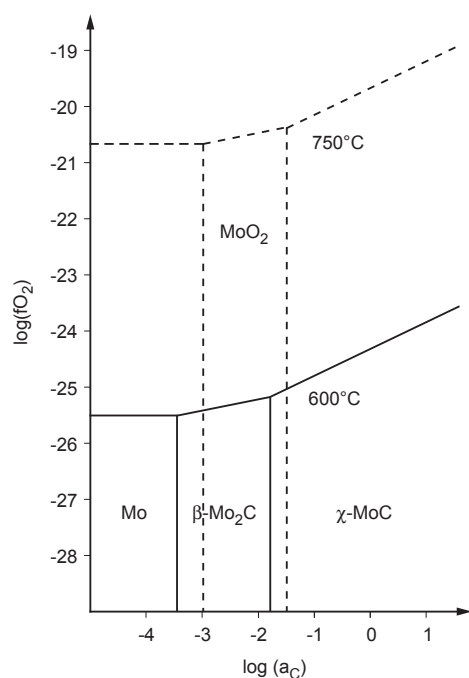


Fig. 8: Phase diagram of the Mo-O-C system at 600°C and 750°C.

The carbide phase evolution observed in the present experiments is similar to previous results obtained

from combined *in-situ* thermogravimetric and *ex-situ* XRD diffraction analysis of the carbothermic reduction of molybdenum oxide [30,32]. As intermediate phase between the starting oxides and the final stable hexagonal Mo₂C, metallic molybdenum [32] or MoO_xC_y [30] were reported, but never both together. Molybdenum metal was observed in experiments with carbon black powder. In such a system Mo₂C should be the stable phase [Figure 8]. Sealing of the oxide grains by a carbide layer and the slow carbon diffusivity through the latter may lower the carbon activity in the interior of the grains enough to stabilize the metal.

In the present experiment both metallic molybdenum and an oxycarbide phase were observed immediately after acetylene inlet. The peak shift observed for the oxycarbide phase, MoO_xC_y, may indicate an increase in carbon content. The direction of the shift is compatible for a transformation of MoO_xC_y to cubic Mo₂C, peaks of which are clearly identified after 10 minutes. The only difference to the previous experiments is the appearance of a monocarbide phase. This phase is stable for carbon activities > -1.776 (600°C) and > -1.513 (750°C) respectively [Figure 8]. In previous carbon nanotube synthesis experiments with iron as catalyst, it has been shown that for the temperatures and gas mixtures used in the present experiments, carbon activity exceeds 1.0. Metastable cementite is formed in those experiments, which requires carbon supersaturation [33]. The monocarbide phase was not observed in the (failed) experiments, where no acetylene was added. The carbon concentration in the latter experiments was obviously not as high as in the experiments with acetylene. In CVD experiments by Herrera et al. [34] and Alvarez et al. [20] molybdenum carbide formation was only observed in the presence of a second metal e.g. cobalt, which according to the authors will promote the formation of active carbon species necessary to generate the carbide. It cannot be excluded, that in the present experiments platinum, the material the sample holder is made of, took over this role. There are, however, also examples of CVD experiments, where Mo₂C is formed without the presence of a second metal [21].

In previous experiments with molybdenum as the only metal present in the catalyst, the carbon nanotube yields, however, were very low or even zero [22,34]. Exceptions are experiments at high temperatures (1200°C) [19] and in which Mo(CO)₃₆ was both the catalyst and the carbon source [35]. The picture is completely different for experiments with molybdenum as part of a bimetallic catalyst. In

synthesis runs with cobalt as second catalyst metal, Mo/Co ratios have a tremendous effect on the type and the yield of CNT's [20,22,24,34] Although the exact role of molybdenum is still unclear, there is consensus, that molybdenum is quickly inactivated as nucleation site for CNT's. In the present experiments the number of nanotubes observed in the samples was also very low. The nucleation of these tubes is confined to the short time span when metallic molybdenum is present in concentrations detectable by X-ray diffraction. The transformation to the carbide phases definitely inactivates the molybdenum grains as nucleation sites. The experiments in which CNT's were grown on pure molybdenum [19,35], the carbon activity was probably too low to stabilize the carbide phases, thus molybdenum remained in the metallic state during the whole experiment. Dai et al. [19] performed the experiments at 1200°C where the stability field of molybdenum metal as a function of carbon activity is increased relative to lower temperatures.

The behaviour of the molybdenum catalyst is in contrast with experiments in which iron was used as catalyst. The iron oxide precursor transformed also directly to a carbide phase, Fe₃C (cementite), nevertheless CNT nucleation could be observed from the start of the acetylene inlet. The difference between the iron and molybdenum system is that cementite is a metastable phase at temperatures below 800°C. After one hour, *in-situ* X-ray diffraction revealed the appearance of metallic iron, due to the breakdown of cementite. In experiments made in larger furnaces, the cementite breakdown was reflected by a strong increase of the CNT nucleation rate [36]. The iron system is thus a special case. Metal-carbon system in which stable carbides occur seemed to be not suited as catalysts.

5. Conclusions

Only an extensive hydrogen pre-treatment led to the formation of metallic molybdenum that can act as nucleation site for carbon nanotubes. The formation of carbon nanotubes is depressed through the formation of stable carbide phases.

6. References

- [1] Iijima S. Helical microtubules of graphitic carbon. *Nature* 1991; 354 (6348): 56-58
- [2] Kuettel OM, Groening O, Emmenegger C, Schlapbach L. Electron field emission from phase pure nanotube films grown in a methane/hydrogen plasma. *Appl Phys Lett* 1998; 73 (15): 2113-2115
- [3] Dillon AC, Jones KM, Bekkedahl TA, Kiang CH, Bethune DS. Storage of hydrogen in single-wall carbon nanotubes, *Nature* 1997; 386: 377-379
- [4] Lee SM, An KH, Lee YH, Seifert G, Frauenheim T. Novel mechanism of hydrogen storage in carbon nanotubes. *Journal of the Korean Physical Society* 2001; 38: 686-691
- [5] Martel R, Schmidt T, Shea HR, Hertel T, Avouris P. Single- and multi-wall carbon nanotube field-effect transistors. *Appl Phys Lett* 1998; 73: 2447-2449
- [6] Tans SJ, Devoret MH, Groeneveld RJA, Dekker C. Electron-electron correlations in carbon nanotubes. *Nature* 1998; 394: 761-764
- [7] Dai H, Hafner JH, Ginzler AG, Colbert DT, Smalley RE. Nanotubes as nanoprobe in scanning probe microscopy. *Nature* 1996; 384 (6605): 147-150
- [8] Journet C, Bernier P. Production of carbon nanotubes. *Appl Phys A-Mater* 1998; 67 (1): 1-9
- [9] Jung M, Eun KY, Lee JK, Baik YJ, Lee KR, Park JW. Growth of carbon nanotubes by chemical vapour deposition. *Diam Relat Mater* 2001; 10 (3-7): 1235-1240
- [10] Oberlin A, Endo M, Koyama T. Filamentous growth of carbon through benzene decomposition. *J Cryst Growth* 1976; 32 (3): 335-349
- [11] Baker RTK, Harris PS. The formation of filamentous carbon. *Chem Phys Carbon* 1978; 14: 83
- [12] Cassell AM, Raymakers JA, Kong J, Dai H, Large scale CVD synthesis of single-walled carbon nanotubes. *J. Phys. Chem. B* 1999; 103 (31), 6484 -6492
- [13] Colomer JF, Stephan C, Lefrant S, Van Tendeloo G, Willems I, Kónya Z, et al. Large-scale synthesis of single-wall carbon nanotubes by catalytic chemical vapour deposition (CCVD) method. *Chem Phys Lett* 2000; 317: 83-89
- [14] Huang ZP, Wang DZ, Wen JG, Sennett M, Gibson H, Ren ZF. Effect of nickel, iron and cobalt on growth of aligned carbon nanotubes. *Appl Phys A-Mater* 2002; 74 (3): 387-391
- [15] Huh Y, Lee JY, Cheon J, Hong YK, Koo JY,

- Lee TJ, et al. Controlled growth of carbon nanotubes over cobalt nanoparticles by thermal chemical vapour deposition. *J Mater Chem* 2003; 13: 2297-2300
- [16] Lee CJ, Park J, Yu JA. Catalyst effect on carbon nanotubes synthesized by thermal chemical vapour deposition. *Chem Phys Lett* 2002; 360 (3-4): 250-255
- [17] Lee CJ, Park J, Huh Y, Le JY. Temperature effect on the growth of carbon nanotubes using thermal chemical vapour deposition. *Chem Phys Lett* 2001; 343: 33-38
- [18] Matzinger K, Grob ty B. The evolution of cobalt nitrate hexahydrate coated silicon substrate during CVD synthesis of carbon nanotubes: An *in-situ* high temperature X-ray diffraction investigation. Submitted to *Appl Phys Lett A* 2005
- [19] Dai H, Rinzler AG, Nikolaev P, Thess A, Colbert DT, Smalley RE. Single-wall nanotubes produced by metal-catalyzed disproportionation of carbon monoxide. *Chem Phys Lett* 1996; 260: 471-475
- [20] Alvarez WE, Kitiyanan B, Borgna A, Resasco DE. Synergism of Co and Mo in the catalytic production of single-wall carbon nanotubes by decomposition of CO. *Carbon* 2001; 39: 547-558
- [21] Flahaut E, Peigney A, Bacsa WS, Bacsa RR, Laurent C. CCVD synthesis of carbon nanotubes from (Mg, Co, Mo)O catalysts: Influence of the proportions of cobalt and molybdenum. *J Mater Chem* 2004; 14: 646-653
- [22] P rez-Mendoza M, Vall s C, Maser WK, Mart nez MT, Benito AM. Influence of molybdenum on the chemical vapour deposition production of carbon nanotubes. *Nanotechnology* 2005; 16: 224-225
- [23] Tang S, Zhong Z, Xiong Z, Sun L, Liu L, Lin J, et al. Controlled growth of single-walled carbon nanotubes by catalytic decomposition of CH₄ over Mo/Co/MgO catalysts. *Chem Phys Lett* 2001; 350: 19-26
- [24] Kitiyanan B, Alvarez WE, Harwell JH, Resasco DE. Controlled production of single-wall carbon nanotubes by catalytic decomposition of CO on bimetallic Co-Mo catalysts. *Chem Phys Lett* 2000; 317: 497-503
- [25] Matzinger K, Grob ty B. The evolution of nickel nitrate hexahydrate coated silicon substrate during CVD synthesis of carbon nanotubes: An *in-situ* high temperature X-ray diffraction investigation. Submitted to *Carbon* 2005
- [26] Emmenegger C, Mauron P, Zuettel A, Nuetzenadel C, Schneuwly A, Schlapbach L, et al. Carbon nanotube synthesized on metallic substrates. *Appl Surf Sci* 2000; 162: 452-456
- [27] Leisegang T, Levin AA, Walter J, Meyer DC. In-situ X-ray analysis of MoO₃ reduction. *Cryst Res Technol* 2005; 40 (1/2): 95-105
- [28] Bouchy C, Derouane-Abd Hamid SB, Derouane EG. A new route to the metastable fcc molybdenum carbide α - MoC_{1-x}. *Chem Commun* 2000; 125-126
- [29] Xiao T, York APE, Coleman KS, Claridge JB, Sloan J, Chanock J, Green MLH. Effect of carburising agent on the structure of molybdenum carbides. *J Mater Chem* 2001; 11: 3094-3098
- [30] Hanif A, Xiao T, York APE, Sloan J, Green MLH. Study on the structure and formation mechanism of molybdenum carbides. *Chem Mater* 2002; 14: 1009-1015
- [31] Li S, Lee JS, Hyeon T, Suslick KS. Catalytic hydrodenitrogenation of indole over molybdenum nitride and carbides with different structures. *Appl Catal A* 1999; 184: 1-9
- [32] Chaudhury S, Mukerjee SK, Vaidya VN, Venugopal V. Kinetics and mechanism of carbothermic reduction of MoO₃ to Mo₂C. *J Alloy Comp* 1997; 261: 105-113
- [33] Matzinger K, L pora A, Grob ty B, Zuettel A. The evolution of iron and nickel films during CVD synthesis of carbon nanotubes: An *in-situ* high temperature X-ray diffraction investigation, Extended Abstract for Carbon 2004, 11 – 16 July 2004, Brown University, Providence, Staten Island, USA
- [34] Herrera JE, Balzano L, Borgna A, Alvarez WE, Resasco DE. Relationship between the structure/composition of Co-Mo catalysts and their ability to produce single-walled carbon nanotubes by CO disproportionation. *J Catal* 2001; 204: 129-149
- [35] Motiei M, Calderon-Moreno J, Gedanken A. Forming multiwalled carbon nanotubes by the thermal decomposition of Mo(CO)₆. *Chem Phys Lett* 2002; 357: 267-271
- [36] Emmenegger C, Bonard JM, Mauron P, Sudan P, Lepora A, Grob ty B, Z ttel A, Schlapbach L. Synthesis of carbon nanotubes over Fe catalyst on aluminium and suggested growth mechanism. *Carbon* 2003; 44 (3): 539-547

APPENDICES

1. The Evolution of Chromium Nitrate Nonahydrate coated Glass Substrate during CVD Synthesis of Carbon Nanotubes: An *in-situ* High Temperature X-Ray Diffraction Investigation

1.1 Experimental Methods

1.1.1 Starting Materials

The substrate (thin glass AF 45, PGO GmbH, Iserlohn, Germany) was coated with chromium nitrate nonahydrate ($\text{Cr}(\text{NO}_3)_3 \cdot 9(\text{H}_2\text{O})$; 27080, Fluka Chemie GmbH, Buchs, Switzerland, crystallized $\geq 97.0\%$) and was either deposited as crystals or as solution dissolved, in ethanol onto the glass substrate. The support material, an alkali free borosilicate glass, has a softening temperature (883°C) well above the temperatures used during the experiments. About 5 mg of crystals or one drop of nitrate solution (approx. 35 - 40 μl) in three different concentrations, 1 mol/l, 0.1 mol/l and 0.05 mol/l of $\text{Cr}(\text{NO}_3)_3 \cdot 9\text{H}_2\text{O}$, were deposited into the support by pipetting or spin coating on the substrate and subsequently dried on air. The crystals were slightly wetted with ethanol to guarantee a better adhesion to the substrate. The glass platelets were chosen because of their non-crystallinity and ease to use in the XRD set-up.

The gases were of high purity grade: N_2 99.995%, impurities: $\text{O}_2 < 10$ ppm, $\text{H}_2\text{O} < 10$ ppm; C_2H_2 99.6%, impurities: N_2 , $\text{PH}_3 < 10$ ppm; H_2 99.99%, $\text{O}_2 < 5$ ppm, $\text{H}_2\text{O} < 10$ ppm, $\text{N}_2 < 300$ ppm. All gases were used without prior cleaning nor drying.

1.1.2 High Temperature Diffractometer Experiments and Electron Microscopy

The apparatus and the synthesis conditions were identical as described in Matzinger et al. [1] and the phase changes were monitored by scanning individual peaks of the reactant phases ((1 0 4) reflection of chromium oxide (Eskolaite, Cr_2O_3) at $33.59^\circ 2\theta$ (JCPDS No. 38-1479); (-1 1 1) reflection of chromium nitrate nonahydrate ($\text{Cr}(\text{NO}_3)_3 \cdot 9\text{H}_2\text{O}$) at $13.40^\circ 2\theta$ (JCPDS No. 31-0409) and product phase ((1 1 0) reflection of metallic chromium at $44.39^\circ 2\theta$ (JCPDS No. 06-0694)).

1.2.1 Phase Evolution of the Catalyst

The chromium nitrate nonahydrate ($\text{Cr}(\text{NO}_3)_3 \cdot 9\text{H}_2\text{O}$) is used as starting material. The observed X-ray

peaks corresponded to the reference pattern (JCPDS No. 31-0409) and the starting material dissolved completely in ethanol.

Under nitrogen (300 sccm), as well as under air, the dehydration reaction of chromium nitrate hydrate starts at 50°C [2]. Already at 70°C the chromium nitrate salt has completely been decomposed (mp at 66.3°C) to an X-ray amorphous layer. While under ambient air Cr_2O_3 (Eskolaite, rhombohedral) appears for the first time at 370°C , under nitrogen atmosphere the appearance of eskolaite is delayed to 420°C . During further heating to 750°C no further phase changes were observed neither under nitrogen nor normal atmosphere conditions [Figure 1].

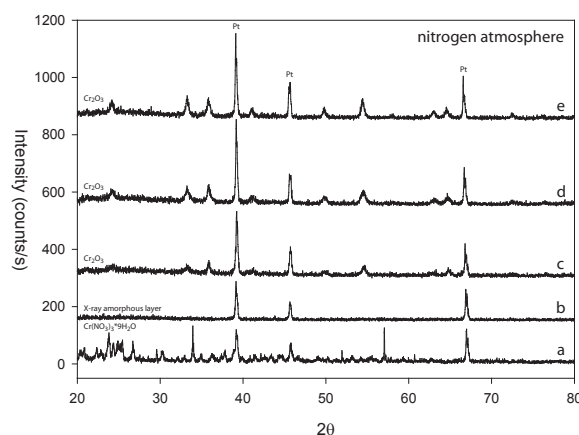


Fig. 1: X-ray diffractograms of quenched samples annealed at various temperatures under nitrogen heating conditions. (a) Chromium nitrate hydrate crystals at room temperature (25°C). Sample annealed at 100°C (b) reveals an X-ray amorphous layer. (c) at 450°C only rhombohedral Cr_2O_3 can be observed. Heating up to 600°C (d) and 750°C (e) revealed no further phase changes.

At 600°C and 750°C various acetylene concentrations (5, 25, 75, 150 sccm) was introduced but neither reduction to metallic chromium nor formation of chromium carbides took place within 4 hours of exposure. A little grain growth right after acetylene inlet is detected but during the following entire reaction remains constant.

A pre-treatment of the samples with hydrogen (25 sccm) at 600°C or 750°C for 10 minutes before subsequent exposure to acetylene reveals no reactions, starting the hydrogen pre-treatment already at 400°C did not change the situation. Chromium oxide remained stable and no metallic chromium was observed.

1.2.2 Morphological Evolution of the Catalyst

The SEM pictures for the description of the morphological evolution were taken from samples prepared by depositing a drop of the 0.01 mol/l cobalt nitrate solution on a glass platelets.

Samples heated up to 400°C under nitrogen atmosphere reveal very fine rhombohedral chromium oxide crystals with diameter of 10 nm to 20 nm. A thin eskolaite film covers the eskolaite grains forming a smooth surface, which is only interrupted

by sealed cracks [Figure 2a]. Temperature increase to 600°C [Figure 2b] and 750°C [Figure 2c] reveal no significant changes. The surface is still covered by a smooth layer, and only inside cracks and destructed particles, grain size of single non-sintered particles are visible and measured to 10 nm to 30 nm. The X-ray derived grain sizes of the chromium oxide show a doubling of grain size with continuously heating. The values are slightly smaller than the average grain sizes observed in SEM images.

Images of samples treated with acetylene are similar

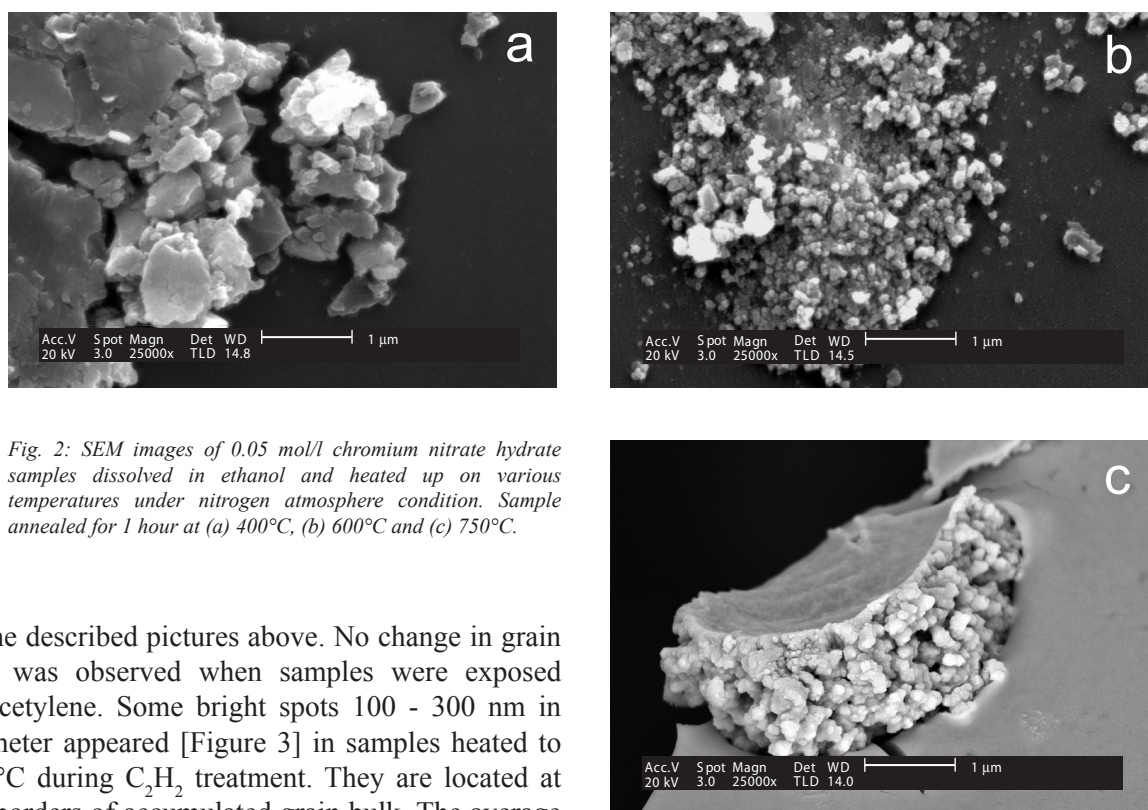


Fig. 2: SEM images of 0.05 mol/l chromium nitrate hydrate samples dissolved in ethanol and heated up on various temperatures under nitrogen atmosphere condition. Sample annealed for 1 hour at (a) 400°C, (b) 600°C and (c) 750°C.

to the described pictures above. No change in grain size was observed when samples were exposed to acetylene. Some bright spots 100 - 300 nm in diameter appeared [Figure 3] in samples heated to 750°C during C_2H_2 treatment. They are located at the borders of accumulated grain bulk. The average particle size of Cr_2O_3 independent of the treatment (hydrogen, hydrogen/acetylene) remained at constant values in between 20 – 25 nm.

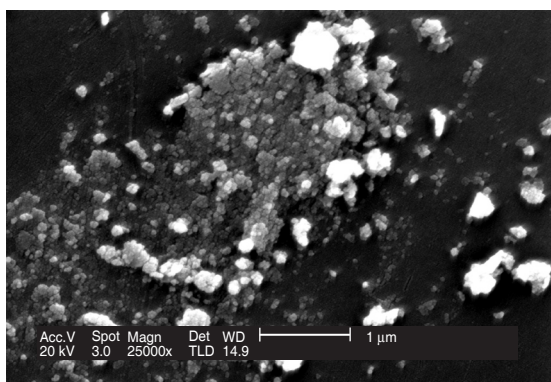


Fig. 3: SEM image of a sample treated with acetylene for 1 hour at 750°C. No nanotubes were observed but some bright spots in the range of 100 to 300 nm occur.

1.3 Discussion

The break-down of the initial chromium nitrate during heating sequence is similar to the evolution in the iron system [3]. First an amorphous layer is formed and with higher temperature Cr_2O_3 . The grain growth observed during heating stage is the result of agglomeration of grains in the thicker part of the catalyst similar to the iron system.

The equilibrium $\log(f_{O_2})$ for the reaction eskolaite – metallic chromium at 600°C is -35.97 [4] e.g. about 10 log unites below the Fe–FeO. The gases used for the experiments, though of highest purity, contain impurities among others oxygen. Assuming an overall impurity of 10 ppm of oxygen in mixture of 5 vol% H_2 and 95 vol% N_2 , the equilibrium oxygen concentration $\log(f_{O_2})$ calculated with the

CHEMKIN calculator [5] at 600°C is $4.5 \cdot 10^{-32}$ mol%. Assuming ideal gas behaviour this translate to a $\log(f_{O_2})$ of -31.35 e.g. a value which is above the Cr_2O_3 -Cr-buffer. To get below the buffer value at 873°C the minimum fraction of hydrogen in the mixture has to be > 0.3 (≈ 130 sccm), which is five times larger than the amount used in the present experiment [Figure 4].

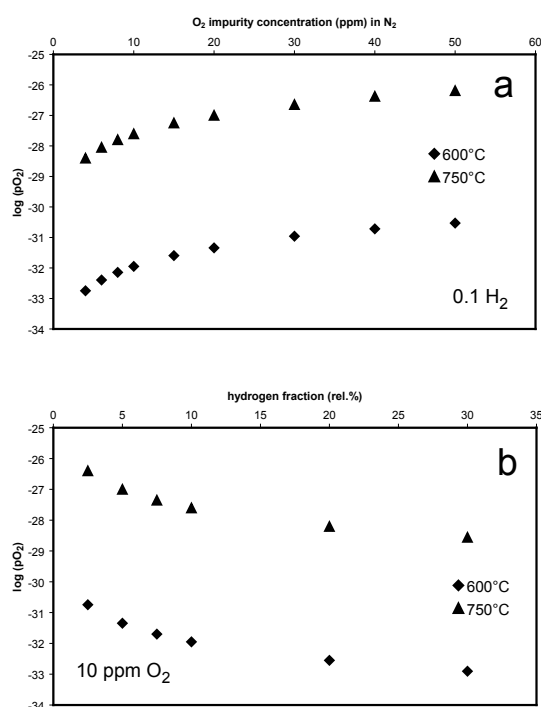


Fig. 4: Oxygen fugacity in the reaction chamber depending on the oxygen impurity of the used nitrogen at constant hydrogen rate (a), and depending on hydrogen fraction at constant oxygen impurity (10 ppm) of the nitrogen (b).

For security reasons, such high hydrogen concentration can not be used with the current set up. For the case the oxygen fugacity can be controlled to levels low enough to stabilize the metal phase, the addition of carbon species would immediately lead to the formation of carbide phases [Figure 5]. Considering that during the time span the gas is in the chamber, equilibrium is hardly attained, it is not surprising the eskolaite could not be reduced within the reaction chamber.

The strong sintering of the surface-close grains to a smooth layer, protecting the bulk from the chamber atmosphere is another obstacle to the reduction of eskolaite. Adding acetylene does not improve the situation.

The bright spots (s. fig. 3) may derive from carbon deposition on the metal oxide phase as it was observed in the cobalt system [6] but signal strength was too small to obtain reliable results determining as metal carbide phases.

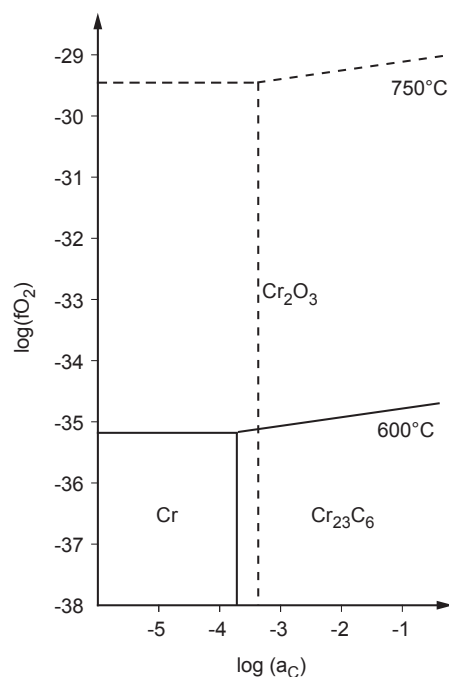


Fig. 5: Phase diagram of the Cr-O-C system at 600°C and 750°C.

1.4 References

- [1] Matzinger K, Grobóty B. The evolution of nickel nitrate hexahydrate coated silicon substrate during CVD synthesis of carbon nanotubes: An *in-situ* high temperature X-ray diffraction investigation. Submitted to Carbon 2005
- [2] Lide DR. Handbook of Chemistry and Physics. CRD Press Inc. 1995-1996; Vol. 76: No. 594, 4-52
- [3] Matzinger K, Lepora A, Grobóty B, Zuetzel A, The evolution of iron and nickel films during CVD synthesis of carbon nanotubes: An *in-situ* high temperature X-ray diffraction investigation, Extended Abstract for Carbon 2004, 11 – 16 July 2004, Brown University, Providence, Staten Island, USA
- [4] Barin I. Thermodynamical data of pure substances. VCH, Verlagsgesellschaft mbH, D-6940 Weinheim, Germany, 1989, Part I & II
- [5] CHEMKIN/EQUIL[®], <http://www.ca.sandia.gov/>
- [6] Matzinger K, Grobóty B. The evolution of cobalt nitrate hexahydrate coated silicon substrate during CVD synthesis of carbon nanotubes: An *in-situ* high temperature X-ray diffraction investigation. Submitted to J Appl Phys 2005

2. Log-Book of all obtained X-Ray Diffraction Experiments

Sample #	Temp. (°C)	Sample	sec/step	°/step	Blenden	2theta	gasflow	pressure (bar)	concentration	notes
0	25	nickel powder	1.0	0.02	1/0.1/1	20-80	air		powder	powder fixed on glass plate with ZAPONLA
1	100-500 (100)	nickel powder	1.0	0.02	1/0.1/1	20-80	air		powder	powder fixed on glass plate with ZAPONLA
2	100-800 (50)	Ni(NO ₃) ₂ * 6H ₂ O	1.0	0.02	1/0.1/1	20-80	air		crystals dissolved in ethanol	
3	25	Ni(NO ₃) ₂ * 6H ₂ O	1.0	0.02	1/0.1/1	20-80	air		crystals dissolved in ethanol	
4	100	Ni(NO ₃) ₂ * 6H ₂ O	1.0	0.02	1/0.1/1	20-80	air		crystals dissolved in ethanol	same sample used as in #4
5	150	Ni(NO ₃) ₂ * 6H ₂ O	1.0	0.02	1/0.1/1	20-80	air		crystals dissolved in ethanol	same sample used as in #4
6	200	Ni(NO ₃) ₂ * 6H ₂ O	1.0	0.02	1/0.1/1	20-80	air		crystals dissolved in ethanol	same sample used as in #4
7	25	Ni(NO ₃) ₂ * 6H ₂ O	1.0	0.02	1/0.1/1	20-80	air		crystals dissolved in ethanol	same sample used as in #4
8	25	Ni(NO ₃) ₂ * 6H ₂ O	1.0	0.02	1/0.1/1	20-80	air		crystals dissolved in ethanol	No signal, measurement aborted
9	50, 80, 220-380 (20)	Ni(NO ₃) ₂ * 6H ₂ O	1.0	0.02	1/0.1/1	20-80	air		crystals dissolved in ethanol	
10	180, 200	Ni(NO ₃) ₂ * 6H ₂ O	1.0	0.02	1/0.1/1	20-80	air		crystals dissolved in ethanol	2 h waited after heating on desired temperature
11	220, 240, 260, 280, 300	Ni(NO ₃) ₂ * 6H ₂ O	1.0	0.02	1/0.1/1	20-80	air		crystals dissolved in ethanol	2 h waited after heating on desired temperature, same sample used as in #11
12	25, 50	Ni(NO ₃) ₂ * 6H ₂ O	1.0	0.02	1/0.1/1	15-80	N ₂ (100%)	N ₂ : 1.5	crystals dissolved in ethanol	2 h waited after heating on desired temperature
13	60, 100	Ni(NO ₃) ₂ * 6H ₂ O	1.0	0.02	1/0.1/1	15-80	N ₂ (100%)	N ₂ : 1.5	crystals dissolved in ethanol	2 h waited after heating on desired temperature, same sample used as in #13
14	150, 200	Ni(NO ₃) ₂ * 6H ₂ O	1.0	0.02	1/0.1/1	15-80	N ₂ (100%)	N ₂ : 1.5	crystals dissolved in ethanol	2 h waited after heating on desired temperature, same sample used as in #13
15	250	Ni(NO ₃) ₂ * 6H ₂ O	1.0	0.02	1/0.1/1	15-80	N ₂ (100%)	N ₂ : 0.5	crystals dissolved in ethanol	2 h waited after heating on desired temperature (measuring overnight)
16	300, 350, 400, 450, 500	Ni(NO ₃) ₂ * 6H ₂ O	1.0	0.02	1/0.1/1	15-80	N ₂ (100%)	N ₂ : 0.5	crystals dissolved in ethanol	2 h waited after heating on desired temperature
17	550, 600	Ni(NO ₃) ₂ * 6H ₂ O	1.0	0.02	1/0.1/1	15-80	N ₂ (100%)	N ₂ : 0.5	crystals dissolved in ethanol	2 h waited after heating on desired temperature
18	180, 220, 240, 260, 280, 320, 340	Ni(NO ₃) ₂ * 6H ₂ O	1.0	0.02	1/0.1/1	15-80	N ₂ (100%)	N ₂ : 0.5	crystals dissolved in ethanol	2 h waited after heating on desired temperature
19, Test 1	25	Ni(NO ₃) ₂ * 6H ₂ O	1.0	0.02	1/0.1/1	15-20	air		solution, 0.1 mol	Test 1, 0.1 mol Lösung, Plättchen überflutet, 15-20 °2theta --> No signal
20, Test 2	200	Ni(NO ₃) ₂ * 6H ₂ O	1.0	0.02	1/0.1/1	15-20	air		solution, 0.1 mol	Test 2, 0.1 mol Lösung, 1 Tropfen, 15-20 °2theta --> No signal
21, Test 3	200	Ni(NO ₃) ₂ * 6H ₂ O	1.0	0.02	1/0.1/1	15-20	air		solution, 1.0 mol	Test 3, 1 mol Lösung, Plättchen überflutet, 15-20 °2theta --> No signal
22, Test 4	200	Ni(NO ₃) ₂ * 6H ₂ O	1.0	0.02	1/0.1/1	15-20	air		solution, 1.0 mol	Test 4, 1 mol Lösung, 1 Tropfen verteilt auf Plättchen, 15-20 °2theta --> No signal
23, Test 5	200	Ni(NO ₃) ₂ * 6H ₂ O	5.0	0.02	1/0.1/1	15-20	air		solution, 1.0 mol	Test 5, 1 mol Lösung, 1 Tropfen über Nacht eingedampft
24, Test 5	400	Ni(NO ₃) ₂ * 6H ₂ O	1.0	0.02	1/0.1/1	15-40	air		solution, 1.0 mol	same sample used as in #023
25, Test 6	25, 200, 300, 400	Ni(NO ₃) ₂ * 6H ₂ O	5.0	0.02	1/0.1/1	15-80	air		solution, 1.0 mol	1 mol Lösung, 1 Tropfen
26, Test 7	200	AF45 + Klebstreifen	1.0	0.02	1/0.1/1	15-45	air			AF45 glasplate mit Klebstreifen Spuren versehen --> No signal at all
27	200	Ni(NO ₃) ₂ * 6H ₂ O	1.0	0.02	1/0.1/1	keine	air		solution, 1.0 mol	1 mol Lösung, 1 Tropfen, 2 h on desired temperature
28	400	Ni(NO ₃) ₂ * 6H ₂ O	1.0	0.02	1/0.1/1	keine	air		solution, 1.0 mol	1 mol Lösung, 1 Tropfen, 2 h on desired temperature
29	100	Ni(NO ₃) ₂ * 6H ₂ O	1.0	0.02	1/0.1/1	keine	air		solution, 1.0 mol	1 mol Lösung, 1 Tropfen, 2 h on desired temperature
30	100	Ni(NO ₃) ₂ * 6H ₂ O	1.0	0.02	1/0.1/1	keine	air		solution, 0.1 mol	1 mol Lösung, 1 Tropfen, 2 h on desired temperature
31	200	Ni(NO ₃) ₂ * 6H ₂ O	1.0	0.02	1/0.1/1	keine	air		solution, 0.1 mol	1 mol Lösung, 1 Tropfen, 2 h on desired temperature
32	400	Ni(NO ₃) ₂ * 6H ₂ O	1.0	0.02	1/0.1/1	keine	air		solution, 0.1 mol	1 mol Lösung, 1 Tropfen, 2 h on desired temperature
33	100	Ni(NO ₃) ₂ * 6H ₂ O	1.0	0.02	1/0.1/1	keine	air		solution, 0.05 mol	1 mol Lösung, 1 Tropfen, 2 h on desired temperature
34	200	Ni(NO ₃) ₂ * 6H ₂ O	1.0	0.02	1/0.1/1	keine	air		solution, 0.05 mol	1 mol Lösung, 1 Tropfen, 2 h on desired temperature
35	400	Ni(NO ₃) ₂ * 6H ₂ O	1.0	0.02	1/0.1/1	keine	air		solution, 0.05 mol	1 mol Lösung, 1 Tropfen, 2 h on desired temperature
36	25	Ni(NO ₃) ₂ * 6H ₂ O	5.0	0.02	1/0.1/1	15-80	air		crystals dissolved in ethanol	presentation for "women in science" day
37	600	Ni(NO ₃) ₂ * 6H ₂ O	1.0	0.02	1/0.1/1	35-53	N ₂ (100%), C ₂ H ₂ (2%)	N ₂ : 0.5 ; C ₂ H ₂ : 0.26	solution, 1.0 mol	1 drop, heated up under N ₂ , 10 min waited, flow 2% C ₂ H ₂ during measurement
38	25	Ni(NO ₃) ₂ * 6H ₂ O	1.0	0.02	1/0.1/1	15-80	air		platinum strip	#037 poisoned pt-strip (carbon soot), check if reaction with pt-strip took place --> no reaction
39	600	Ni(NO ₃) ₂ * 6H ₂ O	1.0	0.02	1/0.1/1	58-80	N ₂ (100%), C ₂ H ₂ (2%)	N ₂ : 0.5 ; C ₂ H ₂ : 0.26	solution, 1.0 mol	1 drop, heated up under N ₂ , 10 min waited, flow 2% C ₂ H ₂ during measurement
40	25, 225	Ni(NO ₃) ₂ * 6H ₂ O	2.0	0.02	1/0.1/1	5-120	N ₂ (100%)	N ₂ : 0.5	crystals dissolved in ethanol	measurement performed to do structural analyses (Rietveldmethode)

Sample #	Temp. (°C)	Sample	sec/step	%step	Blenden	2theta	gasflow	pressure (bar)	concentration	notes
41	600	Ni(NO ₃) ₂ * 6H ₂ O	1.0	0.1	1/0.1/1	43.3-44.8	N ₂ (100%), C ₂ H ₂ (2%)	N ₂ : 0.5 ; C ₂ H ₂ : 0.46	crystals dissolved in ethanol	measurement aborted
42	600	Ni(NO ₃) ₂ * 6H ₂ O	1.0	0.1	1/0.1/1	43.3-44.8	N ₂ (100%), C ₂ H ₂ (2%)	N ₂ : 0.5 ; C ₂ H ₂ : 0.46	crystals dissolved in ethanol	heated up under N ₂ , 1 minute waited, flow 2% C ₂ H ₂ ; repetition of measurement during 9 minutes due to examination of Ni peak behaviour
43	600	Ni(NO ₃) ₂ * 6H ₂ O	1.0	0.1	1/0.1/1	42.2-43.7	N ₂ (100%), C ₂ H ₂ (2%)	N ₂ : 0.5 ; C ₂ H ₂ : 0.46	crystals dissolved in ethanol	heated up under N ₂ , 1 minute waited, flow 2% C ₂ H ₂ ; repetition of measurement during 9 minutes due to examination of NiO peak behaviour
44	600	Ni(NO ₃) ₂ * 6H ₂ O	1.0	0.1	1/0.1/1	70.3-71.8	N ₂ (100%), C ₂ H ₂ (2%)	N ₂ : 0.5 ; C ₂ H ₂ : 0.46	crystals dissolved in ethanol	heated up under N ₂ , 1 minute waited, flow 2% C ₂ H ₂ ; repetition of measurement during 9 minutes due to examination of Ni ₃ C peak behaviour
45	600	Ni(NO ₃) ₂ * 6H ₂ O	1.0	0.02	1/0.1/1	42-46	N ₂ (100%), C ₂ H ₂ (2%)	N ₂ : 0.5 ; C ₂ H ₂ : 0.46	crystals dissolved in ethanol	heated up under N ₂ , 1 minute waited, flow 2% C ₂ H ₂ ; repetition of measurement during 2 hours due to examination of Ni, NiO, Ni ₃ C peak behaviour
46	600	Ni(NO ₃) ₂ * 6H ₂ O	1.0	0.02	1/0.1/1	35-53	N ₂ (100%), C ₂ H ₂ (2%)	N ₂ : 0.5 ; C ₂ H ₂ : 0.46	crystals dissolved in ethanol	heated up under N ₂ , 10 minutes waited, flow 2% C ₂ H ₂ ; repetition of measurement during 3 hours due to examination of Ni, NiO, Ni ₃ C peak behaviour
47	600	Ni(NO ₃) ₂ * 6H ₂ O	1.0	0.02	1/0.1/1	35-53	N ₂ (100%), C ₂ H ₂ (6%)	N ₂ : 0.5 ; C ₂ H ₂ : 0.65	crystals dissolved in ethanol	heated up under N ₂ , 1 minute waited, flow 6% C ₂ H ₂ ; first scan check due to examination of Ni, NiO, Ni ₃ C are present
48	600	Ni(NO ₃) ₂ * 6H ₂ O	1.0	0.1	1/0.1/1	43.3-44.8	N ₂ (100%), C ₂ H ₂ (6%)	N ₂ : 0.5 ; C ₂ H ₂ : 0.65	crystals dissolved in ethanol	heated up under N ₂ , 1 minute waited, flow 6% C ₂ H ₂ ; repetition of measurement during 9 minutes due to examination of Ni peak behaviour
49	600	Ni(NO ₃) ₂ * 6H ₂ O	1.0	0.1	1/0.1/1	42.2-43.7	N ₂ (100%), C ₂ H ₂ (6%)	N ₂ : 0.5 ; C ₂ H ₂ : 0.65	crystals dissolved in ethanol	heated up under N ₂ , 1 minute waited, flow 6% C ₂ H ₂ ; repetition of measurement during 9 minutes due to examination of NiO peak behaviour
50	600	Ni(NO ₃) ₂ * 6H ₂ O	1.0	0.02	1/0.1/1	42-46	N ₂ (100%), C ₂ H ₂ (6%)	N ₂ : 0.5 ; C ₂ H ₂ : 0.65	crystals dissolved in ethanol	heated up under N ₂ , 1 minute waited, flow 6% C ₂ H ₂ ; repetition of measurement during 3 hours due to examination of Ni, NiO, Ni ₃ C peak behaviour
51	750	Ni(NO ₃) ₂ * 6H ₂ O	1.0	0.02	1/0.1/1	35-53	N ₂ (100%), C ₂ H ₂ (2%)	N ₂ : 0.5 ; C ₂ H ₂ : 0.46	crystals dissolved in ethanol	heated up under N ₂ , 1 minute waited, flow 2% C ₂ H ₂ ; first scan check due to examination of Ni, NiO, Ni ₃ C are present
52	750	Ni(NO ₃) ₂ * 6H ₂ O	1.0	0.02	1/0.1/1	35-53	N ₂ (100%), C ₂ H ₂ (6%)	N ₂ : 0.5 ; C ₂ H ₂ : 0.65	crystals dissolved in ethanol	heated up under N ₂ , 1 minute waited, flow 6% C ₂ H ₂ ; first scan check due to examination of Ni, NiO, Ni ₃ C are present
53	225	Ni(NO ₃) ₂ * 6H ₂ O	2.0	0.02	1/0.1/1	5-120	N ₂ (100%)	N ₂ : 0.5	solution, 1.0 mol	heated up under N ₂ , 2 h waited --> ongoing measurement performed with PW 1800 due to structural analyses (Rietveldmethode)
54	25	Alufolie auf AF45	1.0	0.02	1/0.1/1	10-90	air		alufolie on AF45	scan check due to determination of Al-peaks
55	25	Ni(NO ₃) ₂ * 6H ₂ O	2.0	0.02	1/0.2/1	10-90	N ₂ (100%)	N ₂ : 0.5	crystals dissolved in ethanol	measurement performed to do structural analyses (Rietveldmethode)
56	225	Ni(NO ₃) ₂ * 6H ₂ O	2.0	0.02	1/0.2/1	10-90	N ₂ (100%)	N ₂ : 0.5	crystals dissolved in ethanol	measurement performed to do structural analyses (Rietveldmethode)
57	600	Ni(NO ₃) ₂ * 6H ₂ O					air		solution, 0.05 mol	0.05 mol Lösung, 1 Tropfen, 1 h heizen --> SEM
58	750	Ni(NO ₃) ₂ * 6H ₂ O					air		solution, 0.05 mol	0.05 mol Lösung, 1 Tropfen, 1 h heizen --> SEM
59	600	Ni(NO ₃) ₂ * 6H ₂ O					air		solution, 1.0 mol	1.0 mol Lösung, 1 Tropfen, 1 h heizen --> SEM
60	750	Ni(NO ₃) ₂ * 6H ₂ O					air		solution, 1.0 mol	1.0 mol Lösung, 1 Tropfen, 1 h heizen --> SEM
61	25, 50, 60, 100, 150, 200, 225, 250, 400, 600, 750	Ni(NO ₃) ₂ * 6H ₂ O	1.0	0.02	1/0.2/1	10-90	air		crystals dissolved in ethanol	measurement performed for diffractogram change during heating process from 25° to 750°C, used for SEM pictures and illustration
62	25	Ni(NO ₃) ₂ * 6H ₂ O	1.0	0.02	1/0.2/1	10-90	N ₂ (100%)	N ₂ : 0.8	crystals dissolved in ethanol	1 drop, 5 times repetition of measurement due to give statements about the behaviour of educt over time
63	160, 180, 200, 220, 240	Ni(NO ₃) ₂ * 6H ₂ O	1.0	0.02	1/0.2/1	10-90	N ₂ (100%)	N ₂ : 0.8	crystals dissolved in ethanol	1 drop, measurement --> 2 h break --> measurement --> temperature rise ==> appearance of Ni(NO ₃) ₂ peak, disappearance of Hydrate-phases
64	25, 400, 800	Platinum strip	1.0	0.02	1/0.2/1	35-125	air		blank	platinum strip due to thermal expansion coefficient
65	600	Ni(NO ₃) ₂ * 6H ₂ O	1.0	0.02	1/0.2/1	20-80	N ₂ (100%), C ₂ H ₂ (2%)	N ₂ : 0.8 ; C ₂ H ₂ : 0.65	solution, 0.05 mol	0.05 mol Lösung, 1 Tropfen, heating on temperature, 10 waited --> acetylene for 1 hour ==> SEM
66	600	Ni(NO ₃) ₂ * 6H ₂ O	1.0	0.02	1/0.2/1	40-50	N ₂ (100%), C ₂ H ₂ (2%)	N ₂ : 0.8 ; C ₂ H ₂ : 0.65	solution, 0.05 mol	0.05 mol Lösung, 1 Tropfen, heating on temperature, 10 waited --> acetylene for 10 min ==> SEM
67	600	Ni(NO ₃) ₂ * 6H ₂ O	1.0	0.02	1/0.2/1	43.5-44.5	N ₂ (100%), C ₂ H ₂ (2%)	N ₂ : 0.8 ; C ₂ H ₂ : 0.65	solution, 0.05 mol	0.05 mol Lösung, 1 Tropfen, heating on temperature, 10 waited --> acetylene for 1 min ==> SEM
68	750	Ni(NO ₃) ₂ * 6H ₂ O	1.0	0.02	1/0.2/1	40-50	N ₂ (100%), C ₂ H ₂ (2%)	N ₂ : 0.8 ; C ₂ H ₂ : 0.65	solution, 0.05 mol	0.05 mol Lösung, 1 Tropfen, heating on temperature, 10 waited --> acetylene for 10 min ==> SEM
69	750	Ni(NO ₃) ₂ * 6H ₂ O	1.0	0.02	1/0.2/1	20-80	N ₂ (100%), C ₂ H ₂ (2%)	N ₂ : 0.8 ; C ₂ H ₂ : 0.65	solution, 0.05 mol	0.05 mol Lösung, 1 Tropfen, heating on temperature, 10 waited --> acetylene for 1 hour ==> SEM
70	750	Ni(NO ₃) ₂ * 6H ₂ O	1.0	0.02	1/0.2/1	43.5-44.5	N ₂ (100%), C ₂ H ₂ (2%)	N ₂ : 0.8 ; C ₂ H ₂ : 0.65	solution, 0.05 mol	0.05 mol Lösung, 1 Tropfen, heating on temperature, 10 waited --> acetylene for 1 min ==> SEM

Sample #	Temp. (°C)	Sample	sec/step	%step	Blenden	2theta	gasflow	pressure (bar)	concentration	notes
71	600	Ni(NO ₃) ₂ * 6H ₂ O	1.0	0.02	1/0.2/1	43.5-44.5	N ₂ (100%), C ₂ H ₂ (6%)	N ₂ ; 0.8 ; C ₂ H ₂ ; 0.65	solution, 0.05 mol	0.05 mol Lösung, 1 Tropfen, heating on temperature, 10 waited --> acetylene for 1 min ==> SEM
72	600	Ni(NO ₃) ₂ * 6H ₂ O	1.0	0.02	1/0.2/1	40-50	N ₂ (100%), C ₂ H ₂ (6%)	N ₂ ; 0.8 ; C ₂ H ₂ ; 0.65	solution, 0.05 mol	0.05 mol Lösung, 1 Tropfen, heating on temperature, 10 waited --> acetylene for 10 min ==> SEM
73	600	Ni(NO ₃) ₂ * 6H ₂ O	1.0	0.02	1/0.2/1	20-80	N ₂ (100%), C ₂ H ₂ (6%)	N ₂ ; 0.8 ; C ₂ H ₂ ; 0.65	solution, 0.05 mol	0.05 mol Lösung, 1 Tropfen, heating on temperature, 10 waited --> acetylene for 1 hour ==> SEM
74	750	Ni(NO ₃) ₂ * 6H ₂ O	1.0	0.02	1/0.2/1	20-80	N ₂ (100%), C ₂ H ₂ (6%)	N ₂ ; 0.8 ; C ₂ H ₂ ; 0.65	solution, 0.05 mol	0.05 mol Lösung, 1 Tropfen, heating on temperature, 10 waited --> acetylene for 1 hour ==> SEM
75	750	Ni(NO ₃) ₂ * 6H ₂ O	1.0	0.02	1/0.2/1	40-50	N ₂ (100%), C ₂ H ₂ (6%)	N ₂ ; 0.8 ; C ₂ H ₂ ; 0.65	solution, 0.05 mol	0.05 mol Lösung, 1 Tropfen, heating on temperature, 10 waited --> acetylene for 1 hour ==> SEM
76	750	Ni(NO ₃) ₂ * 6H ₂ O	1.0	0.02	1/0.2/1	43.5-44.5	N ₂ (100%), C ₂ H ₂ (6%)	N ₂ ; 0.8 ; C ₂ H ₂ ; 0.65	solution, 0.05 mol	0.05 mol Lösung, 1 Tropfen, heating on temperature, 10 waited --> acetylene for 10 min ==> SEM
77	600	Ni(NO ₃) ₂ * 6H ₂ O	1.0	0.02	1/0.2/1	20-80	N ₂ (100%)	N ₂ ; 0.8	solution, 0.05 mol	0.05 mol Lösung, 1 Tropfen, heating on temperature, 10 waited --> acetylene for 1 min ==> SEM
78	600	Ni(NO ₃) ₂ * 6H ₂ O	1.0	0.02	1/0.2/1	20-80	N ₂ (100%), C ₂ H ₂ (2%)	N ₂ ; 0.8 ; C ₂ H ₂ ; 0.65	crystals dissolved in ethanol	0.05 mol Lösung, 1 Tropfen, heating on temperature, 10 waited --> waiting 1 h on temperature
79	25, 400, 800	Platinum strip	1.0	0.02	1/0.2/1	35-125	air		blank	platinum strip due to thermal expansion coefficient
80	25, 45, 50, 55, 90	Co(NO ₃) ₂ * 6H ₂ O	1.0	0.02	1/0.2/1	5-80	air		crystals dissolved in ethanol	1 drop of solution, measurement --> 2 h break --> measurement ==> measurement aborted due to automatic switch of HT overnight
81	25	Co(NO ₃) ₂ * 6H ₂ O	1.0	0.02	1/0.2/1	5-80	air		crystals dissolved in ethanol	1 drop of solution --> measurement stopped, no waterflow
82	25	Co(NO ₃) ₂ * 6H ₂ O	1.0	0.02	1/0.2/1	5-80	air		crystals dissolved in ethanol	same sample as 081, measurement right after 081 --> 3 times repetition of measurement, in total 4 h --> Measurement stopped, no waterflow
83	25, 50, 55, 60, 90, 100, 110	Co(NO ₃) ₂ * 6H ₂ O	1.0	0.02	1/0.2/1	5-80	air		crystals dissolved in ethanol	measurement stopped after first measurement at 110°C was performed
84	150, 200, 250, 300	Co(NO ₃) ₂ * 6H ₂ O	1.0	0.02	1/0.2/1	5-80	air		crystals dissolved in ethanol	measurement due to detection of phase transformation
85	350, 400, 450, 500, 550, 600, 650, 700, 750	Co(NO ₃) ₂ * 6H ₂ O	1.0	0.02	1/0.2/1	5-80	air		crystals dissolved in ethanol	same sample used as in experiment #084 --> measurement aborted due to a thunderstorm, 650, 700, 750°C not measured
86	650, 700, 750	Co(NO ₃) ₂ * 6H ₂ O	1.0	0.02	1/0.2/1	5-80	air		crystals dissolved in ethanol	completion of the aborted #084 measurement
87	25	Co(NO ₃) ₂ * 6H ₂ O	1.0	0.02	1/0.2/1	5-80	air		crystals dissolved in ethanol	repetition of measurement for 15 hours
88	600	Co(NO ₃) ₂ * 6H ₂ O	1.0	0.02	1/0.2/1	5-80	air		crystals dissolved in ethanol	2 hours waited on temperature before measured --> change in structure?
89	25, 50, 90, 100, 110, 150, 200, 250, 300, 400, 500, 600	Ni(NO ₃) ₂ * 6H ₂ O + Fe(NO ₃) ₃ * 9H ₂ O	1.0	0.02	1/0.2/1	5-80	air		0.5 mol/l solution	mix-solution of 0.5 mol/l Fe(NO ₃) ₃ *9H ₂ O and 0.5 mol/l Ni(NO ₃) ₂ *6H ₂ O
90	25, 400, 800	Platinum strip	1.0	0.02	1/0.2/1	15-125	air		blank	platinum strip due to thermal expansion coefficient --> alloying may possible (21.5 peak in every diffractogram)
91	25, 600	Ni(NO ₃) ₂ * 6H ₂ O + Fe(NO ₃) ₃ * 9H ₂ O	1.0	0.02	1/0.2/1	5-80	air		0.5 mol/l solution + crystals	mix-solution of 0.5 mol/l + (crystals) Fe(NO ₃) ₃ *9H ₂ O and 0.5 mol/l Ni(NO ₃) ₂ *6H ₂ O
92	25, 550 - 595 alle 5	SiO ₂ pure	1.0	0.02	1/0.2/1	18-28	air		crystals of pure SiO ₂	crystals fixed with ZAPONLAC on AF45 glass platelets --> calibration of HT-Diffractometer based on α-β transition of SiO ₂
93	25, 500, 650	SiO ₂ pure	1.0	0.02	1/0.2/1	15-80	air		crystals of pure SiO ₂	crystals fixed with ZAPONLAC on AF45 glass platelets --> calibration of HT-Diffractometer based on α-β transition of SiO ₂
94	550 - 590 (steps, 5 and 2.5)	SiO ₂ pure	1.0	0.02	1/0.2/1	15-80	air		crystals of pure SiO ₂	crystals fixed with ZAPONLAC on AF45 glass platelets --> calibration of HT-Diffractometer based on α-β transition of SiO ₂
95	25, 600	Ni(NO ₃) ₂ * 6H ₂ O + Fe(NO ₃) ₃ * 9H ₂ O	1.0	0.02	1/0.2/1	5-80	air		0.5 mol/l solution + crystals	mix-solution of 0.5 mol/l + (crystals) Fe(NO ₃) ₃ *9H ₂ O and 0.5 mol/l Ni(NO ₃) ₂ *6H ₂ O
96	25, 550 - 590 alle 2.5	SiO ₂ pure	1.0	0.02	1/0.2/1	38-43	air		crystals of pure SiO ₂	crystals fixed with ZAPONLAC on AF45 glass platelets --> calibration of HT-Diffractometer based on α-β transition of SiO ₂
97	590, 592.5, 595	SiO ₂ pure	1.0	0.02	1/0.2/1	38-43	air		crystals of pure SiO ₂	same sample as used in #096, same aims
98	25, 570 - 590 alle 5	SiO ₂ pure	3.0	0.02	1/0.2/1	41.25-43.01	air		crystals of pure SiO ₂	crystals fixed with ZAPONLAC on AF45 glass platelets --> calibration of HT-Diffractometer based on α-β transition of SiO ₂
99	25, 600, 750	pure AF45 platelets	1.0	0.02	1/0.2/1	2-90	air		AF45 glass platelets	AF45 measurement due to possible contamination of the AF45 platelets or the platinum strip
100	25, 600, 750	Fe(NO ₃) ₃ * 9H ₂ O	1.0	0.02	1/0.2/1	10-90	air		crystals dissolved in ethanol	first overview with iron nitrate nonahydrate

Sample #	Temp. (°C)	Sample	sec/step	%step	Blendn	2theta	gasflow	pressure (bar)	concentration	notes
101	25 - 750	Fe(NO ₃) ₃ * 9H ₂ O	1.0	0.02	1/0.2/1	10-90	air		crystals dissolved in ethanol	evolution of Fe(NO ₃) ₃ * 9H ₂ O during heating procedure from 25°C to 750°C under oxygen conditions
102	25, 600	Ni(NO ₃) ₂ * 6H ₂ O + Fe(NO ₃) ₃ * 9H ₂ O	1.0	0.02	1/0.2/1	5-80	air		crystals dissolved in ethanol	special mix-solution where the percentage is 50% Fe and 50% Ni
103	25, 600	Ni(NO ₃) ₂ * 6H ₂ O + Fe(NO ₃) ₃ * 9H ₂ O	1.0	0.02	1/0.2/1	5-80	air		crystals dissolved in ethanol	special mix-solution where the percentage is 75% Fe and 25% Ni
104	25, 400	Platinum strip	1.0	0.02	1/0.2/1	15-125	air		blank	platinum strip, huge deformation, maybe peak movement after refilating of the pt-strip
105	600, 800	Platinum strip	1.0	0.02	1/0.2/1	15-125	air		blank	platinum strip, huge deformation, maybe peak movement after refilating of the pt-strip. Peak movement iteration conversions
106	25, 50, 60, 90	Co(NO ₃) ₂ * 6H ₂ O	1.0	0.02	1/0.2/1	5-80	N ₂ (10%)	N ₂ : 0.5	crystals dissolved in ethanol	heated up under nitrogen atmosphere, annealed for 1 hour at temperature before measurement obtained --> first overview of cobalt nitrate hydrate
107	100, 110, 150, 175	Co(NO ₃) ₂ * 6H ₂ O	1.0	0.02	1/0.2/1	5-80	N ₂ (10%)	N ₂ : 0.5	crystals dissolved in ethanol	heated up under nitrogen atmosphere, annealed for 1 hour at temperature before measurement obtained --> first overview of cobalt nitrate hydrate
108	200, 400, 600	Co(NO ₃) ₂ * 6H ₂ O	1.0	0.02	1/0.2/1	5-80	N ₂ (10%)	N ₂ : 0.5	crystals dissolved in ethanol	heated up under nitrogen atmosphere, annealed for 1 hour at temperature before measurement obtained --> first overview of cobalt nitrate hydrate
109	250, 300	Co(NO ₃) ₂ * 6H ₂ O	1.0	0.02	1/0.2/1	5-80	N ₂ (10%)	N ₂ : 0.5	crystals dissolved in ethanol	heated up under nitrogen atmosphere, annealed for 1 hour at temperature before measurement obtained --> first overview of cobalt nitrate hydrate
110	25, 600	Fe50Ni50 @ 1000°C	1.0	0.02	1/0.2/1	5-80	N ₂ (10%)	N ₂ : 0.5	crystals dissolved in ethanol	special mix-solution where the percentage is 50% Fe and 50% Ni heated for 5h to 1000°C before measurement
111	25, 90-190 alle 10	Co(NO ₃) ₂ * 6H ₂ O	1.0	0.02	1/0.2/1	5-80	air		crystals dissolved in ethanol	evolution of Co(NO ₃) ₂ * 6H ₂ O during heating procedure from 25°C to 190°C under oxygen conditions (compare measurement 083-086) --> absorbed due to no x-ray signal??
112	70-190 alle 10	Co(NO ₃) ₂ * 6H ₂ O	1.0	0.02	1/0.2/1	5-80	air		crystals dissolved in ethanol	repetition of measurement #111
113	750	Co(NO ₃) ₂ * 6H ₂ O	1.0	0.02	1/0.2/1	5-80	air		crystals dissolved in ethanol	heated up under nitrogen atmosphere, annealed for 1 hour at temperature before measurement obtained
114	25-750	Co(NO ₃) ₂ * 6H ₂ O	1.0	0.02	1/0.2/1	5-80	N ₂ (10%)	N ₂ : 0.5	crystals dissolved in ethanol	heated up under nitrogen atmosphere, annealed for 1 hour at temperature before measurement obtained
115	600	Fe50Ni50	1.0	0.02	1/0.2/1	5-80	N ₂ (10%), C ₂ H ₂ (2%)	N ₂ : 0.5, C ₂ H ₂ : 1.0	crystals dissolved in ethanol	heated up under nitrogen atmosphere, waited 10 minutes, 10 minutes acetylene (2%) exposure, measurement --> Carbides?
116	600	Fe50Ni50	1.0	0.02	1/0.2/1	5-80	N ₂ (10%), C ₂ H ₂ (2%)	N ₂ : 0.5, C ₂ H ₂ : 1.0	crystals dissolved in ethanol	heated up under nitrogen atmosphere, waited 10 minutes, 10 minutes acetylene (2%) exposure, measurement --> Carbides?
117	25, 600	Fe50Ni50	1.0	0.02	1/0.2/1	10-80	N ₂ (10%)	N ₂ : 0.5	crystals dissolved in ethanol	heated up under nitrogen atmosphere, annealed for 1 hour at temperature before measurement obtained
118	600	Co(NO ₃) ₂ * 6H ₂ O	1.0	0.02	1/0.2/1	10-80	N ₂ (10%), C ₂ H ₂ (2%)	N ₂ : 0.5, C ₂ H ₂ : 1.0	crystals dissolved in ethanol	heated up under nitrogen atmosphere, 10 minutes acetylene (2%) exposure, measurement --> Co ₂ C present or not, first overview
119	25-500	Co(NO ₃) ₂ * 6H ₂ O	1.0	0.02	1/0.2/1	5-80	air		crystals dissolved in ethanol	evolution of Co(NO ₃) ₂ * 6H ₂ O during heating procedure from 200°C to 500°C under oxygen conditions --> measurement absorbed due to no signal
120	600	Fe75Ni25	1.0	0.02	1/0.2/1	10-80	N ₂ (10%), C ₂ H ₂ (2%)	N ₂ : 0.5, C ₂ H ₂ : 1.0	crystals dissolved in ethanol	first acetylene treatment (2%, 10 minutes) for Fe75Ni25 due to carbide detection
121	600	Co(NO ₃) ₂ * 6H ₂ O	1.0	0.02	1/0.2/1	10-80	N ₂ (10%), C ₂ H ₂ (2%)	N ₂ : 0.5, C ₂ H ₂ : 1.0	crystals dissolved in ethanol	heated up under nitrogen atmosphere, 1 minute acetylene (2%) exposure, measurement --> Co ₂ C present or not, first overview
122	600	Co(NO ₃) ₂ * 6H ₂ O	1.0	0.02	1/0.2/1	10-80	N ₂ (10%), C ₂ H ₂ (2%)	N ₂ : 0.5, C ₂ H ₂ : 1.0	crystals dissolved in ethanol	heated up under nitrogen atmosphere, 10 seconds acetylene (2%) exposure, measurement --> Co ₂ C present or not, first overview
123	25-500	Co(NO ₃) ₂ * 6H ₂ O	1.0	0.02	1/0.2/1	5-80	air		crystals dissolved in ethanol	repetition of #119 due to weak signal
124	600	Co(NO ₃) ₂ * 6H ₂ O	1.0	0.02	1/0.2/1	10-80	N ₂ (10%), C ₂ H ₂ (2%)	N ₂ : 0.5, C ₂ H ₂ : 1.0	crystals dissolved in ethanol	heated up under nitrogen atmosphere, 2 minutes acetylene (2%) exposure, measurement --> Co ₂ C present or not, first overview
125	600	Co(NO ₃) ₂ * 6H ₂ O	1.0	0.02	1/0.2/1	10-80	N ₂ (10%), C ₂ H ₂ (2%)	N ₂ : 0.5, C ₂ H ₂ : 1.0	crystals dissolved in ethanol	heated up under nitrogen atmosphere, 1 hour acetylene (2%) exposure, measurement --> Co ₂ C present or not, first overview
126	600	Co(NO ₃) ₂ * 6H ₂ O	1.0	0.02	1/0.2/1	10-80	N ₂ (10%), C ₂ H ₂ (2%)	N ₂ : 0.5, C ₂ H ₂ : 1.0	crystals dissolved in ethanol	heated up under nitrogen atmosphere, 90 seconds acetylene (2%) exposure, measurement --> Co ₂ C present or not, first overview
127	600	Co(NO ₃) ₂ * 6H ₂ O	1.0	0.02	1/0.2/1	10-80	N ₂ (10%), C ₂ H ₂ (2%)	N ₂ : 0.5, C ₂ H ₂ : 1.0	crystals dissolved in ethanol	heated up under nitrogen atmosphere, 5 minutes acetylene (2%) exposure, measurement --> Co ₂ C present or not, first overview
128	200-500	Co(NO ₃) ₂ * 6H ₂ O	1.0	0.02	1/0.2/1	5-80	air		crystals dissolved in ethanol	repetition of # 119 and #123 due to weak signal
129	600	Co(NO ₃) ₂ * 6H ₂ O	1.0	0.02	1/0.2/1	10-80	N ₂ (10%), C ₂ H ₂ (2%)	N ₂ : 0.5, C ₂ H ₂ : 1.0	crystals dissolved in ethanol	heated up under nitrogen atmosphere, 20 minutes acetylene (2%) exposure, measurement --> Co ₂ C present or not, first overview
130	600	Co(NO ₃) ₂ * 6H ₂ O	1.0	0.02	1/0.2/1	10-80	N ₂ (10%), C ₂ H ₂ (2%)	N ₂ : 0.5, C ₂ H ₂ : 1.0	crystals dissolved in ethanol	heated up under nitrogen atmosphere, 40 minutes acetylene (2%) exposure, measurement --> Co ₂ C present or not, first overview

Sample #	Temp. (°C)	Sample	sec/step	%step	Blenden	2theta	gasflow	pressure (bar)	concentration	notes
131	600	Co(NO ₃) ₂ * 6H ₂ O	1.0	0.02	1/0.2/1	10-80	N ₂ (10%), C ₂ H ₂ (2%)	N ₂ : 0.5, C ₂ H ₂ : 1.0	crystals dissolved in ethanol	heated up under nitrogen atmosphere, 210 seconds acetylene (2%) exposure, measurement -> Co,C present or not, first overview
132	600	Co(NO ₃) ₂ * 6H ₂ O	0.25	0.02	1/0.2/1	10-80	N ₂ (10%), C ₂ H ₂ (2%)	N ₂ : 0.5, C ₂ H ₂ : 1.0	crystals dissolved in ethanol	heated up under nitrogen atmosphere, 1 hour acetylene (2%) exposure, kinetic measurement (repetition of 43-45)
133	25	Co(NO ₃) ₂ * 6H ₂ O	1.0	0.02	1/0.2/1	5-80	air		crystals dissolved in ethanol	repetition of measurement during 14 hours due to investigation of cobalt nitrate hydrate states
134	600	Co(NO ₃) ₂ * 6H ₂ O	1.0	0.02	1/0.2/1	30-80	N ₂ (10%), C ₂ H ₂ (2%)	N ₂ : 0.5, C ₂ H ₂ : 1.0	crystals dissolved in ethanol	heated up under nitrogen atmosphere, stepwise exposure to acetylene (2%) due to reproducibility of past Co-Ac-N ₂ measurements
135	25, 50, 60	Co(NO ₃) ₂ * 6H ₂ O	1.0	0.02	1/0.2/1	5-80	air		crystals dissolved in ethanol	repetition of measurement during 14 hours due to investigation of cobalt nitrate hydrate states
136	600	Fe50Ni50	1.0	0.02	1/0.2/1	30-70	N ₂ (10%), C ₂ H ₂ (2%)	N ₂ : 0.5, C ₂ H ₂ : 1.0	crystals dissolved in ethanol	heated up under nitrogen atmosphere, stepwise exposure to acetylene (2%), measurement -> Carbides?
137	600	Co(NO ₃) ₂ * 6H ₂ O	1.0	0.5	1/0.2/1	58-60.2	N ₂ (10%), C ₂ H ₂ (2%)	N ₂ : 0.5, C ₂ H ₂ : 1.0	crystals dissolved in ethanol	kinetic measurement of Co ₂ O ₃ peak at 59.359 (58-60°2theta)
138	600	Co(NO ₃) ₂ * 6H ₂ O	1.0	0.1	1/0.2/1	64-66	N ₂ (10%), C ₂ H ₂ (2%)	N ₂ : 0.5, C ₂ H ₂ : 1.0	crystals dissolved in ethanol	kinetic measurement of Co ₂ O ₃ peak at 65.238 (64-66°2theta)
139	600	Co(NO ₃) ₂ * 6H ₂ O	0.5	0.05	1/0.2/1	41-43	N ₂ (10%), C ₂ H ₂ (2%)	N ₂ : 0.5, C ₂ H ₂ : 1.0	crystals dissolved in ethanol	kinetic measurement of peak at 41-43°2theta
140	600	Co(NO ₃) ₂ * 6H ₂ O	1.0	0.1	1/0.2/1	43-45	N ₂ (10%), C ₂ H ₂ (2%)	N ₂ : 0.5, C ₂ H ₂ : 1.0	crystals dissolved in ethanol	kinetic measurement of peak at 43-45°2theta
141	600	Co(NO ₃) ₂ * 6H ₂ O	1.0	0.1	1/0.2/1	30-70	air		crystals dissolved in ethanol	kinetic measurement between 30-70°2theta (after 1 h C ₂ H ₂ -> 25°C -> 600°C (air) -> only Co ₂ O ₃ visible)
142	600	Co(NO ₃) ₂ * 6H ₂ O	1.0	0.1	1/0.2/1	36-38	N ₂ (10%), C ₂ H ₂ (2%)	N ₂ : 0.5, C ₂ H ₂ : 1.0	crystals dissolved in ethanol	kinetic measurement of peak at 36-38°2theta
143	600	Co(NO ₃) ₂ * 6H ₂ O					N ₂ (10%)	N ₂ : 0.5	solution, 0.05 mol/l	0.05 mol Lösung, 1 Tropfen, heating on temperature, 1 h waited ==> SEM
144	400	Co(NO ₃) ₂ * 6H ₂ O					N ₂ (10%)	N ₂ : 0.5	solution, 0.05 mol/l	0.05 mol Lösung, 1 Tropfen, heating on temperature, 1 h waited ==> SEM
145	600	Co(NO ₃) ₂ * 6H ₂ O	1.0	0.1	1/0.2/1	41-43	N ₂ (10%), C ₂ H ₂ (2%)	N ₂ : 0.5, C ₂ H ₂ : 1.0	crystals dissolved in ethanol	kinetic measurement of peak at 41-43°2theta
146	600	Co(NO ₃) ₂ * 6H ₂ O	1.0	0.04	1/0.2/1	35-55	N ₂ (10%), C ₂ H ₂ (2%)	N ₂ : 0.5, C ₂ H ₂ : 1.0	crystals dissolved in ethanol	kinetic measurement of peak at 35-55°2theta, C ₂ H ₂ for 5 minutes (test)
147	600	Co(NO ₃) ₂ * 6H ₂ O	1.0	0.04	1/0.2/1	35-55	N ₂ (10%), C ₂ H ₂ (2%)	N ₂ : 0.5, C ₂ H ₂ : 1.0	crystals dissolved in ethanol	kinetic measurement of peak at 35-55°2theta, C ₂ H ₂ for 10 minutes (test) ==> something doesn't work with the gas-system, acetylene flows not through the chamber
148	600	Co(NO ₃) ₂ * 6H ₂ O	1.0	0.04	1/0.2/1	35-55	N ₂ (10%), C ₂ H ₂ (2%)	N ₂ : 0.5, C ₂ H ₂ : 1.0	crystals dissolved in ethanol	kinetic measurement of peak at 35-55°2theta, C ₂ H ₂ for 5 minutes, confirmation of #146
149	200	Co(NO ₃) ₂ * 6H ₂ O					N ₂ (10%)	N ₂ : 0.5	solution, 0.05 mol/l	0.05 mol Lösung, 1 Tropfen, heating on temperature, 1 h waited ==> SEM
150	100	Co(NO ₃) ₂ * 6H ₂ O					N ₂ (10%)	N ₂ : 0.5	solution, 0.05 mol/l	0.05 mol Lösung, 1 Tropfen, heating on temperature, 1 h waited ==> SEM
151/151	750	Co(NO ₃) ₂ * 6H ₂ O					N ₂ (10%)	N ₂ : 0.5	solution, 0.05 mol/l	0.05 mol Lösung, 1 Tropfen, heating on temperature, 1 h waited ==> SEM
151/151	600	Co(NO ₃) ₂ * 6H ₂ O	1.0	0.04	1/0.2/1	35-55	N ₂ (10%), C ₂ H ₂ (2%)	N ₂ : 0.5, C ₂ H ₂ : 1.0	crystals dissolved in ethanol	kinetic measurement of peak at 35-55°2theta, stepwise exposure, 0-15 minutes
152	25, 400, 800	Platinum strip	1.0	0.02	1/0.2/1	15-125	air		platinum strip	floating with N ₂ after change of capton-windows and cleaning of reaction chamber
154	600	Co(NO ₃) ₂ * 6H ₂ O	1.0	0.1	1/0.2/1	41-43	N ₂ (10%), C ₂ H ₂ (2%)	N ₂ : 0.5, C ₂ H ₂ : 1.0	crystals dissolved in ethanol	kinetic measurement of peak at 41-43°2theta, repetition of #139 and #145 -> immer noch ein Leck -> Schrauben noch fester angezogen bei Kapton-Fenster
155	600	Co(NO ₃) ₂ * 6H ₂ O	1.0	0.1	1/0.2/1	43-44	N ₂ (10%), C ₂ H ₂ (2%)	N ₂ : 0.5, C ₂ H ₂ : 1.0	crystals dissolved in ethanol	kinetic measurement of peak at 43-45°2theta, repetition of #140 (scheint brauchbare Resultate zu liefern)
156	600	Co(NO ₃) ₂ * 6H ₂ O	1.0	0.1	1/0.2/1	36-38	N ₂ (10%), C ₂ H ₂ (4%)	N ₂ : 0.5, C ₂ H ₂ : 1.0	crystals dissolved in ethanol	kinetic measurement of peak at 36-38°2theta, repetition of #142 (scheint brauchbare Resultate zu liefern, doch zu schnelle Bildung des Co)
157	600	Co(NO ₃) ₂ * 6H ₂ O	1.0	0.04	1/0.2/1	35-55	N ₂ (10%), C ₂ H ₂ (2%)	N ₂ : 0.5, C ₂ H ₂ : 1.0	crystals dissolved in ethanol	kinetic measurement of peak at 35-55°2theta, stepwise exposure, 0-60 minutes, confirmation of #151
158	600	Co(NO ₃) ₂ * 6H ₂ O	1.0	0.04; 0.1	1/0.2/1	35-55, 35.7-37.5	N ₂ (20%), C ₂ H ₂ (2%)	N ₂ : 0.5, C ₂ H ₂ : 1.0	crystals dissolved in ethanol	kinetic measurement of peak at 35-55°2theta, then kinetic measurement between 35.5-37.5 for 20 minutes; N ₂ : 2.5 ; C ₂ H ₂ : 2.6
159	600	Co(NO ₃) ₂ * 6H ₂ O	1.0	0.04; 0.1	1/0.2/1	35-55, 35.7-37.5	N ₂ (20%), C ₂ H ₂ (2%)	N ₂ : 0.5, C ₂ H ₂ : 1.0	crystals dissolved in ethanol	kinetic measurement of peak at 35-55°2theta, then kinetic measurement between 35.5-37.5 for 20 minutes; N ₂ : 2.5 ; C ₂ H ₂ : 2.6
160	600	Co(NO ₃) ₂ * 6H ₂ O	1.0	0.04; 0.1	1/0.2/1	35-55, 35.7-37.5	N ₂ (20%), C ₂ H ₂ (6%)	N ₂ : 0.5, C ₂ H ₂ : 1.0	crystals dissolved in ethanol	kinetic measurement of peak at 35-55°2theta, then kinetic measurement between 35.5-37.5 for 20 minutes; N ₂ : 2.5 ; C ₂ H ₂ : 7.6

Sample #	Temp. (°C)	Sample	sec/step	%stop	Blendn	°2theta	gasflow	pressure (bar)	concentration	notes
161	600	Co(NO ₃) ₂ * 6H ₂ O	1.0	0.04; 0.1	1/0.2/1	35-55, 35.7-37.5	N ₂ (50%), C ₂ H ₂ (2%)	N ₂ : 0.5, C ₂ H ₂ : 1.0	crystals dissolved in ethanol	kinetic measurement of peak at 35-55°2theta, then kinetic measurement between 35.5-37.5 for 20 minutes; N ₂ : 6.8 ; C ₂ H ₂ : 2.6
162	600	Co(NO ₃) ₂ * 6H ₂ O	1.0	0.04; 0.1	1/0.2/1	35-55, 35.7-37.5	N ₂ (50%), C ₂ H ₂ (6%)	N ₂ : 0.5, C ₂ H ₂ : 1.0	crystals dissolved in ethanol	kinetic measurement of peak at 35-55°2theta, then kinetic measurement between 35.5-37.5 for 20 minutes; N ₂ : 6.8 ; C ₂ H ₂ : 7.6
163	600	Co(NO ₃) ₂ * 6H ₂ O	1.0	0.04; 0.1	1/0.2/1	35-55, 35.7-37.5	N ₂ (20%), C ₂ H ₂ (4%)	N ₂ : 0.5, C ₂ H ₂ : 1.0	crystals dissolved in ethanol	kinetic measurement of peak at 35-55°2theta, then kinetic measurement between 35.5-37.5 for 20 minutes; N ₂ : 2.5 ; C ₂ H ₂ : 5.0
164	600	Co(NO ₃) ₂ * 6H ₂ O					N ₂ (20%), C ₂ H ₂ (2%)	N ₂ : 0.5, C ₂ H ₂ : 1.0	solution, 0.05 mol/l	0.05 mol Lösung, 1 Tropfen, heating on temperature, 1 h waited, then exposed to acetylene (2%) for 10 minutes==> SEM
165	600	Co(NO ₃) ₂ * 6H ₂ O					N ₂ (20%), C ₂ H ₂ (6%)	N ₂ : 0.5, C ₂ H ₂ : 1.0	solution, 0.05 mol/l	0.05 mol Lösung, 1 Tropfen, heating on temperature, 1 h waited, then exposed to acetylene (6%) for 10 minutes==> SEM
166	25 - 600	Co(NO ₃) ₂ * 6H ₂ O	1.0	0.02	1/0.2/1	5-80	air		crystals dissolved in ethanol	repetition of #166
167	25 - 600	Co(NO ₃) ₂ * 6H ₂ O	1.0	0.02	1/0.2/1	5-80	air		crystals dissolved in ethanol	repetition of #166 --> Sample sloped, no useful signal obtained
168	25 - 150	Co(NO ₃) ₂ * 6H ₂ O	1.0	0.02	1/0.2/1	5-80	air		crystals dissolved in ethanol	repetition of # 112and #128, due to definition of crystals structure changemant
169	25 - 70	Co(NO ₃) ₂ * 6H ₂ O	1.0	0.02	1/0.2/1	10-70	air		crystals dissolved in ethanol	repetition of #166 --> dissolution of dehydration reaction of Ni(NO ₃) ₂ * 6H ₂ O
170	70	Co(NO ₃) ₂ * 6H ₂ O	1.0	0.02	1/0.2/1	10-70	air		crystals dissolved in ethanol	repetition of #166 --> dissolution of dehydration reaction of Ni(NO ₃) ₂ * 6H ₂ O
171	110 - 300	Co(NO ₃) ₂ * 6H ₂ O	1.0	0.02	1/0.2/1	10-70	air		crystals dissolved in ethanol	repetition of #166 --> dissolution of dehydration reaction of Ni(NO ₃) ₂ * 6H ₂ O
172	25 - 600	Co(NO ₃) ₂ * 6H ₂ O	1.0	0.02	1/0.2/1	10-70	N ₂ (25%); 3.4	N ₂ : 0.5	crystals dissolved in ethanol	repetition of #106 - #109
173	600	Co(NO ₃) ₂ * 6H ₂ O	1.0	0.04; 0.1	1/0.2/1	35-55, 35.7-37.5	N ₂ (20%), C ₂ H ₂ (2%)	N ₂ : 0.5, C ₂ H ₂ : 1.0	crystals dissolved in ethanol	kinetic measurement of peak at 35-55°2theta, then kinetic measurement between 35.5-37.5 for 60 minutes; N ₂ : 2.5 ; C ₂ H ₂ : 2.5
174	600	Co(NO ₃) ₂ * 6H ₂ O	1.0	0.04; 0.1	1/0.2/1	35-55, 35.7-37.5	N ₂ (20%), C ₂ H ₂ (3%)	N ₂ : 0.5, C ₂ H ₂ : 1.0	crystals dissolved in ethanol	kinetic measurement of peak at 35-55°2theta, then kinetic measurement between 35.5-37.5 for 40 minutes; N ₂ : 2.5 ; C ₂ H ₂ : 3.8
175	600	Co(NO ₃) ₂ * 6H ₂ O	1.0	0.04; 0.1	1/0.2/1	35-55, 35.7-37.5	N ₂ (20%), C ₂ H ₂ (2.5%)	N ₂ : 0.5, C ₂ H ₂ : 1.0	crystals dissolved in ethanol	kinetic measurement of peak at 35-55°2theta, then kinetic measurement between 35.5-37.5 for 20 minutes; N ₂ : 2.5 ; C ₂ H ₂ : 3.1
176	600	Co(NO ₃) ₂ * 6H ₂ O	1.0	0.04; 0.1	1/0.2/1	35-55, 35.7-37.5	N ₂ (20%), C ₂ H ₂ (2.25%)	N ₂ : 0.5, C ₂ H ₂ : 1.0	crystals dissolved in ethanol	kinetic measurement of peak at 35-55°2theta, then kinetic measurement between 35.5-37.5 for 20 minutes; N ₂ : 2.5 ; C ₂ H ₂ : 2.8
177	600	Co(NO ₃) ₂ * 6H ₂ O	1.0	0.04; 0.1	1/0.2/1	35-55, 35.7-37.5	N ₂ (20%), C ₂ H ₂ (2.25%)	N ₂ : 0.5, C ₂ H ₂ : 1.0	crystals dissolved in ethanol	repetition of #176 due to formation of CoO and Co ₃ O ₄ at 600°C instead of only Co ₃ O ₄ (another leak???)
178	600	Co(NO ₃) ₂ * 6H ₂ O	1.0	0.04; 0.1	1/0.2/1	35-55, 35.7-37.5	N ₂ (20%), C ₂ H ₂ (2.25%)	N ₂ : 0.5, C ₂ H ₂ : 1.0	crystals dissolved in ethanol	repetition of #177
179	600	Co(NO ₃) ₂ * 6H ₂ O	1.0	0.04; 0.1	1/0.2/1	35-55, 57-59	N ₂ (20%), C ₂ H ₂ (2.25%)	N ₂ : 0.5, C ₂ H ₂ : 1.0	crystals dissolved in ethanol	doesn't Co3C really not exist?
180	600	Co(NO ₃) ₂ * 6H ₂ O	1.0	0.04; 0.1	1/0.2/1	35-55, 43.5-45.5	N ₂ (20%), C ₂ H ₂ (2.25%)	N ₂ : 0.5, C ₂ H ₂ : 1.0	crystals dissolved in ethanol	doesn't Co3C really not exist?
181	600	Co(NO ₃) ₂ * 6H ₂ O					N ₂ (20%), C ₂ H ₂ (6%)	N ₂ : 0.5, C ₂ H ₂ : 1.0	solution, 0.05 mol/l	0.05 mol Lösung, 1 Tropfen, heating on temperature, 30 min waited, then exposed to acetylene (6%) for 10 minutes ==> SEM
182	600	Co(NO ₃) ₂ * 6H ₂ O					N ₂ (20%), C ₂ H ₂ (2%)	N ₂ : 0.5, C ₂ H ₂ : 1.0	solution, 0.05 mol/l	0.05 mol Lösung, 1 Tropfen, heating on temperature, 30 min waited, then exposed to acetylene (2%) for 1 minute ==> SEM
183	600	Co(NO ₃) ₂ * 6H ₂ O					N ₂ (20%), C ₂ H ₂ (2%)	N ₂ : 0.5, C ₂ H ₂ : 1.0	solution, 0.05 mol/l	0.05 mol Lösung, 1 Tropfen, heating on temperature, 30 min waited, then exposed to acetylene (2%) for 60 minutes ==> SEM
184	600	Co(NO ₃) ₂ * 6H ₂ O					N ₂ (20%), C ₂ H ₂ (6%)	N ₂ : 0.5, C ₂ H ₂ : 1.0	solution, 0.05 mol/l	0.05 mol Lösung, 1 Tropfen, heating on temperature, 30 min waited, then exposed to acetylene (6%) for 60 minutes ==> SEM
185	600	Co(NO ₃) ₂ * 6H ₂ O					N ₂ (20%), C ₂ H ₂ (6%)	N ₂ : 0.5, C ₂ H ₂ : 1.0	solution, 0.05 mol/l	0.05 mol Lösung, 1 Tropfen, heating on temperature, 30 min waited, then exposed to acetylene (6%) for 1 minute ==> SEM
186	750	Co(NO ₃) ₂ * 6H ₂ O					N ₂ (20%), C ₂ H ₂ (6%)	N ₂ : 0.5, C ₂ H ₂ : 1.0	solution, 0.05 mol/l	0.05 mol Lösung, 1 Tropfen, heating on temperature, 30 min waited, then exposed to acetylene (6%) for 10 minutes ==> SEM
187	750	Co(NO ₃) ₂ * 6H ₂ O					N ₂ (20%), C ₂ H ₂ (2%)	N ₂ : 0.5, C ₂ H ₂ : 1.0	solution, 0.05 mol/l	0.05 mol Lösung, 1 Tropfen, heating on temperature, 30 min waited, then exposed to acetylene (2%) for 10 minutes ==> SEM
188	600	Co(NO ₃) ₂ * 6H ₂ O					N ₂ (20%), C ₂ H ₂ (2.25%)	N ₂ : 0.5, C ₂ H ₂ : 1.0	solution, 0.05 mol/l	0.05 mol Lösung, 1 Tropfen, heating on temperature, 30 min waited, then exposed to acetylene (2.25%) for 10 minutes ==> SEM
189	750	Co(NO ₃) ₂ * 6H ₂ O					N ₂ (20%), C ₂ H ₂ (2.25%)	N ₂ : 0.5, C ₂ H ₂ : 1.0	solution, 0.05 mol/l	0.05 mol Lösung, 1 Tropfen, heating on temperature, 30 min waited, then exposed to acetylene (2.25%) for 10 minutes ==> SEM
190	600	Fe50Ni50					N ₂ (20%), C ₂ H ₂ (2%)	N ₂ : 0.5, C ₂ H ₂ : 1.0	solution, 0.05 mol/l	0.05 mol Lösung, 1 Tropfen, heating on temperature, 30 min waited, then exposed to acetylene (2%) for 10 minutes ==> SEM

Sample #	Temp. (°C)	Sample	sec/step	%stop	Blenden	2theta	gasflow	pressure (bar)	concentration	notes
191	600	Fe50Ni50					N ₂ (20%), C ₂ H ₂ (6%)	N ₂ : 0.5, C ₂ H ₂ : 1.0	solution, 0.05 mol/l	0.05 mol Lösung, 1 Tropfen, heating on temperature, 30 min waited, then exposed to acetylene (6%) for 10 minutes ==> SEM
192	600	Fe75Ni25					N ₂ (20%), C ₂ H ₂ (6%)	N ₂ : 0.5, C ₂ H ₂ : 1.0	solution, 0.05 mol/l	0.05 mol Lösung, 1 Tropfen, heating on temperature, 30 min waited, then exposed to acetylene (6%) for 10 minutes ==> SEM
193	600	Fe75Ni25					N ₂ (20%), C ₂ H ₂ (2%)	N ₂ : 0.5, C ₂ H ₂ : 1.0	solution, 0.05 mol/l	0.05 mol Lösung, 1 Tropfen, heating on temperature, 30 min waited, then exposed to acetylene (2%) for 10 minutes ==> SEM
194	600	Fe75Ni25					N ₂ (20%)	N ₂ : 0.5	solution, 0.05 mol/l	0.05 mol Lösung, 1 Tropfen, heating on temperature, 30 min waited ==> SEM
195	600	Fe50Ni50					N ₂ (20%)	N ₂ : 0.5	solution, 0.05 mol/l	0.05 mol Lösung, 1 Tropfen, heating on temperature, 30 min waited ==> SEM
196	600	Co(NO ₃) ₂ * 6H ₂ O	1.0	0.04; 0.1	1/0.2/1	35-55, 35.5-37.5	N ₂ (20%), C ₂ H ₂ (2.25%)	N ₂ : 0.5, C ₂ H ₂ : 1.0	crystals dissolved in ethanol	kinetic measurement of peak at 35-55°2theta, then kinetic measurement between 35.5-37.5 for 20 minutes; N ₂ : 2.25; C ₂ H ₂ : 2.25% (2.8)
197	600	Co(NO ₃) ₂ * 6H ₂ O	1.0	0.04; 0.1	1/0.2/1	35-55, 35.5-37.5	N ₂ (20%), C ₂ H ₂ (6%)	N ₂ : 0.5, C ₂ H ₂ : 1.0	crystals dissolved in ethanol	kinetic measurement of peak at 35-55°2theta, then kinetic measurement between 35.5-37.5 for 20 minutes; N ₂ : 2.0; C ₂ H ₂ : 6% (7.6)
198	600	Co(NO ₃) ₂ * 6H ₂ O	1.0	0.04; 0.1	1/0.2/1	35-55, 69.5-71.5	N ₂ (20%), C ₂ H ₂ (2.25%)	N ₂ : 0.5, C ₂ H ₂ : 1.0	crystals dissolved in ethanol	kinetic measurement of peak at 35-55°2theta, then kinetic measurement between 43.5-45.5 for 20 minutes; N ₂ : 2.25; C ₂ H ₂ : 3.1 ==> Carbides???
199	750	Co(NO ₃) ₂ * 6H ₂ O	1.0	0.04; 0.1	1/0.2/1	35-55, 35.5-37.5	N ₂ (20%), C ₂ H ₂ (2%)	N ₂ : 0.5, C ₂ H ₂ : 1.0	crystals dissolved in ethanol	kinetic measurement of peak at 35-55°2theta, then kinetic measurement between 35.5-37.5 for 60 minutes; N ₂ : 2.0; C ₂ H ₂ : 2% (2.5)
200	750	Co(NO ₃) ₂ * 6H ₂ O	1.0	0.04; 0.1	1/0.2/1	35-55, 35.5-37.5	N ₂ (20%), C ₂ H ₂ (2%)	N ₂ : 0.5, C ₂ H ₂ : 1.0	crystals dissolved in ethanol	kinetic measurement of peak at 35-55°2theta, then kinetic measurement between 35.5-37.5 for 60 minutes; N ₂ : 2.0; C ₂ H ₂ : 2% (2.5)
201	750	Co(NO ₃) ₂ * 6H ₂ O	1.0	0.04; 0.1	1/0.2/1	35-55, 35.5-37.5	N ₂ (20%), C ₂ H ₂ (2%)	N ₂ : 0.5, C ₂ H ₂ : 1.0	crystals dissolved in ethanol	kinetic measurement of peak at 35-55°2theta, then kinetic measurement between 35.5-37.5 for 60 minutes; N ₂ : 2.0; C ₂ H ₂ : 2% (2.5) --> should be reduced after a moment to Co. Chamber was greased --> 600°C only Co ₃ O ₄
202	25, 225, 25	Ni(NO ₃) ₂ * 6H ₂ O	2.0	0.02	1/0.2/1	5-80	N ₂ (20%)	N ₂ : 0.5	crystals dissolved in ethanol	measurement performed at 225°C due to determination of crystal structure and ongoing rietveld-refinements
203	25, 225, 25	Platglas	2.0	0.02	1/0.2/1	5-80				AF 45 platelets on platinum strip enables to elimination during rietveld-refinements
204	25, 225, 25	Platinum strip	2.0	0.02	1/0.2/1	5-80				Platinum strip
205	25, 225, 25	Co(NO ₃) ₂ * 6H ₂ O	2.0	0.02	1/0.2/1	10-80				measurement performed at 175°C due to determination of crystal structure and ongoing rietveld-refinements
206	600	Co(NO ₃) ₂ * 6H ₂ O					N ₂ (20%), C ₂ H ₂ (2.25%)	N ₂ : 0.5, C ₂ H ₂ : 1.0	solution, 0.05 mol/l	0.05 mol Lösung, 1 Tropfen, heating on temperature, 30 min waited, then exposed to acetylene (2.25%) for 1 minute ==> SEM
207	600	Co(NO ₃) ₂ * 6H ₂ O					N ₂ (20%), C ₂ H ₂ (2.25%)	N ₂ : 0.5, C ₂ H ₂ : 1.0	solution, 0.05 mol/l	0.05 mol Lösung, 1 Tropfen, heating on temperature, 30 min waited, then exposed to acetylene (2.25%) for 2 minutes ==> SEM
208	600	Co(NO ₃) ₂ * 6H ₂ O					N ₂ (20%), C ₂ H ₂ (2.25%)	N ₂ : 0.5, C ₂ H ₂ : 1.0	solution, 0.05 mol/l	0.05 mol Lösung, 1 Tropfen, heating on temperature, 30 min waited, then exposed to acetylene (2.25%) for 3 minutes ==> SEM
209	600	Co(NO ₃) ₂ * 6H ₂ O					N ₂ (20%), C ₂ H ₂ (2.25%)	N ₂ : 0.5, C ₂ H ₂ : 1.0	solution, 0.05 mol/l	0.05 mol Lösung, 1 Tropfen, heating on temperature, 30 min waited, then exposed to acetylene (2.25%) for 4 minutes ==> SEM
210	600	Co(NO ₃) ₂ * 6H ₂ O					N ₂ (20%), C ₂ H ₂ (2.25%)	N ₂ : 0.5, C ₂ H ₂ : 1.0	solution, 0.05 mol/l	0.05 mol Lösung, 1 Tropfen, heating on temperature, 30 min waited, then exposed to acetylene (2.25%) for 5 minutes ==> SEM
211	600	Co(NO ₃) ₂ * 6H ₂ O					N ₂ (20%), C ₂ H ₂ (2.25%)	N ₂ : 0.5, C ₂ H ₂ : 1.0	solution, 0.05 mol/l	0.05 mol Lösung, 1 Tropfen, heating on temperature, 30 min waited, then exposed to acetylene (2.25%) for 10 minutes ==> SEM
212	600	Co(NO ₃) ₂ * 6H ₂ O					N ₂ (20%), C ₂ H ₂ (2.25%)	N ₂ : 0.5, C ₂ H ₂ : 1.0	solution, 0.05 mol/l	0.05 mol Lösung, 1 Tropfen, heating on temperature, 30 min waited, then exposed to acetylene (2.25%) for 60 minutes ==> SEM
213	600	Co(NO ₃) ₂ * 6H ₂ O					N ₂ (20%)	N ₂ : 0.5	solution, 0.05 mol/l	0.05 mol Lösung, 1 Tropfen, heating on temperature, 30 min waited ==> SEM
214	600	Co(NO ₃) ₂ * 6H ₂ O	1.0	0.04; 0.1	1/0.2/1	35-55	N ₂ (20%), C ₂ H ₂ (2.25%)	N ₂ : 0.5, C ₂ H ₂ : 1.0	crystals dissolved in ethanol	exposure to acetylene (2.25%) during 3 hours due to exploration of peak-shift (is carbon liquified in cobalt structure, as seen by nickel?)
215	600	Co(NO ₃) ₂ * 6H ₂ O	1.0	0.04; 0.1	1/0.2/1	43.5-45.5	N ₂ (20%), C ₂ H ₂ (6%)	N ₂ : 0.5, C ₂ H ₂ : 1.0	crystals dissolved in ethanol	kinetic measurement of peak 43.5-45.5; N ₂ : 2.0; C ₂ H ₂ : 6% (7.8) due to peak evolution of the Co-peak
216	600	Co(NO ₃) ₂ * 6H ₂ O	1.0	0.04; 0.1	1/0.2/1	35-55	N ₂ (20%), C ₂ H ₂ (6%)	N ₂ : 0.5, C ₂ H ₂ : 1.0	crystals dissolved in ethanol	exposure to acetylene (6%) during 3 hours due to exploration of peak-shift (is carbon liquified in cobalt structure, as seen by nickel?)
217	600, 750	Co(NO ₃) ₂ * 6H ₂ O	1.0	0.02	1/0.2/1	5-80	N ₂ (20%)	N ₂ : 0.5	solution, 0.5 mol/l	0.5 mol Lösung, 1 Tropfen, due to testing of lowest peak resolution
218	25	quartz	1.0	0.1	1/0.2/1	35-45				
219	600, 750	Co(NO ₃) ₂ * 6H ₂ O	1.0	0.02	1/0.2/1	5-80	N ₂ (20%)	N ₂ : 0.5	solution, 0.1 mol/l	0.1 mol Lösung, 1 Tropfen, due to testing of lowest peak resolution
220	600	Co(NO ₃) ₂ * 6H ₂ O	1.0	0.02	1/0.2/1	35-55	N ₂ (20%)	N ₂ : 0.5	crystals dissolved in ethanol	is Co ₃ O ₄ stable at 600°C under nitrogen or does it transform to CoO after a while?

Sample #	Temp. (°C)	Sample	sec/step	%step	Blenden	2theta	gasflow	pressure (bar)	concentration	notes
221	750	Co(NO ₃) ₂ * 6H ₂ O	1.0	0.02	1/0.2/1	5-80	N ₂ (20%)	N ₂ : 0.5	solution, 0.1 mol/l	0.1 mol Lösung, 1 Tropfen, due to testing of lowest peak resolution, maybe repetition useful because not enough signal
222	600	Co(NO ₃) ₂ * 6H ₂ O	1.0	0.04; 0.2	1/0.2/1	43.5-45.5; 35-45	N ₂ (25%), C ₂ H ₂ (3%)	N ₂ : 0.5, C ₂ H ₂ : 1.0	crystals; 0.05 mol/l	crystals for measurement and TEM sample, 0.05 mol/l for SEM, 10 minutes C ₂ H ₂ (3%, 3.8) exposure --> magnetism
223	600	Co(NO ₃) ₂ * 6H ₂ O	1.0	0.04; 0.2	1/0.2/1	35.5-37.5; 35-45	N ₂ (25%), C ₂ H ₂ (3%)	N ₂ : 0.5, C ₂ H ₂ : 1.0	crystals; 0.05 mol/l	crystals for measurement and TEM sample, 0.05 mol/l for SEM, 5 minutes C ₂ H ₂ (3%, 3.8) exposure --> magnetism
224	600	Co(NO ₃) ₂ * 6H ₂ O	1.0	0.04; 0.2	1/0.2/1	35.5-37.5; 35-45	N ₂ (25%), C ₂ H ₂ (3%)	N ₂ : 0.5, C ₂ H ₂ : 1.0	crystals; 0.05 mol/l	crystals for measurement and TEM sample, 0.05 mol/l for SEM, 4 minutes C ₂ H ₂ (3%, 3.8) exposure --> magnetism
225	600	Co(NO ₃) ₂ * 6H ₂ O	1.0	0.1	1/0.2/1	35-55	N ₂ (25%)	N ₂ : 0.5	crystals	crystals for measurement and TEM sample, 0.05 mol/l for SEM, 20 minutes at 600°C --> as well magnetic??? --> no magnetism
226	600	Co(NO ₃) ₂ * 6H ₂ O	1.0	0.04; 0.2	1/0.2/1	43.5-45.5; 35-45	N ₂ (25%), C ₂ H ₂ (3%)	N ₂ : 0.5, C ₂ H ₂ : 1.0	crystals; 0.05 mol/l	crystals for measurement and TEM sample, 0.05 mol/l for SEM, 3 minutes C ₂ H ₂ (3%, 3.8) exposure
227	600	Co(NO ₃) ₂ * 6H ₂ O	1.0	0.04; 0.2	1/0.2/1	43.5-45.5; 35-45	N ₂ (25%), C ₂ H ₂ (3%)	N ₂ : 0.5, C ₂ H ₂ : 1.0	crystals; 0.05 mol/l	crystals for measurement and TEM sample, 0.05 mol/l for SEM, 3 minutes C ₂ H ₂ (3%, 3.8) exposure
228	600	Co(NO ₃) ₂ * 6H ₂ O	1.0	0.04; 0.2	1/0.2/1	43.5-45.5; 35-45	N ₂ (25%), C ₂ H ₂ (3%)	N ₂ : 0.5, C ₂ H ₂ : 1.0	crystals; 0.05 mol/l	crystals for measurement and TEM sample, 0.05 mol/l for SEM, 3 minutes C ₂ H ₂ (3%, 3.8) exposure
229	600	Co(NO ₃) ₂ * 6H ₂ O	1.0	0.02	1/0.2/1	35-55	N ₂ (25%), C ₂ H ₂ (3%)	N ₂ : 0.5, C ₂ H ₂ : 1.0	crystals	crystals for measurement and TEM sample, 0.05 mol/l for SEM, 0 - 3 hours C ₂ H ₂ (3%, 3.8) exposure due to possible peak shift (liquefaction of C in Co)
230	600	Co(NO ₃) ₂ * 6H ₂ O	1.0	0.02	1/0.2/1	35-55	N ₂ (25%), C ₂ H ₂ (6%)	N ₂ : 0.5, C ₂ H ₂ : 1.0	crystals	crystals for measurement and TEM sample, 0.05 mol/l for SEM, 0 - 3 hours C ₂ H ₂ (6%, 7.6) exposure due to possible peak shift (liquefaction of C in Co)
231	25, 400, 800	Platinum strip	1.0	0.02	1/0.2/1	5-120	air		platinum strip	platinum strip after change of capton-windows and cleaning of reaction chamber
232	25, 565 - 605	SiO ₂ pure	2.0	0.02	1/0.2/1	38-43	air		SiO ₂ pure	crystals dissolved in ethanol --> calibration of HT-Diffractometer based on α : β transition in SiO ₂
233	25, 565 - 605	SiO ₂ pure	2.0	0.02	1/0.2/1	38-43	air		SiO ₂ pure	crystals dissolved in ethanol --> calibration of HT-Diffractometer based on α : β transition in SiO ₂ --> Repetition of #232
234	25, 400, 800	Platinum strip	1.0	0.02	1/0.2/1	30-120	air		platinum strip	platinum strip after change of capton-windows and cleaning of reaction chamber
235	25 - 750	Cr(NO ₃) ₃ * 9H ₂ O	1.0	0.02	1/0.2/1	10-80	air		crystals dissolved in ethanol	first overview of Cr(NO ₃) ₃ 9H ₂ O, behaviour under normal atmosphere conditions --> sample slipped on the pt-strip --> no signals
236	25 - 750	Cr(NO ₃) ₃ * 9H ₂ O	1.0	0.02	1/0.2/1	10-80	air		crystals dissolved in ethanol	first overview of Cr(NO ₃) ₃ 9H ₂ O, behaviour under normal atmosphere conditions
237	25, 600	Cr(NO ₃) ₃ * 9H ₂ O	1.0	0.02	1/0.2/1	10-80	air		crystals dissolved in ethanol	first overview of Cr(NO ₃) ₃ 9H ₂ O, behaviour under normal atmosphere conditions
238	25 - 750	Cr(NO ₃) ₃ * 9H ₂ O	1.0	0.02	1/0.2/1	10-80	air		crystals dissolved in ethanol	first overview of Cr(NO ₃) ₃ 9H ₂ O, behaviour under normal atmosphere conditions; sample dried for 3 days on air
239	25	Cr(NO ₃) ₃ * 9H ₂ O	1.0	0.02	1/0.2/1	10-80	air		crystals dissolved in ethanol	same sample as #238, drop removed and glass platelets with the rest measured
240	50	Cr(NO ₃) ₃ * 9H ₂ O	1.0	0.02	1/0.2/1	10-80	air		crystals dissolved in ethanol	sample dried for 3 days on air
241	100	Cr(NO ₃) ₃ * 9H ₂ O	1.0	0.02	1/0.2/1	10-80	air		crystals dissolved in ethanol	same sample as #240
242	150	Cr(NO ₃) ₃ * 9H ₂ O	1.0	0.02	1/0.2/1	10-80	air		crystals dissolved in ethanol	same sample as #240
243	200	Cr(NO ₃) ₃ * 9H ₂ O	1.0	0.02	1/0.2/1	10-80	air		crystals dissolved in ethanol	same sample as #240
244	200	Cr(NO ₃) ₃ * 9H ₂ O	1.0	0.02	1/0.2/1	10-80	air		crystals dissolved in ethanol	same sample as #240, drop removed and glass platelets with the rest measured
245	250	Cr(NO ₃) ₃ * 9H ₂ O	1.0	0.02	1/0.2/1	10-80	air		crystals dissolved in ethanol	same sample as #240, drop removed and glass platelets with the rest measured
246	300	Cr(NO ₃) ₃ * 9H ₂ O	1.0	0.02	1/0.2/1	10-80	air		crystals dissolved in ethanol	rest measured new sample
247	300	Cr(NO ₃) ₃ * 9H ₂ O	1.0	0.02	1/0.2/1	10-80	air		crystals dissolved in ethanol	same sample as #246, but drop removed, crushed and again dissolved in ethanol, than dried on air on the glass platelets --> measured
248	350, 400	Cr(NO ₃) ₃ * 9H ₂ O	1.0	0.02	1/0.2/1	10-80	air		crystals dissolved in ethanol	same sample as #246
249	450, 500, 600, 750	Cr(NO ₃) ₃ * 9H ₂ O	1.0	0.02	1/0.2/1	10-80	air		crystals dissolved in ethanol	same sample as #246
250	310 - 390	Cr(NO ₃) ₃ * 9H ₂ O	1.0	0.02	1/0.2/1	10-80	air		crystals dissolved in ethanol	sample annealed at 300°C, drop removed, crushed and again dissolved in ethanol, than subsequent dried on air on the glass platelets --> measurement

Sample #	Temp. (°C)	Sample	sec/step	%step	Blendn	2theta	gasflow	pressure (bar)	concentration	notes
251	25 - 150	Cr(NO ₃) ₃ * 9H ₂ O	1.0	0.02	1/0.2/1	10-80	N ₂ (25%), 3.2	N ₂ : 0.5	crystals dissolved in ethanol	sample dried on air for one week. Heating procedure under nitrogen atmosphere. first overview
252	300	Cr(NO ₃) ₃ * 9H ₂ O	1.0	0.02	1/0.2/1	10-80	N ₂ (25%), 3.2	N ₂ : 0.5	crystals dissolved in ethanol	sample heated up to 300°C
253	300 - 750	Cr(NO ₃) ₃ * 9H ₂ O	1.0	0.02	1/0.2/1	10-80	N ₂ (25%), 3.2	N ₂ : 0.5	crystals dissolved in ethanol	sample annealed at 300°C, drop removed, crushed and again dissolved in ethanol, then subsequent dried on air on the glass platelets --> measurement
254	60 - 90	Cr(NO ₃) ₃ * 9H ₂ O	1.0	0.02	1/0.2/1	10-80	N ₂ (25%), 3.2	N ₂ : 0.5	crystals dissolved in ethanol	new sample
255	60 - 90	Cr(NO ₃) ₃ * 9H ₂ O	1.0	0.02	1/0.2/1	10-80	air		crystals dissolved in ethanol	new sample
256	410 - 440	Cr(NO ₃) ₃ * 9H ₂ O	1.0	0.02	1/0.2/1	10-80	N ₂ (25%), 3.2	N ₂ : 0.5	crystals dissolved in ethanol	sample annealed at 300°C, drop removed, crushed and again dissolved in ethanol, then subsequent dried on air on the glass platelets --> measurement
257	25, 400, 800	Platinum strip	1.0	0.02	1/0.2/1	30-130	air		platinum strip	measurement due to clarification of pt-strip contamination
258	100	Cr(NO ₃) ₃ * 9H ₂ O	1.0	0.02	1/0.2/1	25-70	N ₂ (25%), 3.2	N ₂ : 0.5	0.05 mol/l, crystals dis. Eth	SEM-Sample, 0.05 mol/l, 1 h revealed on temperature; measurement due to affirmation of atmospheric conditions
259	200	Cr(NO ₃) ₃ * 9H ₂ O	1.0	0.02	1/0.2/1	25-70	N ₂ (25%), 3.2	N ₂ : 0.5	0.05 mol/l, crystals dis. Eth	SEM-Sample, 0.05 mol/l, 1 h revealed on temperature; measurement due to affirmation of atmospheric conditions
260	300	Cr(NO ₃) ₃ * 9H ₂ O	1.0	0.02	1/0.2/1	25-70	N ₂ (25%), 3.2	N ₂ : 0.5	0.05 mol/l, crystals dis. Eth	SEM-Sample, 0.05 mol/l, 1 h revealed on temperature; measurement due to affirmation of atmospheric conditions
261	400	Cr(NO ₃) ₃ * 9H ₂ O	1.0	0.02	1/0.2/1	25-70	N ₂ (25%), 3.2	N ₂ : 0.5	0.05 mol/l, crystals dis. Eth	SEM-Sample, 0.05 mol/l, 1 h revealed on temperature; measurement due to affirmation of atmospheric conditions and grain growth with ongoing heating procedure
262	500	Cr(NO ₃) ₃ * 9H ₂ O	1.0	0.02	1/0.2/1	25-70	N ₂ (25%), 3.2	N ₂ : 0.5	0.05 mol/l, crystals dis. Eth	SEM-Sample, 0.05 mol/l, 1 h revealed on temperature; measurement due to affirmation of atmospheric conditions and grain growth with ongoing heating procedure
263	600	Cr(NO ₃) ₃ * 9H ₂ O	1.0	0.02	1/0.2/1	25-70	N ₂ (25%), 3.2	N ₂ : 0.5	0.05 mol/l, crystals dis. Eth	SEM-Sample, 0.05 mol/l, 1 h revealed on temperature; measurement due to affirmation of atmospheric conditions and grain growth with ongoing heating procedure
264	750	Cr(NO ₃) ₃ * 9H ₂ O	1.0	0.02	1/0.2/1	25-70	N ₂ (25%), 3.2	N ₂ : 0.5	0.05 mol/l, crystals dis. Eth	SEM-Sample, 0.05 mol/l, 1 h revealed on temperature; measurement due to affirmation of atmospheric conditions and grain growth with ongoing heating procedure
265	200 - 750	Cr(NO ₃) ₃ * 9H ₂ O	1.0	0.02	1/0.2/1	25-70	N ₂ (25%), 3.2	N ₂ : 0.5	crystals dissolved in ethanol	Sample used for grain size evolution (FVHM)
267	25, 400, 800	Platinum strip	1.0	0.02	1/0.2/1	30-110	air		platinum strip	measurement due to clarification of pt-strip contamination
268	600	Co(NO ₃) ₂ * 6H ₂ O	1.0	0.04	1/0.2/1	35-55	N ₂ (25%, 3.0), C ₂ H ₂ (25sccm)	N ₂ : 0.5, C ₂ H ₂ : 1.0	crystals dissolved in ethanol	peak shift of Co during acetylene treatment for 4 hours --> measurement aborbed due to sample sided, no signal
269	600	Co(NO ₃) ₂ * 6H ₂ O	1.0	0.04	1/0.2/1	35-55	N ₂ (25%, 3.0), C ₂ H ₂ (25sccm)	N ₂ : 0.5, C ₂ H ₂ : 1.0	crystals dissolved in ethanol	peak shift of Co during acetylene treatment for 4 hours
270	750	Co(NO ₃) ₂ * 6H ₂ O	1.0	0.04	1/0.2/1	35-55	N ₂ (25%, 3.0), C ₂ H ₂ (25sccm)	N ₂ : 0.5, C ₂ H ₂ : 1.0	crystals dissolved in ethanol	peak shift of Co during acetylene treatment for 4 hours
271	600	Co(NO ₃) ₂ * 6H ₂ O	1.0	0.04	1/0.2/1	35-55	N ₂ (25%, 3.0), C ₂ H ₂ (25sccm)	N ₂ : 0.5, C ₂ H ₂ : 1.0	crystals dissolved in ethanol	peak shift of Co during acetylene treatment for 4 hours
272	600	Co(NO ₃) ₂ * 6H ₂ O	1.0	0.04	1/0.2/1	35-55; 35.5-37.5	N ₂ (25%, 3.0), C ₂ H ₂ (25sccm)	N ₂ : 0.5, C ₂ H ₂ : 1.0	crystals dissolved in ethanol	peak vs. Time
273	750	Co(NO ₃) ₂ * 6H ₂ O	1.0	0.04	1/0.2/1	35-55; 35.5-37.5	N ₂ (25%, 3.0), C ₂ H ₂ (25sccm)	N ₂ : 0.5, C ₂ H ₂ : 1.0	crystals dissolved in ethanol	peak vs. Time
274	750	Co(NO ₃) ₂ * 6H ₂ O	1.0	0.04	1/0.2/1	35-55; 43.5-45.5	N ₂ (25%, 3.0), C ₂ H ₂ (25sccm)	N ₂ : 0.5, C ₂ H ₂ : 1.0	crystals dissolved in ethanol	peak vs. Time
275	600	Cr(NO ₃) ₃ * 9H ₂ O	1.0	0.02	1/0.2/1	30-50	N ₂ (25%, 3.0), C ₂ H ₂ (25sccm)	N ₂ : 0.5, C ₂ H ₂ : 1.0	crystals dissolved in ethanol	first overview, sample not useful due to foam formation --> All Cr-samples have to be heated up to 300°C, then crushed and again dissolved in ethanol before measurement
276	750	Co(NO ₃) ₂ * 6H ₂ O	1.0	0.04	1/0.2/1	35-55; 43.5-45.5	N ₂ (25%, 3.0), C ₂ H ₂ (75sccm)	N ₂ : 0.5, C ₂ H ₂ : 1.0	crystals dissolved in ethanol	peak vs. Time
277	750	Co(NO ₃) ₂ * 6H ₂ O	1.0	0.04	1/0.2/1	35-55; 35.5-37.5	N ₂ (25%, 3.0), C ₂ H ₂ (75sccm)	N ₂ : 0.5, C ₂ H ₂ : 1.0	crystals dissolved in ethanol	peak vs. Time
278	750	Cr(NO ₃) ₃ * 9H ₂ O	1.0	0.02	1/0.2/1	30-50	N ₂ (25%, 3.0), C ₂ H ₂ (25sccm)	N ₂ : 0.5, C ₂ H ₂ : 1.0	crystals dissolved in ethanol	first overview
279	600	Cr(NO ₃) ₃ * 9H ₂ O	1.0	0.02	1/0.2/1	30-50	N ₂ (25%, 3.0), C ₂ H ₂ (75sccm)	N ₂ : 0.5, C ₂ H ₂ : 1.0	crystals dissolved in ethanol	first overview, but 3 times more C ₂ H ₂ than #275 --> no reaction at all, no reduction of the chromium oxide
280	750	Cr(NO ₃) ₃ * 9H ₂ O	1.0	0.02	1/0.2/1	30-50	N ₂ (25%, 3.0), C ₂ H ₂ (75sccm)	N ₂ : 0.5, C ₂ H ₂ : 1.0	crystals dissolved in ethanol	first overview, but 3 times more C ₂ H ₂ than #276 --> no reaction at all, no reduction of the chromium oxide

Sample #	Temp. (°C)	Sample	sec/step	%step	Blend	θ	gasflow	pressure (bar)	concentration	notes
281	600	Cr(NO ₃) ₃ * 9H ₂ O	1.0	0.02	1/0.2/1	30-50	N ₂ (25%, 3.0), C ₂ H ₂ (150sccm)	N ₂ : 0.5, C ₂ H ₂ : 1.0	crystals dissolved in ethanol	first overview, but twice more C ₂ H ₂ than #279 --> no reaction at all, no reduction of the chromium oxide
282	600	Cr(NO ₃) ₃ * 9H ₂ O	1.0	0.02	1/0.2/1	30-50	N ₂ (25%, 3.0), C ₂ H ₂ (5sccm)	N ₂ : 0.5, C ₂ H ₂ : 1.0	crystals dissolved in ethanol	all cr-samples seemed to be covered by a carbon layer, this may cause no reduction of the chromium oxide --> idea of very small C ₂ H ₂ amount
283	600	Cr(NO ₃) ₃ * 9H ₂ O	1.0	0.02	1/0.2/1	30-40	N ₂ (25%, 3.0), C ₂ H ₂ (25sccm)	N ₂ : 0.5, C ₂ H ₂ : 1.0	0.05 mol/l, crystals dis. Eth	SEM-Sample, 0.05 mol/l, 10 min revealed on temperature before measurement obtained; 10 minutes exposed to 25sccm C ₂ H ₂
284	600	Cr(NO ₃) ₃ * 9H ₂ O	1.0	0.02	1/0.2/1	30-40	N ₂ (25%, 3.0), C ₂ H ₂ (75sccm)	N ₂ : 0.5, C ₂ H ₂ : 1.0	0.05 mol/l, crystals dis. Eth	SEM-Sample, 0.05 mol/l, 10 min revealed on temperature before measurement obtained; 10 minutes exposed to 75sccm C ₂ H ₂
285	750	Cr(NO ₃) ₃ * 9H ₂ O	1.0	0.02	1/0.2/1	30-40	N ₂ (25%, 3.0), C ₂ H ₂ (75sccm)	N ₂ : 0.5, C ₂ H ₂ : 1.0	0.05 mol/l, crystals dis. Eth	SEM-Sample, 0.05 mol/l, 10 min revealed on temperature before measurement obtained; 10 minutes exposed to 75sccm C ₂ H ₂
286	750	Cr(NO ₃) ₃ * 9H ₂ O	1.0	0.02	1/0.2/1	30-40	N ₂ (25%, 3.0), C ₂ H ₂ (25sccm)	N ₂ : 0.5, C ₂ H ₂ : 1.0	0.05 mol/l, crystals dis. Eth	SEM-Sample, 0.05 mol/l, 10 min revealed on temperature before measurement obtained; 10 minutes exposed to 25sccm C ₂ H ₂
287	600	Cr(NO ₃) ₃ * 9H ₂ O	1.0	0.02	1/0.2/1	20-70	N ₂ (25%, 3.0)	N ₂ : 0.5, C ₂ H ₂ : 1.0	crystals dissolved in ethanol	Peak evolution during heating procedure
288	25 - 750	MoO ₂	1.0	0.02	1/0.2/1	20-70	N ₂ (25%, 3.0)	N ₂ : 0.5	crystals dissolved in ethanol	Peak evolution during heating procedure
289	25 - 750	MoO ₂	1.0	0.02	1/0.2/1	20-70	air		crystals dissolved in ethanol	Peak evolution during heating procedure
290	625 - 725, step 25	MoO ₂	1.0	0.02	1/0.2/1	20-70	N ₂ (25%, 3.0)	N ₂ : 0.5	crystals dissolved in ethanol	Peak evolution during heating procedure
291	325 - 725	MoO ₂	1.0	0.02	1/0.2/1	20-70	air		crystals dissolved in ethanol	Peak evolution during heating procedure
292	600	Mo-Ac-N2	1.0	0.02	1/0.2/1	20-70	N ₂ (25%, 3.0), C ₂ H ₂ (25sccm)	N ₂ : 0.5, C ₂ H ₂ : 1.0	crystals dissolved in ethanol	First overview after 50 minutes of C ₂ H ₂ (25sccm) inlet
293	750	Mo-Ac-N2	1.0	0.02	1/0.2/1	20-70	N ₂ (25%, 3.0), C ₂ H ₂ (25sccm)	N ₂ : 0.5, C ₂ H ₂ : 1.0	crystals dissolved in ethanol	First overview after 50 minutes of C ₂ H ₂ (25sccm) inlet
294	600	Mo-Ac-N2	1.0	0.02	1/0.05/1	20-70	N ₂ (25%, 3.0), C ₂ H ₂ (75sccm)	N ₂ : 0.5, C ₂ H ₂ : 1.0	crystals dissolved in ethanol	peak-shift and evolution after C ₂ H ₂ (75sccm) inlet
295	750	Mo-Ac-N2	1.0	0.02	1/0.2/1	20-70	N ₂ (25%, 3.0), C ₂ H ₂ (75sccm)	N ₂ : 0.5, C ₂ H ₂ : 1.0	crystals dissolved in ethanol	peak-shift and evolution after C ₂ H ₂ (75sccm) inlet
296	25, 400, 800	Platinum strip	1.0	0.02	1/0.2/1	10-120	air		platinum strip	measurement due to clarification of pt-strip contamination
297	600	Fe-Ac-N2	1.0	0.04	1/0.2/1	30-70	N ₂ (25%, 3.0), C ₂ H ₂ (25sccm)	N ₂ : 0.5, C ₂ H ₂ : 1.0	crystals dissolved in ethanol	Peak evolution and peak movement during C ₂ H ₂ treatment for 5 h (carbide decomposition, peak shift of Fe) --> no carbide peaks, weak signals!
298	600	Fe-Ac-N2	1.0	0.04	1/0.2/1	30-70	N ₂ (25%, 3.0), C ₂ H ₂ (75sccm)	N ₂ : 0.5, C ₂ H ₂ : 1.0	crystals dissolved in ethanol	Peak evolution and peak movement during C ₂ H ₂ treatment for 5 h (carbide decomposition, peak shift of Fe)
299	25, 600	Fe-Ac-N2	1.0	0.04	1/0.2/1	30-70	N ₂ (25%, 3.0)	N ₂ : 0.5	crystals dissolved in ethanol	Peak evolution before acetylene treatment
300	600	Fe-Ac-N2	1.0	0.04	1/0.2/1	30-70	N ₂ (25%, 3.0), C ₂ H ₂ (75sccm)	N ₂ : 0.5, C ₂ H ₂ : 1.0	crystals dissolved in ethanol	Peak evolution and peak movement during C ₂ H ₂ treatment for 5 h (carbide decomposition, peak shift of Fe)
301	600	Fe-Ac-N2	1.0	0.04	1/0.2/1	30-70	N ₂ (25%, 3.0), C ₂ H ₂ (75sccm)	N ₂ : 0.5, C ₂ H ₂ : 1.0	crystals dissolved in ethanol	repetition of #300 due to confirmation
302	600	Fe-Ac-N2	1.0	0.04	1/0.2/1	30-70	N ₂ (25%, 3.0), C ₂ H ₂ (75sccm)	N ₂ : 0.5, C ₂ H ₂ : 1.0	crystals dissolved in ethanol	same sample as #302, continuation with acetylene treatment
303	600	Cr(NO ₃) ₃ * 9H ₂ O	1.0	0.03	1/0.2/1	20-50	N ₂ (25%, 3.0), C ₂ H ₂ (75sccm)	N ₂ : 0.5, C ₂ H ₂ : 1.0	crystals dissolved in ethanol	repetition of #282, but with better soler slit 0.2 (better signals) --> carbides???
304	750	Fe-Ac-N2	1.0	0.04	1/0.2/1	30-70	N ₂ (25%, 3.0), C ₂ H ₂ (75sccm)	N ₂ : 0.5, C ₂ H ₂ : 1.0	crystals dissolved in ethanol	Peak evolution and peak movement during C ₂ H ₂ treatment for 5 h (carbide decomposition, peak shift of Fe)
305	600	Fe-Ac-N2	1.0	0.04	1/0.2/1	30-70	N ₂ (25%, 3.0), C ₂ H ₂ (75sccm)	N ₂ : 0.5, C ₂ H ₂ : 1.0	crystals dissolved in ethanol	Peak evolution and peak movement during C ₂ H ₂ treatment for 5 h (carbide decomposition, peak shift of Fe)
306	600	Fe-Ac-N2	1.0	0.04	1/0.2/1	30-70	N ₂ (25%, 3.0), C ₂ H ₂ (75sccm)	N ₂ : 0.5, C ₂ H ₂ : 1.0	crystals dissolved in ethanol	same sample as #305 but again treated with C ₂ H ₂ for 4 h
307	600	Ni-H2-N2	1.0	0.04	1/0.2/1	30-70	N ₂ (30%, 3.5), H ₂ (25sccm)	N ₂ : 0.5, H ₂ : 0.5	crystals dissolved in ethanol	Heated up under nitrogen to 600°C, waited 30 min before inlet of H ₂ --> Peak-shift of NiO and Ni visible?
308	600	Ni-H2-N2	1.0	0.04	1/0.2/1	30-70	N ₂ (30%, 3.5), H ₂ + C ₂ H ₂ (25sccm)	N ₂ : 0.5, H ₂ + C ₂ H ₂ : 0.5	crystals dissolved in ethanol	Heated up under nitrogen to 400°C, then added 25 sccm H ₂ while heating on 600°C, waited 30 min before inlet of C ₂ H ₂ --> Peak-shift of Ni visible?
309	25, 400, 800	Platinum strip	1.0	0.02	1/0.2/1	10-120	air		platinum strip	measurement due to clarification of pt-strip contamination
310	600	Ni-H2-N2	1.0	0.04	1/0.2/1	30-70	N ₂ (25%, 3.0), C ₂ H ₂ (25sccm)	N ₂ : 0.5, C ₂ H ₂ : 0.5	crystals dissolved in ethanol	Heated up under nitrogen to 600°C, waited 30 min before inlet of C ₂ H ₂ --> Peak-shift of Ni visible?

Sample #	Temp. (°C)	Sample	sec/step	%stop	Blendn	2theta	gasflow	pressure (bar)	concentration	notes
311	600	Ni-H2-N2	1.0	0.04	1/0.2/1	30-70	N ₂ (25%, 3.0), H ₂ + C ₂ H ₂ (25sccm)	N ₂ : 0.5, H ₂ + C ₂ H ₂ : 0.5	crystals dissolved in ethanol	Repetition of #308
312	600	Ni-H2-N2	1.0	0.04	1/0.2/1	43.5-45.5	N ₂ (25%, 3.0), C ₂ H ₂ (5sccm)	N ₂ : 0.5, C ₂ H ₂ : 0.5	crystals dissolved in ethanol	minimal requirement of acetylene flow rate for the reduction of NiO to pure nickel
313	600	Ni-H2-N2	1.0	0.04	1/0.2/1	43.5-45.5	N ₂ (25%, 3.0), C ₂ H ₂ (10sccm)	N ₂ : 0.5, C ₂ H ₂ : 0.5	crystals dissolved in ethanol	minimal requirement of acetylene flow rate for the reduction of NiO to pure nickel
314	600	Ni-H2-N2	1.0	0.04	1/0.2/1	43.5-45.5	N ₂ (25%, 3.0), C ₂ H ₂ (15sccm)	N ₂ : 0.5, C ₂ H ₂ : 0.5	crystals dissolved in ethanol	minimal requirement of acetylene flow rate for the reduction of NiO to pure nickel → Reduction after about 20 minutes to nickel observed
315	600	Co-H2-N2	1.0	0.02	1/0.2/1	35-55	N ₂ (25%, 3.0), H ₂ (25sccm)	N ₂ : 0.5, H ₂ : 0.5	crystals dissolved in ethanol	heated up under nitrogen to 600°C, waited 30 min before inlet of H ₂ → Peak-shift of Co ₃ O ₄ , CoO and finally of pure Co
316	600	Co-Ac-N2	1.0	0.02	1/0.2/1	35-55	N ₂ (25%, 3.0), C ₂ H ₂ (25sccm)	N ₂ : 0.5, C ₂ H ₂ : 0.5	crystals dissolved in ethanol	heated up under nitrogen to 600°C, waited 30 min before inlet of C ₂ H ₂ → Peak-shift of Co ₃ O ₄ , CoO and finally of pure Co
317	600	Co-H2-N2	1.0	0.02	1/0.2/1	35-55	N ₂ (25%, 3.0), H ₂ + C ₂ H ₂ (25sccm)	N ₂ : 0.5, H ₂ + C ₂ H ₂ : 0.5	crystals dissolved in ethanol	Heated up under nitrogen to 400°C, then added 25 sccm H ₂ while heating on 600°C, waited 30 min before inlet of C ₂ H ₂ → Carbide present????
318	600	Ni-H2-N2	1.0	0.04	1/0.2/1	30-70	N ₂ (30%, 3.5), H ₂ + C ₂ H ₂ (25sccm)	N ₂ : 0.5, H ₂ + C ₂ H ₂ : 0.5	crystals dissolved in ethanol	Repetition of #317, Heated up under nitrogen to 400°C, then added 25 sccm H ₂ while heating on 600°C, waited 30 min before inlet of C ₂ H ₂ → Carbide present????
319	600	Co-H2-N2	1.0	0.02	1/0.2/1	35-55	N ₂ (25%, 3.0), H ₂ + C ₂ H ₂ (25sccm)	N ₂ : 0.5, H ₂ + C ₂ H ₂ : 0.5	crystals dissolved in ethanol	Repetition of #317, Heated up under nitrogen to 400°C, then added 25 sccm H ₂ while heating on 600°C, waited 30 min before inlet of C ₂ H ₂ → Carbide present????
320	600	Co-H2-N2	1.0	0.02	1/0.2/1	35-55	N ₂ (25%, 3.0), H ₂ (25sccm)	N ₂ : 0.5, H ₂ : 0.5	crystals dissolved in ethanol	Repetition of #316, Heated up under nitrogen to 600°C, waited 30 min before inlet of H ₂ → Peak-shift of Co ₃ O ₄ , CoO and finally of pure Co
321	600	Ni-H2-N2	1.0	1.00	1/0.2/1	43-46.6	N ₂ (30%, 3.5), H ₂ + C ₂ H ₂ (25sccm)	N ₂ : 0.5, H ₂ + C ₂ H ₂ : 0.5	crystals dissolved in ethanol	Heated up under nitrogen to 400°C, then added 25 sccm H ₂ while heating on 600°C, waited 30 min before inlet of C ₂ H ₂ → what happen within the first ten minutes?
322	600	Co-SEM	1.0	0.04	1/0.2/1	35-55	N ₂ (25%, 3.0)	N ₂ : 0.5	0.05 mol/l, crystals dis. Eth	SEM-Sample, 1 drop of 0.05 mol/l solution, 10 minutes revealed on temperature
323	600	Co-SEM	1.0	0.04	1/0.2/1	35-55	N ₂ (25%, 3.0), H ₂ (25sccm)	N ₂ : 0.5, H ₂ : 0.5	0.05 mol/l, crystals dis. Eth	SEM-Sample, 1 drop of 0.05 mol/l solution, 10 minutes revealed on temperature, before H ₂ treatment for 5 minutes
324	600	Co-SEM	1.0	0.04	1/0.2/1	35-55	N ₂ (25%, 3.0), H ₂ (25sccm)	N ₂ : 0.5, H ₂ : 0.5	0.05 mol/l, crystals dis. Eth	SEM-Sample, 1 drop of 0.05 mol/l solution, 10 minutes revealed on temperature, before H ₂ treatment for 5 minutes
325	600	Co-SEM	1.0	0.04	1/0.2/1	35-55	N ₂ (30%, 3.5), H ₂ + C ₂ H ₂ (25sccm)	N ₂ : 0.5, H ₂ + C ₂ H ₂ : 0.5	0.05 mol/l, crystals dis. Eth	SEM-Sample, 1 drop of 0.05 mol/l solution, heated up to 400°C, then H ₂ added by subsequent heating to 600°C, remained for 10 minutes, before acetylene inlet
326	600	Co-SEM	1.0	0.04	1/0.2/1	35-55	N ₂ (30%, 3.5), H ₂ + C ₂ H ₂ (25sccm)	N ₂ : 0.5, H ₂ + C ₂ H ₂ : 0.5	0.05 mol/l, crystals dis. Eth	SEM-Sample, 1 drop of 0.05 mol/l solution, heated up to 400°C, then H ₂ added by subsequent heating to 600°C, remained for 10 minutes, then 5 minutes C ₂ H ₂ treatment
327	600	Co-SEM	1.0	0.04	1/0.2/1	35-55	N ₂ (30%, 3.5), H ₂ + C ₂ H ₂ (25sccm)	N ₂ : 0.5, H ₂ + C ₂ H ₂ : 0.5	0.05 mol/l, crystals dis. Eth	SEM-Sample, 1 drop of 0.05 mol/l solution, heated up to 400°C, then H ₂ added by subsequent heating to 600°C, remained for 10 minutes, then 25 minutes C ₂ H ₂ treatment
328	600	Co-SEM	1.0	0.04	1/0.2/1	35-55	N ₂ (30%, 3.5), C ₂ H ₂ (25sccm)	N ₂ : 0.5, C ₂ H ₂ : 0.5	0.05 mol/l, crystals dis. Eth	SEM-Sample, 1 drop of 0.05 mol/l solution, 10 minutes revealed on temperature, then C ₂ H ₂ treatment for 5 minutes
329	600	Co-SEM	1.0	0.04	1/0.2/1	35-55	N ₂ (30%, 3.5), C ₂ H ₂ (25sccm)	N ₂ : 0.5, C ₂ H ₂ : 0.5	0.05 mol/l, crystals dis. Eth	SEM-Sample, 1 drop of 0.05 mol/l solution, 10 minutes revealed on temperature, then C ₂ H ₂ treatment for 5 minutes
330	600	Ni-SEM	1.0	0.04	1/0.2/1	35-55	N ₂ (30%, 3.5), C ₂ H ₂ (25sccm)	N ₂ : 0.5, C ₂ H ₂ : 0.5	0.05 mol/l, crystals dis. Eth	SEM-Sample, 1 drop of 0.05 mol/l solution, 10 minutes revealed on temperature, then C ₂ H ₂ treatment for 5 minutes
331	600	Ni-SEM	1.0	0.04	1/0.2/1	35-55	N ₂ (30%, 3.5), C ₂ H ₂ (25sccm)	N ₂ : 0.5, C ₂ H ₂ : 0.5	0.05 mol/l, crystals dis. Eth	SEM-Sample, 1 drop of 0.05 mol/l solution, 10 minutes revealed on temperature, then C ₂ H ₂ treatment for 5 minutes
332	600	Ni-SEM	1.0	0.04	1/0.2/1	35-55	N ₂ (30%, 3.5)	N ₂ : 0.5	0.05 mol/l, crystals dis. Eth	SEM-Sample, 1 drop of 0.05 mol/l solution, 10 minutes revealed on temperature
333	600	Ni-SEM	1.0	0.04	1/0.2/1	35-55	N ₂ (30%, 3.5), H ₂ (25sccm)	N ₂ : 0.5, H ₂ : 0.5	0.05 mol/l, crystals dis. Eth	SEM-Sample, 1 drop of 0.05 mol/l solution, 10 minutes revealed on temperature, then H ₂ treatment for 5 minutes
334	600	Ni-SEM	1.0	0.04	1/0.2/1	35-55	N ₂ (30%, 3.5), H ₂ (25sccm)	N ₂ : 0.5, H ₂ : 0.5	0.05 mol/l, crystals dis. Eth	SEM-Sample, 1 drop of 0.05 mol/l solution, 10 minutes revealed on temperature, then H ₂ treatment for 5 minutes
335	600	Ni-SEM	1.0	0.04	1/0.2/1	35-55	N ₂ (30%, 3.5), H ₂ + C ₂ H ₂ (25sccm)	N ₂ : 0.5, H ₂ + C ₂ H ₂ : 0.5	0.05 mol/l, crystals dis. Eth	SEM-Sample, 1 drop of 0.05 mol/l solution, heated up to 400°C, then H ₂ added by subsequent heating to 600°C, remained for 10 minutes, before acetylene inlet
336	600	Ni-SEM	1.0	0.04	1/0.2/1	35-55	N ₂ (30%, 3.5), H ₂ + C ₂ H ₂ (25sccm)	N ₂ : 0.5, H ₂ + C ₂ H ₂ : 0.5	0.05 mol/l, crystals dis. Eth	SEM-Sample, 1 drop of 0.05 mol/l solution, heated up to 400°C, then H ₂ added by subsequent heating to 600°C, remained for 10 minutes, then 5 minutes C ₂ H ₂ treatment
337	600	Ni-SEM	1.0	0.04	1/0.2/1	35-55	N ₂ (30%, 3.5), H ₂ + C ₂ H ₂ (25sccm)	N ₂ : 0.5, H ₂ + C ₂ H ₂ : 0.5	0.05 mol/l, crystals dis. Eth	SEM-Sample, 1 drop of 0.05 mol/l solution, heated up to 400°C, then H ₂ added by subsequent heating to 600°C, remained for 10 minutes, then 25 minutes C ₂ H ₂ treatment
338	25, 400, 800	Platinum strip	1.0	0.04	1/0.2/1	10-100	air		platinum strip	measurement due to clarification of pt-strip contamination
339	400, 450, 500, 550, 600	Ni-H2-N2	1.0	0.04	1/0.2/1	30-70	N ₂ (30%, 3.5), H ₂ (25sccm)	N ₂ : 0.5, H ₂ : 0.5	crystals dissolved in ethanol	Heated up under nitrogen to 400°C, after measurement added 25 sccm hydrogen and subsequent measurement up to 600°C every 50°C → observation of strange peak-form
340	600	Co-Ac-N2	1.0	0.02	1/0.2/1	35-55	N ₂ (25%, 3.0), C ₂ H ₂ (25sccm)	N ₂ : 0.5, C ₂ H ₂ : 0.5	crystals dissolved in ethanol	heated up under nitrogen to 600°C, 10 minutes revealed on temperature, then C ₂ H ₂ treatment for 4 h → bad results

Sample #	Temp. (°C)	Sample	sec/step	%stop	Blenden	2theta	gasflow	pressure (bar)	concentration	notes
341	600	Co-Ac-N2	1.0	0.02	1/0.2/1	30-70	N ₂ (25%, 3.0), C ₂ H ₂ (25sccm)	N ₂ : 0.5, C ₂ H ₂ : 0.5	crystals dissolved in ethanol	heated up under nitrogen to 600°C, 10 minutes revealed on temperature, than C ₂ H ₂ treatment for 4 h -> Measurement absorbed
342	600	Co-Ac-N2	1.0	0.02	1/0.2/1	30-70	N ₂ (25%, 3.0), C ₂ H ₂ (25sccm)	N ₂ : 0.5, C ₂ H ₂ : 0.5	crystals dissolved in ethanol	heated up under nitrogen to 600°C, 10 minutes revealed on temperature, than C ₂ H ₂ treatment for 4 h -> CoO at the beginning
343	600	Platinum strip	1.0	0.04	1/0.2/1	10-100	air	N ₂ : 0.5	platinum strip	measurement due to clarification of pt-strip contamination
344	400	Ni-SEM					N ₂ (25%, 3.0)	N ₂ : 0.5	0.05 mol/l, crystals dis. Eth	SEM-Sample, 1 drop of 0.05 mol/l solution, heated up to 400°C under nitrogen
345	400	Ni-SEM					N ₂ (30%, 3.5), H ₂ (25sccm)	N ₂ : 0.5, H ₂ : 0.5	0.05 mol/l, crystals dis. Eth	SEM-Sample, 1 drop of 0.05 mol/l solution, heated up to 400°C under nitrogen, then treated with H ₂ for 20 minutes
346	500	Ni-SEM					N ₂ (30%, 3.5), H ₂ (25sccm)	N ₂ : 0.5, H ₂ : 0.5	0.05 mol/l, crystals dis. Eth	SEM-Sample, 1 drop of 0.05 mol/l solution, heated up to 400°C under nitrogen, then subsequent heating to 500°C under H ₂ + N ₂ , treated waiting for 20 minutes
347	600	Co-Ac-N2	1.0	0.02	1/0.2/1	30-70	N ₂ (25%, 3.0), C ₂ H ₂ (25sccm)	N ₂ : 0.5, C ₂ H ₂ : 0.5	crystals dissolved in ethanol	heated up under nitrogen to 600°C, 10 minutes revealed on temperature, than C ₂ H ₂ treatment for 4 h -> Co ₃ O ₄ at the beginning, sample sliced after 2 h C ₂ H ₂ treatment
348	600	Co-Ac-N2	1.0	0.02	1/0.2/1	30-70	N ₂ (25%, 3.0), C ₂ H ₂ (25sccm)	N ₂ : 0.5, C ₂ H ₂ : 0.5	crystals dissolved in ethanol	same sample as #347, but new dissolved in ethanol
349	25, 400, 600, 750, 800	Platinum strip	1.0	0.04	1/0.2/1	10-100	air		platinum strip	ht-diffractometer calibration based on platinum thermal expansion coefficient
350	25, 400, 600, 800	Platinum strip	1.0	0.04	1/0.2/1	10-100	air		platinum strip	ht-diffractometer calibration based on platinum thermal expansion coefficient
351	600	Co-SEM					N ₂ (25%, 3.0)	N ₂ : 0.5	0.05 mol/l, crystals dis. Eth	SEM-Sample, 1 drop of 0.05 mol/l solution, heated up to 600°C under nitrogen and remained for 10 minutes
352	600	Co-SEM					N ₂ (25%, 3.0), C ₂ H ₂ (25sccm)	N ₂ : 0.5, C ₂ H ₂ : 0.5	0.05 mol/l, crystals dis. Eth	SEM-Sample, 1 drop of 0.05 mol/l solution, heated up to 600°C under nitrogen and remained for 10 minutes before treated 20 minutes with acetylene
353	600	Co-SEM					N ₂ (25%, 3.0)	N ₂ : 0.5	0.05 mol/l, crystals dis. Eth	SEM-Sample, 1 drop of 0.05 mol/l solution, heated up to 600°C under nitrogen and remained for 10 minutes
354	600	Co-SEM					N ₂ (25%, 3.0), C ₂ H ₂ (25sccm)	N ₂ : 0.5, C ₂ H ₂ : 0.5	0.05 mol/l, crystals dis. Eth	SEM-Sample, 1 drop of 0.05 mol/l solution, heated up to 600°C under nitrogen and remained for 10 minutes before treated 20 minutes with acetylene
355	600	Co-Ac-N2	1.0	0.03	1/0.2/1	30-60	N ₂ (25%, 3.0), C ₂ H ₂ (25sccm)	N ₂ : 0.5, C ₂ H ₂ : 0.5	crystals dissolved in ethanol	Behaviour of sample after C ₂ H ₂ treatment under nitrogen under oxygen atmosphere -> Re-reaction of same phases, are they stable?
356	600	Ni-Ac-N2	1.0	0.03	1/0.2/1	30-60	N ₂ (25%, 3.0), C ₂ H ₂ (25sccm)	N ₂ : 0.5, C ₂ H ₂ : 0.5	crystals dissolved in ethanol	Behaviour of sample after C ₂ H ₂ treatment under nitrogen under oxygen atmosphere -> Re-reaction of same phases, are they stable?
357	600	Ni-Ac-N2	1.0	0.03	1/0.2/1	30-60	air		crystals dissolved in ethanol	Same sample as #356, leave 12 hours in the chamber before measured under oxygen atmosphere conditions
358	600	Co-Ac-N2	1.0	0.03	1/0.2/1	30-60	air		crystals dissolved in ethanol	Same sample as #355, leave 12 hours in the chamber before measured under oxygen atmosphere conditions
359	600	Co-Ac-N2	1.0	0.03	1/0.2/1	30-60	air		crystals dissolved in ethanol	Same sample as #355, but pt-strip was rearranged (pushed a little bit up) -> Peak shift of platinum recognizable
360	600	Co-Ac-N2	1.0	0.03	1/0.2/1	30-60	air		crystals dissolved in ethanol	Same sample as #355, but pt-strip was rearranged (pushed a little bit down) -> Peak shift of platinum recognizable, now same position as #355
361	300	Cr(NO3)3 * 9H2O								
362	600	Cr(NO3)3 * 9H2O	1.0	0.08	1/0.2/1	30-70	N ₂ (25%, 3.0), H ₂ (25sccm)	N ₂ : 0.5, H ₂ : 0.5	crystals dissolved in ethanol	Sample heated up to 600°C under N ₂ , waited 10 min, H ₂ inlet for 10 minutes, measurement at last under N ₂ atmosphere -> No reduction to metallic chromium observed
363	600	Cr(NO3)3 * 9H2O	1.0	0.08	1/0.2/1	30-70	N ₂ (25%, 3.0), H ₂ + C ₂ H ₂ (25sccm)	N ₂ : 0.5, H ₂ + C ₂ H ₂ : 0.5	crystals dissolved in ethanol	Sample heated up to 400°C under N ₂ , then exposed to H ₂ by subsequent heating to 600°C and remained for 20 minutes before C ₂ H ₂ was introduced -> no reduction to metallic chromium at all observed
364	600	MoO ₂	1.0	0.08	1/0.2/1	30-70	N ₂ (25%, 3.0), H ₂ (25sccm)	N ₂ : 0.5, H ₂ : 0.5	crystals dissolved in ethanol	Sample heated up to 600°C under N ₂ , waited 10 min, H ₂ inlet for 3 hours -> no reduction to metallic molybdenum observed
365	600	MoO ₂	1.0	0.08	1/0.2/1	30-70	N ₂ (25%, 3.0), H ₂ + C ₂ H ₂ (25sccm)	N ₂ : 0.5, H ₂ + C ₂ H ₂ : 0.5	crystals dissolved in ethanol	Sample heated up to 400°C under N ₂ , then exposed to H ₂ by subsequent heating to 600°C and remained for 20 minutes before C ₂ H ₂ was introduced -> no reduction to metallic chromium at all observed
366	600	Cr(NO3)3 * 9H2O	1.0	0.08	1/0.2/1	30-70	N ₂ (25%, 3.0), H ₂ (25sccm)	N ₂ : 0.5, H ₂ : 0.5	crystals dissolved in ethanol	Sample heated up to 600°C under N ₂ , waited 10 min, H ₂ inlet for 10 minutes, measurement at last under N ₂ atmosphere -> observation of Cr-oxide peak shift
367	750	MoO ₂	1.0	0.08	1/0.2/1	30-70	N ₂ (25%, 3.0), H ₂ (25sccm)	N ₂ : 0.5, H ₂ : 0.5	crystals dissolved in ethanol	Sample heated up to 750°C under N ₂ , waited 10 min, H ₂ inlet for 3 hours -> reduction to Mo, but after 10 - 15 minutes formation of Mo ₂ C ₂ O ₇ -> contamination of the chamber -> repetition
368	750	MoO ₂	1.0	0.08	1/0.2/1	30-70	N ₂ (25%, 3.0), H ₂ (25sccm)	N ₂ : 0.5, H ₂ : 0.5	crystals dissolved in ethanol	Sample heated up to 750°C under N ₂ , waited 10 min, H ₂ inlet for 3 hours -> no reduction
369	750	MoO ₂	1.0	0.08	1/0.2/1	30-70	N ₂ (25%, 3.0), H ₂ (25sccm)	N ₂ : 0.5, H ₂ : 0.5	crystals dissolved in ethanol	Sample heated up to 750°C under N ₂ , waited 10 min, H ₂ inlet for 3 hours -> no reduction
370	750	MoO ₂	1.0	0.08	1/0.2/1	30-70	N ₂ (25%, 3.0), H ₂ (25sccm)	N ₂ : 0.5, H ₂ : 0.5	crystals dissolved in ethanol	Sample heated up to 750°C under N ₂ , waited 10 min, H ₂ inlet for 3 hours -> no reduction

Sample #	Temp. (°C)	Sample	sec/step	%step	Blendn	2theta	gasflow	pressure (bar)	concentration	notes
371	750	MoO ₂	1.0	0.08	1/0.2/1	30-70	N ₂ (25%, 3.0), H ₂ + C ₂ H ₂ (25sccm)	N ₂ : 0.5, H ₂ + C ₂ H ₂ : 0.5	crystals dissolved in ethanol	Sample heated up to 400°C under N ₂ , then exposed to H ₂ by subsequent heating to 600°C and remained for 20 minutes before C ₂ H ₂ was introduced -> "MoO ₂ " before and after C ₂ H ₂ inlet
372	25, 500, 800	Platinum strip	1.0	0.04	1/0.2/1	40-100	air	N ₂ : 0.5, H ₂ : 0.5	platinum strip	measurement due to clarification of pt-strip contamination
373	750	Cr(NO ₃) ₃ * 9H ₂ O	1.0	0.08	1/0.2/1	30-70	N ₂ (25%, 3.0), H ₂ (25sccm)	N ₂ : 0.5, H ₂ : 0.5	crystals dissolved in ethanol	Sample heated up to 750°C under N ₂ , waited 10 min, H ₂ inlet for 10 minutes -> no reduction of Cr-oxide to metallic chromium
374	750	Cr(NO ₃) ₃ * 9H ₂ O	1.0	0.08	1/0.2/1	30-70	N ₂ (25%, 3.0), H ₂ + C ₂ H ₂ (25sccm)	N ₂ : 0.5, H ₂ + C ₂ H ₂ : 0.5	crystals dissolved in ethanol	Sample heated up to 400°C under N ₂ , then exposed to H ₂ by subsequent heating to 750°C and remained for 20 minutes before C ₂ H ₂ was introduced -> no reduction of Cr ₂ O ₃ to metallic chromium
375	750	MoO ₂	1.0	0.08	1/0.2/1	30-70	N ₂ (25%, 3.0), H ₂ (25sccm)	N ₂ : 0.5, H ₂ : 0.5	crystals dissolved in ethanol	Sample heated up to 400°C under N ₂ , then exposed to H ₂ by subsequent heating to 750°C in steps of 50°C
376	400 - 750 / 50	MoO ₂	1.0	0.08	1/0.2/1	30-70	N ₂ (25%, 3.0), H ₂ (75sccm)	N ₂ : 0.5, H ₂ : 0.5	crystals dissolved in ethanol	Sample heated up to 750°C under N ₂ , waited 10 min, H ₂ inlet for 3 hours -> same reaction as before, no significant change in time
377	750	MoO ₂	1.0	0.08	1/0.2/1	30-70	N ₂ (25%, 3.0), H ₂ (150sccm)	N ₂ : 0.5, H ₂ : 0.5	crystals dissolved in ethanol	Sample heated up to 750°C under N ₂ , waited 10 min, H ₂ inlet for 3 hours -> same reaction as before, no significant change in time
378	750	MoO ₂	1.0	0.08	1/0.2/1	35-45	N ₂ (25%, 3.0), H ₂ + C ₂ H ₂ (25sccm)	N ₂ : 0.5, H ₂ + C ₂ H ₂ : 0.5	crystals dissolved in ethanol	Sample heated up to 400°C under N ₂ , then exposed to H ₂ by subsequent heating to 750°C and remained for 20 minutes before C ₂ H ₂ was introduced -> kinetic measurements of Mo-oxide and metallic Mo peaks
379	750	MoO ₂	1.0	0.08	1/0.2/1	35-45	N ₂ (25%, 3.0), H ₂ (25sccm)	N ₂ : 0.5, H ₂ : 0.5	crystals dissolved in ethanol	Sample heated up to 750°C under N ₂ , waited 10 min, H ₂ inlet for 3 hours -> kinetic measurement between 35-45 (no appearance of metallic Mo)
380	750	MoO ₂	1.0	0.08	1/0.2/1	30-70	N ₂ (25%, 3.0), H ₂ (25sccm)	N ₂ : 0.5, H ₂ : 0.5	crystals dissolved in ethanol	Sample heated up to 750°C under N ₂ , waited 10 min, H ₂ inlet for 3 hours -> same reaction as before, no significant change in time
381	750	MoO ₂	1.0	0.08	1/0.2/1	30-70	N ₂ (25%, 3.0), H ₂ (25sccm)	N ₂ : 0.5, H ₂ : 0.5	crystals dissolved in water	Sample heated very to 100°C (30 minutes), then normally heated up to 750°C under N ₂ , waited 10 min, H ₂ inlet for 3 hours
382	750	MoO ₂	1.0	0.08	1/0.2/1	30-70	N ₂ (25%, 3.0)	N ₂ : 0.5	0.05 mol/l, crystals dis. Eth	SEM sample, heated to 750°C under N ₂ , waited 10 minutes
382	750	MoO ₂	1.0	0.08	1/0.2/1	51.5-61.5	N ₂ (25%, 3.0), H ₂ (25sccm)	N ₂ : 0.5, H ₂ : 0.5	crystals dissolved in ethanol	Sample heated up to 750°C under N ₂ , waited 10 min, H ₂ inlet for 3 hours -> kinetic measurement between 51.5-61.5
383	750	MoO ₂	1.0	0.08	1/0.2/1	51.5-61.5	N ₂ (25%, 3.0), H ₂ + C ₂ H ₂ (25sccm)	N ₂ : 0.5, H ₂ + C ₂ H ₂ : 0.5	crystals dissolved in ethanol	Sample heated up to 750°C under N ₂ , waited 10 min, H ₂ inlet for 3 hours -> kinetic measurement between 51.5-61.5
384	750	MoO ₂	1.0	0.08	1/0.2/1	30-70	N ₂ (25%, 3.0), C ₂ H ₂ (25sccm)	N ₂ : 0.5, C ₂ H ₂ : 0.5	crystals dissolved in ethanol	Sample heated up to 750°C under N ₂ , waited 10 min, C ₂ H ₂ inlet
385	750	MoO ₂	1.0	0.08	1/0.2/1	30-70	N ₂ (25%, 3.0), C ₂ H ₂ (25sccm)	N ₂ : 0.5, C ₂ H ₂ : 0.5	crystals dissolved in ethanol	Sample heated up to 750°C under N ₂ , waited 10 min, C ₂ H ₂ inlet (repetition of #384)
386	750	MoO ₂	1.0	0.08	1/0.2/1	30-70	N ₂ (25%, 3.0), C ₂ H ₂ (25sccm)	N ₂ : 0.5, C ₂ H ₂ : 0.5	crystals dissolved in ethanol	Sample heated up to 750°C under N ₂ , waited 10 min, C ₂ H ₂ inlet (repetition of #385)
387	750	Cr(NO ₃) ₃ * 9H ₂ O	1.0	0.08	1/0.2/1	30-70	N ₂ (25%, 3.0), C ₂ H ₂ (25sccm)	N ₂ : 0.5, C ₂ H ₂ : 0.5	crystals dissolved in ethanol	Sample heated up to 750°C under N ₂ , then exposed to C ₂ H ₂ for 3 hours -> no reduction of Cr ₂ O ₃ to metallic chromium, no appearance of chromium carbide phases
388	750	MoO ₂	1.0	0.08	1/0.2/1	30-70	N ₂ (25%, 3.0), H ₂ (25sccm)	N ₂ : 0.5, H ₂ : 0.5	0.05 mol/l, crystals dis. Eth	SEM sample, heated to 750°C under N ₂ , waited 10 minutes, then treated for 10 minutes with hydrogen
389	750	MoO ₂	1.0	0.08	1/0.2/1	30-70	N ₂ (25%, 3.0), H ₂ (25sccm)	N ₂ : 0.5, H ₂ : 0.5	0.05 mol/l, crystals dis. Eth	SEM sample, heated to 750°C under N ₂ , waited 10 minutes, then treated for 2.5 minutes with hydrogen
390	750	MoO ₂	1.0	0.08	1/0.2/1	30-70	N ₂ (25%, 3.0), H ₂ (25sccm)	N ₂ : 0.5, H ₂ : 0.5	0.05 mol/l, crystals dis. Eth	SEM sample, heated to 750°C under N ₂ , waited 10 minutes, then treated for 60 minutes with hydrogen
391	750	MoO ₂	1.0	0.08	1/0.2/1	30-70	N ₂ (25%, 3.0), H ₂ (25sccm)	N ₂ : 0.5, H ₂ : 0.5	0.05 mol/l, crystals dis. Eth	SEM sample, heated to 750°C under N ₂ , waited 10 minutes, then treated for 5 minutes with hydrogen
392	750	MoO ₂	1.0	0.08	1/0.2/1	30-70	N ₂ (25%, 3.0), H ₂ (25sccm)	N ₂ : 0.5, H ₂ : 0.5	0.05 mol/l, crystals dis. Eth	SEM sample, heated to 750°C under N ₂ , waited 10 minutes, then treated for 7.5 minutes with hydrogen
393	750	MoO ₂	1.0	0.08	1/0.2/1	30-70	N ₂ (25%, 3.0), H ₂ (25sccm)	N ₂ : 0.5, H ₂ : 0.5	0.05 mol/l, crystals dis. Eth	SEM sample, heated to 750°C under N ₂ , waited 10 minutes, then treated for 20 minutes with hydrogen
394	750	MoO ₂	1.0	0.08	1/0.2/1	30-70	N ₂ (25%, 3.0), H ₂ + C ₂ H ₂ (25sccm)	N ₂ : 0.5, H ₂ + C ₂ H ₂ : 0.5	0.05 mol/l, crystals dis. Eth	SEM sample, heated to 750°C under N ₂ , then added hydrogen for 5 minutes before treated with acetylene for 2.5 minutes
395	750	MoO ₂	1.0	0.08	1/0.2/1	30-70	N ₂ (25%, 3.0), H ₂ + C ₂ H ₂ (25sccm)	N ₂ : 0.5, H ₂ + C ₂ H ₂ : 0.5	0.05 mol/l, crystals dis. Eth	SEM sample, heated to 750°C under N ₂ , then added hydrogen for 5 minutes before treated with acetylene for 60 minutes
396	750	MoO ₂	1.0	0.08	1/0.2/1	30-70	N ₂ (25%, 3.0), H ₂ + C ₂ H ₂ (25sccm)	N ₂ : 0.5, H ₂ + C ₂ H ₂ : 0.5	0.05 mol/l, crystals dis. Eth	SEM sample, heated to 750°C under N ₂ , then added hydrogen for 5 minutes before treated with acetylene for 5 minutes
397	750	MoO ₂	1.0	0.08	1/0.2/1	30-70	N ₂ (25%, 3.0), H ₂ + C ₂ H ₂ (25sccm)	N ₂ : 0.5, H ₂ + C ₂ H ₂ : 0.5	0.05 mol/l, crystals dis. Eth	SEM sample, heated to 750°C under N ₂ , then added hydrogen for 5 minutes before treated with acetylene for 20 minutes
398	750	MoO ₂	1.0	0.08	1/0.2/1	30-70	N ₂ (25%, 3.0), H ₂ + C ₂ H ₂ (25sccm)	N ₂ : 0.5, H ₂ + C ₂ H ₂ : 0.5	0.05 mol/l, crystals dis. Eth	SEM sample, heated to 750°C under N ₂ , then added hydrogen for 5 minutes before treated with acetylene for 7.5 minutes
399	750	MoO ₂	1.0	0.08	1/0.2/1	30-70	N ₂ (25%, 3.0), H ₂ + C ₂ H ₂ (25sccm)	N ₂ : 0.5, H ₂ + C ₂ H ₂ : 0.5	0.05 mol/l, crystals dis. Eth	SEM sample, heated to 750°C under N ₂ , then added hydrogen for 5 minutes before treated with acetylene for 10 minutes
400	600	MoO ₂	1.0	0.08	1/0.2/1	30-70	N ₂ (25%, 3.0)	N ₂ : 0.5	0.05 mol/l, crystals dis. Eth	SEM sample, heated to 600°C under N ₂ and remained 10 minutes

Sample #	Temp. (°C)	Sample	sec/step	%step	Blenden	°2theta	gasflow	pressure (bar)	concentration	notes
401	600	MoO ₂					N ₂ (25%, 3.0), H ₂ (25sccm)	N ₂ : 0.5, H ₂ : 0.5	0.05 mol/l, crystals dis.	Eth SEM sample, heated to 600°C under N ₂ and remained 10 minutes
402	600	Cr(NO ₃) ₃ * 9H ₂ O					N ₂ (25%, 3.0), H ₂ (25sccm)	N ₂ : 0.5, H ₂ : 0.5	0.05 mol/l, crystals dis.	Eth SEM sample, heated to 600°C under N ₂ and treated with hydrogen for 10 minutes
403	750	Cr(NO ₃) ₃ * 9H ₂ O					N ₂ (25%, 3.0), H ₂ (25sccm)	N ₂ : 0.5, H ₂ : 0.5	0.05 mol/l, crystals dis.	Eth SEM sample, heated to 750°C under N ₂ and treated with hydrogen for 10 minutes
404	600	MoO ₂					N ₂ (25%, 3.0), H ₂ + C ₂ H ₂ (25sccm)	N ₂ : 0.5, H ₂ + C ₂ H ₂ : 0.5	0.05 mol/l, crystals dis.	Eth SEM sample, heated to 600°C under N ₂ , then added hydrogen for 5 minutes before treated with acetylene for 10 minutes
405	600	MoO ₂					N ₂ (25%, 3.0), C ₂ H ₂ (25sccm)	N ₂ : 0.5, C ₂ H ₂ : 0.5	0.05 mol/l, crystals dis.	Eth SEM sample, heated to 600°C under N ₂ , waited 10 minutes before treated with acetylene for 10 minutes --> no reaction observed
406	750	MoO ₂					N ₂ (25%, 3.0), C ₂ H ₂ (25sccm)	N ₂ : 0.5, C ₂ H ₂ : 0.5	0.05 mol/l, crystals dis.	Eth SEM sample, heated to 750°C under N ₂ , waited 10 minutes before treated with acetylene for 10 minutes --> reaction observed, glass coated by carbon
407	750	MoO ₂					N ₂ (25%, 3.0), H ₂ + C ₂ H ₂ (25sccm)	N ₂ : 0.5, H ₂ + C ₂ H ₂ : 0.5	0.05 mol/l, crystals dis.	Eth Sample heated up to 400°C under N ₂ , then exposed to H ₂ by subsequent heating to 750°C and remained for 10 minutes before C ₂ H ₂ for 10 minutes was introduced

3. Oxygen Fugacity and Carbon Activity Calculations

Oxygen fugacity calculation in the Mo-O-C system:

Basic equation for the chemical reaction is



The equation relating the Gibbs free energy of reaction and the equilibrium constant K is

$$\Delta G_r = -RT \ln K \quad (2)$$

and K can be calculated as following:

$$K = \frac{[Mo] * [O_2]}{[MoO]} = \left[\frac{p_{O_2}}{p_0} \right] \quad (3)$$

$$\rightarrow p_{O_2} = K * p_0$$

With p_0 equal to the reference pressure e.g. 1 bar, the Gibbs free energy of reaction is given by:

$$\begin{aligned} \Delta G_r &= \Delta G_f(Mo) - \Delta G_f(MoO_2) = \\ &= (0 \text{ kJ/mol}) - (-428.293 \text{ kJ/mol}) = \\ &= 428.293 \text{ kJ/mol} \end{aligned} \quad (4)$$

The equilibrium partial pressure of oxygen for the reaction can be calculated from:

$$\begin{aligned} p_{O_2} &= K * p_0 = \left(e^{\frac{\Delta G_r}{-RT}} \right) * 1 = \\ &= e^{\left(\frac{428.293 * 1000}{-8.31451 * 873} \right)} = 2.678 * 10^{-26} \text{ bar} \end{aligned} \quad (6)$$

$$\Rightarrow \log(p_{O_2}) = -25.626$$

Carbon activity calculation in the Mo-O-C system:

Basic equation for the chemical reaction:



K is given by:

$$K = \frac{[Mo_2C]}{[Mo]^2 * [C]} = \left[\frac{p_0}{a_C} \right] \quad (9)$$

$$\rightarrow a_C = \frac{1}{K} * p_0$$

The carbon activity can be calculated from:

$$\Delta G_r = -RT \ln K = -RT(\ln 1 - \ln a_C) = RT \ln[a_C]$$

$$\ln[a_C] = \frac{\Delta G_r}{RT} \quad (10)$$

$$\Rightarrow [a_C] = e^{\frac{-\Delta G_r}{RT}} = e^{\left(\frac{-57.289 * 1000}{8.31451 * 873} \right)} = -3.428 * 10^{-4} \text{ bar}$$

$$\Rightarrow \log(a_C) = -3.428$$

Calculation of slopes in $\log(fO_2)$ vs. $\log(a_C)$ diagrams:

General basic equation for the reaction:



A, C: pure solids; B, D: species in solution or gas species

The equation for the Gibbs free energy is

$$\Delta G_r = -RT \ln K \quad (2)$$

and K is given by:

$$K = \frac{C * D^y}{A * B^x} \quad (12)$$

The slope in activation diagrams can be calculated as following:

at equilibrium $\Delta G = 0$, therefore

$$\ln K = \ln C + y * \ln D - \ln A - x * \ln B = 0 \quad (13)$$

with $\ln C, \ln A = 0$ follows

$$y * \ln D = x * \ln B \quad (14)$$

$$\Rightarrow \ln B = \frac{y}{x} * \ln D$$

The boundary of reaction (1) has a slope of y/x in a $\ln D$ vs. $\ln B$ diagram.

Slope of the boundary of reaction $MoO_2 - \beta-Mo_2C$.



At equilibrium $\Delta G = 0$

$$K = \ln[Mo_2C] + 2 * [\ln O_2] - 2 * \ln[MoO_2] - \ln[C]$$

$$\ln[Mo_2C], 2 * \ln[MoO_2] = 0$$

$$2 * \ln[O_2] = \ln[C] \quad (16)$$

$$\ln[O_2] = \frac{1}{2} \ln[C]$$

$$\Rightarrow \frac{\ln[O_2]}{\ln[C]} = \frac{1}{2}$$

A summary of all calculated equilibrium values for oxygen fugacities and carbon activities for the formation from the elements is given in the following table.

	ΔG_f 873K ²	$\log(K_f)$ 873K	ΔG_f 1023K ³	$\log(K_f)$ 1023K
NiO	-160.178	-19.168	-147.251	-15.037
Ni ₃ C	54.872*	3.283*	52.412*	2.676*
Ni	0	0	0	0
Fe ₃ O ₄	-827.183	-24.371	-782.543	-19.148
¹ FeO	-207.84	-24.871	-198.345	-20.893
Fe ₃ C	3.848	0.23	0.786	0.08
Fe	0	0	0	0
Co ₃ O ₄	-544.937	-3.824	-486.405	-0.554
CoO	-170.995	-20.462	-160.327	-16.372
Co	0	0	0	0
Cr ₂ O ₃	-901.787	-35.970	-863.556	-29.395
Cr ₃ C ₂	-93.218	-2.789	-95.908	-2.546
Cr ₂₃ C ₆	-374.484	-3.734	-386.005	-3.285
Cr	0	0	0	0
MoO ₃	-524.293	-11.488	-488.349	-9.965
MoO ₂	-428.293	-25.626	-405.074	-20.683
Mo ₂ C	-57.289	-3.428	-58.464	-2.985
MoC	-29.675	-1.776	-29.638	-1.513
Mo	0	0	0	0

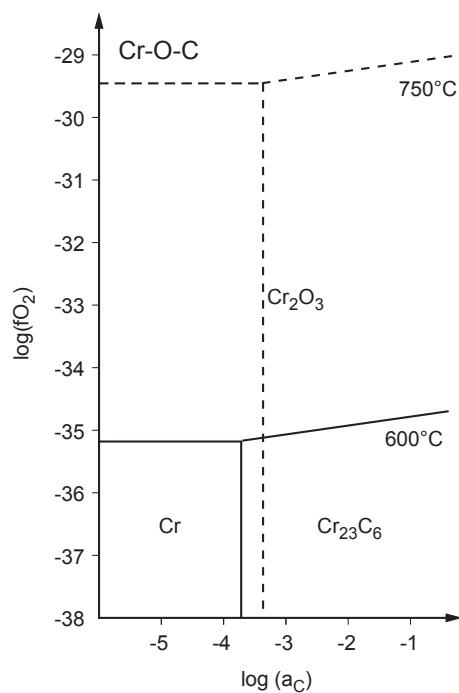
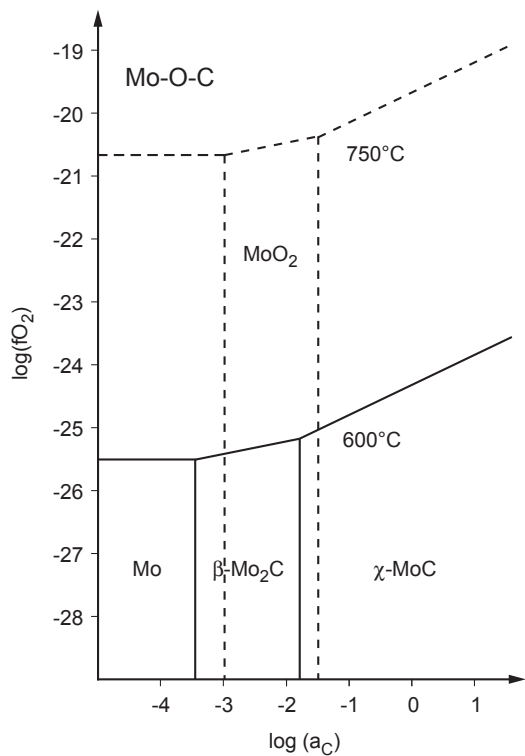
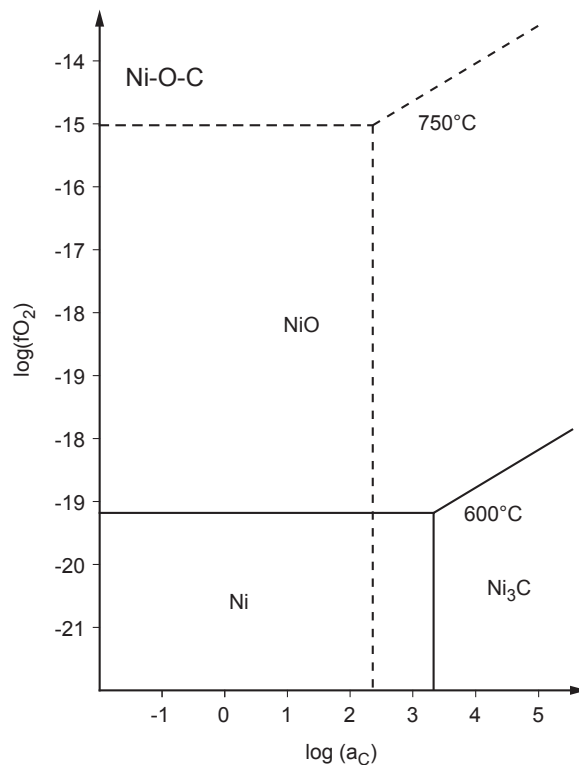
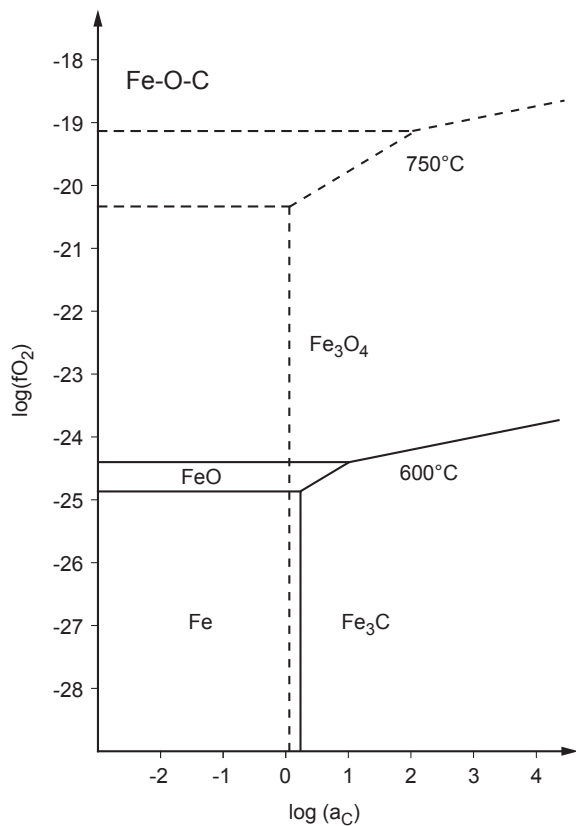
¹ Taken from sub-stoichiometric Fe_{0.94}O_x

² ΔG_f kJ/mol

³ extrapolated

all data taken from book Ihsan Barin, Thermodynamical data of pure substances Part I or II, 1989, VCH Verlagsgesellschaft mbH, D-6940 Weinheim, Germany

4. Metal-O-C Phase Diagrams



5. Calculations of Solid Volume Changes

Calculation of solid volume changes during heat and gas treatments in the nickel system:

Nickel nitrate [14-0593; Ni(NO₃)₂]

Cell volume: 390.62 Å³ (cubic: a = 7.31 Å)

Z: 4 molecules per cell

Ref.: Weigel, Imelik and Lafitte, Bull. Soc. Chim. Fr., 544 (1962)

Nickel oxide [47-1049; NiO]

Cell volume: 72.88 Å³ (cubic: a = 4.177 Å)

Z: 4

Ref.: Marti, McCarthy, North Dakota State University, Fargo, North Dakota, USA, ICDD Grant-in-Aid (1991)

Nickel [04-0850; Ni]

Cell volume: 43.76 Å³ (cubic: a = 3.524 Å)

Z: 4

Ref.: Swanson, Tatge, Natl. Bur. Stand. (U.S.), Circ. 539, I, 13 (1953)

Solid volume loss during decomposition reaction of Ni(NO₃)₂ to NiO:

$$\frac{\text{Volume}[\text{Ni}(\text{NO}_3)_2] - \text{Volume}[\text{NiO}]}{\text{Volume}[\text{Ni}(\text{NO}_3)_2]} =$$

$$= \frac{390.62\text{Å} - 72.88\text{Å}}{390.62\text{Å}} * 100\% = 81.34\% \approx 81\%$$

Solid volume loss during decomposition reaction of NiO to Ni:

$$\frac{\text{Volume}[\text{NiO}] - \text{Volume}[\text{Ni}]}{\text{Volume}[\text{NiO}]} =$$

$$= \frac{72.88\text{Å} - 43.76\text{Å}}{72.88\text{Å}} * 100\% = 39.96\% \approx 40\%$$

Total solid volume loss during decomposition reaction of Ni(NO₃)₂ to Ni:

$$\frac{\text{Volume}[\text{Ni}(\text{NO}_3)_2] - \text{Volume}[\text{Ni}]}{\text{Volume}[\text{Ni}(\text{NO}_3)_2]} =$$

$$= \frac{390.62\text{Å} - 43.76\text{Å}}{390.62\text{Å}} * 100\% = 88.80\% \approx 88\%$$

The total solid volume loss of the decomposition reaction of Ni(NO₃)₂ to small Ni-nuclei is about 88%. The solid volume loss in the nickel system (≈ 53%, after A. Lepora et al.) is about 60% higher than in the iron system.

Calculation of solid volume changes during heat and gas treatments in the cobalt system:

Cobalt nitrate [19-0356; Co(NO₃)₂]

Cell volume: 406.87 Å³ (cubic: a = 7.41 Å)

Z: 4 molecules per cell

Ref.: Weigel, Imelik and Prettre, Bull. Soc. Chim. Fr., 2600, 1964

Cobalt oxide [42-1467; Co₃O₄]

Cell volume: 528.24 Å³ (cubic: a = 8.084 Å)

Z: 8

Ref.: Martin, McCarthy, North Dakota State University, Fargo, North Dakota, USA, ICDD Grant-in-Aid, 1990

Cobalt oxide [43-1004; CoO]

Cell volume: 77.31 Å³ (cubic: a = 4.26 Å)

Z: 4

Ref.: Grier, McCarthy, North Dakota State University, Fargo, North Dakota, USA, ICDD Grant-in-Aid, 1991

Cobalt [15-0806; Co]

Cell volume: 44.55 Å³ (cubic: a = 3.545 Å)

Z: 4

Ref.: Natl. Bur. Stand. (U.S.) Monogr. 25, 4, 10 (1966)

Solid volume loss during decomposition reaction of Co(NO₃)₂ to Co₃O₄:

$$\frac{\text{Volume}[\text{Co}(\text{NO}_3)_2] - \frac{1}{6} \text{Volume}[\text{Co}_3\text{O}_4]}{\text{Volume}[\text{Co}(\text{NO}_3)_2]} =$$

$$= \frac{406.87\text{Å} - \frac{1}{6} * 528.24\text{Å}}{406.87\text{Å}} * 100\% = 78.36\% \approx 78\%$$

Solid volume loss during decomposition reaction of Co₃O₄ to CoO:

$$\frac{\frac{1}{6} * \text{Volume}[\text{Co}_3\text{O}_4] - \text{Volume}[\text{CoO}]}{\frac{1}{6} * \text{Volume}[\text{Co}_3\text{O}_4]} =$$

$$= \frac{\frac{1}{6} * 528.24\text{Å} - 77.31\text{Å}}{\frac{1}{6} * 528.24\text{Å}} * 100\% = 12.19\% \approx 12\%$$

Solid volume loss during decomposition reaction of CoO to Co:

$$\frac{\text{Volume}[\text{CoO}] - \text{Volume}[\text{Co}]}{\text{Volume}[\text{CoO}]} =$$

$$= \frac{77.31\text{\AA} - 44.55\text{\AA}}{77.31\text{\AA}} * 100\% = 42.37\% \approx 42\%$$

Total solid volume loss during decomposition reaction of Co_3O_4 to Co:

$$\frac{\frac{1}{6} * \text{Volume}[\text{Co}_3\text{O}_4] - \text{Volume}[\text{Co}]}{\frac{1}{6} * \text{Volume}[\text{Co}_3\text{O}_4]} =$$

$$= \frac{\frac{1}{6} * 528.24\text{\AA} - 44.55\text{\AA}}{\frac{1}{6} * 528.24\text{\AA}} * 100\% = 49.4\% \approx 49\%$$

Solid volume loss during decomposition reaction of $\text{Co}(\text{NO}_3)_2$ to CoO:

$$\frac{\text{Volume}[\text{Co}(\text{NO}_3)_2] - \text{Volume}[\text{CoO}]}{\text{Volume}[\text{Co}(\text{NO}_3)_2]} =$$

$$= \frac{406.87\text{\AA} - 77.31\text{\AA}}{406.87\text{\AA}} * 100\% = 80.99\% \approx 81\%$$

Total solid volume loss during decomposition reaction of $\text{Co}(\text{NO}_3)_2$ to Co:

$$\frac{\text{Volume}[\text{Co}(\text{NO}_3)_2] - \text{Volume}[\text{Co}]}{\text{Volume}[\text{Co}(\text{NO}_3)_2]} =$$

$$= \frac{406.87\text{\AA} - 44.55\text{\AA}}{406.87\text{\AA}} * 100\% = 89.05\% \approx 89\%$$

The total solid volume loss of the decomposition reaction of Co_3O_4 to small Co-nucleuses is about 49%. The solid volume loss in the cobalt system is comparable with the one in the nickel system.

Calculation of solid volume changes during heat and gas treatments in the chromium system:

Chromium (III) nitrate nonahydrate [31-0409 ; $\text{Cr}(\text{NO}_3)_3 * 9\text{H}_2\text{O}$]

Cell volume: 400.15\AA^3 (monoclinic: $a = 13.967\text{\AA}$, $c = 9.6545$, $\beta = 95.39$)

Z: 4

Ref.: Visser, J., Technisch Physische Dienst, Delft, Netherlands, ICDD Grant-in-Aid, (1978)

Chromium oxide [38-1479; Cr_2O_3 ; Eskolaite]

Cell volume: 289.49\AA^3 (rhombohedral: $a = 4.95876\text{\AA}$, $c = 13.5942$, $C = 2.7415$)

Z: 6

Ref.: McMurdie et al., Powder Diffraction, 2, 45 (1987)

Chromium [06-0694; Cr]

Cell volume: 23.99\AA^3 (cubic: $a = 2.88\text{\AA}$)

Z: 2

Ref.: Swanson et al., Natl. Bur. Stand. (U.S.), Circ. 539, Vol. 20 (1955)

Total solid volume loss during decomposition reaction of $\text{Cr}(\text{NO}_3)_3 * 9\text{H}_2\text{O}$ to Cr_2O_3 :

$$\frac{3 * \text{Volume}[\text{Cr}(\text{NO}_3)_3 * 9\text{H}_2\text{O}] - \frac{2}{2} * \text{Volume}[\text{Cr}_2\text{O}_3]}{3 * \text{Volume}[\text{Cr}(\text{NO}_3)_3 * 9\text{H}_2\text{O}]} =$$

$$= \frac{3 * 400.15\text{\AA} - \frac{2}{2} * 289.49\text{\AA}}{3 * 400.15\text{\AA}} * 100\% = 75.88\% \approx 76\%$$

Total solid volume loss during decomposition reaction of Cr_2O_3 to Cr:

$$\frac{\text{Volume}[\text{Cr}_2\text{O}_3] - 2 * \text{Volume}[\text{Cr}]}{\text{Volume}[\text{Cr}_2\text{O}_3]} =$$

$$= \frac{289.49\text{\AA} - 3 * 2 * 23.99\text{\AA}}{289.49\text{\AA}} * 100\% = 50.28\% \approx 50\%$$

Calculation of solid volume changes during heat and gas treatments in the molybdenum system:

Molybdenum oxide [32-0671; MoO₂] Tugarinovite
Cell volume: 131.48 Å³ (monoclinic: a = 5.6068 Å, b: 4.8595 Å, c: 5.5373 Å, β: 119.37)

Z: 4

Ref.: Natl. Bur. Stand. (U.S.) Monogr. 25, 18, 44 (1981)

Molybdenum oxide [47-1320; MoO₃]

Cell volume: 100.47 Å³ (monoclinic: a = 3.954 Å, b = 3.687 Å, c = 7.095 Å, β = 103.75)

Z: 2

Ref.: McCarron, III, E. Calabrese, J. J. Solid State Chem. 91, 121 (1991)

Molybdenum carbide [15-0457; Mo₂C]

Cell volume: 71.73 Å³ (cubic: a = 4.155 Å)

Z: 2

Ref.: Read, Bell Telephone Laboratory, Private Communication (1962)

Molybdenum carbide [35-0787; α-Mo₂C]

Cell volume: 37.21 Å³ (hexagonal: a = 3.012 Å, c = 4.735 Å)

Z: 1

Ref.: Natl. Bur. Stand. (U.S.) Monogr. 25, 21, 95 (1984)

Molybdenum carbide [45-1015; γ-MoC]

Cell volume: 20.31 Å³ (hexagonal: a = 2.901 Å, c = 2.786 Å)

Z: 1

Ref.: Velikanova T, Kublii V, Khaenko B, Soviet Powder Metall. and Met. Ceramics, 27, 891 (1988)

Molybdenum [42-1120; Mo]

Cell volume: 31.17 Å³ (cubic: a = 3.147 Å)

Z: 2

Ref.: Schreiner W, Intelligent Controls Inc., Amawalk, NY, USA, ICDD grant-in-aid (1991)

Solid volume loss during decomposition reaction of MoO₃ to MoO₂:

$$\frac{\text{Volume}[\text{MoO}_3] - \text{Volume}[\text{MoO}_2]}{\text{Volume}[\text{MoO}_3]} =$$

$$= \frac{2 * 100.47 \text{Å}^3 - 131.48 \text{Å}^3}{2 * 100.47 \text{Å}^3} * 100\% = 34.57\% \approx 35\%$$

Solid volume change during reaction of MoO₂ to MoO₃:

$$\frac{\text{Volume}[\text{MoO}_2] - \text{Volume}[\text{MoO}_3]}{\text{Volume}[\text{MoO}_2]} =$$

$$= \frac{131.48 \text{Å}^3 - 2 * 100.47 \text{Å}^3}{131.48 \text{Å}^3} * 100\% = -52.83\% \approx -53\%$$

Solid volume change during reaction of MoO₃ to Mo₂C:

$$\frac{\text{Volume}[\text{MoO}_3] - \frac{1}{2} \text{Volume}[\text{Mo}_2\text{C}]}{\text{Volume}[\text{MoO}_3]} =$$

$$= \frac{100.47 \text{Å}^3 - \frac{1}{2} * 71.73 \text{Å}^3}{100.47 \text{Å}^3} * 100\% = 64.30\% \approx 64\%$$

Solid volume change during reaction of MoO₂ to α-Mo₂C:

$$\frac{\text{Volume}[\text{MoO}_2] - \frac{1}{2} \text{Volume}[\alpha - \text{Mo}_2\text{C}]}{\text{Volume}[\text{MoO}_2]} =$$

$$= \frac{131.48 \text{Å}^3 - \frac{4}{2} * 37.48 \text{Å}^3}{131.48 \text{Å}^3} * 100\% = 42.98\% \approx 43\%$$

Total solid volume loss during decomposition reaction of MoO₃ to Mo:

$$\frac{\text{Volume}[\text{MoO}_3] - \text{Volume}[\text{Mo}]}{\text{Volume}[\text{MoO}_3]} =$$

$$= \frac{100.47 \text{Å}^3 - 31.17 \text{Å}^3}{100.47 \text{Å}^3} * 100\% = 68.98\% \approx 69\%$$

Total solid volume loss during decomposition reaction of MoO₂ to Mo:

$$\frac{\text{Volume}[\text{MoO}_2] - \text{Volume}[\text{Mo}]}{\text{Volume}[\text{MoO}_2]} =$$

$$= \frac{131.48 \text{Å}^3 - 2 * 31.17 \text{Å}^3}{131.48 \text{Å}^3} * 100\% = 52.59\% \approx 53\%$$

Total solid volume change during reaction of Mo₂C to α-Mo₂C:

$$\frac{\text{Volume}[\text{Mo}_2\text{C}] - \text{Volume}[\alpha - \text{Mo}_2\text{C}]}{\text{Volume}[\text{Mo}_2\text{C}]} =$$

$$= \frac{71.73 \text{Å}^3 - 2 * 37.21 \text{Å}^3}{71.73 \text{Å}^3} * 100\% = -3.75\% \approx -4\%$$

Total solid volume change during reaction of Mo₂C to γ -MoC:

$$\frac{\text{Volume}[\text{Mo}_2\text{C}] - \text{Volume}[\chi - \text{MoC}]}{\text{Volume}[\text{Mo}_2\text{C}]} =$$

$$= \frac{71.73\text{\AA} - 2 * 2 * 20.31\text{\AA}}{71.73\text{\AA}} * 100\% = -13.25\% \approx 13\%$$

Total solid volume change during reaction of γ -MoC to α -Mo₂C:

$$\frac{\text{Volume}[\chi - \text{MoC}] - \frac{1}{2} \text{Volume}[\alpha - \text{Mo}_2\text{C}]}{\text{Volume}[\chi - \text{MoC}]} =$$

$$= \frac{20.31\text{\AA} - \frac{1}{2} 37.21\text{\AA}}{20.31\text{\AA}} * 100\% = 8.39\% \approx 8\%$$

Total solid volume change during reaction of Mo to γ -MoC:

$$\frac{\text{Volume}[\text{Mo}] - \text{Volume}[\chi - \text{MoC}]}{\text{Volume}[\text{Mo}]} =$$

$$= \frac{31.17\text{\AA} - 2 * 20.31\text{\AA}}{31.17\text{\AA}} * 100\% = -30.32 \approx -30\%$$

The total solid volume loss of the decomposition reaction of MoO₃ to small Mo-nucleuses is about 69%.

Summary of solid volume loss datas:

phases	solid volume loss (%)
Ni(NO ₃) ₂ --> NiO	81.34
NiO --> Ni	39.96
Ni(NO ₃) ₂ --> Ni	88.8
Co(NO ₃) ₂ --> Co ₃ O ₄	78.36
Co ₃ O ₄ --> CoO	12.19
CoO --> Co	42.37
Co ₃ O ₄ --> Co	49.4
Co(NO ₃) ₂ --> Co	89.05
Co(NO ₃) ₂ --> CoO	81
Cr(NO ₃) ₃ *9H ₂ O --> Cr ₂ O ₃	75.88
Cr ₂ O ₃ to Cr	50.28
MoO ₃ --> MoO ₂	34.57
MoO ₃ --> Mo ₂ C	64.3
MoO ₃ --> Mo	68.98
MoO ₂ --> Mo	52.59
Mo --> χ -MoC	-30.32
Mo ₂ C --> α -Mo ₂ C	-3.75

6. Calculation of Unit Cell Parameters

Sample #316, Co₃O₄-precursor exposed to C₂H₂

time [min]	a-parameter [Å] [*]	°2theta [1 1 1] [°]
20	3.592	43.605
40	3.589	43.645
60	3.584	43.705
80	3.575	43.827
120	3.569	43.899
180	3.566	43.941
240	3.566	43.947
calculated	3.564	43.962

Pt-measured: 39.22
rel. Peak shift: -0.284

Sample #342, CoO-precursor exposed to C₂H₂

time [min]	a-parameter [Å] [*]	°2theta [1 1 1] [°]
20	3.577	43.794
60	3.573	43.853
120	3.570	43.893
180	3.567	43.925
240	3.565	43.959
calculated	3.564	43.962

Pt-measured: 45.69
rel. Peak shift: -0.279

Sample #315, Co₃O₄-precursor exposed to H₂

time [min]	a-parameter [Å] [*]	°2theta [1 1 1] [°]
20	3.561	44.007
40	3.561	44.007
60	3.562	43.998
120	3.563	43.987
180	3.563	43.979
240	3.563	43.982
calculated	3.564	43.968

Pt-measured: 39.19
rel. Peak shift: -0.314

Sample #317, Co pre-treated with H₂ (400°C) at 600°C and exposed to C₂H₂ for 4 hours

time [min]	a-parameter [Å] [*]	°2theta [1 1 1] [°]
0	3.573	43.857
20	3.571	43.878
40	3.570	43.894
60	3.568	43.910
80	3.568	43.917
120	3.567	43.933
180	3.566	43.940
240	3.564	43.965
calculated	3.564	43.968

Pt-measured: 39.37
rel. Peak shift: -0.188

Cobalt at 25°C: 3.544
Cobalt at 600°C: 3.564

*: Calculated after equation 2.5 for a cubic unit cell
°: Data obtained after peak correction described in chapter 2

Sample #046, NiO-precursor exposed to C₂H₂

time [min]	a-parameter [Å] [*]	°2theta [1 1 1] [°]
20	3.557	44.057
40	3.556	44.074
60	3.553	44.114
80	3.552	44.128
100	3.551	44.135
120	3.548	44.172
140	3.545	44.213
160	3.542	44.256
180	3.539	44.289
200	3.538	44.313
220	3.536	44.331
240	3.534	44.36
calculated	3.531	44.395

Pt-measured: 39.35
rel. Peak shift: -0.154

Nickel at 25°C: 3.523
Nickel at 600°C: 3.531

*: Calculated after equation 2.5 for a cubic unit cell
°: Data obtained after peak correction described in chapter 2

Calculation of metal cell parameters after peak shift corrections. The used equations (5) are described in chapter 2.

7. Calibration Conversion from Reference Gases

The calibration conversion incorporates the K factor. It is derived from gas density and the coefficient of specific heat. The following equations [1] are only correct for diatomic gases:

$$K_{\text{gas}} = \frac{1}{d * C_p} \tag{1}$$

d = gas density (g/l)

C_p = coefficient of specific heat (cal/g)

In the above relationship d and C_p are chosen at standard conditions of one atmosphere and 25°C.

If the flow range of a mass flow meter or controller remains unchanged, a relative factor is used to relate the calibration of the actual gas to the reference gas (1).

$$K = \frac{Q_a}{Q_r} = \frac{K_a}{K_r} \tag{2}$$

Q_a = mass flow rate of an actual gas (sccm, standard cubic cm per minute)

Q_r = mass flow rate of a reference gas (sccm)

K_a = K factor of an actual gas

K_r = K factor of a reference gas

In our case following calibration conversions were applied:

$$K_1 = \frac{K_{\text{CO}_2}}{K_{\text{N}_2}} = K_{\text{N}_2}^{\text{CO}_2}$$

$$K_2 = \frac{K_{\text{C}_2\text{H}_2}}{K_{\text{N}_2}} = K_{\text{N}_2}^{\text{C}_2\text{H}_2} \tag{3}$$

$$K_3 = \frac{K_{\text{H}_2}}{K_{\text{C}_2\text{H}_2}} = K_{\text{C}_2\text{H}_2}^{\text{H}_2}$$

$$Q_{\text{CO}_2} = K_1 * Q_{\text{N}_2}$$

$$\Rightarrow Q_{\text{N}_2} = \frac{1}{K_1} * Q_{\text{CO}_2} = \frac{1}{0.7382} * Q_{\text{CO}_2} \approx 1.35 * Q_{\text{CO}_2} \tag{4}$$

$$Q_{\text{C}_2\text{H}_2} = K_2 * Q_{\text{N}_2} \Rightarrow Q_{\text{N}_2} = \frac{1}{K_2} * Q_{\text{C}_2\text{H}_2}$$

$$Q_{\text{H}_2} = K_3 * Q_{\text{C}_2\text{H}_2} \Rightarrow Q_{\text{C}_2\text{H}_2} = \frac{1}{K_3} * Q_{\text{H}_2}$$

$$Q_{\text{C}_2\text{H}_2} * \frac{1}{K_2} = Q_{\text{CO}_2} * \frac{1}{K_1}$$

$$\Rightarrow Q_{\text{CO}_2} = K_1 * Q_{\text{C}_2\text{H}_2} * \frac{1}{K_2} = Q_{\text{C}_2\text{H}_2} * \frac{0.7382}{0.5829} \approx 1.27 * Q_{\text{C}_2\text{H}_2} \tag{5}$$

$$Q_{\text{H}_2} * \frac{1}{K_3} = Q_{\text{CO}_2} * \frac{1}{K_1}$$

$$\Rightarrow Q_{\text{CO}_2} = K_1 * Q_{\text{H}_2} * \frac{1}{K_3} = Q_{\text{C}_2\text{H}_2} * \frac{0.5829}{1.0106} \approx 0.58 * Q_{\text{H}_2}$$

All calibration results were calculated and listed in following table.

desired amount of N ₂ (%)	on display CO ₂ (%)
98	13.28
98.1	13.29
98.2	13.30
98.3	13.32
98.4	13.33
98.5	13.34
98.6	13.36
98.7	13.37
98.8	13.38
98.9	13.40
99	13.41
99.1	13.42
99.2	13.44
99.3	13.45
99.4	13.46
99.5	13.48
99.6	13.49
99.7	13.51
99.8	13.52
99.9	13.53
100	13.55

desired amount C ₂ H ₂ (sccm)	on display (%)
5	2.50
10	5.00
15	7.50
20	10.00
25	12.50
30	15.00
35	17.50
40	20.00
45	22.50
50	25.00
55	27.50
60	30.00
65	32.50
70	35.00
75	37.50
80	40.00
85	42.50
90	45.00
95	47.50
100	50.00
105	52.50

References

[1] Operating Manual for AFC-2600 Mass Flowmeters & Controllers, AALBORG® Instruments & Controls, Inc. Orangeburg, New York USA.

8. SEM Samples

# Nr.	composition	Temp (°C)	N ₂ (%)	C ₂ H ₂ (%)	H ₂ (%)	exp. time (min) (C ₂ H ₂)
143	Co(NO ₃) ₂ *6H ₂ O	600	20			30
144	Co(NO ₃) ₂ *6H ₂ O	400	20			30
149	Co(NO ₃) ₂ *6H ₂ O	200	20			30
150	Co(NO ₃) ₂ *6H ₂ O	100	20			30
151	Co(NO ₃) ₂ *6H ₂ O	750	20			30
164	Co(NO ₃) ₂ *6H ₂ O	600	20	2		10
165	Co(NO ₃) ₂ *6H ₂ O	600	20	6		10
181	Co(NO ₃) ₂ *6H ₂ O	600	20	6		10
182	Co(NO ₃) ₂ *6H ₂ O	600	20	2		1
183	Co(NO ₃) ₂ *6H ₂ O	600	20	2		60
184	Co(NO ₃) ₂ *6H ₂ O	600	20	6		60
185	Co(NO ₃) ₂ *6H ₂ O	600	20	6		1
186	Co(NO ₃) ₂ *6H ₂ O	750	20	6		10
187	Co(NO ₃) ₂ *6H ₂ O	750	20	2		10
188	Co(NO ₃) ₂ *6H ₂ O	600	20	2.25		10
189	Co(NO ₃) ₂ *6H ₂ O	750	20	2.25		10
190	Fe ₅₀ Ni ₅₀	600	20	2		10
191	Fe ₅₀ Ni ₅₀	600	20	6		10
192	Fe ₇₅ Ni ₂₅	600	20	6		10
193	Fe ₇₅ Ni ₂₅	600	20	2		10
194	Fe ₇₅ Ni ₂₅	600	20			30
195	Fe ₅₀ Ni ₅₀	600	20			30
258	Cr(NO ₃) ₃ *9H ₂ O	100	30			
259	Cr(NO ₃) ₃ *9H ₂ O	200	30			
260	Cr(NO ₃) ₃ *9H ₂ O	300	30			
261	Cr(NO ₃) ₃ *9H ₂ O	400	30			
262	Cr(NO ₃) ₃ *9H ₂ O	500	30			
263	Cr(NO ₃) ₃ *9H ₂ O	600	30			
264	Cr(NO ₃) ₃ *9H ₂ O	750	30			
283	Cr(NO ₃) ₃ *9H ₂ O	600	30	2		10
286	Cr(NO ₃) ₃ *9H ₂ O	750	30	2		10
287	Cr(NO ₃) ₃ *9H ₂ O	600	30	2		60
322	Co(NO ₃) ₂ *6H ₂ O	600	30			0
323	Co(NO ₃) ₂ *6H ₂ O	600	30		2 (600°C)	5
324	Co(NO ₃) ₂ *6H ₂ O	600	30		2 (600°C)	25
325	Co(NO ₃) ₂ *6H ₂ O	600 (400 H ₂)	30		2 (400°C)	0
326	Co(NO ₃) ₂ *6H ₂ O	600 (400 H ₂)	30	2	2 (400°C)	5
327	Co(NO ₃) ₂ *6H ₂ O	600 (400 H ₂)	30	2	2 (400°C)	25
328	Co(NO ₃) ₂ *6H ₂ O	600	30	2		5
329	Co(NO ₃) ₂ *6H ₂ O	600	30	2		25
330	Ni(NO ₃) ₂ *6H ₂ O	600	30	2		25
331	Ni(NO ₃) ₂ *6H ₂ O	600	30	2		5
332	Ni(NO ₃) ₂ *6H ₂ O	600	30			0
333	Ni(NO ₃) ₂ *6H ₂ O	600	30		2 (600°C)	5
334	Ni(NO ₃) ₂ *6H ₂ O	600	30		2 (600°C)	25
335	Ni(NO ₃) ₂ *6H ₂ O	600 (400 H ₂)	30		2 (400°C)	0

# Nr.	composition	Temp (°C)	N ₂ (%)	C ₂ H ₂ (%)	H ₂ (%)	exp. time (min) (C ₂ H ₂)
336	Ni(NO ₃) ₂ *6H ₂ O	600 (400 H ₂)	30	2	2 (400°C)	5
337	Ni(NO ₃) ₂ *6H ₂ O	600 (400 H ₂)	30	2	2 (400°C)	25
344	Ni(NO ₃) ₂ *6H ₂ O	400	30			0
345	Ni(NO ₃) ₂ *6H ₂ O	400 (H ₂)	30		2 (400°C)	0
346	Ni(NO ₃) ₂ *6H ₂ O	500 (400 H ₂)	30		2 (400°C)	0
351	Co(NO ₃) ₂ *6H ₂ O	600	30			0
352	Co(NO ₃) ₂ *6H ₂ O	600	30	2		20
353	Co(NO ₃) ₂ *6H ₂ O	600	30			0
354	Co(NO ₃) ₂ *6H ₂ O	600	30	2		20
382	MoO ₂	750	30			0
388	MoO ₂	750	30		2	10
389	MoO ₂	750	30		2	2.5
390	MoO ₂	750	30		2	60
391	MoO ₂	750	30		2	5
392	MoO ₂	750	30		2	7.5
393	MoO ₂	750	30		2	20
394	MoO ₂	750	30	2	2 (5min)	2.5
395	MoO ₂	750	30	2	2 (5min)	60
396	MoO ₂	750	30	2	2 (5min)	5
397	MoO ₂	750	30	2	2 (5min)	20
398	MoO ₂	750	30	2	2 (5min)	7.5
399	MoO ₂	750	30	2	2 (5min)	10
400	MoO ₂	600	30			0
401	MoO ₂	600	30		2	10
402	Cr(NO ₃) ₃ *9H ₂ O	600	30		2	10
403	Cr(NO ₃) ₃ *9H ₂ O	750	30		2	10
404	MoO ₂	600	30	2	2 (5min)	10
405	MoO ₂	600	30	2		10
406	MoO ₂	750	30	2		10
407	MoO ₂	750	30	2	2 (400°C)	10

Acknowledgements

I express my gratitude to many people who supported and helped me during the PhD thesis over the last three years.

I am deeply grateful to Bernard Grobéty who initiated and directed this project. Thank you Bernard, your help and support during my entire PhD was kind and generous and your scientific advices straightforward.

Anna Lepora is owed particular thanks. She was the outrider of the project and paved the way for my thesis. Her introduction in the high temperature diffractometry and her bibliographical help was immaculate.

Thanks to Christoph Neururer for helping me in all electrotechnical problems. Your support in Scanning Electron Microscopy and your help in the refinement of the gas mixing facility were milestones in my work.

A very special thank to Andri Vital and Andreas Züttel who accepted to revise my thesis although very busy.

Thanks to Marino Maggetti for the financing, Nicole Brügger for her administrative work, Odette Marbacher for the chemical advise and laboratory support and Paulo Bourqui for the jamoke.

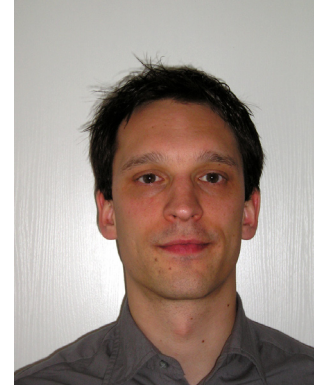
Many thanks to Pierre Vonlanthen for the numberless fruitful discussions, the bi-weekly French lessons and holiday organisations. You are an exemplary bureau workmate. I'm also thankful to Peter Berner and Simon Fischer for their support and simple daily chats, you are buccaneers.

Another very big thanks to all my colleagues and friends I met here in Fribourg, André, Andrea, Cédric, Christina, Christophe, Claire, Claudius, Cordula, Corinne, Daniel, Elias, Giacomo, Gianfranco, Gisela, Hajnalka, Jean Pierre, Jeanne, Jessica, Jon, Jonas, Katja, Luc, Maëlle, Martin, Michèle, Mikaël, Mustafa, Nico, Niels, Patrick, Rémi, Sabina, Sébastien, Sherkan, Silvia, Sophie, Srdan, Stephan, Stéphanie, Vincent, etc.

Thanks to my flatmate Lars for sharing with me everyday life and to accord me a job beside my PhD, Richard for the English revision and my sister for many lunch invitations. All my gratitude goes to my family and my friends. Thank you Cécile for your presence, your care and for having helped and pushed me to finish this work.

Kuno Matzinger

Holenackerstrasse 35
3027 Bern
phone: +41 79 232 02 44
kuno.matzinger@bluewin.ch



born 11th of october 1977 in Lucerne, Switzerland

Education

- 2002 – 2006 University of Fribourg, Switzerland
▪ **PhD in Technical Mineralogy**
- 1997 – 2002 University of Berne, Switzerland
▪ **Master of Science in Earth Sciences**

Work experience

- 2002 – 2006 **University of Fribourg**, Switzerland
▪ Evolution of transition metal nitrate films during chemical vapour deposition (CVD) of carbon nanotubes. An *in-situ* high temperature X-ray diffraction study with complementary SEM and TEM investigations
▪ Organisation and leadership of practical training
▪ Compilation of an extensive collection of minerals
▪ Teaching assistant of the X-ray course
- 2005 – 2006 **Armasuisse**
▪ Implementation of a Secure Network Communication System for SAP
- 2001 – 2002 **University of Berne**, Diploma Thesis
▪ Field work at the Selati Game Reserve, South Africa
▪ Design of a digital geological map based on GIS skills
▪ Age determination by Pb/Pb Stepwise Leaching (PbSL) method on garnet, staurolite, sillimanite and andalusite
- 2001 **EMPA Dübendorf**, Laboratory for High Performance Ceramics
▪ Work placement in science and production of nano-particles via flame-synthesis with additional TEM investigations and BET measurements.
- 2001 Geologische Beratungen, Dr. Franz Schenker
▪ Work placement for a geological consulting agency
- 2000 Vocational School Biel
▪ Substitute teacher in mathematics
- 1998 – 2003 Wesser & Partner (Swiss Red-Cross)
▪ Acquisition, field research and data processing

Language skills

- German Mother tongue
English Fluent, Edition of diploma and PhD thesis
French Fluent, Language of education
Italian School knowledge

Publications and Communications

K. Matzinger, A. Lepora, B. Grobéty, A. Zuetzel (2004), The evolution of iron and nickel nitrate films during CVD synthesis of carbon nanotubes: An *in-situ* high temperature X-ray diffraction investigation, Journal of Conference Abstracts, C051, 192; Carbon 2004, Providence, Rhode Island, USA, 11-16 July 2004

K. Matzinger, B. Grobéty, The evolution of nickel nitrate hexahydrate coated glass substrate during CVD synthesis of carbon nanotubes: An *in-situ* high temperature X-ray diffraction investigation, Carbon (submitted 2005).

K. Matzinger, B. Grobéty, The evolution of cobalt nitrate hexahydrate coated glass substrate during CVD synthesis of carbon nanotubes: An *in-situ* high temperature X-ray diffraction investigation. Journal of Applied Physics A (to be submitted).

K. Matzinger, B. Grobéty, The evolution of molybdenum oxide coated glass substrate during CVD synthesis of carbon nanotubes: An *in-situ* high temperature X-ray diffraction investigation (to be submitted).